HIGH RESOLUTION ELECTRIC FIELD PROBES WITH APPLICATIONS IN HIGH EFFICIENCY RF POWER AMPLIFIER DESIGN

Nelo Dehghan

A thesis submitted to Cardiff University
for the degree of Doctor of Philosophy

September 2014

Declaration

This work has not previously been accepted in substance for any degree and is not concurrently submitted in candidature for any other higher degree.

Signed:……………………………..(Candidate) Date:………………………….

Statement 1

This thesis is being submitted in partial fulfilment of the requirements for the degree of ……………..(insert as appropriate PhD, MPhil, EngD)

Signed:……………………………..(Candidate) Date:………………………….

Statement 2

This thesis is the result of my own independent work/investigation, except where otherwise stated. Other sources are acknowledged by explicit references.

Signed:……………………………..(Candidate) Date:………………………….

Statement 3

I hereby give consent for my thesis, if accepted, to be available for photocopying, inter-library loan and for the title and summary to be made available to outside organisations.

Signed:……………………………..(Candidate) Date:………………………….

ACKNOWLEDGMENTS

I would like to start off by expressing my deepest appreciation and gratitude to my supervisors Professor Steve Cripps and Professor Adrian Porch, thank you for all your guidance and support.

The path felt long during the journey, but looking back the time seemed to disappear. I am grateful to the memories I have, the people I have met and the experience I am left with.

I'd like to thank my fellow colleagues: Dr David Rowe, thank you for allowing me to pester you, constantly. Thank you also to Dr Alex Morgan, I am still waiting on my wish list.

I would also like to thank Dr Jonny Lees, Dr Randeep Saini and Dr Jack Naylon for their wisdom, time and help.

I would like to say a thank you to my friends and family. Your support saw me to the end. Mr. P, I hope you liked the input. With a final thank you to Jonathan Cox, my shoe. Thank you for finding my commas,,,,

ABSTRACT

The evolution of high power transistors has ultimately increased the complexity of their design, interaction and incorporation within microwave frequency power amplifiers. The requirement for high efficiency and high linearity for a wide band frequency by the consumer has put pressure on designers. Due to unexpected and unpredictable failures, device characterisation of the transistor in operational conditions is a highly valuable advantage. The proposed work will describe a non-intrusive, ultra-miniaturised, high resolution electric field probe system; with the capability of measuring relative voltage and waveforms distribution of complex active devices within their operating conditions.

The design, construction and evolution of the probing system will be described displaying a resolution of better than 100μm, with a flat frequency response of up to 8GHz. Due to the miniaturised size and the flexibility in positioning, the probe has the ability to measure on-chip, at the device plane, across the device periphery. Results will show direct observation of device plane voltages in high power RFPAs, where the device can exhibit variation in the voltage distribution across the periphery. Such variation will be a function of the internal behaviour and not evident in the output characteristics of the device. This work will also describe a novel method for absolute calibration of the probing system which can be implemented with every movement of the measurement plane. Therefore presenting a successful and calibrated EFP system capable of device characterisation and diagnostics.

Contents

1. Introduction 1

1.1. Research Overview 1

1.1.1. Introduction to Electric field probing techniques and literature Review: Outline of Chapter 2 1

1.1.2. Initial work performed on Coaxial EF probes: Outline of chapter 3 2

1.1.3. The EDM electric field probe: Outline of chapter 4 2

1.1.4. MMIC amplified EDM Electric field probe: Outline of chapter 5 3

1.1.5. High power amplifier diagnostic: Outline of chapter 6 3

1.1.6. Doherty power amplifier diagnostic: Outline of chapter 7 4

1.1.7. Asymmetrical Doherty power amplifier diagnostics: Outline of chapter 8 4

1.1.8. “In-Situ” calibration method for EFP: Outline of chapter 9 4

1.1.9. Discussion: Outline of chapter 10 5

1.1.10. Conclusions and future works: Outline of chapter 11 5

1.2. Novel work presented and publications list 5

2. Introduction to EFP techniques and literature Review 7

2.1. The role of the radio frequency power amplifier 9

2.1.1. Introduction to the transistor and its characteristics 9

2.1.2. The Doherty power amplifier 12

2.1.3. Inside the transistor 17

2.2. Measurement apparatus 20

2.2.1. Scattering parameters 20

2.2.2. Vector network analyser 22

2.2.3. Digital storage oscilloscope 24

2.2.4. RF measurements and characterisation 25

2.3. Electric field probe 26

2.3.1. Open-ended coaxial probe 27

2.3.2. Capacitive probe analogy 31

2.4. Electric field at the device plane 33

2.4.1. Electric field at the surface of a metal. 33

2.4.2. Orthogonal components of electric field. 35

2.5. Literature review of EFP design considerations and techniques 36

2.5.1. Increasing the spatial resolution 38

2.5.2. Increasing the sensitivity 43

2.5.3. Measurement of orthogonal electric field components 47

2.5.4. Discussion of the literature review 51

2.6. Alternative methods for electric field measurements and device characterisation 54

2.6.1. Electrooptic field mapping 54

2.6.2. Load-pull measurements for device plane voltages 56

3. Initial work performed on Coaxial EF probes 58

3.1. Initial design stage of electric field probe 60

3.1.1. Design of EFP1 and EFP2 60

3.1.2. Passive device under test 65

3.1.3. Automation of the results 70

3.1.4. Spatial resolution capability of EFP1 and EFP2 73

3.1.5. Design of EFP3 76

3.2. The EFP and resonant electric field probe 82

3.2.1. The design and comparison of the resonant electric field probe to EFP2 82

3.2.2. Experimental results of EFP2 and REFP 84

3.2.3. The effect of increasing the measurement separation 88

3.2.4. The effect of the probe and the resulting measured field 90

3.3. Conclusion 91

4. The EDM electric field probe 93

4.1. Construction of the EDM EFP and EDM REFP 94

4.1.1. EDM electric field probe and resonant electric field probe 94

4.1.2. Resolution of the EDM EFP and REFP 97

4.1.3. The effect of inner conductor protrusion on the spatial resolution . 101

4.1.4. Frequency calibration.... 104

4.1.5. The effect of the separation between probe tip and DUT.... 106

4.2. The ultra-fine mini-coaxial EFP 110

4.2.1. Construction of the ultra-fine coaxial EFP 110

4.3. Conclusion.... 117

5. MMIC amplified EDM Electric field probe 118

5.1. Design and construction of the low-noise MMIC 118

5.1.1. Design of the low-noise MMIC.... 119

5.1.2. Construction of the MMIC EDM EDF 122

5.2. MMIC EDM EFP characteristics and resolution capability.... 125

5.2.1. Design of the flat inter-digital test fixture 125

5.2.2. Frequency calibration of the MMIC EDM EFP 127

5.2.3. Spatial resolution of the MMIC EDM EFP 129

5.2.4. Spatial resolution capability beyond 100μm.... 132

5.3. Design and characteristics of alternative MMIC EDM EFP.... 137

5.3.1. Glass dielectric EDM EFP.... 137

5.3.2. Construction of the ‘control’ EDM EFP.... 139

5.4. MMIC design improvements.... 143

5.4.1. Extending the frequency response of the MMIC amplifier.... 143

5.4.2. Frequency calibration of improved MMIC EFP.... 145

5.5. Conclusion.... 147

6. High power amplifier diagnostic.... 149

6.1. The high power amplifier, the transistor and its test circuit 149

6.1.1. Device characterisation before and after de-lidding process 151

6.1.2. Automated spatial resolution and the electric field distribution 152

6.1.3. Calibration and Data processing of waveform information 154

6.1.4. Waveform distribution with varying input power................................ 156

6.1.5. Waveform distribution before and after broken bondwire................ 158

6.1.6. Amplitude calibration.. 160

6.2. Conclusion.. 161

7. Doherty power amplifier diagnostic... 163

7.1. Symmetrical Doherty power amplifier.. 163

7.1.1. Theoretical DPA behaviour 163

7.1.2. RF input output characteristics before and after transistor de-lidding 165

7.1.3. Spatial resolution scans along the bondwire of the transistors......... 166

7.1.4. Experimental waveform measurements and fundamental voltage component... 171

7.2. Conclusion.. 175

8. Asymmetrical Doherty power amplifier diagnostics 176

8.1. EFP diagnostic evolution of the A-DPA... 177

8.1.1. Theoretical behaviour of the A-DPA 177

8.1.2. RF Pin-Pout characteristics before and after the de-lidding process 178

8.1.3. Spatial resolution analysis of the A-DPA.. 180

8.1.4. Waveform analysis of the A-DPA 189

8.1.5. Waveform analysis of the A-DPA at band-edge frequencies 196

8.2. Conclusion.. 199

9. "In-Situ" calibration method for EFP... 201

9.1. Basic concepts of proposed technique.. 201

9.1.1. Low frequency analysis.. 203

9.1.2. RF input and output characteristics of the 10W GaAs device 206
9.1.3. Measurement setup 206
9.1.4. Experimental results 207
9.2. Conclusion 210
10. Discussion 211
10.1. Design methodology of the EFP 211
10.2. Continuity of the measurement plane and the resulting output 212
10.3. Response of true voltage 212
10.4. Calibration 213
11. Conclusions and future works 215
11.1. Conclusions 215
11.2. Future works 219
12. Bibliography 222
13. Appendix 1 226
INTRODUCTION 226
PROBE CONSTRUCTION 227
MEASUREMENTS. 227
CONCLUSION 229
REFERENCES 229
14. Appendix 2 230
INTRODUCTION 230
PROBE DESIGN AND CONSTRUCTION 230
PROBE CALIBRATION 231
HIGH POWER PA (HPA) MEASUREMENTS 232
DOHERTY POWER AMPLIFIER (DPA) MEASUREMENTS 233
CONCLUSIONS 234
REFERENCES 234
15. Appendix 3 235

INTRODUCTION 235
LOW FREQUENCY RESPONSE 236
THEORY 236
MEASUREMENT SETUP 237
EXPERIMENTAL RESULTS 237
CONCLUSION 238
REFERENCES 238
16. Appendix 4 239
17. Appendix 5 241

1. INTRODUCTION

The work presented within this thesis ultimately achieves two specific goals. One; the development and evolution of a high-resolution Electric Field Probe (EFP) for use at GHz frequencies and two; the successful application of the EFP for in-situ measurements of complex active devices within operational high power microwave amplifier systems. Unconventionally, the initial goal of the outlined work was to develop an alternative method for the measurement and device characterisation of high power transistors within a functioning amplifier system, specifically the Doherty Power Amplifier (DPA). The DPA provides an excellent solution as an efficiency enhancement technique, however is prone to unexplainable failure, both catastrophic and unexpected performance. Existing characterisation methods, such as load-pull systems and ElectroMagnetic (EM) simulators, at times, are unable to pre-empt such failures. For this reason the initial research conducted within the presented work required the design and development of an ultra-miniaturised, high-resolution EFP capable of extracting on-chip waveform information for the given Device Under Test (DUT).

1.1. Research Overview

1.1.1. Introduction to EFP techniques and literature Review: Outline of Chapter 2

This chapter provides the outline of the theory presented within this work. Preliminary explanations will be provided regarding the importance of the work, before an in depth discussion regarding the models and concepts utilised for the upcoming research. The literature review will firstly seek to understand the conceptual idea of the transistor and its function within a DPA system before concentration is focused to the EFP and alternative methods of characterisation. By fully understanding the needs, requirements and topology of the transistor, the requirements of the EFP system can be set. Alternative design methods of the EFP will be shown and discussed, though it will be evident that their design and resolution capabilities are not sufficient for the requirements of the work presented.

1.1.2. Initial work performed on Coaxial EF probes: Outline of chapter 3

Chapter 3 will outline preliminary work on the EFP, where initial resolution capability was much greater than 100µm. A novel feature is introduced with the positioning of a small buffer amplifier close to the probe tip, providing a much needed increase in output as well as reducing the level of stray pick-up. The non-satisfactory resolution is result of the materials used for the construction of the EFP, as probes were fabricated with the smallest commercially available coaxial cables. However, an important design feature was discovered by the work presented within this chapter; the resulting spatial resolution was dependent on both the diameter of the inner and outer conductor of the probe tip. Though theoretical expectation predicts this dependence mainly as a function of inner diameter as this is the region which couples to the field produced by the DUT.

1.1.3. The EDM electric field probe: Outline of chapter 4

The work continued within this chapter shows further evolution of the EFP. The attainment of further reduced commercially available coaxial cables proved difficult, for this reason the study concentrated on the custom design of a coaxial line. Sourcing of copper tubes with an outer diameter of 0.24mm and threading an enamelled copper wire with a diameter of 0.07mm resulted in a custom EFP fabrication. This subsequent reduction in both the inner and outer diameter of the EFP resulted in an improved resolution of greater than 100µm. Within this chapter

both the probe tip length and probe tip protrusion is investigated, yielding the conclusion that the length of probe line dictates the resonance present in the frequency response, while the presence of probe tip protrusion decreases the resolution capability of the EFP. The importance of a constant measurement plane is shown within this chapter, with the most important conclusion being a decay of half the output requires an increase in the measurement plane of up to 100μm. This finding is extremely important when considering the results shown within chapter 7 and 8.

1.1.4. MMIC amplified EDM Electric field probe: Outline of chapter 5

With the spatial resolution to the required level, this chapter focussed on the improvement of the frequency response of the EFP. The incorporation of the buffer amplifier introduced in chapters 3 and 4 yielded a flat response up to 4GHz before resonance as parasitic components dominated. The design and implementation of a Monolithic Microwave Integrated Circuit (MMIC) will result in a flattening of the frequency response to a much higher frequency, greater than 8GHz. The probe tip line length, tip protrusion and alternative design of the EFP is investigated within this chapter. Consistent evidence is shown that the length of the probe line dictates the resonance present in the response, where shorter the line length results in a resonance at a higher frequency. Further evidence is presented that the inclusion of a probe tip protrusion will increase the output of the probe but at the expense of the spatial resolution.

Alternative EFP probe designs are presented and include the incorporation of an ultra-fine coaxial cable and the construction of a control EFP (with no buffer amplifier). The construction of the control EFP displays the importance of the buffer amplifier and its incorporation as well as showing the high frequency response is solely due to parasitic components as a result of the MMIC design. Therefore the high frequency response can be further improved with modification to the buffer amplifier and not the design of the EFP tip.

1.1.5. High power amplifier diagnostic: Outline of chapter 6

Previous chapters have shown the design, fabrication and calibration measurements of the EFP concluding entities such as; resolution, output, response and sensitivity to the local geometry. However measurements thus far have been

conducted on simple passive structures. This chapter shows initial measurements conducted on high power and complex structures. All investigations shown will require the removal of the transistors protective ceramic casing, vital for direct chip access. Important key features presented include; the ability to detect device plane variation and provide diagnostics of broken bondwires. These anomalies are not present or cannot be detect at the output of the device, thus highlighting the importance of the EFP as a diagnostic tool.

1.1.6. Doherty power amplifier diagnostic: Outline of chapter 7

With successful high power measurements conducted within chapter 6; chapter 7 will focus on a more complicated system, a DPA. The EFP is lowered over the drain manifold of both the main and peaking devices, for the most accurate measurement of drain voltage. Substantial variation along the device periphery resulted in a difference of up to two times in the measured V_{pp} values, where the maximum voltage held by the peaking device was at a higher value. Again, these anomalies are not seen in the output characteristic of the amplifier and therefore can go potentially undetected.

1.1.7. Asymmetrical Doherty power amplifier diagnostics: Outline of chapter 8

Chapter 8 will display and discuss the results of an asymmetrical DPA, usually regarded as more complex system than a symmetrical DPA due to the use of different sub-amplifiers. The EFP will successfully measure the voltage and waveform distribution along both devices highlighting unexpected measurements such as; the main device exhibiting a clear and visible trend, whereby the maximum voltage is measured in the central position of the device with substantial roll-off at each edge and the peaking device displays significant variation along the device periphery. The variation measured will be shown to have a proportional effect on the waveform distribution, thus the fundamental components of the drain voltage will display differences in the measured peak values depending on the point of comparison along the device.

1.1.8. "In-Situ" calibration method for EFP: Outline of chapter 9

Chapter 9 will show a novel in-situ method for absolute calibration of the EFP. Unconventionally this chapter is placed at the end of the thesis due to the relevance in the timeline of events. This method was designed at the latest stage of

this work, although proving a successful method for calibration, and was not applied as a measurement standard in prior chapters. The in-situ calibration technique of the EFP takes advantage of low frequency behaviour of complex structures. By 'illuminating' the DUT with a low frequency of 1MHz, the voltage distribution along all entities of the DUT will appear to be uniform and equal. Therefore the output of the EFP, when placed over the drain manifold, can be compared to direct measurement of a high impedance contact oscilloscope probe. The subsequent comparison will yield a suitable scaling factor as the output of the probe will be significantly smaller than the output of the contact oscilloscope probe. This scaling factor can therefore be applied to EFP measurements at the correct operational frequency. Thus providing an absolute in-situ calibration of the EFP not restricted to a specific position.

1.1.9. Discussion: Outline of chapter 10

Chapter 10 will provide a discussion point of the whole work presented. Further commenting on the design standard utilised with relevance to the resulting output and spatial resolution of the EFP. The full effect of the measurement plane with links to final DPA and A-DPA results. Majority of the measurements presented within this work have been conducted on the assumption that the output of the EFP is a 'relevant' measurement. Although absolute calibration will be supplied at the final stage of this work, discussion will be presented regarding the importance of the information provided by the relevant measurements.

1.1.10. Conclusions and future works: Outline of chapter 11

The final chapter within this thesis will state a summary of the results presented in the form of conclusions. This chapter will also discuss the potential future works with an outlined method of execution.

1.2. Novel work presented and publications list

This thesis will present both novel techniques as well as discovered aspects that question the current standards of EFP design. A summary of the highlighted features that will be discussed in the following chapters are given below:

- Miniaturised size and positioning flexibility of the proposed EFP.
- Dismissal of the requirement of inner conductor protrusion for signal gain.

- Incorporation of a buffer amplifier placed close to the probe tip for the amplification of low pick-up and alleviation of unwanted stray pick-up.
- Determination of an optimal distance of the measurement plane between DUT and EFP.
- EFPs capability of time domain waveform measurements.
- The flexibly of the EFP system; with the ability for on-chip, device plane measurements of high power transistors in operational amplifiers.
- The design and utilisation of an absolute in-situ calibration for the EFP.

The publications achieved during the course of the work are as follows.

Conference proceedings:

N. Dehghan*, S. C. Cripps, A. Porch and J. Lees, "An improved electric field probe with applications in high efficiency PA design and diagnostics," in *81st ARFTG*, Seattle, 2013 (*presenter, oral). See Appendix 1.

N. Dehghan*, A. Porch, S. C. Cripps and P. H. Aaen, "A Novel High Resolution E-Field Microscope System with Applications in HPA Diagnostics," in *ARFTG-978-1-4673-0282-1/11*, Tempe, 2011 (*presenter, oral). See Appendix 2.

It should be noted the following submission has been made to the May 2015 International Microwave Symposium proceedings:

N. Dehghan, S. C. Cripps , A. Porch, "A Novel In-Situ Calibration Technique for a High Resolution E-Field Probe" 2014.

The submission was successful as an oral presentation, confirmed one week after VIVA examination of the author.

2. INTRODUCTION TO EFP TECHNIQUES AND LITERATURE REVIEW

The increasing growth and complexity of Radio Frequency Power Amplifiers (RFPA) to support the need for high data rate, for a wide frequency band, has been an ongoing process in recent times. With the sophistication of smartphones and the consumer demand for more simultaneous use from a multifunctional device, designers are under pressure to meet demands. Maintaining and improving the efficiency and linearity of the RFPA in such systems is therefore an ongoing necessity.

While the consumer is demanding faster, lighter and smarter mobile phones, there is not much thought in the resultant carbon footprint from such action. This has resulted in government 'think green' initiatives, which caused many telecommunication companies to feel the pressure to improve efficiency, not only for financial reasons, but in order to reduce the carbon footprint. The improvements in circuit design, semi-conductor technology and cooling techniques of RFPAs within base stations have all contributed to this movement.

The main device under investigation within this thesis is a Field Effect Transistor (FET). Although conceptually a simple unipolar device, it displays many complexities when used in the design of high power and high efficiency RFPA's. The revival of the Doherty Power Amplifier (DPA), a technique utilised for its efficiency enhancement, has produced many unexpected behavioural

characteristics such as, memory effects, deviation from theoretical expectations and device malfunction.

Understanding these complexities requires an understanding of the interactions between the components of a RFPA. While Computer Aided Design (CAD) packages allow the user to manipulate the output for a given input, the user may have no conceptual idea of the waveform information or indeed the actual behaviour internally within the transistor package.

Load-pull systems, a favourite among designers, have been developed for the characterisation and understanding of transistors at GHz frequencies. Entities such as output power, efficiency and gain can be measured [1, 2, 3, 4, 5] under engineered operating conditions for a given frequency range; by tuning the load impedance presented to the transistor, the desired or maximum output power condition can be achieved for the required frequency. By measuring at the device plane, current and voltage time domain waveforms can be obtained at both the input and the output of the device under test (DUT) [1]. However this method of characterisation is not based on the measurements of the DUT under conditions within an operational power amplifier. Therefore the resulting behaviour of the DUT can deviate from the expected measurements when placed within an operational RFPA. However it is understood that this configuration of characterisation allows for the design of the desired matching network for the amplifier, based on the ideal load impedance chosen through tuning. The load-pull analysis relies on the assumption that the device under test is a three port system, where in reality the high power transistor is a large distributed device much more complex than the initial assumption. Therefore, such information as the internal waveform distribution along the device plane can give a valuable insight to the complexity of the device behaviour and help aid its understanding.

The proposed measurement system described within this thesis will allow for in-situ, non-intrusive waveform and relative voltage distribution monitoring within a packaged high-power transistor device. The non-intrusive technique will arise from the development of an Electric Field Probe (EFP), with the capability of measuring internal voltages, within a given operating system. The EFP will function as a diagnostic tool, not only providing an alternative method for the understanding of unexplainable behavioural characteristics present in PA systems,

but providing vital internal information not available through other measurement techniques.

2.1. The role of the radio frequency power amplifier

The main function of an RFPA is to deliver high power for the communication frequency band, frequencies in the range of 500MHz to 3GHz, for a given power supply ("DC") input. The RFPA is normally designed for optimum efficiency within a specific bandwidth, depending on the application of the amplifier. The main active component in an amplifier is the transistor; there are many different transistors available depending on the requirements and application of the amplifier.

This chapter will review the basics of the transistor before understanding its action within an amplifier system. In this thesis the measurements are required at the device plane; therefore it is vital to have an understanding of the transistor topology, once the pre-packaged ceramic casing has been removed. The final section within this chapter will explain the EFP system for the measurement of internal device plane voltages of operational RFPAs.

This thesis will concentrate on the following two transistors: laterally diffused metal oxide semiconductor (LDMOS) and the GaAs pseudomorphic high-electron mobility transistor (pHEMT). It should be noted however, the EFP system is not confined to these two devices for successful measurement, but applicable to a wide range of DUT.

2.1.1. Introduction to the transistor and its characteristics

The FET is a three-terminal, unipolar, device, i.e. dependant on either electron or hole conduction, comprising of a gate (G), drain (D) and source (S) terminals.

The voltage on the gate controls the current flowing from the drain to the source, as a variation in magnitude will result in a subsequent variation in the depletion region of the transistor, which in turn can either restrict or increase the current flow.

Figure 2.1 displays the DC characteristics of a generic FET device.

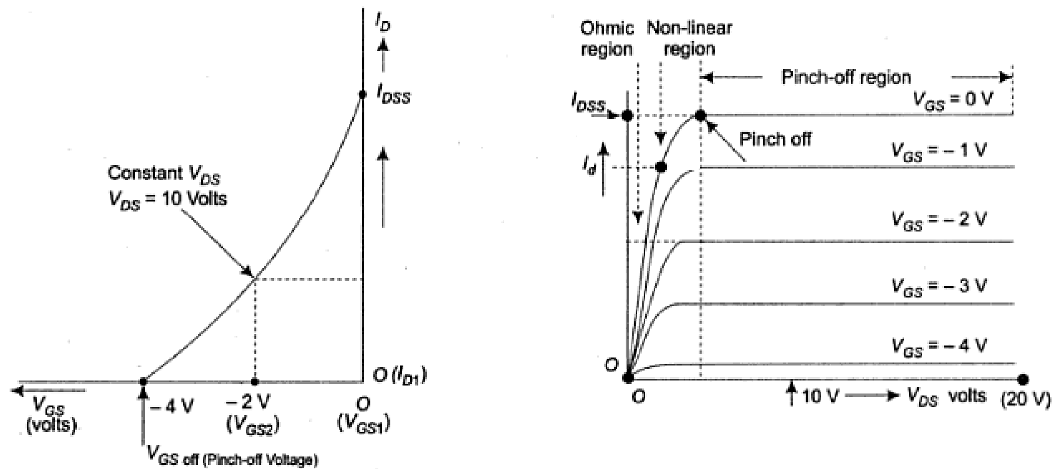

Figure 2.1: DCIV characteristic for a generic FET device detailing the linear and saturation regions. Showing the drain current as a function of gate and drain voltages [6].

For low values of V_{DS}, the transistor behaves according to Ohm's law, this region is known as the linear region. As the value of V_{DS} is increased, the effective depletion region is also increased, resulting in a decrease of the channel width, which in turn limits the flow of current from the drain to the source. The device will reach a point of saturation, whereby a further increase of the V_{DS} value will no longer result in a subsequent increase of I_{DS}, therefore the device is considered to behave like a voltage controlled current source.
The maximum current, I_{DSS}, is achieved when V_{GS} is zero. As V_{GS} becomes more and more negative, the level at which I_{DS} saturates will become lower. Simple device characterisation can be achieved by plotting the DC IV curve, drain current vs. drain voltage, and the transfer characteristics, drain current vs. gate voltage, as shown in figure 2.1. This can be easily achieved through computer simulation or within the lab, with a simple sweep of the gate and drain voltages.

The LDMOS is part of the Metal-Oxide-Silicon Field-Effect Transistor (MOSFET) family, with direct grounding of the source and a laterally opposite drain and source, differentiating it from its counterparts.

The channel length of the LDMOS controls the current which flows across it. The channel current is dependent on both the induced vertical and lateral field, due to the application of gate bias and the lateral field that exists between the drain and the source. The alteration of the applied gate voltage will result in a variation of the induced field, which can in turn reduce the effective channel width and limit the channel current. While the lateral field which exists between the source and drain is dependent on the doping levels present [7].

The channel length of the LDMOS is partly due to the physical length of the gate and the depletion region created by the drain and source while under bias. This depletion region along with the gate induced depletion region, are connected, creating the 'effective channel length'. Depending on the desired I_{DSS} and V_P for the given application, both the physical gate length and dopant levels of drain and source can be varied.

Any transistor device within an amplifier circuit has additional excitation simultaneously supplied along with the DC bias. The additional excitation is provided in the form of RF input drive. Figure 2.2 relates the ac stimulation to the DC operating conditions.

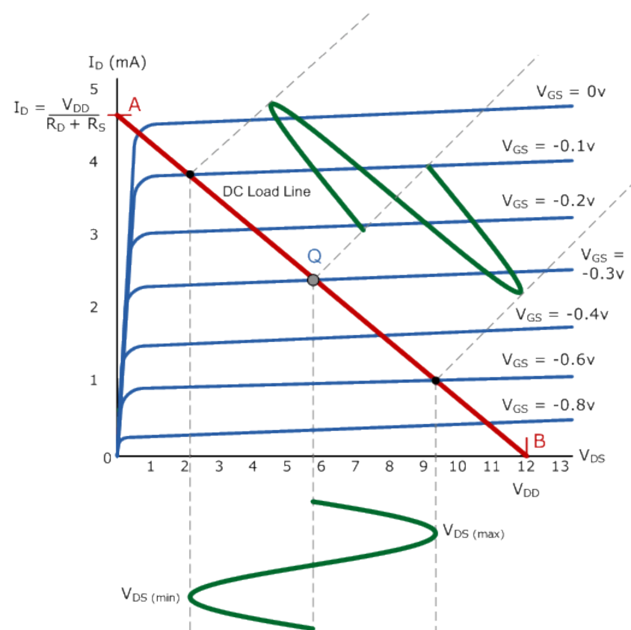

Figure 2.2: ac analysis for a generic FET device relating the input ac signal to the output voltage swing around the quiescent point [8].

The Q denoted in figure 2.2 refers to the quiescent operating condition of the device, which is chosen depending on the class of operation required. As the ac signal is applied to the device, the output voltage swing will vary above and below the DC operating point. Increasing the applied excitation will result in a subsequent increase around the DC bias point. As the applied excitation is increased, this swing around the DC bias point will also increase, until a level of saturation is reached.

The pHEMT takes advantage of the differences present in the energy bands of the semiconductors: gallium and arsenide. The difference in the energy bands between the two elements is known as a heterojunction, which is present at the channel. Many layers of intrinsic and semi-conducting GaAs form the HEMT structure, i.e. undoped and doped n-type GaAs. By separating these layers, high electron mobility can be achieved. The electrons from the doped region can move through the lattice, staying close to the heterojunction. These electrons form a one electron thick layer, meaning that mobility is high due to lack of lattice atoms for collision. It therefore has a high frequency response, due to the so called 'two-dimensional' electron gas [9]. The channel conductivity is controlled by the application of gate bias, as this controls the number of electrons within the channel.

With advancement of nanotechnology, HEMT devices are readily available, which are useable at frequencies above 40GHz [9].

2.1.2. The Doherty power amplifier

Although there are many different existing operating types and configurations of power amplifiers, within this thesis the focus will be placed on the Doherty power amplifier. First introduced in 1936 [10] as an efficiency enhancement technique, has experienced a revival, as a contemporary communication standard for most base stations. For amplifiers operating below their maximum saturated output power (the "back-off region"), the Doherty Power Amplifier (DPA), with the correct phase alignment and power combination, provides an efficiency enhancement over a conventional PA design. Despite its popularity, the DPA is prone to numerous problems, including reliability, memory effects and 'Doherty lite' behaviour. Memory effects are very difficult to pre-determine, as they are a form of additional non-linear behaviour not accounted for in PA models, and can cause subsequent

difficulties in attempts to cancel the distortion DSP (Digital Signal Processing) [1]. 'Doherty lite' behaviour, as the name suggests, is a 'lite' version of the classical Doherty behaviour. A Doherty Lite PA often results from post design adjustment and its behaviour is undesirable, inasmuch as efficiency enhancement is much reduced. Such anomalies have baffled designers; the lack of predictability of such problems in the design phase emphasises the necessity for device plane waveform measurement as demonstrated in this thesis.

The DPA operates in a similar manner to an active load-pull system, consisting of two active devices (this thesis will refer to them as; the "main" and the "peaking" devices), connected by a quarter-wave transmission line. The main and peaking are biased to different classes, Class A or AB while the latter is biased to Class C, respectively, due to the delay required in their activation.
The basic configuration of a DPA and the expected output characteristics are shown below in figure 2.3(a) and (b) respectively.

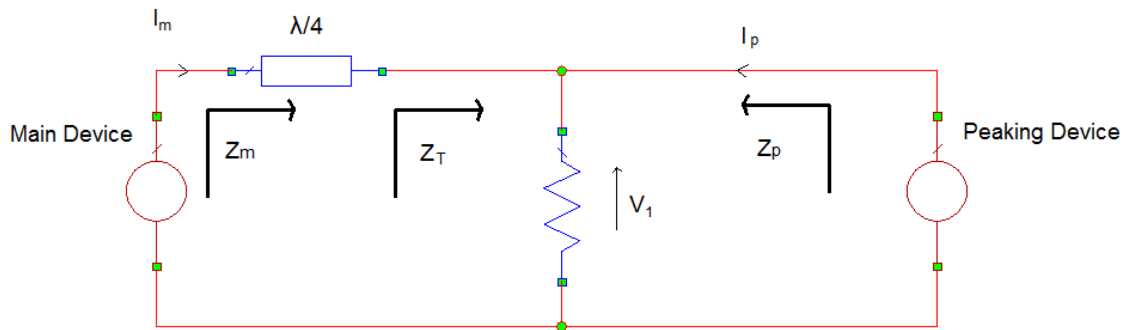

(a)

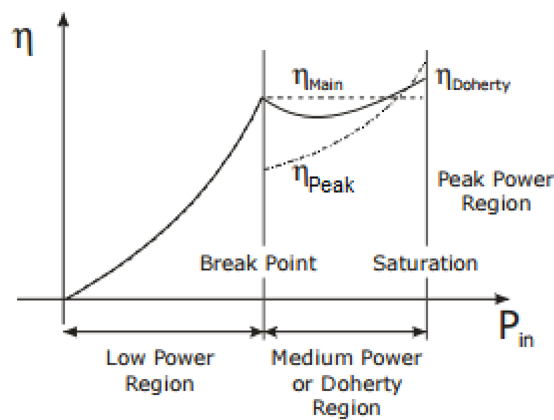

(b)

Figure 2.3: (a) Schematic of Doherty power amplifier, and (b) the theoretical expectation of efficiency versus the input drive, with highlighted low power and medium power regions [1].

At low input power levels, the peaking device is off; this means the main devices receives the entirety of the input signal and sees a high impedance due to the $\lambda/4$ transformer. The role of the $\lambda/4$ transformer within the DPA is to act as an impedance invertor, converting a low to a high impedance, at the output of the main device. At this point, the peaking 'sees' an infinite impedance due to its 'off' state. As the power level is increased, the main device reaches a level of voltage saturation. At this point, due to the Class C bias of the peaking device, the peaking device switches on. This switch-on results in a current contribution from the peaking device, which in turn reduces the overall load impedance seen by the main. The main device now behaves as a controlled voltage source; whereas the peaking device is now considered a controlled current source.

As the input drive is further increased, the impedance seen by both devices is now equal to that of the characteristic impedance of the quarter-wave transformer, thus maintaining maximum efficiency over the power range.

The load impedance of main device is therefore modified by the addition of another coherent current device, the peaking. For this reason, the Doherty is an example of an active load-pull system.

With reference to figure 2.3, circuit analysis can be performed for the derivation of the theory below.

At low levels of input power, the main device will see only the load. As the peaking device switches on and contributes current, the voltage across the load becomes dependant on the current generated by the main and peaking device,

$$V = R(I_m + I_p), \tag{2.1}$$

$$R_m = R\left(\frac{I_m + I_p}{I_m}\right) \tag{2.2}$$

and

$$R_p = R\left(\frac{I_m + I_p}{I_p}\right). \tag{2.3}$$

Considering the AC analysis:

$$Z_m = R\left(\frac{I_m + I_p}{I_m}\right) = R\left(1 + \frac{I_p}{I_m}\right) \tag{2.4}$$

Meaning, if the current supplied by the main and peaking devices are in phase, then Z_m is transformed to a higher resistive value. If I_p is out of phase with I_m, then Z_m is transformed to a lower value. This shows that the impedance seen by one device is dependent on the current contribution of the other device. As the value of I_p increases, the quarter-wave transformer acts as an impedance invertor and reduces the impedance seen by the main device, thus maintaining maximum voltage swing and efficiency [1].

The utilisation of this efficiency enhancement technique can result in an improvement by up to a factor of 2; which would not occur if each device was considered individually, as the overall output performance is a combination of each amplifier [1].

In theory, the classical Doherty behaviour is shown to be rather abrupt, literature on the topic will illustrate the efficiency to be similar to that shown above. With a linear efficiency at low input power and a peak efficiency at the 6dB back-off point. The efficiency is somewhat maintained at higher input power, with the contribution to the, now on, peaking device. Same is shown for the drain voltages, shown below in figure 2.4.

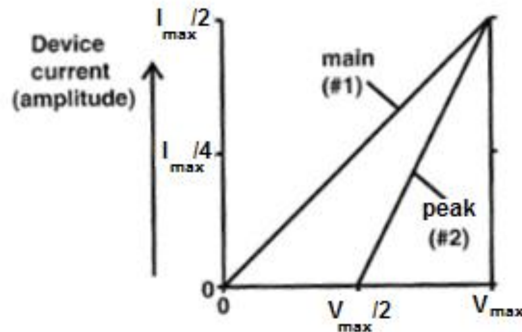

(a)

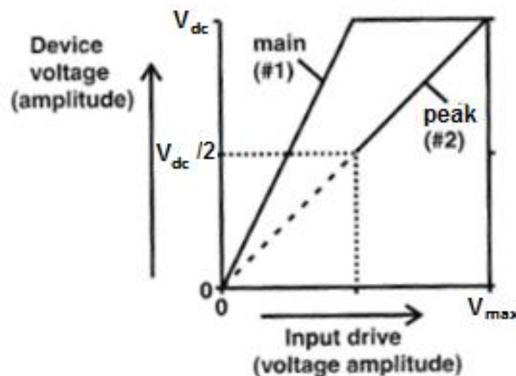

(b)

Figure 2.4: (a) Device currents, and (b) and device voltages, both showing the characteristic response with increasing the input drive [1].

The drain voltages, at low input drive, will show an idealised linear increase in the main device, with sudden saturation around the 6dB back off. This saturation is a result of the instantaneous switch-on of the peaking device, thus maintaining the saturated voltage value of the main device.

In practice, this idealised behaviour is not always evident. Actual measurements of the efficiency and device voltage will show a somewhat much diluted representation of the theoretical expectation.

Efficiency and gain calculations do not require measurements at the device plane, analysis of the input and output power with the consideration of the current from each device is sufficient.

However, the measurement of internal device plane voltages will require an in-situ technique. If such measurement is taken outside the packaged device, this cannot be considered the truest representation, but rather an engineered output for device plane waveforms. Therefore measurements taken at the device-plane, as close to the drain terminal as possible, will be the only correct comparison to the theory.

2.1.3. Inside the transistor

In order to understand the full extent of the proposed measurement system, the physical design of the transistor must be understood. A transistor package ready for integration in a PA circuit consists of a metal drain and gate flanged tabs and a ceramic casing, which encloses the complex internal structure. Removal of the ceramic lid displays a coherent topology amongst most transistor packages within base station amplifiers. Bondwires are required to connect the drain lead to the transistor metallisation, the die, and further connection of the gate lead, laterally opposite. The die of the transistor consists of an inter-digital array, with multiple drain and gate cells. The overall topology of a generic high power 2 GHz transistor is shown below in figure 2.5, with a magnified view of the die metallisation.

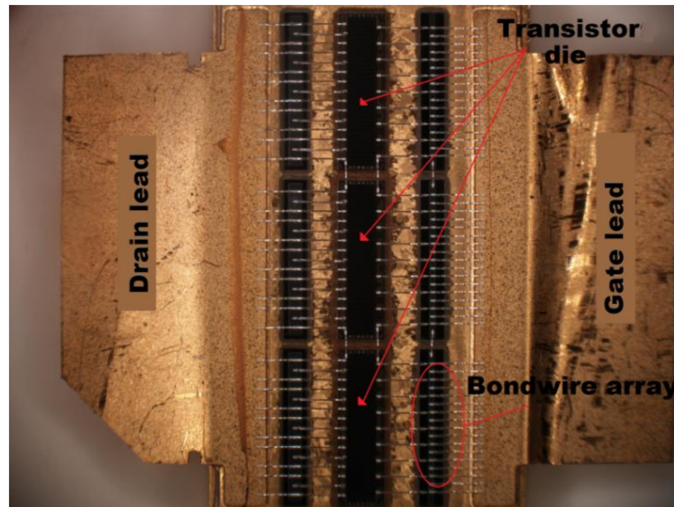

(a)

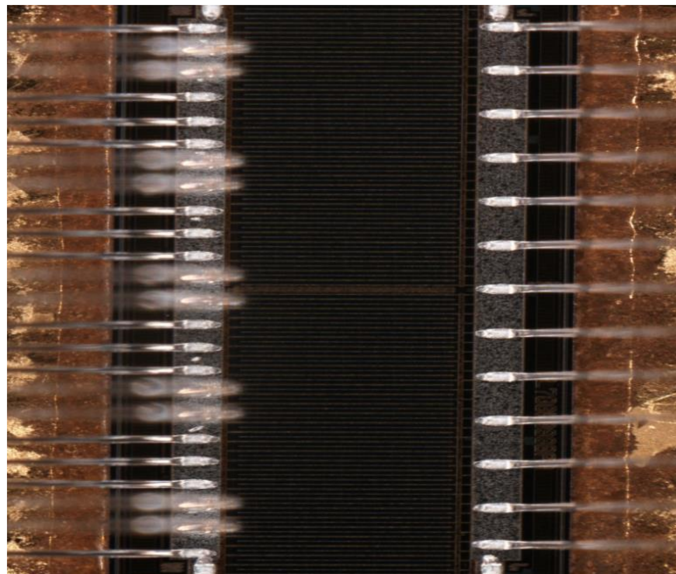

(b)

Figure 2.5: (a) A generic high power 2GHz transistor device with ceramic case removed showing the complex internal structure, and (b) a magnified edit of the interdigital fingers separating the drain and gate bondwire array.

Obtaining experimental data for most high-power transistors does not require the removal of the ceramic casing, with measurements taken only at the input and output terminals of the device. This thesis will explain in subsequent chapters the importance of the exposed circuitry, so that removal of the casing is vital for in-situ

measurements of device plane voltages, which in turn is vital for characterisation and confirmation of theory. In particular, the functionality and interaction of the main and peaking devices can be measured due to this direct access of the drain manifold. Such access will yield the fundamental voltage distribution of the amplifier, in the case of the Doherty, while both transistors are in operational conditions.

Considering the system on a fundamental level, the application of an input drive will evidently result in a movement of current within the circuitry. Electrons will flow through the metallisation of the die and through the bondwires within the package. This flow of electrons will induce a corresponding electric field, which as a result, can be measured as a relative voltage distribution. The resulting measurement system to be described will be a comparable size to the topology of the high power transistor shown.

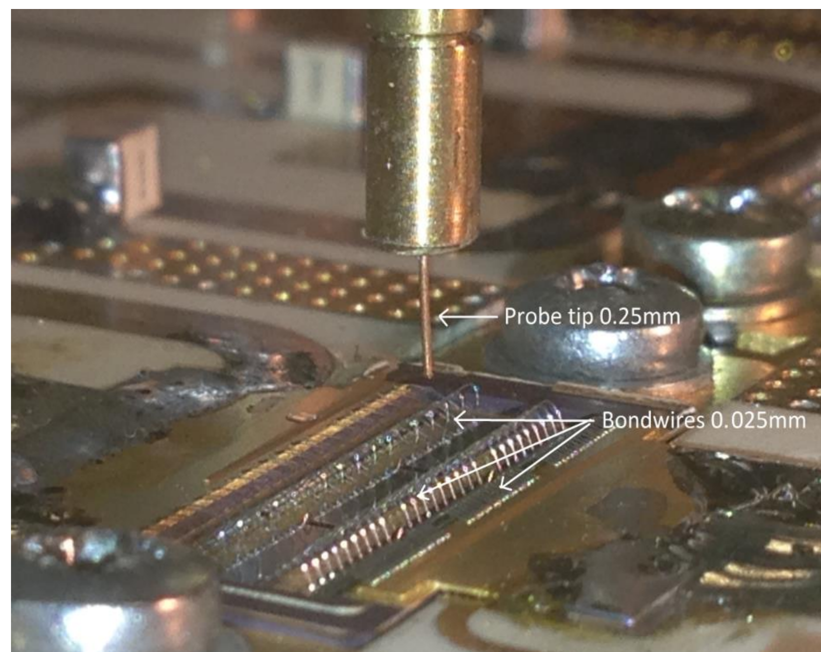

Figure 2.6: Pictorial representation of the resulting EFP system, highlighting the comparable size of the EFP tip and the DUT. Note: the transistor shown belongs to the asymmetrical Doherty power amplifier described within chapter 8.

Figure 2.6 displays the resulting EFP system described within this work. Due to the size and flexibility of the EFP system, measurements can be conducted in various locations across the high power transistor. Resulting in a critically important

measurement of the on-chip device plane drain voltage, the EFP can be lowered directly above the drain manifold.

2.2. Measurement apparatus

In order to generate and acquire the correct data, the measurement apparatus must be fully considered. The proposed in-situ measurement system requires three main components; a DUT, a probe and a measuring scope. Further components will depend on the type of DUT, therefore the type of measurement required, which will then determine the best method for its acquisition.

If the electric field probe is considered as a capacitive probe, further explanation will be provided in section 2.3.2, in which its output is proportional to the local normal electric field component generated by the DUT. Depending on the required data the output of the EFP will be connected to one of two measuring devices, either a Vector Network Analyser (VNA) or a Digital Storage Oscilloscope (DSO). Using the VNA, the relative voltage distribution can be extrapolated with simple calculations. For extraction time-domain waveform information, the EFP will be connected to a DSO.

2.2.1. Scattering parameters

When measuring voltages and currents within a high frequency structure, some difficulty can arise as their values are distributed and can vary within the microwave structure [11]. A method for its simplification requires the consideration of these entities as waves, by describing their behaviour as incident, reflected and transmitted waves, the magnitude and phase of these waves can be measured in a given direction. These waves can be represented within a scattering matrix, and allow for the measurement of voltage waves for any number of ports. An N-port network shown in equation 2.5:

$$\begin{bmatrix} b_1 \\ \vdots \\ b_n \end{bmatrix} = \begin{bmatrix} S_{11} & \dots & S_{1m} \\ \vdots & \ddots & \vdots \\ S_{n1} & \dots & S_{nm} \end{bmatrix} \begin{bmatrix} a_1 \\ \vdots \\ a_m \end{bmatrix}, \tag{2.5}$$

where a_m, is the amplitude of the incident wave on port m and b_n, is the amplitude of the reflected wave from port n.

The work within this thesis will only require the use of a two-port network, shown below in figure 2.7, the resulting scattering (S) parameters within the matrix is shown in equation 2.6.

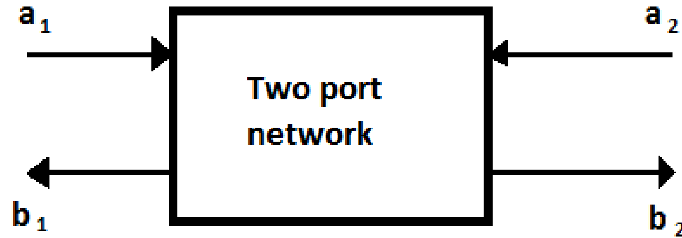

Figure 2.7: An example of a two-port network with identification of the incident and reflected wave direction.

$$\begin{bmatrix} b_1 \\ b_2 \end{bmatrix} = \begin{bmatrix} S_{11} & S_{12} \\ S_{21} & S_{22} \end{bmatrix} \begin{bmatrix} a_1 \\ a_2 \end{bmatrix} \tag{2.6}$$

where:

S_{11} is the reflection from port 1

S_{12} is the transmission from port 2 to port 1

$S_{21}$is the transmission from port 1 to port 2

and S_{22} is the reflection from port 2.

By measuring the S-parameters of a given network, the ratio between the incident and reflected waves can be measured, therefore the transmission behaviour of a network becomes a known entity. Since the characteristic impedance, Z_0, of the system is known, the S-parameters can be interpreted as normalised voltages, currents and power.

For any system, measurement of the S-parameters is a vital tool for its understanding. Information such as voltage standing wave ratio (VSWR), reflection coefficient (Γ) etc. will arise from S-parameter measurements.

If the characteristic impedance of the network is the ratio of voltage to current:

$$Z_0 = \frac{V_0^+}{I_0^+} \tag{2.7}$$

A network terminated by a load, Z_L, the reflection coefficient can be considered as the amplitude of the reflected wave normalised to the amplitude of the incident wave.

$$\Gamma = \frac{V_0^-}{V_0^+} = \frac{Z_L - Z_0}{Z_L + Z_0} \tag{2.8}$$

With respect to the S-parameter, from the input and output voltages at the port, S_{11} is the input reflection coefficient Γ_1 and S_{21} is the output reflection coefficient Γ_2.

If there is a mismatch between the load and the generator, all of the available power will not be successfully delivered. This degree of mismatch is termed a return loss, RL and defined in dB [12].

$$RL = -20\log|\Gamma|\ dB \tag{2.9}$$

The mismatch between the load and the line results in the reflected wave, which leads to a standing wave. The ratio between the maximum voltage value and the minimum voltage value is called the standing wave ratio, SWR, which is the mismatch of the line.

$$SWR = \frac{V_{max}}{V_{min}} = \frac{1 + |\Gamma|}{1 - |\Gamma|} \tag{2.10}$$

Therefore if the line is presented with the condition of a matched load, the $\Gamma = 0$ and hence the $SWR = 1$.

2.2.2. Vector network analyser

The vector network analyser (VNA) is a tuned receiver; with the capability of measuring the magnitude and phase at the ports of a given system. At high frequencies, the wavelength is comparable to or smaller than its physical length, for a transmission line. Therefore the resulting transmission of power can be considered in terms of travelling waves. A VNA has the ability of measuring the incident, transmitted and reflected waves along the transmission line, which is required for the measurement of S-parameters. If the output of the probe is

connected to the VNA, the resulting measurement is of the normalised power which is proportional to the local electric field of the DUT. With sensitivity to the local geometry, sequential measurements conducted with movement of the EFP position along the x or y-axis, (for a constant separation of the z-axis) will result in the relative voltage distribution.

For initial characterisation of the probe, a wide band frequency VNA, Agilent Technologies 300kHz-20GHz PNA-L Network Analyzer, is used. In order to test the frequency response of each probe, the tip is placed over a matched length of 50Ω microstrip line. No reflection will occur along the microstrip line as there is a proper termination. Figure 2.8 shows the setup, where port one of the VNA will be attached to the terminated 50 Ω line, while port two is attached to the output of the probe.

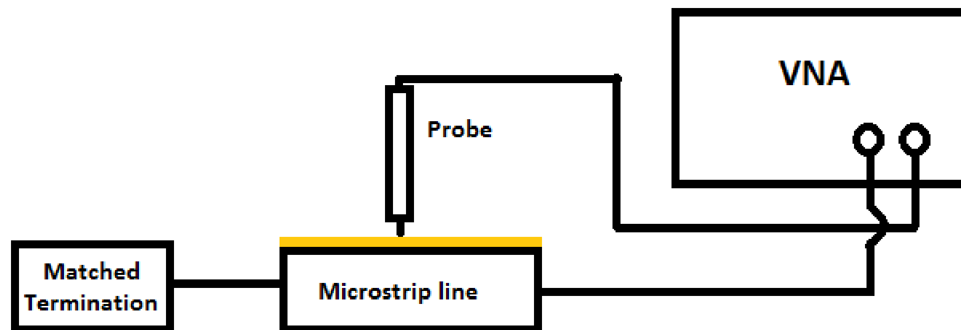

Figure 2.8: Schematic diagram of the setup used for frequency calibration of the EFP. Whereby the probe is placed in a fixed position, 30μm, over the matched microstrip line. The frequency is swept while the output of the probe is used to measure the S_{11} *and* S_{21} *parameters.*

By sweeping the frequency, the response of the probe can be measured for the specified range. The frequency response of the probe holds great importance. In order to minimise distortion of the measured data, a flat response up to three times the fundamental frequency of the DUT is required. The amplifiers used in this thesis operate in the region of 2GHz; a flat frequency response up to 6GHz will allow for minimal corruption of the waveform data for up to three harmonics. Additional frequency and phase calibration must be considered if the response of the probe did not achieve the nominally flat range for the required frequency bandwidth.

The sensitivity of the EFP's to its local geometry and its separation to the DUT is a recurring issue within this thesis, analytical treatment will be provided in sections 2.3.2 and 2.4.2 and experimentally in sections 3.2.3 and 4.1.5. The finalised system will consist of a miniaturised EFP tip, in the region of 250 microns. It will be shown that such small dimensions will inevitably cause a decrease in the signal picked up by the probe. This is shown in the initial characterisation of the probe over the microstrip line. Although final intentions of the EFP are to measure high power active devices, for purposes of characterisation, the EFP will need maximum output for the measurement of passive devices.

2.2.3. Digital storage oscilloscope

The VNA can give vital information about a system, such as s-parameters, return loss, frequency response; however, it is not suitable for producing time-domain waveform measurements. A novel aspect of the proposed measurement system is its miniaturised size and flexibility in its positioning, the probe tip is small enough to be lowered down close to, but not touching, the die metallisation of a transistor. This allows the user to measure the truest representation of time-domain waveforms within a given device, within their normal operating conditions. Triggering of the DSO is achieved through two synchronised i.e. phase locked, signal generators resulting in a fixed trigger point as the drive power to the DUT is varied.

The data obtained from a DSO shows the voltage waveforms with respect to time, ensuring that vital further information can be extrapolated from this data. As the measured waveform is an example of a periodic function, Fourier analysis can be used to extract the fundamental voltage component, which can be plotted as a function of input drive. Once processed, this information will give us the RF characteristics of the measured transistor.

Final measurements described in chapters 6-9 will be conducted within the internal structure of transistor, this will involve the lowering of the EFP to separation of 30μm above the drain manifold, resulting in the highest accuracy for representation of the fundamental drain voltage. The importance of this novel factor will be highlighted for the determination of the transistors functionality in several different PA configurations.

2.2.4. RF measurements and characterisation

In order to correctly characterise a transistor, the power at both the input and the output of the system must be fully considered. All of the PAs investigated within this thesis will require the internal structure of the transistor to be exposed for successful in-situ measurements. De-lidding the transistor will inevitably cause some sort of variance to the proposed measurements, the degree of this variance must be considered before any further characterisation and testing can continue. For this reason before and after the de-lidding process, the transistor will be characterised by the RF input/output measurements taken. This will avoid possible anomalies.

In section 2.1.1, the transistors DC IV characteristics were explained. In order to carry out the RF characteristics, the transistor is set to bias working conditions. For a high power LDMOS device, usually $V_{gs} = 28V$, the transistor is then injected with a continuous wave (cw) of a given frequency, the RF input power is swept uniformly, while I_D and its output power, in dBm, are measured.

The power gain of the system can be described as the ratio of output power by the input power, shown in equation 2.11.

$$Gain = \frac{P_{out}}{P_{in}} \tag{2.11}$$

If the efficiency of the system is defined as the extent to which DC power is converted to RF power, for highest efficiency, an ideal situation would dictate the maximum power delivered to the load while consuming minimum DC power:

$$\eta = \frac{P_{out}}{P_{DC}} \tag{2.12}$$

Where:

$$P_{DC} = I_{DC}V_{DC}. \tag{2.13}$$

Once the transistor has been de-lidded and its internal structure is exposed, the same measurement procedure can be repeated for comparative purposes. The overall efficiency will be shown to vary to an average error of less than 1% and will

therefore be considered negligible. The main issue arising from the de-leading process is the ability of conducting clean lift of the ceramic lid. Beneath this lid, as shown in figure 2.5, lies an extremely delicate bondwire array, the slightest angle in the lift can cause deformation of the bondwires, therefore causing detrimental effect on the transistors performance.

Results shown in chapters 6, 7 and 8, represent seemingly functional PA’s, where no indication of anomaly is perceived in the RF characteristic. However, closer analysis utilised with the EFP will show extensive variation across the periphery of the device. This variation cannot be observed at the output or input terminals, therefore the novel aspect of the size and flexibility of the EFP will allow for accurate diagnostic analysis. The probe can therefore be used as a tool to ‘see’ inside the device and act as a ‘microscope’, thus analytically measuring in the behaviour of transistors and PA systems.

2.3. Electric field probe

The Electric Field Probe (EFP) has been utilised for decades for the measurement of electric field on passive and active arrays [13, 14, 15, 16, 17, 18]. While steady progress has been made in the evolution of the EFP design for improvements in spatial resolution and probe response, to date, EFPs have not been developed that are capable of internal device plane measurements of functional active devices. *This was a key achieved objective in the work reported in this thesis.*

Many variations in the EFP design are in existence; this section will take an unbiased analysis of current procedures while fully considering the design specifications required for the design and development of the EFP.

A circuit with current and voltage will produce electromagnetic waves; the distribution of these waves can be measured, or mapped using an electric field probe. This method of measurement is highly desirable for many reasons; the probe is contactless, there is no direct attachment to the circuitry of the DUT, thus the variation of the output due to the presence of the probe is minimised. EFP manufacturing is generally more cost effective than other measurement techniques available. The system can be used as a verification or alternative

method to existing ElectroMagnetic (EM) simulators, while acting as a characterisation tool, capable of in-situ analysis of the DUT.

Due to the size and design of the proposed miniaturised probes, measurements are not limited to input and output terminals of the DUT, unlike [19], a particular advantage for transistor characterisation.

2.3.1. Open-ended coaxial probe

The simplest electric field probe can be constructed from an open-ended semi-rigid coaxial cable [13, 14, 15, 16, 17, 18, 20]. This simple physical arrangement has been used, both formally and informally for many years, by microwave circuit engineers as a sensor of the voltage at a chosen point in a microwave circuit or system. Published works over several decades have shown a strong preference for the use of a short protruding "monopole" antenna, usually as a means of increasing the coupled signal. The probe operation has frequently been assumed to be that of an antenna which responds to the component of electric field, in the direction parallel to the monopole. This may be a reasonable view in some applications (e.g. antenna pattern mapping) where the monopole far-field response is being used. But in this work, the monopole is essentially removed and only the "ultra-near field" response of the probe is relevant.

During the course of the present work however, and as reported in this thesis, a different explanation of the probe action has been developed, based on lengthy experience and many measurements made under a wide range of physical conditions.

In fact, it is now believed that the probes described in this thesis have a closer affinity to the simple high impedance contact voltage probe, as used with oscilloscopes. As illustrated in section 2.3.2, the inner conductor of the probe forms a capacitor, which "connects" it to the DUT. Physical considerations, along with simulations of the probe response, give a value for this coupling capacitance which is of the order of 10^{-3}pF. This represents a very high impedance (order of 10's kOhm) at GHz frequencies, and this means in turn that the outer conductor of the probe co-axial line can be regarded as a virtual ground, so that the probe is measuring a true scaled voltage at the DUT target point. This can be shown by the construction and measurement of a waveform with a distinct polarity. By injecting

a “class J” waveform along a terminated microstrip line, comparisons can be made with the direct measurement of the source to that of the probe output. Further discussion is provided in section 6.1.3 and the resultant comparison is shown below in figure 2.9.

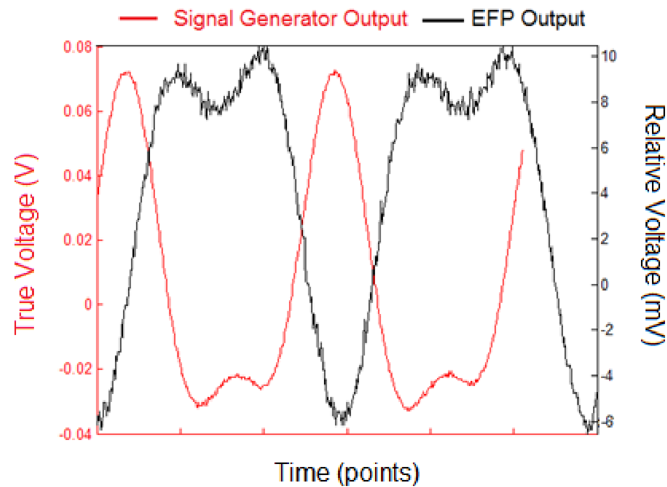

Figure 2.9: Comparison of a Class J waveform measured directly from the signal generator to output of the probe. The probe output results in an inverted and scaled down measurement of the original waveform therefore representing a true scaled voltage at the DUT target.

The “virtual ground assumption” has been widely used in the design of oscilloscope voltage probes [21, 22], and the relative insensitivity of the ground connection demonstrated. An analogous GHz-frequency voltage probe using a high impedance resistive divider has been reported with no physical ground connection, and commercial products are even available although these have much lower impedances, and lower spatial resolution, than the probes developed in the present work.

It should be noted at this point that the introduction of a probe-tip amplifier, a key innovation in the present work, is vital in mainlining a flat frequency response for the probe; this will be described in detail in Chapters 3, 4, and 5.

A coaxial cable is an example of a transmission line, used for the transfer of high frequency. The cable is an example of a two-wire line, consisting of a central conductor surrounded by a dielectric material, shielded by a cylindrical conductor.

Considering the lumped element model of a transmission line for a short defined length of Δz.

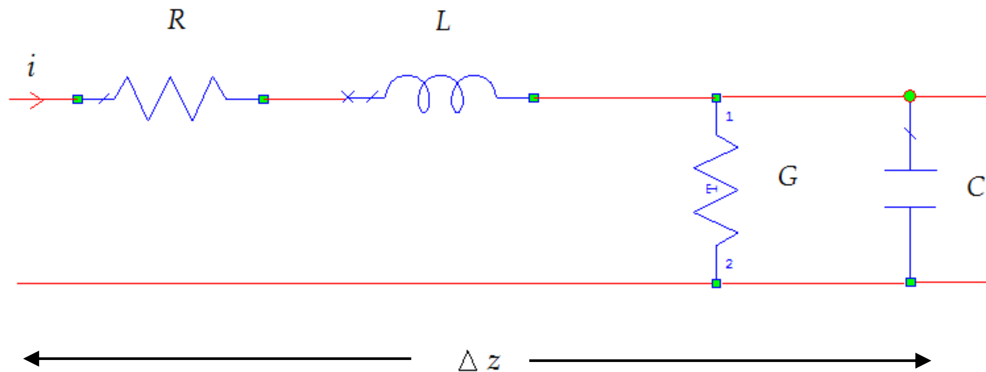

Figure 2.10: Schematic of the lumped element approximation of a transmission line.

Where the R, L, G, C per unit length is defined as the following [12]:

R= series resistance due to the finite conductivity of the conductors.

L=series inductance representing the total self-inductance of the two conductors.

G= shunt conductance due to the dielectric loss of the material between the conductors.

C= shunt capacitance due to the close proximity of the conductors.

The lumped element analysis allows for the calculation of characteristic impedance, phase velocity, the phase and attenuation of the propagation constant. The characteristic impedance of the transmission line is defined as:

$$Z_0 = \sqrt{\frac{R + j\omega L}{G + j\omega C}} \tag{2.14}$$

At high frequencies, $j\omega L \gg R$ and $j\omega C \gg G$, so the characteristic impedance can be considered as:

$$Z_0 = \sqrt{\frac{L}{C}} \tag{2.15}$$

A transmission line in the form of a coaxial cable, the capacitance and inductance is dependent on the diameter of the inner conductor and the inner diameter of the outer conductor, shown in figure 2.11.

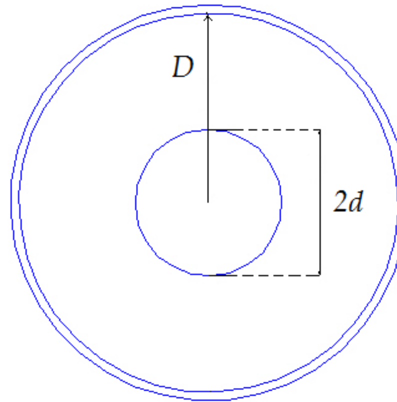

Figure 2.11: Schematic diagram of a concentric coaxial cable indicating the acronyms required for calculation, whereby 2d represents the diameter of the inner conductor and D represents the radius of the inner section of the outer conductor.

Where

$$L = \frac{\mu}{2\pi}\ln\left(\frac{D}{d}\right) \tag{2.16}$$

$$C = \frac{2\pi\varepsilon}{\ln\left({}^{D}/_{d}\right)} \tag{2.17}$$

By inserting equations 2.16 and 2.17 into the equation 2.15, the characteristic impedance of a coaxial cable can defined as:

$$Z_0 = \frac{138}{\sqrt{\varepsilon}}\log\left(\frac{D}{d}\right) \tag{2.18}$$

The propagation of electromagnetic waves along length of the cable must be considered. Potential propagation losses can occur if the central conductor does not hold a concentric position throughout the length of the EFP, as well as non-

uniform impedance. The displacement current across the air-gap has a real current density component along the central conductor, J. By means of Ampere's law, produces an orthogonal magnetic field, B.

$$\nabla \times \mathrm{B} = \mu J \tag{2.19}$$

This ability to support magnetic and electric field allows for the transverse electromagnetic (TEM) mode of propagation along the length of the line. Therefore displacement of the central conductor would cause an uneven distribution of TEM propagating resulting in the potential attenuation of the measured signal.

2.3.2. Capacitive probe analogy

Comparing the two surfaces present within the measurement system, the inner conductor and the DUT, to that of a parallel plate capacitor, then displacement current will flow within the air gap. Essentially, the field measured is proportional to the displacement current across this air gap, which in turn is proportional to the intensity of the field generated by the DUT. The schematic below, shown in figure 2.12, shows how the surfaces of the inner conductor of the EFP and DUT can be comparable to that of a parallel plate capacitor the perspective is magnified.

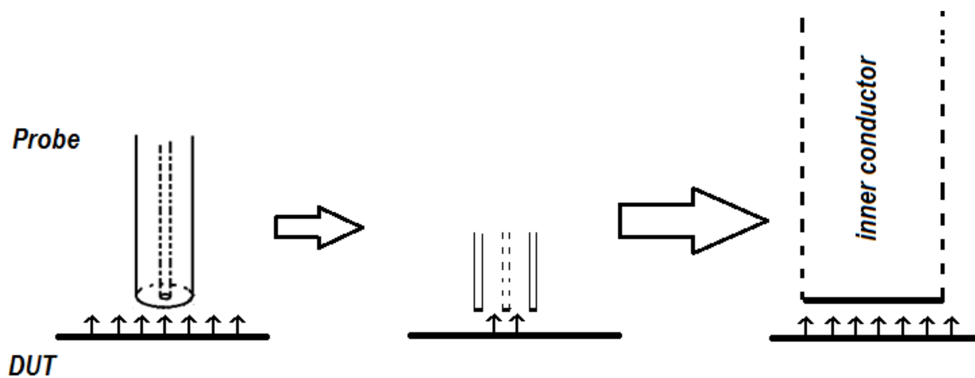

Figure 2.12: Schematic of an open-ended coaxial cable above DUT showing the capacitive analogy in a magnified image. Where the inner conductor and the surface of the DUT can be compared to plates of a capacitor and the effective coupling between them is dependent on their separation and surface area.

Therefore, the electric field between two parallel plates can be expressed as equation 2.20.

$$V = Ed \qquad 2.20$$

According to Gauss's law, a conductor in the state of equilibrium has no charge situated within the plate, but rather, charge is situated on the surface. The charge density for each plate is given by equation 2.21.

$$\sigma = \frac{Q}{A} \qquad 2.21$$

Neglecting the fringing effects of the electric field, equation 2.22 shows the relationship between the charge density and electric field. Where ε_0 is the constant, permittivity of free space.

$$E = \frac{\sigma}{\varepsilon_0} \qquad 2.22$$

Substitution of equation 2.21 into 2.22 yields:

$$E = \frac{Q}{\varepsilon_0 A} \qquad 2.23$$

Since the dielectric in this particular case is air, the permittivity can be considered as $\varepsilon_r = 1$.

Placing equation 2.23 back in to equation 2.20, the voltage across the two surfaces:

$$V = \frac{Qd}{\varepsilon_0 A} \qquad 2.24$$

If the capacitance of a parallel plate capacitor is simply defined in equation 2.25

$$C = \frac{Q}{V} \qquad 2.25$$

Therefore the capacitance across the parallel plate with respect to plate separation and area, can be considered as:

$$C = \frac{\varepsilon_0 A}{d} \quad 2.26$$

Since the dielectric in this scenario is air, the capacitance and therefore maximum coupling is dependent only on plate area and plate separation.

From equation 2.26 it is evident that the overall capacitance is proportional to the area of the plates and inversely proportional to the distance between them. Therefore, decreasing the probe aperture will have a direct effect on the E-field measured, as the effective area of the 'capacitive plates' has been decreased, which in turn will proportionally reduce the output.

The resulting measurement taken by the probe is the voltage which is proportional to the induced displacement current at the probe tip. Therefore, if the probe is connected to a vector network analyser (VNA) the resultant power can be measured and bears a direct relationship with the local DUT voltage.

2.4. Electric field at the device plane

2.4.1. Electric field at the surface of a metal.

Electric field can be a non-uniform entity, with multiple vector components, therefore its divergence can be difficult to measure.

In a 3-D structure it is capable of producing all orthogonal components of electric field, i.e. $E_x, E_y, and\ E_z$. The proposed E-field probe is intended for the measurement of electric field normal to the plane of the DUT, E_z.

When considering field induced at the surface of a metal, it is assumed that only the perpendicular component of electric field, $E_{\perp}$, is present. This is primarily due to the cancelation of tangential components, $E_{\parallel}$, when the orthogonal components are considered as separate vectors. Therefore a metal with an infinitely long surface will exhibit only perpendicular components of electric field, within close proximity to that surface. Conversely, a metal with finite dimensions will exhibit

fringing of the electric field at the metal edge even within close proximity to that surface.

For measurements regarding the electric field distribution at the device plane of high power transistor i.e. at the surface of the die, cannot simply rely on the analogy above. The die of a transistor cannot be assumed merely as a metal surface; in reality the topology of the die is much more complex. Figure 2.13 below shows a magnified view of a transistor die, with visual inspection, the complexity is visible.

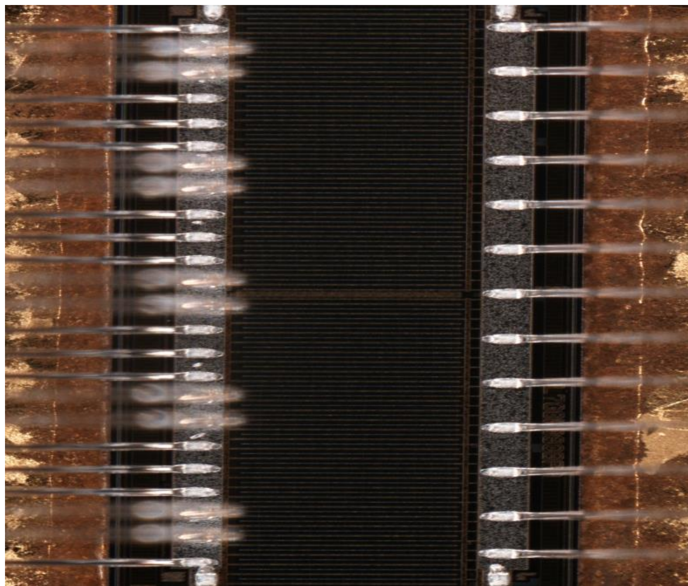

Figure 2.13: A magnified section of the die metallisation present in a generic high power transistor device.

Under this magnified view, the interlocking fingers that connect the drain to the gate side of the transistor are visible.

The underlying question, of whether the surface of the die can be considered as a uniform section of metallisation depends on the resolution capability of the EFP. A closer inspection of figure 2.13, will show the dimensions of the interdigital fingers as considerably smaller than that of the bondwires, and much more closely situated. The average bondwire, within a transistor package, has a diameter thickness in the region of 25μm with a spacing of 100μm. Whereas, the thickness of interdigital fingers are in the region of 10μm, with a spacing of only a few microns.

This thesis will go on to describe an EFP with a resolution of >100μm, therefore the dimensions and spacing of the interdigital fingers are beyond the resolution capability of the proposed system. The EFP in principle will 'see' a uniform section of metal. Confirmation of this theory is shown within section 5.2.4, whereby the EFP will not have the capability of measuring bondwire structure, the lack of resolution can be interpreted as the measurement of a uniform entity.

2.4.2. Orthogonal components of electric field.

The analogy made in section 2.4.1, can only be considered true, for an infinitely long metal conductor close to its surface. A surface with predetermined dimensions will exhibit fringing at the edges of the structure, as well as a divergence of field as the distance from the source is increased. Therefore, orthogonal components of electric field must be considered and analysed further.

As previously described in section 2.2.2, a calibration method for the frequency response of the EFP, requires measurements to be made on a terminated transmission line (TL).

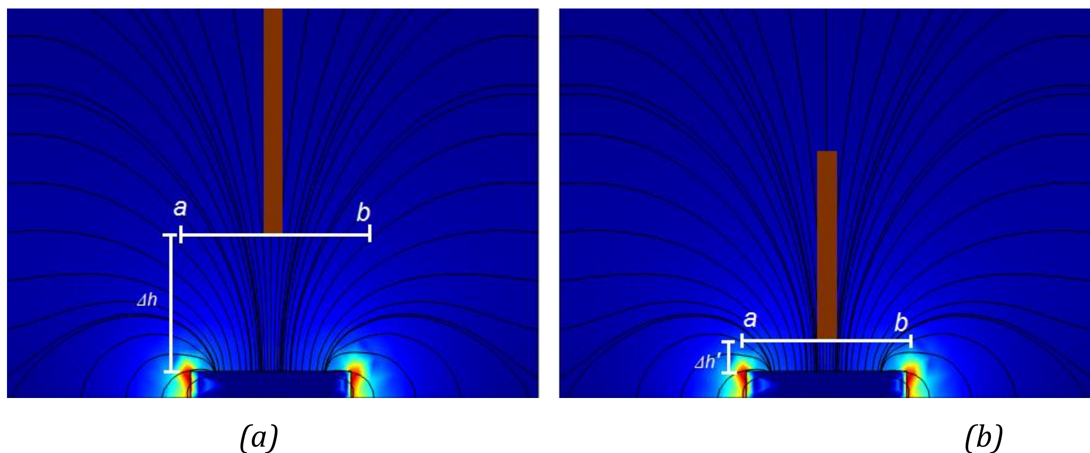

(a) *(b)*

Figure 2.14: A schematic diagram of a metal section with finite dimensions and the resulting electric field distribution. Indicating the measurement plane of (a) Δh and (b) Δh'. Whereby a decrease in the measurement plane, from Δh to Δh', reduces the quantity of orthogonal electric field components present.

From figure 2.14, a typical field distribution for a section of metal with finite dimensions is shown above. Figure 2.14(a) shows the typical divergence of electric field, where fringing occurs at each end of the metal surface and as distance from source is increased. The degree of divergence associated with the measurement is dependent on the plane chosen, i.e. the separation between probe tip and DUT. If

the probe is placed over the metal section at too great a distance i.e. Δh, the electric field can no longer be assumed to be perpendicular to the plane, as divergence has occurred. However, if this separation is reduced and the measurement plane is a smaller value i.e. Δh', the electric field can be assumed to be perpendicular to the metal surface, as proximity of the probe has been reduced sufficiently for divergence to be minimised.

Consideration of the fringed electric field at the metals edge, the orthogonal component will exhibit some angle of E_{θ}. This angle of electric field can be separated and considered as the resultant parallel and perpendicular components:

$$E_{\theta} = E_{\perp} + E_{\parallel}. \tag{2.27}$$

Therefore the resultant EFP output will measure the proportional reduction of the perpendicular component E_z.

Experimental procedure can provide confirmation of this vector analysis, as the measured distribution at the metals edge will show a gradual reduction in the measured field, i.e. as $E_{\parallel} \gg E_{\perp}$ due to the increased degree of fringing.

2.5. Literature review of EFP design considerations and techniques

As previously stated, the simplest method for the measurement of electric field can be merely constructed from an open ended semi-rigid coaxial cable. Consisting of an outer copper conductor and an inner metal conductor separated by a dielectric medium. Although this method can detect the normal field to the device plane, its application is best suited for e-field measurements of larger devices due to its physical size.

$$C = \frac{\varepsilon_0 A}{d} \tag{2.26}$$

From equation 2.26 it can be noted that the coupling of the EFP to the DUT is heavily dependent of the physical dimensions of the probe. The more miniaturised the probe becomes, the lower the coupling factor, therefore the pick-up signal will be weak and may be indistinguishable from stray pick-up. However, the design of the EFP is then directly linked to the device that is being measured. If the intended

measurements are to be taken on miniaturised structures requiring a resolution of 100microns or better, the probe size must be such, that it is a comparable to the size of structure that is to be measured. The evolution of the EFP within this thesis will show substantial spatial resolution improvement as the dimensions of the probes are reduced, this will be shown in the transition between chapters 3 through to chapters 4. It will be seen that the subsequent improvement is a factor of both the inner and outer conductor diameter reduction. However, since the reduction of probe dimensions will have a detrimental effect on the coupling and therefore pick-up of the probe, the trade-off between resolution and sensitivity must be carefully considered.

Previous literature has shown a dedication for an alleviation of such problems, new design and different fabrications methods, along with improvements to the measurement techniques, have all resulted in the advancement of E-field probes [14, 18, 22, 23, 24, 25, 26]. It should be noted that absolute calibration of the probes has posed some difficulty, maybe resulting to the E-field probes unpopularity.

The trade-offs present between resolution and sensitivity will ultimately dictate the design of the probe, with no specific design able to accomplish both, the DUT will set the precedent of the EFP.

The category of the DUT, whether passive or active, will have an influence on the design of the probe, as it will have a direct effect on the generated field. The nature of a passive components will require a much more sensitive probe, due to the lack of power within the component, the electric field to be measured will be small. If this is too small, the signal may be indistinguishable to stray pick-up or the background noise level. However, if the function of the probe is to measure bondwires within an active transistor, then sensitivity is less significant but rather spatial resolution.

The dimensions of the DUT will also have an effect on the design consideration. The spatial resolution of the probe must equal, if not exceed, the minimum element size of the DUT. If the resolution of the probe is less than that of the minimum element size, then an accurate electric field distribution cannot be obtained. This

will also lead to the comparable size of the probe to the DUT. The physical dimensions of the probe tip will affect the interaction it may have with the measured field. The smaller the probe, i.e. the more miniaturised it becomes, the less it will distort the field being measured [20, 23]. Perturbance to the DUT can be further reduced by increasing the impedance presented by the EFP [22]. Confirmation can be achieved by measuring the S_{21} parameter of the DUT and comparing any perturbation that may have occurred by the presence of the EFP.

2.5.1. Increasing the spatial resolution

Modern day advancements in technology have resulted in extensive miniaturisation of components within a given system. For characterisation of these devices, measurement techniques must also undergo the same progression, for accurate analysis.

It has been commonly seen by researchers that decreasing the dimensions of the EFP, the spatial resolution can be improved [14, 18, 24, 20]. Referring back to the magnified image of a section of a de-lidded transistor, the dimensions of bondwires and bondwire separation are highlighted in figure 2.15.

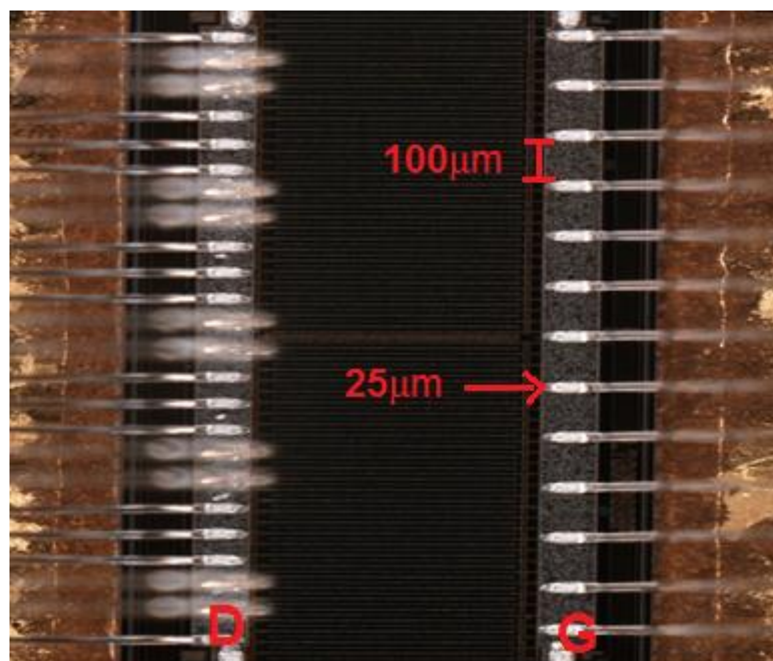

Figure 2.15: A magnified image of a section of generic high power transistor, with ceramic casing removed, highlighting the dimensions of the componentry.

Figure 2.15 shows the delicate array of bondwires, diameter of 25μm, and a separation of 100μm. The drain manifold within the transistor is highlighted, for measurements requiring the fundamental drain voltage component; the EFP must be lowered as close as possible, to this manifold. For such measurements, the size of the EFP is of great importance, too large a probe tip, will cause destruction of the DUT. Therefore the tip of the probe must be small enough in circumference not to make contact with the surrounding bondwire array. Due to the active and high power nature of the measurement, such contact would result in destruction of both the EFP and the transistor. Figure 2.16 depicts the importance of the outer conductor diameter for in-situ drain measurements.

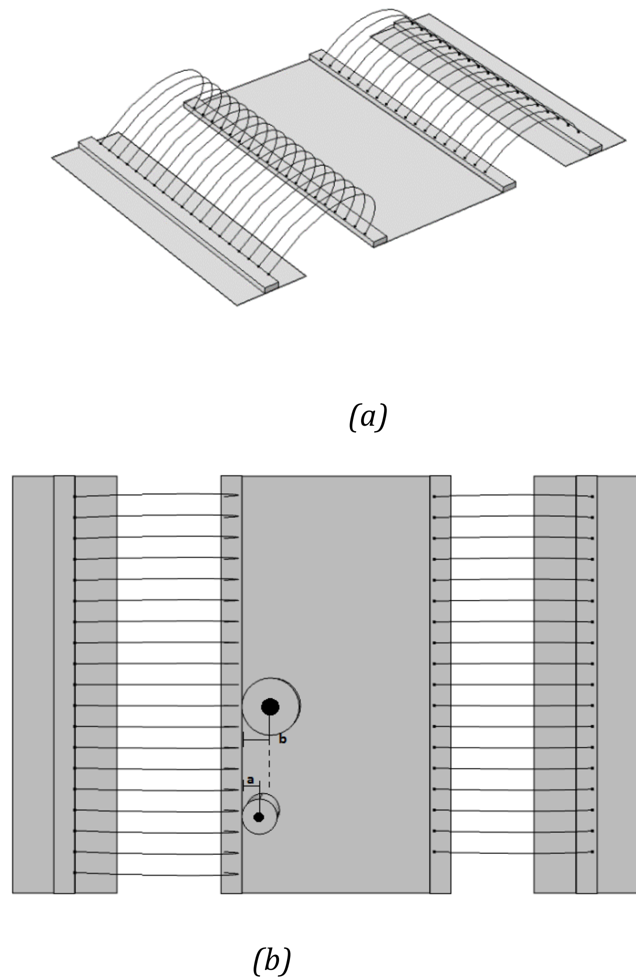

Figure 2.16: (a) Different angle of view for a generic high power transistor device (b) showing the point of measurement required for drain manifold measurements and the importance of the outer conductor of the EFP.

From the figure 2.16, the significance of the outer diameter of the EFP can be seen, as the diameter increases, so too does the distance between the inner conductor to the drain side manifold. The total effective coupling is dependent on the surface of the central conductor, for best representation of the drain voltages, the probe must be positioned as close as possible to the drain manifold. For an EFP with a reduced outer diameter, the position of the central conductor will be situated closer to the probing target. Therefore a suitable reduction must occur in the outer diameter of the EFP to reduce the displacement of the central conductor, since $a<b$, for a more representative measurement. Such design procedures as the 'micro-hole' cap [18],

discussed further within section 2.5.2, would be deemed as an unpractical method for spatial resolution and sensitivity improvement of the EFP.

The coupling which occurs between the EFP and DUT is predominantly dependent on two surfaces; the inner conductor of the probe and the measurement plane (DUT). Theoretical analysis of the expected resolution would dictate that the inner diameter of the EFP must be equal or be smaller than the desired resolution. The figure below illustrates an example whereby the diameter of the inner conductor far exceeds the desired resolution; i.e. an EFP with an ID of 100μm required for 20μm resolution.

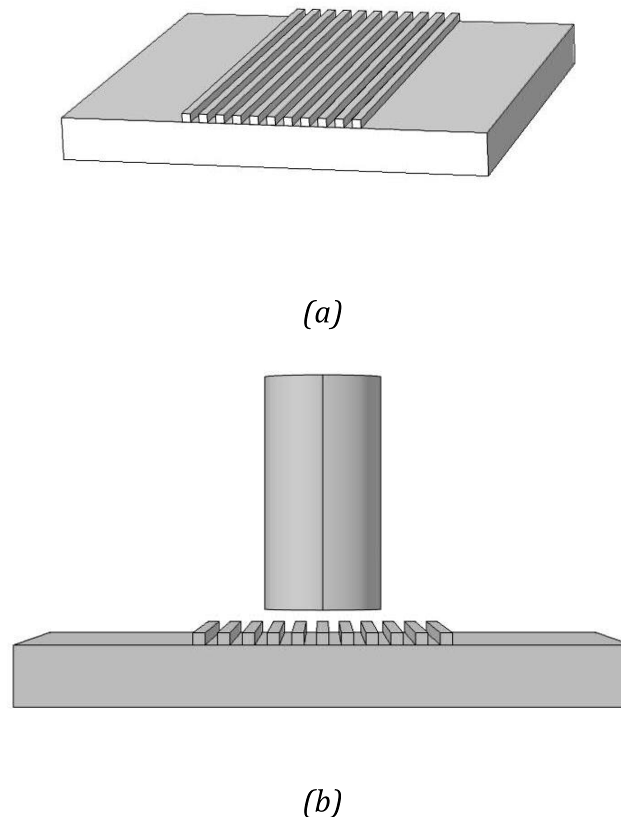

(a)

(b)

Figure 2.17: (a) An example of a structure with 20μm fingers with a separation of 20μm (b) and an EFP, with dimensions greater than the expected and desired resolution in-situ. Note: the EFP is depicted with only the central conductor.

The example mentioned above will result in the effective coupling of multiple abject fingers. Each finger within this device will have its own resulting electric field distribution; an overlap of the coupling area will result in a summation of all

fields present under the inner conductor, at that given point. Therefore a correct depiction of the electric field distribution cannot be made, as the geometry of the EFP surpasses the dimensions of the DUT and therefore its resolution capability. Chapter 3 will go on to show experimentally the direct correlation between the inner diameter of the EFP and the maximum possible resolution. Thus confirming the requisition if 100μm spatial resolution can only occur if the effective diameter of the EFP is comparable in dimensions.

Initial analogy of a simple EFP constructed of a standard open-ended coaxial cable is shown to be an illogical mode of measurement for micron-scale devices. Although many of the novel techniques described in this thesis for the improvement of spatial resolution may be applicable to the coaxial cable, its purpose would prove impossible. A typical spacing between the drain and gate side bondwires is in the region 1mm, a standard semi-rigid cable, with a diameter of 2mm would be impractical and unfeasible for the measurement required. Therefore miniaturisation should be such that, it is sufficient for the proposed application.

However, with miniaturisation certain difficulties will arise. The most common problems encountered are the resultant loss of sensitivity and materials required for construction. Complications with fabrication can also be a limitation, even if the correct materials are sourced [24]. Literature has shown the difficulties in fabrication and further miniaturisation beyond the region of an OD of 230μm and an inner diameter of 8μm. With most work requiring hand-made fabrication methods, limitations are inevitably reached and difficult to overcome without the aid of machining.

Research of EFP resulted in two major discoveries, which then set the path for the improvement of spatial resolution. Miniaturised probes, containing a small protrusion of the inner conductor, were found to have substantial improvement of spatial resolution, if the protrusion length did not exceed the diameter of the outer conductor [20, 23, 24]. The second discovery made, required an alteration to the measurement technique and named the 'position/signal difference method' (PSD) [24]. Experimentation conducted found that the miniaturisation of the EFP

dimensions resulted in a reduction of the probe output, with an inability to fully resolve the DUT. To utilise the PSD method, two successive scans of the same area of the DUT are made with different vertical heights. By scanning the section of the DUT, with the help of an X-Y positioning stage, in a given vertical position, the repetition of the initial scan with a displaced probe height of Δh would result in two sets of poorly resolved distributions. However, by subtracting the two subsequent scans, a third and fully resolved distribution was obtained.

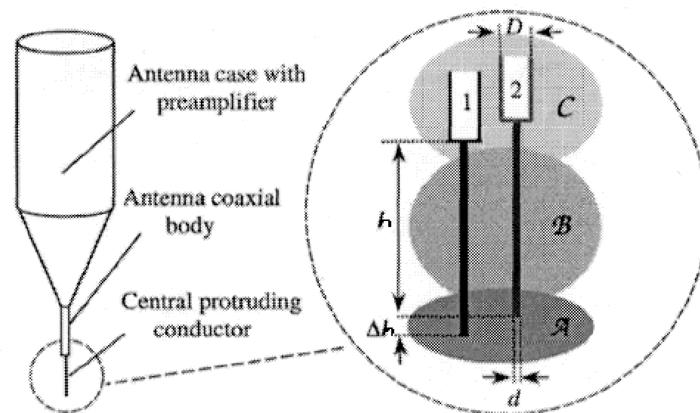

Figure 2.18: PSD method shown pictorially, with the displacement of the protruding central conductor of a distance Δh [24].

Subtraction of the two data plots eliminated the external interfering fields, therefore resulting in a depiction of the required field strength within that displaced region.

PSD is successful method for the attainment improved resolution without the need for EFP design modification, as it is attained through alteration of the measurement technique. However, requirement of two identical scans with displaced height, will subsequently double the scanning time for each measurement.

The trade-offs present between miniaturisation and signal strength, requires alternative methods for increasing the sensitivity of the system.

2.5.2. Increasing the sensitivity

All miniaturised probes will inevitably have an issue of sensitivity. As the EFP is reduced in size, the effective area is decreased and therefore the coupling between the probe tip and DUT also decreases. Returning to the analogy that the EFP is

capacitive probe, the overall coupling between the probe and DUT is known to be dependent on the probe size and the separation of the measuring plane. With reference to the previously mentioned equation 2.26:

$$C = \frac{\varepsilon_0 \varepsilon_r A}{d} \qquad 2.26$$

Where *A,* is the plate area, which will depend on the inner diameter of the probe and d is the separation of the plates. By reducing the probe dimensions the effective capacitance is compromised. Therefore the measurement plane must be kept to a minimum in order to maximise the coupling potential.

The electric field at a metal's surface can be considered at equipotential.

$$\underline{E} = -\underline{\nabla}\phi \qquad 2.28$$

For a given distance above the DUT, the potential will be equal. As the probe is moved transversely across the DUT, the distribution measured will be relative to electric field within that plane. Therefore an accurate depiction of the distribution requires a constant separation between DUT and probe tip. Previous methods of data acquisition have shown the use of a topography probes [24] before EFP measurements. The utilisation of the topography probe indicates the planarity issues of the device under test, thus allowing a predetermined adjustment for the measurement plane i.e. the probe tip to DUT separation is kept constant in accordance to the topography of the device plane. If the topography specifies a change in the subject's planarity, the EFP separation is altered to compensate for the change in height. This method of EFP mapping does not give the truest representation of the measured field but rather an idealised distribution due to the alteration in probe tip to DUT separation.

From previous models of EFPs, measurements have been conducted with a separation plane of the order of 400-500µm [16] [19], with a reported resolution of up to 100µm.

Extensive measurements regarding the degradation of resolution and signal strength will be shown in chapters 3 and 4. Results will indicate the full consequence of increasing the measurement plane to such an extent. The average measurement plane conducted within this thesis consists of a separation of 30μm; data presented within section 4.1.5 will show that an increase to 100μm, will result in an EFP output decay by half the initial magnitude. It will also be shown that this increase will result in a proportional degradation of the achievable resolution, when compared to the initial 30μm measurement plane. Thus questioning the validity of reported work for the measurement of electric field distributions, with a measurement plane of greater than 300μm.

The substantial improvements in the spatial resolution, shown in chapter 4, are a result of strategic reductions in the dimensions of the EFP. The necessity of this reduction will consequently decrease the capacitive coupling to the region of 0.001pF. For absolute maximisation of the resultant coupling, the measurement plane cannot be reduced to zero:

- The proposed measurement system is a contactless in-situ EFP. Contact of any form has a greater potential to distort the measured entity due to the presence of the probe.
- Contact will result in eradication of the air gap between the probe tip and DUT, thus the EFP cannot be considered as a capacitive probe.
- Contact of the EFP and an active device i.e. a transistor within an operating PA system, will provide an undesired path to ground and cause destruction on both the EFP and the DUT.

Therefore the separation of DUT and EFP can only be reduced so far in order to increase and maximise the coupling. Thus, an alternative method for the amplification of already weak coupling signal must be carried out in order to have any validity in the results. This thesis will present the novel incorporation of a low-noise buffer amplifier, placed close to the EFP tip, for the amplification of the probe output. However, literature in this area can become rather vague, and at times, has failed to mention any form of required amplification. An alternative method of amplification of the weakly coupled, miniaturised EFP has yet to be found.

Some literature has referenced the requirement of external amplification [15, 16, 25], however, exact execution is unclear and information has been sparingly revealed.

The most detailed mention for the requirement of external amplification [24, 25] is in the form of a low-noise monolithic-microwave integrated-circuit (MMIC) and its incorporation within the probe, however no further information was mentioned about the design or functionality of this MMIC, or the positioning of the amplifier within the EFP.

A lack of information can be seen across the available literature regarding EFP's that have been recently reported [14, 18, 19]. No indication is made that the miniature probes utilised for experimentation require any form of signal amplification. Since it is a known fact that sensitivity diminishes with miniaturisation, the reasoning behind this equivocality is questioned.

A technique available for increasing the spatial resolution without compromising the sensitivity of the EFP is known as a 'micro-hole' probe [18]. The probe requires the fabrication and utilisation of a custom designed 'micro-hole' cap, covering the end of a commercially available semi-rigid coaxial cable. This cap reduces the apparent size of the inner and outer conductor's diameter which is shown in figure 2.19.

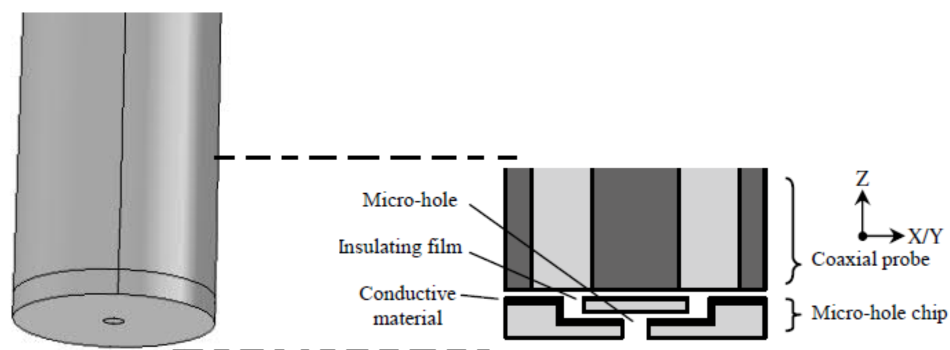

Figure 2.19: Schematic diagram with of an enlargement the micro-hole attachment to the tip of an EFP [18]*. Showing the effective reduction in the dimensions of the probe tip with the micro-hole addition. The resulting output of the probe is not compromised by this reduction as the majority of the probes dimensions have not been reduced.*

In essence, the geometry of the coaxial cable is large enough that external amplification is not required and the design and incorporation of the micro-hole allows for the concentration of the coupling area.

This technique results in the improvement of spatial resolution without the compromise in the probe output. However, its application would best suit specific examples: the measurement of large structures with small componentry and passive structures where sensitivity is a great issue. With no reduction in the overall dimensions; the micro-hole probe would be too large for the measurements of more intricate and delicate structures, where the target area is much smaller than the EFP. For the measurements of drain side voltages on a de-lidded transistor, the micro-hole EFP would prove to be too large for successful results.

2.5.3. Measurement of orthogonal electric field components

Previous probes have been developed specifically for the measurement of orthogonal components of electric field intensity [20, 25], with their topology differing to that of the EFP utilised for E_z measurements.

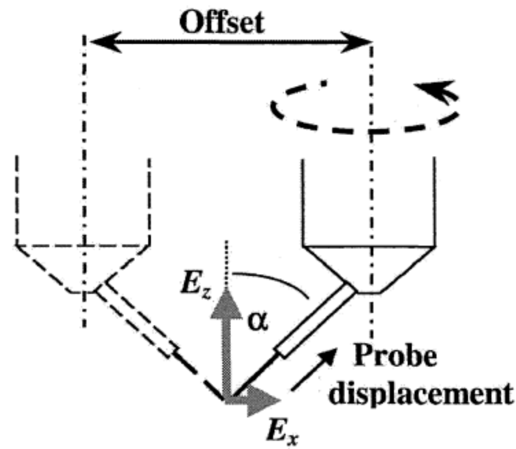

(a)

(b)

Figure 2.20: Schematic layout of the various design alterations required for the measurement of orthogonal electric field components; where (a) is the 45° slanted probe tip [25] *and (c) is the dipole probe* [20].

The probe tip is re-designed with a 45° adjustment relative to the vertical axis. The new arrangement of the EFP requires the measurement at two different 180° rotations around the normal axis. The electric field entities, E_{0° and E_{180° are detected by the EFP before and after the rotation. The vertical and tangential field can be calculated.

$$E_z = \frac{1}{2\cos(\alpha)}(E_{0^\circ} + E_{180^\circ}) \tag{2.28}$$

$$E_t = \frac{1}{2\sin(\alpha)}(E_{0^\circ} + E_{180^\circ}) \tag{2.29}$$

In order to calculate all three orthogonal components of electric field, a further three rotations of the probe and additional calculations are required.

$$E_x = \frac{1}{\sin(\alpha)}(2E_{0^\circ} - E_{120^\circ} - E_{240^\circ}) \tag{2.30}$$

$$E_y = \frac{1}{\sqrt{3}\sin(\alpha)}(E_{120^\circ} - E_{240^\circ}) \tag{2.31}$$

$$E_z = \frac{1}{3\cos(\alpha)}(E_{0^\circ} + E_{120^\circ} + E_{240^\circ}) \tag{2.32}$$

This proposed method for the measurement of orthogonal components of electric field has a high degree of complexity as well as an increase in the total time required for all measurements. With five different probe orientations required at each position, a scan over any given area will take five times as long. In many active measurements this can have a detrimental effect, increasing the scanning time will allow the measured system to heat up, therefore further knowledge of temperature coefficients must be taken in to account.

As previously stated, orthogonal components of electric field diminish, if not vanish close to a metal surface. For valid measurements of these components, the probe must be raised to a sufficient level for these components to be significant and a present entity. This increase in separation, between the probe tip and DUT will have negative effect on the probe output, as the electric field will decay from the source. Therefore this signal must be greater than the background noise in order to be distinguished or to make a valid calculation of E_x *and* E_y.

The measurements discussed in [25] required a measurement plane of 600μm, while comparative measurements of the perpendicular components were taken at separation of 5-50μm [24]. A difference of this magnitude in the measurement plane would raise the question of the validity in the direct comparison as well as the significance in measuring orthogonal components at such distances. The resulting decay of electric field at this increased measurement plane must produce qualitative results such that an increase scanning time by five times can be justified.

The mode of measurement utilised by the dipole EFP, shown in figure 2.20(b), would also require alteration in the measurement orientation. The dipole probe has the capability of measuring the two tangential components of electric field, $E_x \, and \, E_y$, due to the presence of two coaxial cables. The aid of a spectrum analyser allows for the difference in the output to be calculated, along with an additional 90° rotation of the probe (around the z-axis), the correct tangential components can be calculated.

Most methods for the measurement of orthogonal components of electric field have posed some difficulty. No one method has been found that did not require the alteration of the existing measurement apparatus, either by rotation of the EFP or the complete redesign of the EFP. These amendments while necessary for orthogonal component measurements, increase the total time required for a complete scan due to the unavoidable rotation of the EFP.

Electrooptic field mapping can provide an alternative method for the measurement and diagnostics of active and passive devices. With a claimed resolutions varying from 8μm to 580μm [24, 27] and the ability to measure orthogonal field components. Note: the method of its operation will be described in more detail in section 2.6. With the use of a photodiode, an incident beam of photons fired at the DUT, is analysed to detect the change in its polarisation state. This polarisation state is sensitive to the magnitude and phase of the measured RF electric field. The incident beam is focused using a customised electrooptic probe crystal. In order for the measurements of orthogonal electric field components, both the composition of the electrooptic crystal and its orientation must be changed. For measurements requiring the normal component, a bismuth silicate (BSO) crystal is used, while the two tangential components have been found to require lithium

tantalite ($LiTaO_3$) crystals. The use of $LiTaO_3$ crystals requires the rotation about the axis of 90° for the calculation of the two tangential-orthogonal components [24]. Thus meaning the required scanning time of an electrooptic system is tripled for the achievement of the three orthogonal electric field components.

2.5.4. Discussion of the literature review

Before electromagnetic (EM) simulators were widely available or had the accuracy of modern day computer programs, alternative methods for the understanding and mapping electric field intensity was under much analysis. Initial investigations of the EFP required the comparison of physical and analytical expectations of an axially suspended probe over a shielded microstrip between [13]. Preliminary, experimentations were not concerned with the resolution of the probe, nor its design, but rather a confirmation of theoretical calculations for its given application. The evolution of the EPF did not take off until many years later, as components within a microwave circuit became smaller so did the diagnostic tool for its measurement. Early work concluded that a simple open-ended coaxial cable can be used as an inexpensive alternative for electric field mapping, the capacitive coupling of the probe to the DUT resulted in a measureable induced electric current [28]. However, the signal deterioration as a result of increasing the probe tip to DUT separation was not fully considered at this point, as the measurement plane within this example was conducted at 1000μm. Further documentation stated additional increases to the measurement plane, experimental procedure have been reported with measurement planes as large as 2300μm [14] above the DUT. The probe used for such experiments consisted of a miniaturised coaxial cable, with an outer diameter (OD) of 500μm, an inner diameter of 120μm and an inner conductor protrusion of 300μm. Reinvestigation of the probe signal and its dependence on the separation, concluded a rapid decrease in signal strength, about 10dBm for an increase of 300μm [29], which concluded optimal measurement separation of 100μm. However, the probe dimensions between initial experiments and the reinvestigation were not altered, only the measurement plane, yet all recorded data resulted in a depiction in the -50dBm region. In the latter investigation, probe signal was clearly found to be a factor of its separation, yet a

reduction of more than 50% in the separation did not constitute in a subsequent increase in probe signal.

Most literature available on miniature EFP includes the presence of an inner conductor protrusion to some extent; however most fail to mention the negative constraints found between spatial resolution and sensitivity as a function of the protrusion [14, 19]. The trade-off between present entities when mentioned [15, 20], were not fully investigated.

When considering these entities separately, it was found that the length of the protruding inner conductor of the EFP had a great effect on its resolution capabilities. Its length should not exceed the OD of the EPF or that of the desired spatial resolution [24], this means a protrusion of 300μm will yield a similar resolution. It was found that a reduction of the probing geometry to the dimensions mentioned above, required the need for a pre-amplifier, to obtain a signal strength greater than the noise level. For a constant field intensity, the induced current will also be constant, therefore can be fed to a pre-amplifier. The length of the protruding inner conductor has a direct influence on the sensitivity and matching of the high impedance source (the DUT) to the coaxial probe and pre-amplifier. The length of the protruding inner conductor was adjusted for optimal signal matching, if chosen to be a length of $\lambda/4$, the probe will operate at resonance, however for such particular experiment, would yield a protrusion of up to 2mm. However, the probe under investigation had an ID of 8μm, a protrusion of such lengths would result in inevitable bending, deformation or be susceptible to vibration.

Designing a probe for a specific DUT, although resulting in optimisation can restrict the application to limit DUT measurements. Thus requiring alternative probes as the device under investigation alters; if their operation is out of the resonance frequency band. However, the variance in spatial resolution resulting from the intentional design of an inner conductor protrusion was not under full investigation i.e. both protrusion and spatial resolution were not considered simultaneously.

An intentional EFP resonance can be a favourable design method, as is can increase both the sensitivity and resulting output of the probe [26, 30]. The resonant frequency is very sensitive to its local geometry, any changes to the probing target

will result in the measureable shift of the resonance. This shift will occur accordingly to the intensity of the field magnitude and phase, which can be recorded and analysed for the representation of electric field across the section of the DUT.

For measurements not requiring the shift in resonance, the ideal frequency response of an EFP should be flat, and wide a band as the DUT. A resonance in the frequency response not carefully considered can result in the modulation of the field to be measured.

Results shown in this thesis will display strong evidence that increasing the length of protrusion gives an advantageous increase in the signal level of the probe; however it has a detrimental effect on the spatial resolution.

However it is still seen in modern day practice to have an EFP with a protrusion of up to 300μm, and an unrealistic measurement separation of 500μm [19] for the measurement of high power devices. This particular investigation does not require high spatial resolution, but rather the analysis of the probe signal for numerical interpretation of load modulation, in-circuit current and voltages. This method required the comparison of two sets of data, one is obtained by numerically solving the probe reception by an electromagnetic field simulator (ANSYS HFSS) and the second required the magnitude and phase of the E-field. The relative power waves at the input and output are deduced, since this particular device under investigation is a 400W LDMOS DPA, there are four ports that must be taken in consideration. Each measurement must be repeated for the linear combination of the four simulated field distributions.

Although the resulting measurements of voltage and current is considered as 'in-circuit', measurements are taken at the drive, load and biasing ports and not inside the LDMOS transistor. Between the internal periphery of the LDMOS device and the input/output ports, many factors can vary and therefore the result may not be considered as the most accurate representation of the device behaviour. For the most accurate representation of drain voltages and currents, the expectation would be measurements made on-chip, at the LDMOS device plane.

Other disadvantages of this method include: the requirement of electromagnetic modelling for the given DUT. If this is unknown, in-circuit reflection coefficients

cannot be easily determined [17]. Deviation from expected modelling can only arise with access to EM models, without such information strays from normal working conditions will go undetected. This proposed method in reality works as a verification tool rather than a complete diagnostic.

2.6. Alternative methods for electric field measurements and device characterisation

2.6.1. Electrooptic field mapping

Electric field probes are in general, a rather inexpensive method for the analysis of E-field distribution, and a favoured technique to others available. The electrooptic probe, or electrooptic sampling, seen as the more expensive and complicated method of choice, has its own advantages and disadvantages. The costing issues with this method is evident, from materials for the construction of the sophisticated and intricate probe heads to the start-up purchase price of the laser, (required for the incident beam) all add up to a considerable amount. The results achieved by this method must outweigh the disadvantages for it to be a viable and favourable alternative to EFP.

The principle of operation relies on the change in optical index of refraction of the incident beam, usually Ti: sapphire laser, as it passes through the electrooptic probe crystal [31]. This change in optical index is caused by the varying electric field, Pockels effect, which is converted to a relevant change in amplitude and can be reconstructed to a full waveform by methods of sequential sampling. Pockel's effect is proportional change in the refractive index with applied electric field [32], and can only occur in non-centrosymmetric materials. For this reason the probe crystal can only be constructed of a certain material, it must be polished correctly to achieve total internal reflection [33]. A general schematic for electrooptic sampling is shown below in 2.21.

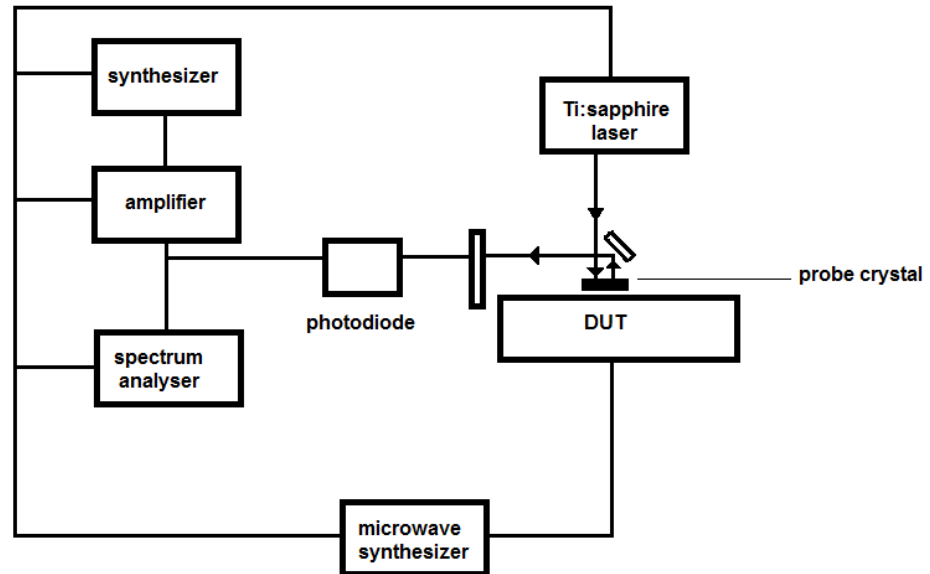

Figure 2.21: Block diagram of a common system utilised in electrooptic sampling.

The magnitude and phase of the time-varying electric field produced by the DUT will cause a relative change in the refractive index of the incident Ti: sapphire laser at the electrooptic crystal. The electrical signal produced by the photodiode is proportional to this change. For faster data acquisition, most electrooptic systems adopt asynchronous sampling, using two locked lasers at different pulse rates. Alleviating the speed at which delays can be realised, this helps provide an intentional time delay for the sampling gate.

For many years, electrooptic systems have been used to measure the electric field distribution for active and passive devices [27, 31, 34], with most methods of evolution resulting in faster data acquisition and better knowledge of crystals used for electrooptic probe tip.

As previously mentioned, the electrooptic system is capable of measuring three orthogonal components of electric field. By changing the composition of the probe crystal and their orientation, the two tangential-orthogonal components of e-field can be determined. For measurements requiring the normal component, a bismuth silicate (BSO) crystal is used, while tangential components have been found to require lithium tantalite $(LiTaO_3)$ crystals. The use of $LiTaO_3$ crystals requires the rotation about the axis, of 90°, for the calculation of the two orthogonal components [27]. As with the 45° slanted EFP [25] (shown in figure 2.19),

measurements of the orthogonal components of electric field with an electrooptic system requires an increased scanning time. Again, thermal effects must be accounted for as a considerable time will elapse before and after the probe orientation is made. The 90° rotation must also be conducted in accordance to the same measured point, unless the error in the automated system is small enough for displacement inaccuracies to be negligible, one full scan cannot be made then repeated at a 90° rotation. Rotation must occur at every measuring point adding more complications in data acquisition.

In some particular systems, the electrooptic circuitry is large and immobile. For full 3-dimentional scans, it is required for the DUT to be attached to a motorised positioner. Practicality of this method occurs only if the DUT is mobile. However, if both the measuring system and the system to be measured are large and immobile, neither can be attached to the motorised stage, required for 3-D scanning.

Spatial resolution can vary from system to system. This is due to the variance in the focus of the Ti: sapphire beams spot size, spatial resolution can vary from a few micrometres [34] to 500μm [27]. The minimum detectable voltage by the electrooptic system is similar to that of the EFP, in the region of 0.5mV or -45dBm [33].

It seems certain factors will dictate if the electrooptic system is a feasible method of choice, with similar spatial resolution and minimum detectable voltage, both EFP and electrooptic probe can be used for the measurement of passive and active components. Two factors dominating the choice of measurement will be: budget and portability of the DUT. Cost of purchasing Ti: sapphire lasers, along with the electrooptic crystals, can cause escalation in the budget. The EFP proposed within this thesis, has both the capability of moving the DUT on a motorised controller stage, or utilising a stationary DUT with an adjustable probe. The EFP systems are much more flexible in terms of the range of devices it can measure and its versatility will be personified throughout this thesis.

2.6.2. Load-pull measurements for device plane voltages

Load-pull systems have been developed for many years as a method for characterisation of transistors at GHz frequencies. Entities such as output power, efficiency and gain can be measured [1, 2, 3, 4, 5], under engineered operating

conditions for a given frequency range. This is achieved by tuning the load impedance presented to the transistor, so that the desired or maximum output power condition can be achieved for the required frequency.

Load-pull systems have successfully measured current and voltage time-domain waveforms within the 50Ω environment. By monitoring the forward and reflected waves using a dual directional coupler. The impedances seen at harmonic frequencies can be engineered using either a passive external tuner, or by injection of suitable signals [4]. However, such measurements rely on the assumption that a complex high power transistor behaves in a much simpler manner than is exposed in the present work. For characterisation of device plane waveforms, the transistor is assumed to behave in a simple 1D manner; where in reality transistors can be very large, distributed structures, with the capability to exhibit variance across the device in a 2D and 3D manner. It will be demonstrated in chapters 6-8 the true level of variation present within a complex high power transistor; therefore such simplifications can result in an inferior method of waveform extrapolation.

Measurements are conducted at both ports of a DUT, the resulting device plane waveform information is a calculation derived by the knowledge of forward and reflected voltages. However these measurements are conducted within the 50Ω environment and as such can be argued not to replicate the DUT under true operational conditions.

The resulting waveform information may thus be inaccurate, as load-pull systems do not take variation along the device to be a significant factor. Furthermore, characterisation can only be considered true for the DUT in optimal conditions. The device is not characterised while in its operational form i.e. within a working high power PA. Therefore the resulting behaviour of the DUT can deviate from the expected measurements when placed within an operational RFPA.

As previously mentioned, load-pull systems do provide an understanding of the DUT characteristics; therefore, can aid the design of resulting matching network required for amplifier systems. The work within this thesis will present actual internal waveform information distributed along the device plane. Due to the position of the measuring system to be described, the resultant drain waveform information can be regarded as the truest representation of on-chip device characterisation.

3. INITIAL WORK PERFORMED ON COAXIAL EF PROBES

This chapter describes the first phase of this PhD project, which was to perform a detailed study of the practical probe structures using commercial, off-the-self (COT) components and materials.

The starting point for the practical work on this project was a clear goal to measure in-situ device plane voltages and the waveform distribution of high power transistors, within a working operational power amplifier. The resultant probe must fulfil this purpose. The final design of the EFP resulted in many design alterations in order to fulfil the initial objective. EFP evolution consisted of intentional reductions in the systematic design, for improvement of the spatial resolution. Such reductions will cause an inevitable loss in the output of the probe and require alternative rectification. A common solution for the improvement and increase of the probes gain has been the introduction of a protruding inner conductor in the EFP design [13, 14, 17, 24]. The presence of protrusion does alleviate the problem of poor signal however, full considerations of its effect has not been investigated with regards to spatial resolution of the EFP. Prior work at Cardiff University [30] found evidence to contradict previous literature [23] whereby is was stated that for a constant measurement plane, the reduction of probe tip protrusion resulted in a subsequent improvement in the spatial resolution and probe output (shown in figure 3.3). This thesis describes intensive investigations of the effect of the probe tip protrusion and the consequence it has on the spatial resolution. Results in section 4.1.3 and throughout chapter 5 will

show that a reduced protrusion, minimised to a flush cut, can achieve maximum spatial resolution, although at the cost to the signal pick-up.
As a result, an alternative method for signal amplification must be considered for the miniaturised EFP. The starting point of the proposed investigation is based on the findings, that a buffer amplifier, close to the probe tip, can provide isolation and termination of the unwanted stray pick-up from the feeder cable as well as the much needed amplification of the small signal pick-up [35]. The amplifier placed in an alternative position, i.e. further away from the probe tip, would result in the compromise of dynamic range and ultimately exaggerate the stray pickup on the outer conductor of the EFP. Thus, this unique configuration allows the amplification of the probe output alone, whilst providing a termination for the feeder line as well as reduction of stray pickup [35].

The EFP described within the next chapters will go through three key stages of development. The first stage will consist of an EFP design containing the smallest coaxial, semi-rigid cable commercially available. This will result in an inevitable limitation of the maximum spatial resolution that can be achieved. With only financial limitations, this lead to the sourcing of fine copper tubes for the construction of smaller custom made coaxial cable probes. Due to the reduction in overall dimensions of the EFP, a low noise, surface mountable pHEMT small-outline transistor (SOT) will be introduced for the amplification of the low signal levels. The final redesign of the EFP requires the improvement of the packaged SOT, for final improvement of the frequency response.

It should be noted that numerous EFP designs mentioned throughout this thesis were in fact fabricated, without prior computer simulation to investigate its expected performance characteristics. This is solely due to the difficulty presented during the construction stage of the EFP. Simulation of ultra-miniaturised EFP of unrealistic proportions can be conducted with ease, while in reality, the outcome and the possibility for successful construction doubtful. Within this chapter and those to follow, the escalating difficulty presented in the construction of EFP, as dimensions are reduced, will be highlighted. Simulations of the EFP's characteristic will be computed after successful construction and testing.

3.1. Initial design stage of electric field probe

The internal structure of a high power transistor is not a consistent entity. With the sensitivity of the EFP to the probing target, a design will be required for the general application and acquisition of data. These requirements will set the initial restrictions in the design plan of the EFP.

In section 2.5.1 it is stated that the overall desired spatial resolution should be comparable, if not dictate, the dimensions of the EFP. Along with additional considerations due to the restricted access of the probing target, preliminary design specifications can be set, with a final objective to improve the spatial resolution beyond 100μm.

In section 2.3.1 it was suggested that an open-ended, semi-rigid coaxial cable can be successfully used for the measurement of electric field intensity, however not optimised for the purpose of in-situ device plane measurements of high power transistor due to its size. For miniaturisation, initial design considerations must include two specific attentions: sourcing of the smallest commercially available miniature coaxial cables, limited only by budget, and the redesign for the step by step fabrication of a customised sub-miniature coaxial cable.

3.1.1. Design of EFP1 and EFP2

During the initial construction stage of the EFP, two different miniature coaxial cable types were found, both different in Outer Diameter (OD) and Inner Diameter (ID). The larger of the two, EFP1, measured with an OD of 0.88mm and an ID of 0.177mm, while the smaller, EFP2, measured at an outer diameter OD of 0.58mm and an inner diameter ID of 0.127mm.

The EFP, as previously mentioned, can be considered as a capacitive probe. It will be stated that the measured output will be a proportional to the corresponding varying electric field, produced by the DUT. Due to the level of miniaturisation required, the anticipated signal probe output is predicted to be very low, possibly close to the electronic noise level. From equation 3.1 the maximum coupling for an EFP can be predetermined.

$$C = \frac{\varepsilon_0 \varepsilon_r A}{d} \tag{3.1}$$

The dielectric within this example is considered negligible as the gap between the probe tip and DUT is air, with a $\varepsilon_r \approx 1$, therefore the coupling can be estimated if their separation is kept constant. Assuming the separation is around 30μm, then capacitance for each probe will be in the region of:

$C_{EFP1} = 7.33 \times 10^{-15} F$

$C_{EFP2} = 3.73 \times 10^{-15} F$.

Where the characteristic impedance of the coaxial probe can be calculated by the capacitance and inductance per unit length,

$$Z_0 = \sqrt{\frac{L}{C}} \tag{3.2}$$

$$C(dl) = \frac{2\pi\varepsilon_r}{\ln\frac{D}{d}} \tag{3.3}$$

where D is the inner diameter of the outer conductor and d is the diameter of the inner conductor:

$$L(dl) = \frac{\mu}{2\pi}\ln\frac{D}{d}. \tag{3.4}$$

By substituting equations 3.3 and 3.4 in to 3.2, the following can be said for the characteristic impedance,

$$Z_0 = \frac{138}{\sqrt{\varepsilon_r}}\log\frac{D}{d} \tag{3.5}$$

therefore

$Z_{0_{EFP1}} = 96.11\Omega$

$Z_{0_{EFP2}} = 91.03\Omega$.

With the sourced coaxial cable of dimensions mentioned above, the reduction in signal pick up is unavoidable. Due to the weak coupling the integration of a buffer amplifier, close to the probe tip, can compensate for the loss in signal. The drain bias of the buffer amplifier is provided by an external biasing network, which for most of this work consisted of a commercial "bias tee". The inner conductor of the probe tip is connected as an open circuit to the gate.

In order for the EFP to be fully integrated to the measurement systems, an initial connection must be made to a vector network analyser (VNA), for characterisation of the probe and the DUT. The subsequent probe will consist of two coaxial cables, of different diameters connected with a custom designed brass ferrule. A standard RG 405 U coaxial cable is used for the integration to a SMA (SubMiniature version A) connection, while the miniature tip consists of a cable with much smaller dimensions. The custom designed small brass ferrule provides a means of connection between the two sub-sections of coaxial cable. Thus resulting in a gradual reduction of the RG 4058 U cable to the chosen miniaturised dimensions.

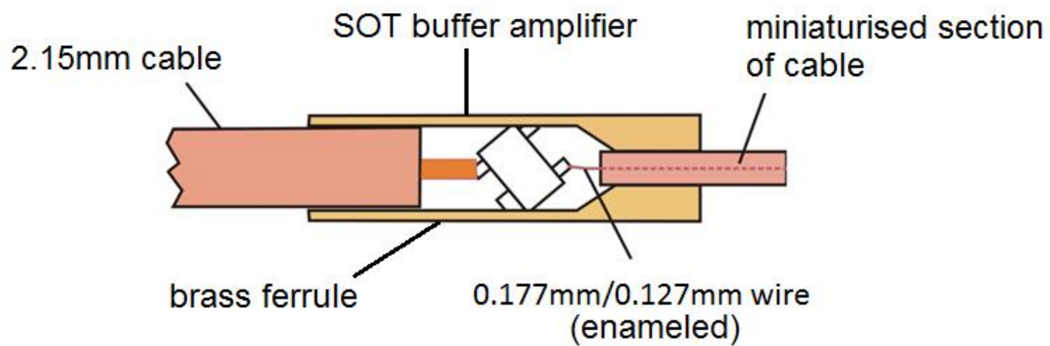

(a)

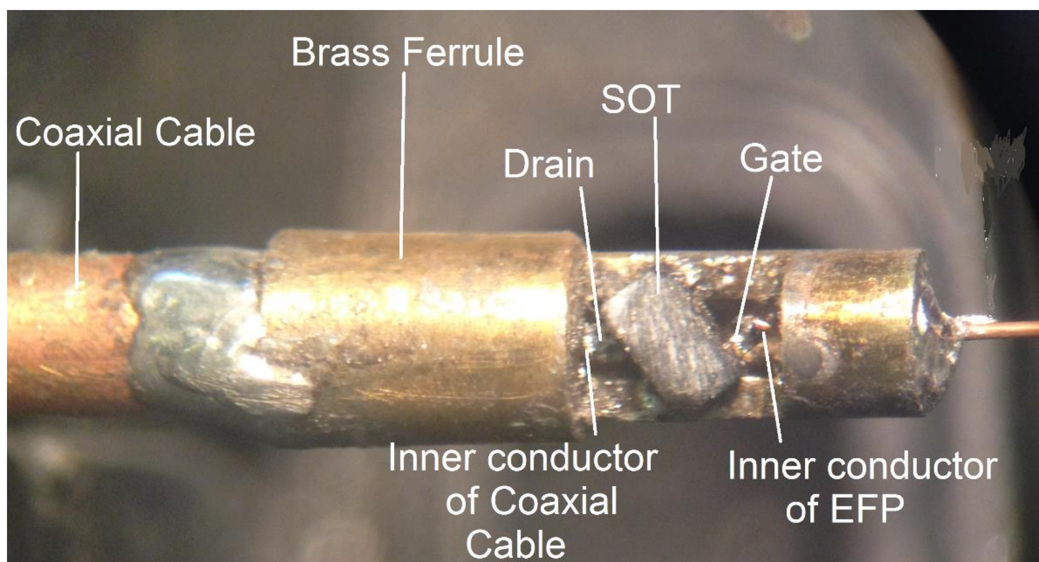

Figure 3.1(a): Schematic diagram of the gradual reduction of the EFP for the integration to the measurement system, showing how the brass ferrule fits over the larger section of co-axial cable and the method of connection to the miniaturised probe tip. Note: the tight fit casing to enclose the brass ferrule is not included in the diagram. (b) Picture of constructed EFP for reference.

The design and integration of the brass section provides many benefits for the functionality of the EFP. It not only acts as a physical connection between the two extremely different outer diameters of coaxial cable, but with slight modifications, i.e. smaller drilled hole, could allow for future smaller probe designs. The brass ferrule, designed with sufficient space, can also house the buffer amplifier, providing a source of ground and a shield to external electrical interference.

Due to the intended in-situ measurements, the EFP will be inevitably exposed to potentially very strong fields. In order to combat external coupling to the buffer amplifier, a tight fit case is designed to fit securely over the brass ferrule, not pictured in figure 3.1. The conductive nature of the tight fit brass case allows for an effective model of a Faraday's cage to exist, whereby surplus charge remains on the outer layer of the brass section. This provides protection to any harmful static electric fields penetrating into the buffer amplifier.

The buffer amplifier used to increase the low input signal pick up is a low noise SOT packaged, small signal, 4-lead PHEMT transistor (Avago ATF34143), with physical package measurements of L 1.30mm, W 1.15mm and H 0.80mm.

The introduction of the SOT amplifier has additional advantages; due to the effective capacitance presented at the probe tip, the system can be considered as a capacitive divider. Figure 3.2 below represents the capacitive divider present within the EFP design, where the outer conductor of the EFP can be considered as the virtual ground connection [22].

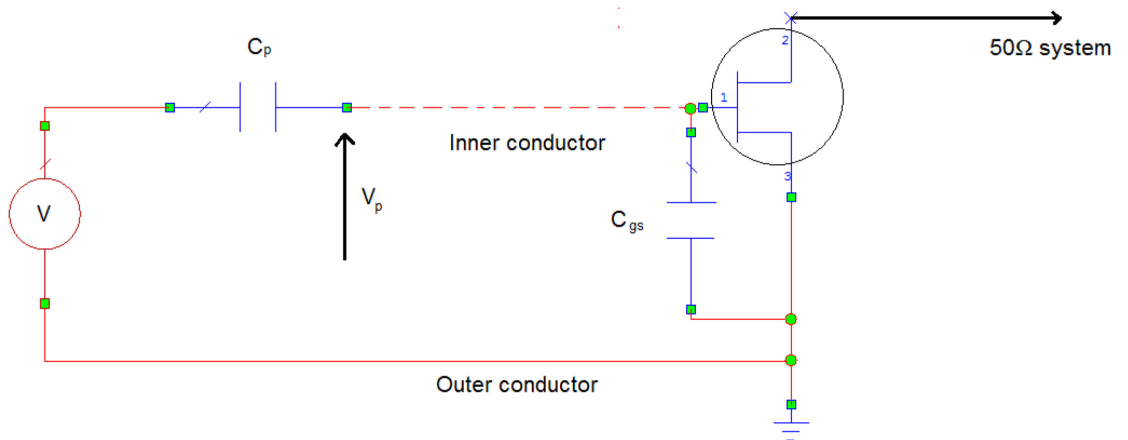

Figure 3.2: Schematic diagram capacitive divider present within the system; where C_p is the capacitance present between the surface of the DUT and the inner conductor of the probe and C_{gs} is the capacitance of the amplifier. The outer conductor of the probe can be considered as the virtual ground of the system.

The ac analysis of the amplifier's voltage can be calculated as:

$$V_{gs} = \frac{V.X_{C_{gs}}}{X_{C_p} + X_{C_{gs}}} \tag{3.6}$$

since $X_{C_p} \gg X_{C_{gs}}$, then;

$$V_{gs} = \frac{V . X_{C_{gs}}}{X_{C_p}} \tag{3.7}$$

The reactance of the capacitance present at the probe tip is:

$$X_{C_p} = \frac{1}{j\omega C_p} \tag{3.8}$$

And the reactance of the of the amplifier is:

$$X_{C_{gs}} = \frac{1}{j\omega C_{gs}} \tag{3.9}$$

Substituting equations 3.8 and 3.9 into 3.6 yields:

$$V_{gs} = \frac{C_p}{C_{gs}}, \tag{3.10}$$

showing that V_{gs} *is independent of frequency,* ω. This is a highly desirable situation, and indicates that such a probe design will have a flat frequency response all the way down to DC. In addition to making waveform measurements much easier due to the flat frequency response, the low frequency characteristic has led to a unique in-situ calibration procedure which is described in chapter 9.

3.1.2. Passive device under test

In order to test the spatial resolution capability of EFP1, EFP2 and any future probes, the test fixture used for this purpose must be applicable to the final measurements made on a high power transistor. In section 2.5.1 the topology of the internal structure of a de-lidded transistor was mentioned and the complex and delicate array of bondwires was evident. In previous literature the spatial resolution of the probe has been shown to be tested in many ways, some include:

- Using the probe to move transversely across a matched microstrip line. By comparing the nulls and peaks achieved to that of an EM simulation, a conclusion of the spatial resolution of different probes can be achieved. The probes with the most similar result to the simulation or the probe which

can achieve the most defined null is deemed the highest resolution [16] [23]. The figure 3.3 below shows the effect of altering the separation of the measurement plane on the spatial resolution and pick-up of the probe. It can be clearly seen that both diminish with a separation increase.

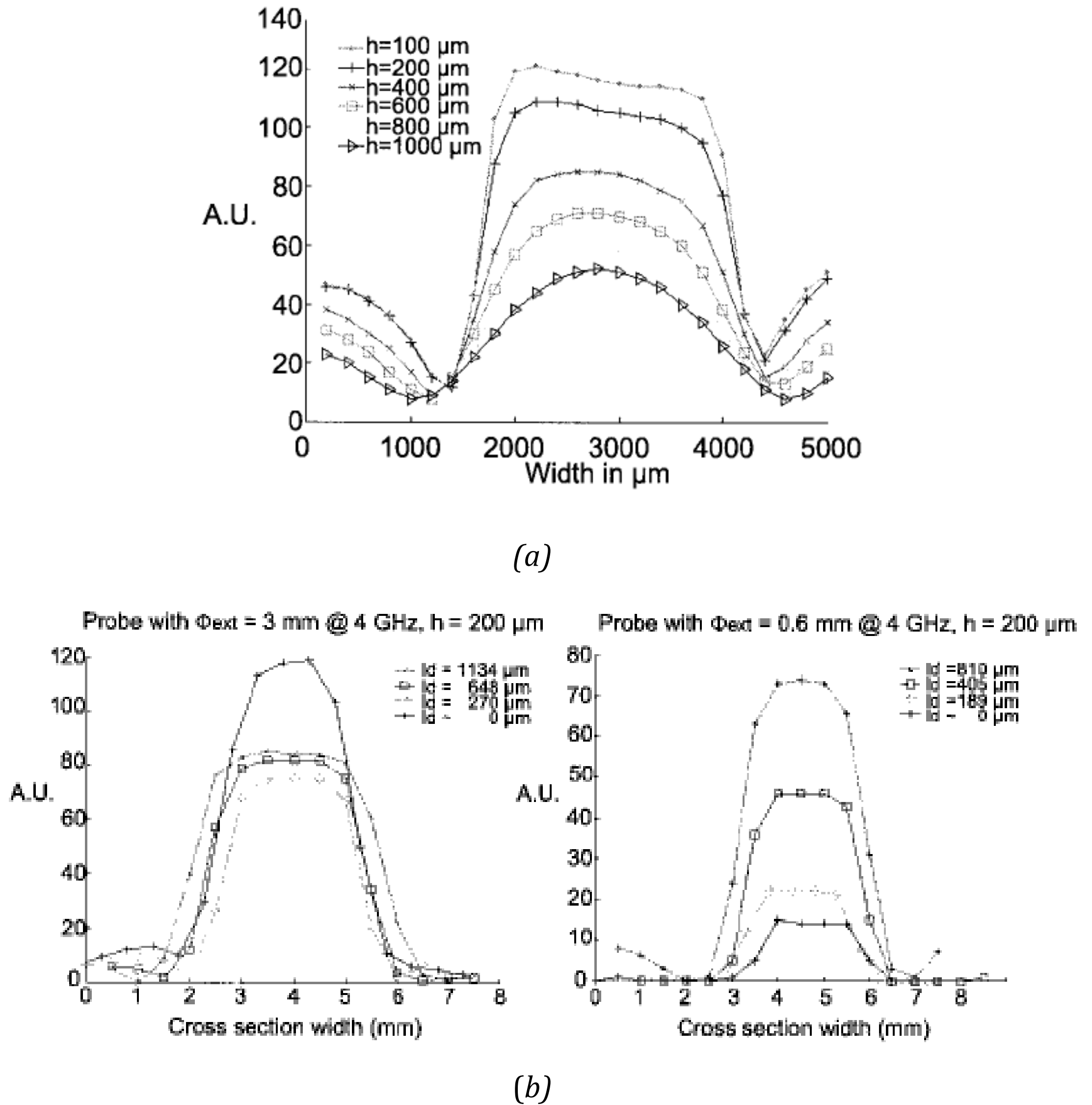

(a)

(b)

Figure 3.3: Cross sectional scans conducted across a section of transmission line (a) at different heights of the measuring plane and (b) two scans acquired by probes with different OD investigating the effect of probe tip protrusion at a constant measuring plane [23]. *Showing a loss of resolution, for a constant measurement plane, as the probe tip protrusion is decreased.*

- Another method for the determination of resolution is the ability to distinguish anomalies [23]. With the addition of purpose drilled defects of 25µm holes to the test fixture, sequential scans of before and after the additions, can determine deviation from the expected result. The EFP's

ability to extricate this defect would show the spatial resolution capability of the probe.

Although both the methods mentioned above can show some aspects of the spatial resolution, a method directly applicable to the intended measurements would better represent the achievable resolution. Figure 3.4 below represents an example of the test fixture used for spatial resolution analysis.

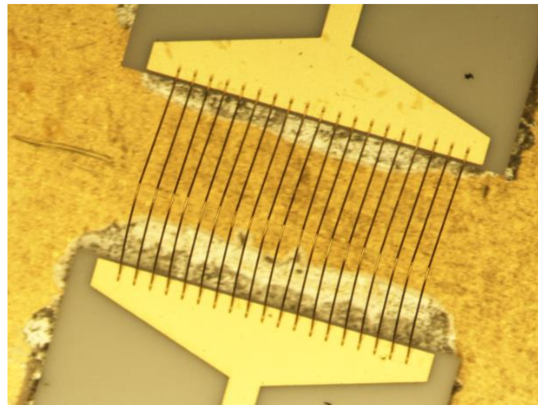

(a)

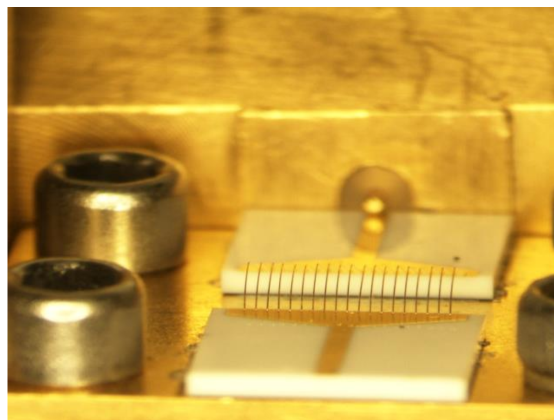

(b)

Figure 3.4(a) and (b): An example of the plan and side view of a 19 bondwire test fixture used for spatial resolution analysis. The excitation to the test fixture is provided by a VNA and terminated by a matched 50Ω load, where resolution is determined by the transverse movement of the EFP across the DUT at constant separation.

Figure 3.4 shows a multiple array of 20µm bondwires, joining two sections of microstrip line. This test structure is made to fit on a standard microstrip test

fixture ("H Block"), allowing it to be measured with SMA connections. The excitation to this structure is provided through port 1, which is connected to a vector network analyser and is terminated through port 2, to a matched 50Ω termination. The test fixture shown above is an example of just one of the many used. Structures varied in bondwire numbers and termination, i.e. some bondwire arrays terminated to ground while others, as shown above in figure 3.4, terminated by bonding to an adjacent section of microstrip line. All structures used resulted in the full investigation of the spatial resolution capability of the EFP.

By placing the probe, whose spatial resolution capability is to be tested, over the bondwire array and moving it transversely across the structure, the output picked up by the probe is proportional to the voltage produced between the bondwires and ground. Between each movement, the corresponding voltage is measured and recorded with respect to that given point.

The resulting scan across the test fixture should achieve a corresponding number of peaks and troughs to the number of bondwires; where the maximum relative voltage measured is proportional to the number of bondwires, while the troughs represent the spacing between the bondwires. Although it has been previously mentioned that the probe is only sensitive to the normal component of electric field, the troughs measured will not yield a relative voltage of zero. This is due to the fact, that the field between the bondwires $E_z \neq 0$ at the chosen measurement plane.

The field between the bondwires can be simplified by only considering the field distribution of two parallel conducting wires. The figure below shows the electric field patters surrounding two conducting wires, note the current is travelling though each wire is in the same direction.

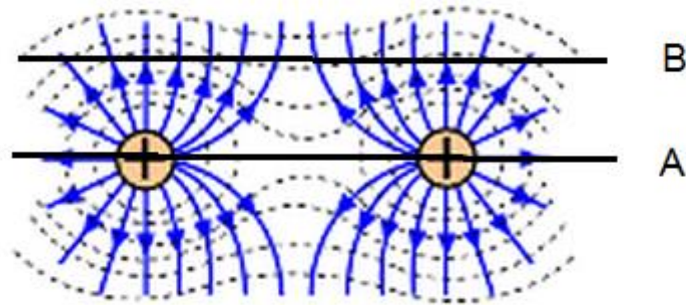

Figure 3.5: Electric field distribution between two parallel wires with two indicated measuring planes, plane A and B; where the blue lines indicate electric field and the dotted lines represent their corresponding equipotential surfaces. To achieve a field measurement of zero between adjacent bondwires, the intended measurement plane must be conducted at A.

The field patterns axially central between the current carrying conductors, will exhibit a null of zero electric field due to the divergence of field, when conducting in the same direction. In order to achieve a measurement of zero electric field and hence zero relative voltage, the EFP would need to be transversely moved across plane A, indicated above. Due to the physical obstacle of the bondwires, the movement across plane A would be impossible and cause irreversible damage to the structure as well as the probe, for this reason the actual measurement made is along plane B. Midway across plane B, it shows clear evidence of an electric field present. However, due to the divergence of field, the resultant perpendicular component is reduced. This therefore shows the probe will measure a proportional and relevant reduction in the electric field distribution.

It should be mentioned that the effective coupling of the probe tip to a bondwire, would in fact be much less than the calculated value in section 3.1.1. The calculation in the previous section was derived from the assumption that the DUT is of a larger area than that of the probe tip, therefore the value calculated is the maximum possible coupling. However, with measurements over the bondwire structure, the maximum possibility of coupling is reduced due to the size

(diameter) of the bondwire. The coupling is further reduced due to the DUT area of 20μm, which is about an 80% reduction in effective area.

3.1.3. Automation of the results

For correct analysis of spatial resolution, the movement of either the DUT or EFP must be carefully controlled. Therefore automation of the measurement plane can aid the investigation while eliminating spatial errors:

- Automation of the test fixture or the probe will allow for repeatability of the results. Given a specific starting and ending point, with a precise number of increments, the measurements taken by different probes will be comparable as well as repeatable.
- Automation of the step size, i.e. the increments between each measurement taken by the probe must be carefully controlled. An unrealistic expectation of a resolution of 100μm would occur, if the increments between each measurement were 200μm. Automation will allow for a much more precise movement as well as fine-tune control.

The initial automation process required the movement of the H-block fixture i.e. to keep the probe stationary while the DUT below is moved. The linear stage used within this work is the Zaber 100mm T-LSM100A with built in controller and optional manual mode (see Appendix 3). The maximum error possible between two positions is 30μm with a repeatability of <1μm, where the repeatability is considered as the maximum deviation possible to the specified position.

The motorised linear stage required programming from scratch with C#, through the use of Microsoft Visual by a RS 232 to USB conversion.

For a successful automation procedure, the following outcomes must be considered and fulfilled:

- Result in a simple, user-friendly program not dependent on the level of the user's computer literacy.
- Allow for measurements to be interchanged between manual or automated modes.
- For automated modes of measurement, the magnitude and phase of each position must be stored in order to produce a full scan.
- The ability to store positions, this will allow the user to return to a specific point with only marginal error of the linear stage.

- Most important, to define the number of points within a given scan and the distance between each increment.

The latter point will have an introduced time delay between each increment within the code, allowing the instrument to have sufficient time to respond to the local environment of the new movement i.e. time to correctly measure the new field component, as well as the time needed for the acquisition of data.

Figure 3.6 below, shows screenshots of the resultant program, figure (a) is the method for individual data point acquisition, figure (b) represents the automated control and definition of starting point while figure (c) is the automated program.

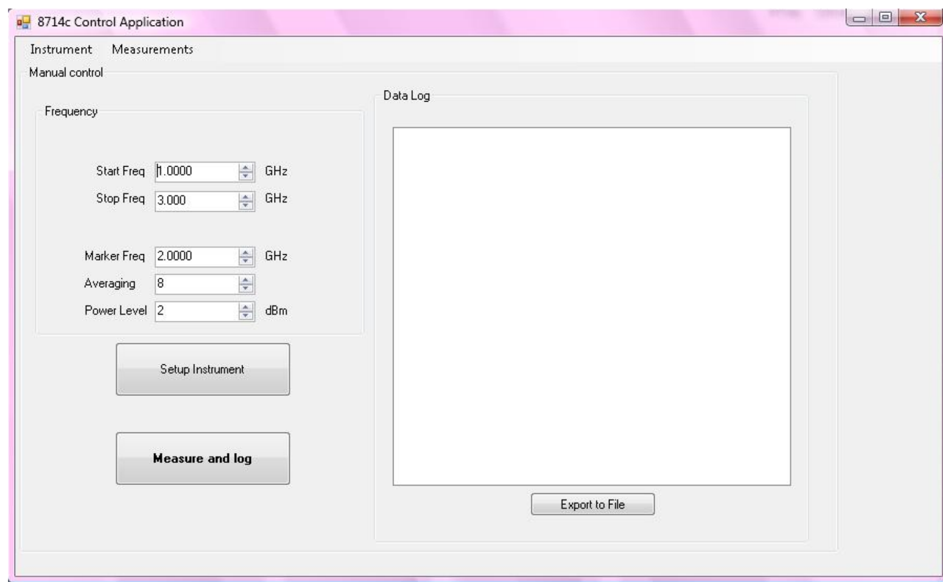

3.6 (a)

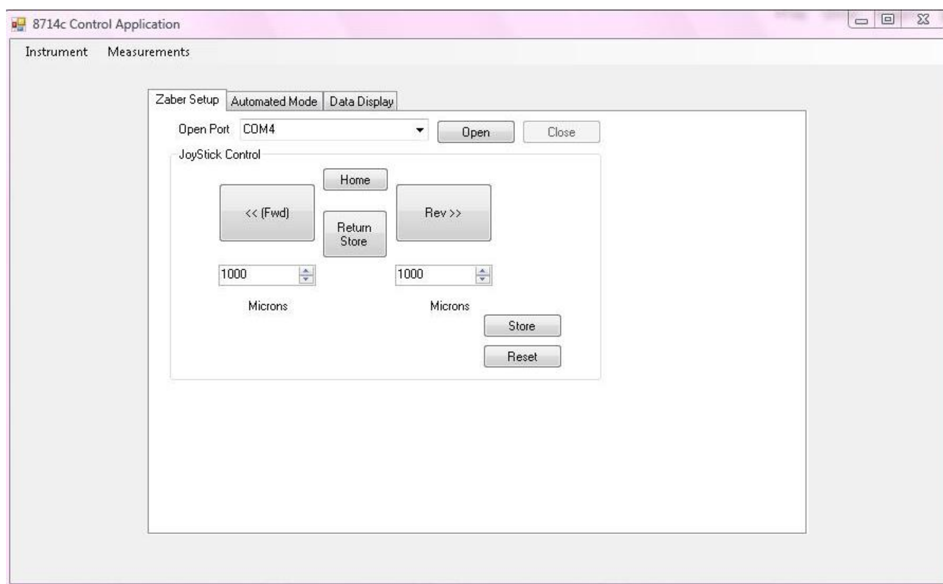

3.6 (b)

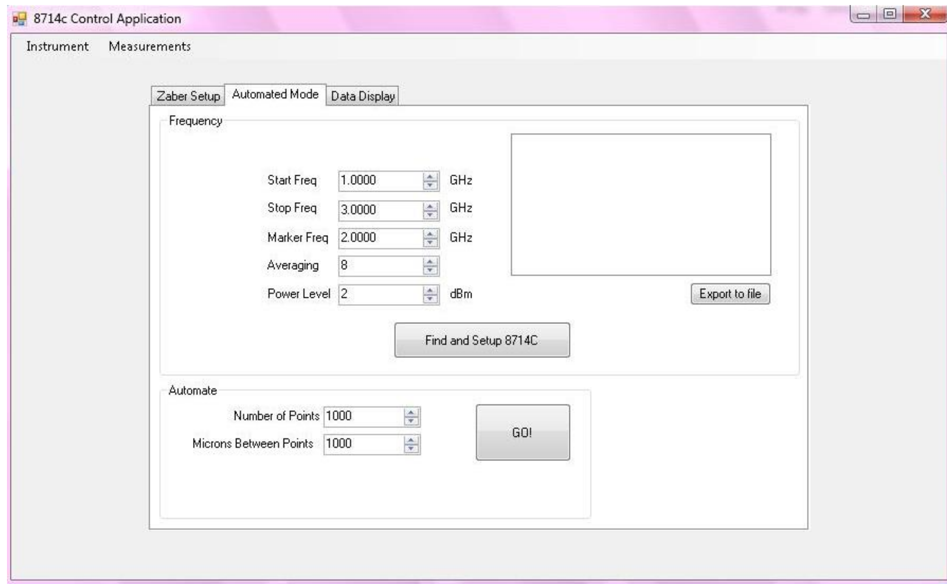

3.6(c)

Figure 3.6: Screenshot of the resulting program from the c# code (a) with manual modes and automated modes of measurement, (b) with the ability to automatically control and define probe position and (c) conduct automated scans with specific dimensions and pre-set levels.

The Zaber automated linear stage includes numerous predefined commands. The incorporation of these demands and further code allowed for an effective program which is used throughout this work.

The automated program undergoes an open loop of commands for a given scan. Firstly, the VNA is initialised, by defining the frequency sweep and marker frequency of the measurement, with additional control of the required power level and averaging. The number of points required for a complete scan and the increments between each movement are predefined by the user. The automated program is then started, the magnitude and phase of the probes output is recorded for a given position. This measurement is relevant to the predefined marker frequency. With an appropriate time delay, the probe is then moved and a new measurement is recorded. The time delay between subsequent measurements can be changed. A longer time delay will result in a better response to the local field, however this will result in a greater scan time. The resultant scan is a data set of all the points acquired within the specific number of points which can be exported for later analysis in a .CSV file.

Two additional significant features in the code include a real-time plot of EFP measurements with respect to magnitude and phase of the output and a 'cancel' button to prevent a chain of disastrous events.

3.1.4. Spatial resolution capability of EFP1 and EFP2

In order to test the spatial resolution of the two probes, EFP1 and EFP2, automated scans were made of the structure shown below.

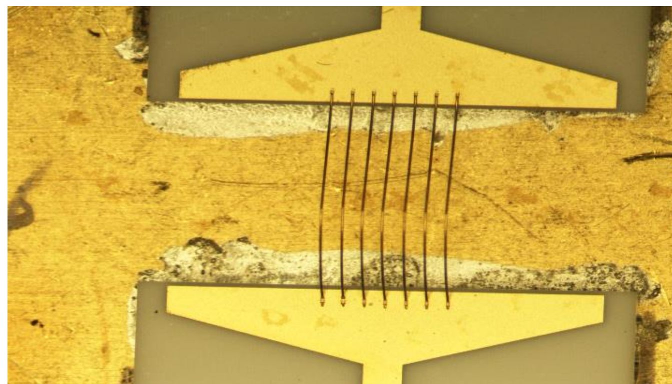

(a)

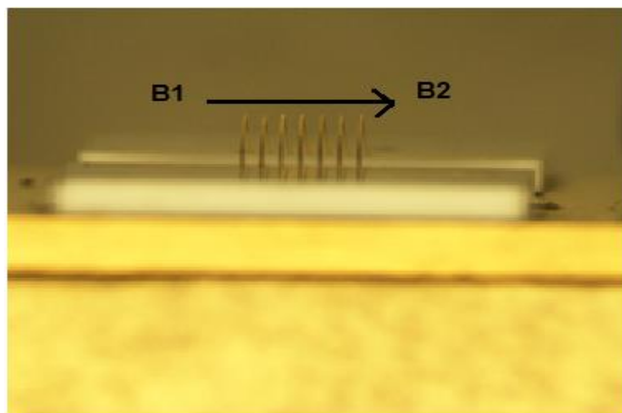

(b)

Figure 3.7(a) and (b): Plan and side view of a 7 bondwire test fixture used for spatial resolution analysis of EFP1 and EFP2, indicating the direction of data acquisition.

Figure 3.7 shows both the plan and side view of a structure consisting of a section of microstrip line, connected by a fan of 20µm diameter bondwires. The 7 bondwires each have a separation measuring 100µm. The probe was placed over the initial measurement point of B1, with a measurement height of 30µm between

the highest bondwire. The probe is kept stationary, while the structure, due to its attachment to the automated stage, is moved from the trajectory B1 to B2. The structure itself is passive, measurements are taken at the frequency sweep of 1GHz to 3GHz, with an input power of 0dBm. To avoid reflection, port 2 of the structure is terminated by a matched 50Ω load. The measurement taken from the probe is the resulting transmission in dB, at a given point, using a VNA. This output is converted to a relative voltage measurement by means of:

$$V = 10^{P/20}, \tag{3.11}$$

where P is the output measured by the VNA in dB.

Figure 3.8 shows the results yielded from the respective scans from EFP1 and EFP2 for the 7 bondwire structure, where the horizontal scale represents the relative distance from position B1 to B2.

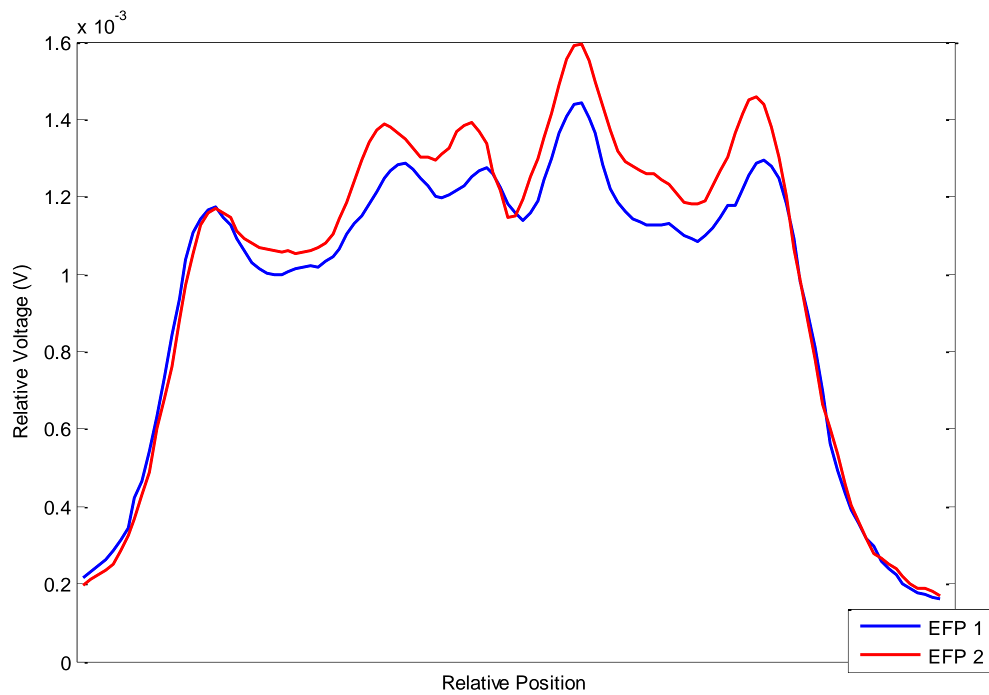

Figure 3.8: Resultant spatial resolution scans, with the transverse movement across the measurement plane of the device shown in figure 3.7 using EFP1 and EFP2; where the horizontal scale represents a relative measurement of distance.

From the spatial resolution analysis of EFP1 and EFP2, it can be easily concluded the resolution capability is beyond the required 100µm. Clear resolution of the

individual bondwires cannot be fully distinguished. With only a slight improvement in resolution due to a reduction of probe dimension, one probe cannot be clearly labelled as superior.

This outcome is rather expected when considering the analogy presented in section 2.5.1. If the diameter of the inner conductor exceeds the area of intended measurement, the spatial resolution will degrade. (Note that in this thesis “increased resolution” is used to indicate “improved resolution”).

With consideration of the smaller probe, EFP2, its ID measures at 127μm, whereas the proposed DUT has a bondwire diameters of 20μm with a separation of 100μm. This will result in the situation whereby the probe tip can potentially couple to two adjacent bondwires, therefore clear resolution of the bondwires cannot be achieved. The illustration shown in figure 3.9 is to help reinforce this analogy.

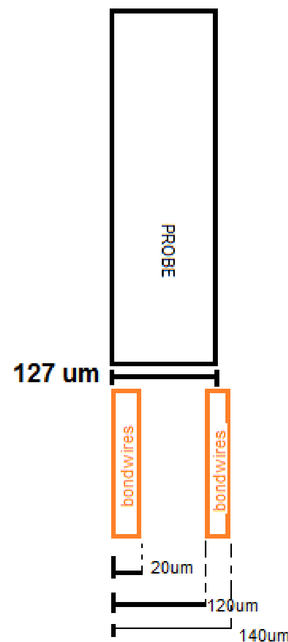

Figure 3.9: Schematic highlighting possible simultaneous coupling of two adjacent bondwires due to the diameter of the inner conductor exceeding the required resolution. Note: that the schematic is showing only, the inner conductor and not the outer conductor.

For clear distinction of individual bondwires, the diameter of the inner conductor must be equal or less than the required resolution (<100μm).

Resolution capability of the EFP can be quantified with a resolution factor scale (RFS), such a quantity can allow the user for a much clearer interpretation of the results. Equation 3.12 provides a simple calculation that can be applied to a given resolution scan by considering the maximum peak and minimum trough, relative voltage values.

$$RFS = \frac{V_{Peak_{max}} - V_{Trough_{min}}}{V_{Peak_{max}} + V_{Trough_{min}}}, \tag{3.12}$$

Application of equation 3.12 to figure 3.8 results in the following RFS:
$EFP1 = 0.15$ and $EFP2 = 0.18$.
Thus showing that the resolution capability of EFP2 is slightly better than that of EFP1.

3.1.5. Design of EFP3

From the results presented in the section 3.1.4, it is true to say that by reducing the overall dimensions of the probe, the spatial resolution of the probe can be improved. With difficulty sourcing coaxial cables with smaller dimensions than that of EFP2, a design alteration has to be made to reduce the dimensions further, this can be achieved by modifying the existing design. The inner conductor of the EFP is extracted and replaced with a wire smaller in dimensions; consisting of an enamelled copper wire with a diameter of 0.1mm. However, the diameter of the EFP remains the same. In order to reduce the effective OD of the EFP, the inner conductor is extended further from the probe tip, to present a protrusion. The protruding inner conductor is coated with an application of a thin layer of silver paint. This layer of conductive paint allows for a continuation of the outer conductor path, thus connecting the larger OD to a much smaller diameter only slightly larger than the ID of the inner conductor. The enamel coating of the wire will now act as the effective dielectric medium separating the silver painted OD to the ID of the copper wire.
By replacing the inner conductor to that of a smaller diameter, the reduction to 100μm should allow for individual measurements of the bondwire structure, unlike its predecessor which measured 127μm.

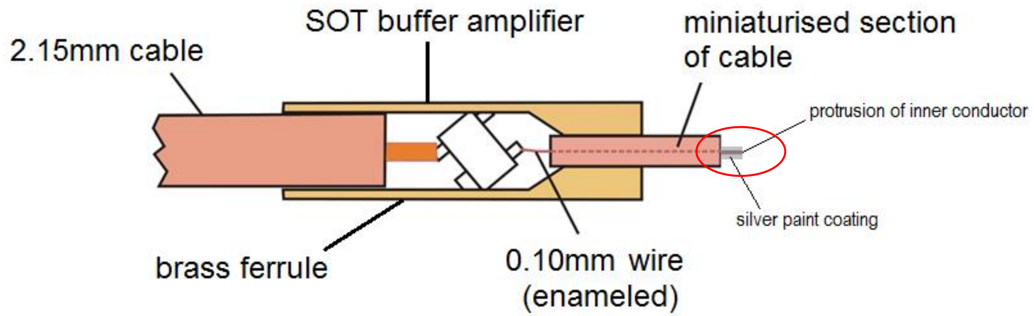

Figure 3.10: Schematic diagram of the further reduction of the EFP by addition of inner conductor protrusion and silver paint coating, highlighting key components. Note: the red circle highlights the novel design alteration from that shown in figure 3.1.

Figure 3.11 highlights the differences between EFP1, EFP2 and EFP3, while table 3.1 reiterates their measurements.

Table 3.1: Recap of the dimensions of OD and ID of EFP1, EFP2 and EFP3.

EFP1		EFP2		EFP3	
OD(mm)	ID(mm)	OD(mm)	ID(mm)	OD(mm)	ID(mm)
0.88	0.1778	0.58	0.127	0.111	0.101

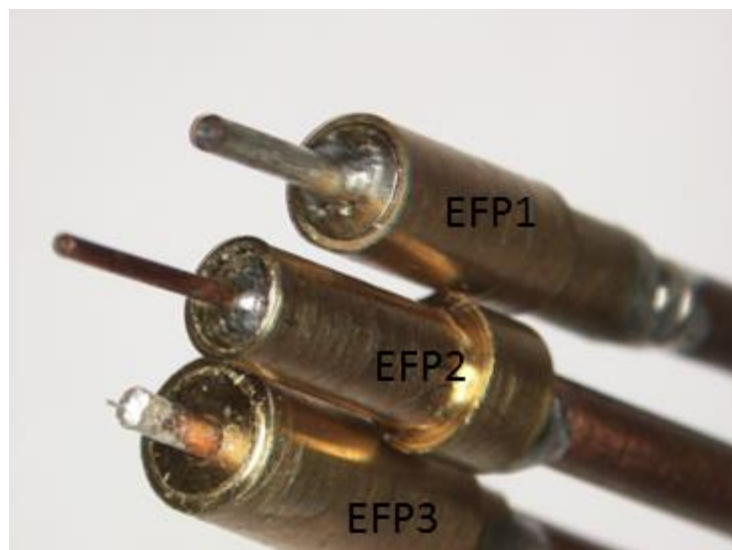

(a)

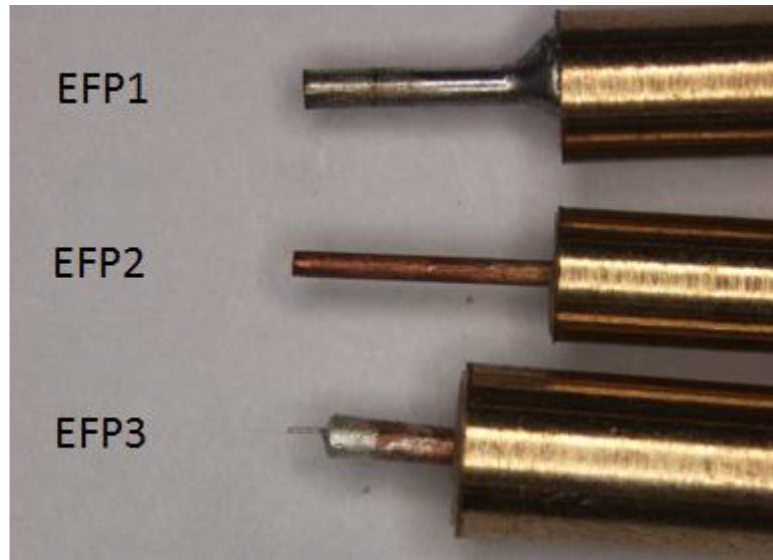

(b)

Figure 3.11(a) and (b): Pictorial representation of the EFP1, EFP2 and EFP3, with visual depiction of varying OD and ID.

The coupling between the newly refurbished EFP3 and the DUT differs from EFP1 and EFP2. The resulting measurement plane is reduced to 20μm to compensate for the anticipated reduction in the effective coupling. The maximum capacitance is calculated, from equation 3.1, to be in the order of:

$$C_{EFP3} = 3.54 \times 10^{-15} F.$$

Although the coupling is further reduced, due to the additional reduction in probe dimensions, the resultant reduction is only at the expense of the output not the resolution. The resulting scan conducted on the same 7 bondwire test fixture shows substantial improvement in the spatial resolution of EFP3, this is shown in figure 3.12.

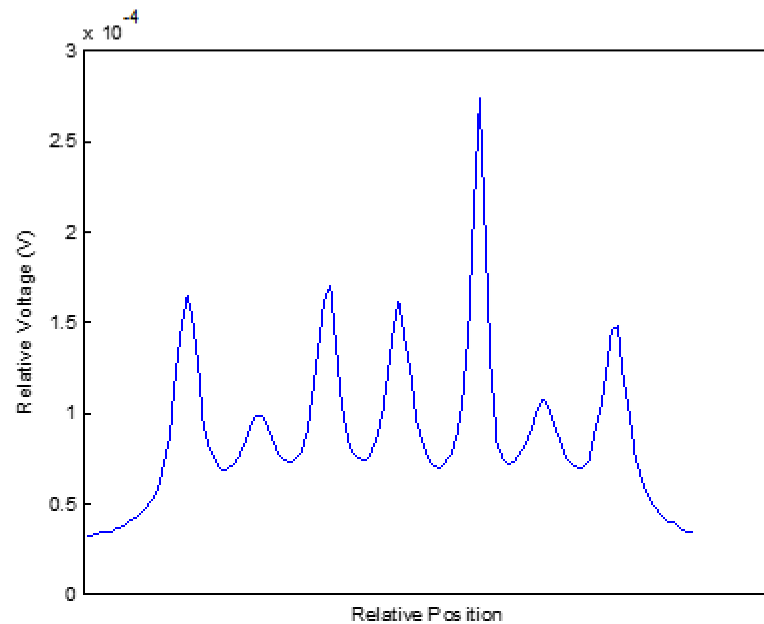

Figure 3.12: Resultant spatial resolution scans, with the transverse movement across the measurement plane, of the 7 bondwire structure using, EFP3.

Clear resolution of individual bondwires can be distinguished, much at the expense of output. This represents the reduction in the effective coupling will not dictate the subsequent resolution achieved, but the maximum voltage measured.

The relative voltage distribution of the 7 finger device exhibits a variation in the magnitude of the measured peaks. Closer inspection of the device revealed significant variation in the curvature of the bondwire, and therefore variation in the ground to peak height of each bondwire. This variation in height constituted in a proportional change in the magnitude of the measured voltage, thus making the EFP3 very sensitive to the geometry of the probing target.

The spatial resolution capability of EFP3 was further investigated with a more extensive structure, shown below in figure 3.13. This new test fixture consisted of section of microstrip line section connected to a 19 bondwire array with a diameter of 20µm terminated to ground, the spacing between bondwires was again 100µm.

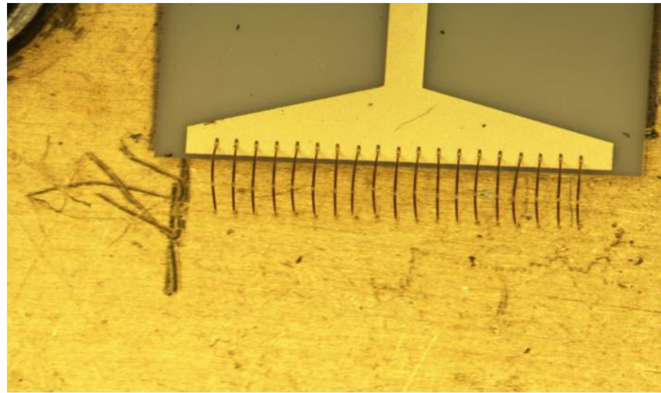

(a)

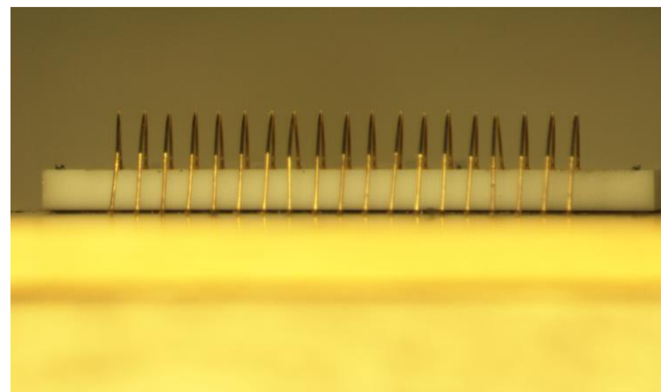

(b)

Figure 3.13(a) and (b): Plan and side view of a 19 bondwire test fixture, terminated to ground, used for further spatial resolution analysis.

The transverse scan of the structure shown in figure 3.14 with EFP3 yielded a voltage distribution with a clear visible trend; whereby the field exhibited maximum magnitude in the middle with substantial roll off towards the edges.

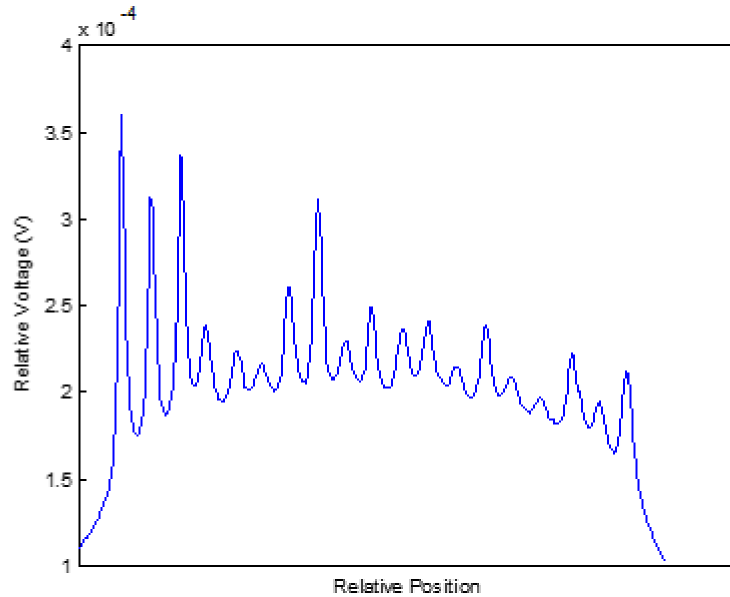

Figure 3.14: Resultant spatial resolution scans, with the transverse movement across the measurement plane using EFP3. Showing clear resolution of individual bondwires of the structure shown in figure 3.13.

The movement of the DUT on the linear stage could account for the observed anomaly, however this unexpected behaviour is visible in the various repeats of the scan. A gradient capable of producing an 'umbrella' like trend would be extremely difficult to achieve. Therefore the most probable outcome of a tilt present in the movement of the stage, would result in a comparative gradient in the measurement. So if in fact the separation between probe tip and DUT was decreasing along the scan, the decrease would continue past the middle section and inevitably hit the remaining bondwires. This is in contradiction to the results achieved, whereby the separation decreases then again increases.

This contradiction continues when comparisons are made to EM simulations of the 19 bondwire structure. EM simulation agrees with the increase of field at the centre of the structure, but would also expect an increase in field at both of the outermost edges.

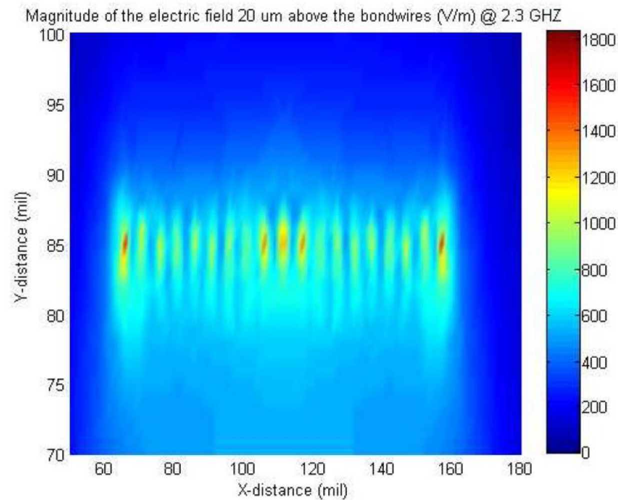

Figure 3.15: EM simulation at 2.3GHz, 20µm above bondwires [36]*. The resultant distribution is predicted to achieve a maximum at the structures edges as well as mid-way along the device. Contradicting the experimental achievement of an 'umbrella' distribution.*

3.2. The EFP and resonant electric field probe

3.2.1. The design and comparison of the resonant electric field probe to EFP2

Previous work at Cardiff University on microwave microscopy has shown many advantages for the use of resonant transmission lines. By designing an intentional resonance, improvements can be made in the spatial resolution and a 15dB increase in the frequency response of the EFP [30]. Improvements in spatial resolution can be achieved due to the sensitivity of the resonant frequency. Slight changes in the local geometry i.e. what is placed in front of the probe tip, can cause a consequent and measurable shift. Thus variation in the magnitude and phase of electric field, at the device plane, can be analysed and mapped for a proportional relative voltage distribution.

The length of the probe tip will cause an unavoidable resonance in the frequency response of the EFP, but by intentionally increasing this line and introducing a capacitance in the inner conductor a Resonant Electric Field Probe (REFP) can be designed.

Although the results obtained within section 3.1.5 have shown that a 100μm resolution requires an ID of comparable dimensions, work conducted within this section occurred prior to this discovery.

The REFP was constructed with the same probe dimensions as EFP2, for comparative reasons. Spatial resolution scans conducted within this section will be compared with EFP2. The EFP consisted of a probe line length of 9mm, whereas the REFP consisted of a probe line length of 34.9mm

(a)

(b)

Figure 3.16: Pictorial representation of (a) EFP4 and (b) EFP2 with visual depiction of different conductor length.

The REFP was designed to have a resonance at 2.15GHz, with the introduction of a series capacitive element, as show in in figure 3.17. The frequency response of the REFP yielded a resonant frequency with a fundamental $f_0 = 2.15$GHz, 1st harmonic of $f_1 = 4.31$GHz and a third harmonic of $f_2 = 6.45$GHz. The resulting probe orientation is shown below in figure 3.17.

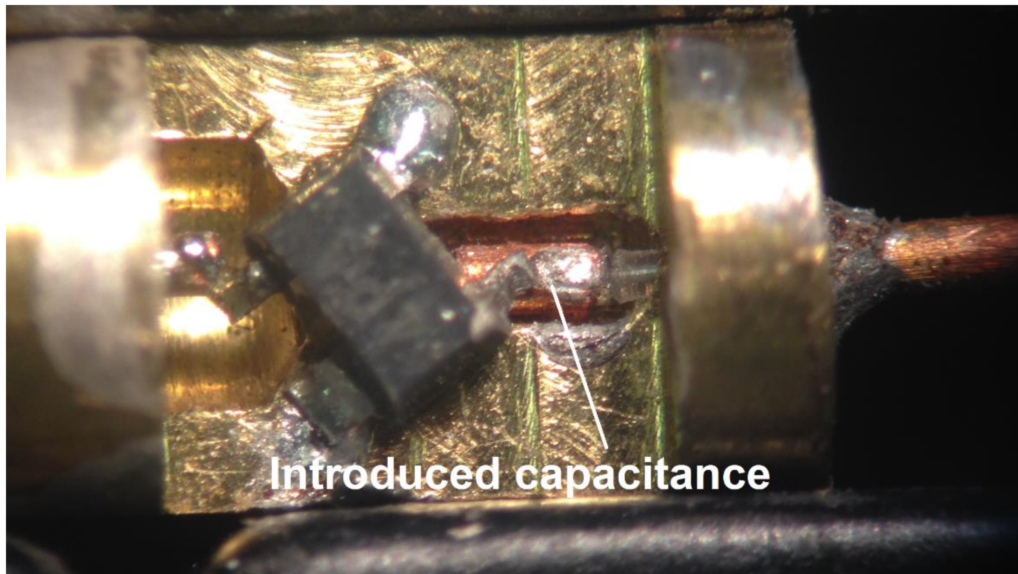

Figure 3.17: A magnified pictorial representation of REFP, within the brass housing, highlighting the introduced capacitance.

3.2.2. Experimental results of EFP2 and REFP

EFP2 and REFP are conceptually the same probe, differing only in the length of cable required for the probe tip. Constituting the same materials and method for construction. Both probes were used to scan the same structure shown in section 3.1.4, and results are given in figure 3.18, where the horizontal axis represents the relative distance across the device.

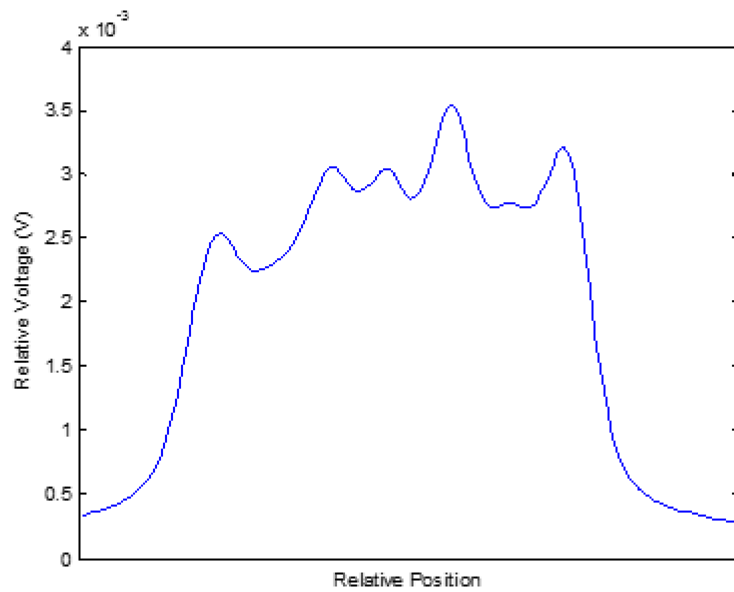

(a)

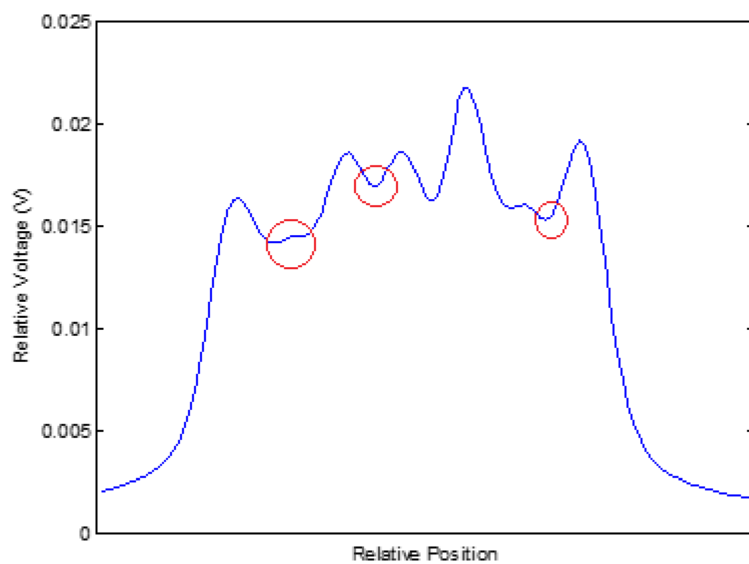

(b)

Figure 3.18: Resultant spatial resolution scans, with the transverse movement across the measurement plane using (a) EFP2 and (b) REFP with highlighted improvements in resolution.

Although neither probe is able to make clear resolution of the individual bondwires with regards to the 7 finger structure, there is a slight improvement from the scan achieved by REFP. This improvement could be a result of the increased probe output, however literature would expect a greater improvement in the spatial resolution [30].

Nonetheless, taking into account only the subsequent scans produced by EFP2 and REFP, there is clear difference in the magnitude of the measured relative voltage. The resonant probe has a greater response of about 15dB. However, further analysis is required to determine if the slight improvement in resolution is a result of the increased probe output.
Continuity of measurements are shown by the consistent detection comparable bondwires. Both probes, regardless of initial output, are extremely sensitive to the planarity of the bondwires. The display of comparable bondwires in this section is consistent to those completed in sections 3.1.4 and 3.1.5.

Further analysis of the two probes on a different structure, yielded further discontinuity. Figure 3.19 below shows the resulting scan of a 19 bondwire structure, this structure differs to that shown in section 3.1.2, as the bondwire array is not terminated to ground, but rather connects to a symmetrical section of microstrip line. For continuity, ideally, the same structure shown in section 3.1.2 would be used for measurement and analysis, unfortunately during experimental procedure; this structure was damaged beyond functionality.

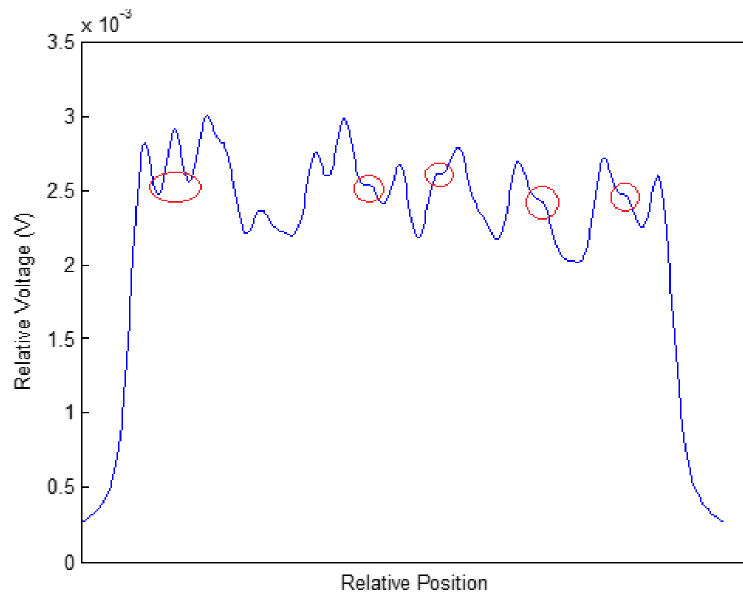

(a)

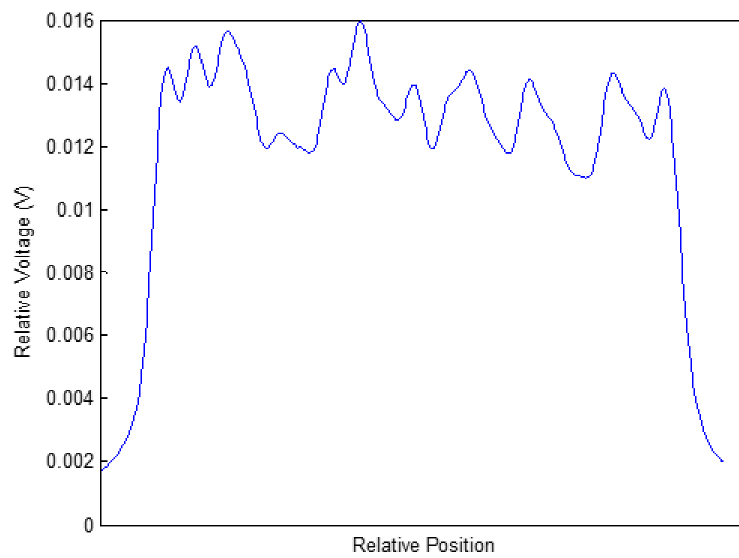

(b)

Figure 3.19: Resultant spatial resolution scans, with the transverse movement across the measurement plane using (a) EFP2 and (b) REFP with highlighted improvements in resolution.

The measured magnitude of voltage is much higher in the resonant probe when compared to the non-resonant, of the order of 15dB. With this particular scan, the non-resonant probe is showing signs of improved resolution. The highlighted

sections in figure 3.19 (a) indicate the major differences between the two plots. The work conducted within this section has concluded that an increase in the output of the probe will not constitute a proportional increase to the spatial resolution. From the analysis provided in section 3.1.5, the lack of resolution seen within figures 3.18 and 3.19 is to be expected. With both probes consisting of an inner diameter of 0.127mm, resolution of a 100µm is beyond the expectation.

Application of equation 3.12 to figure 3.19 results in the following RFS:

$EFP2 = 0.39$ and $REFP = 0.21$.

Thus showing that the resolution capability of EFP2 is slightly better than that of REFP.

3.2.3. The effect of increasing the measurement separation

For full consideration of the separation of the probe tip and DUT the same measurements performed in the previous section were repeated with both, EFP2 and REFP, at different measurement planes.

The code written for the automation of the linear stage beneath the DUT, allowed for various positions to be stored, meaning that the same scan can be repeated as the probe height separation is varied manually on the z-axis.

The measurements shown below are conducted with an initial separation of 30µm, and re-scanned with increments of 10µm, with the separation never exceeding 100µm.

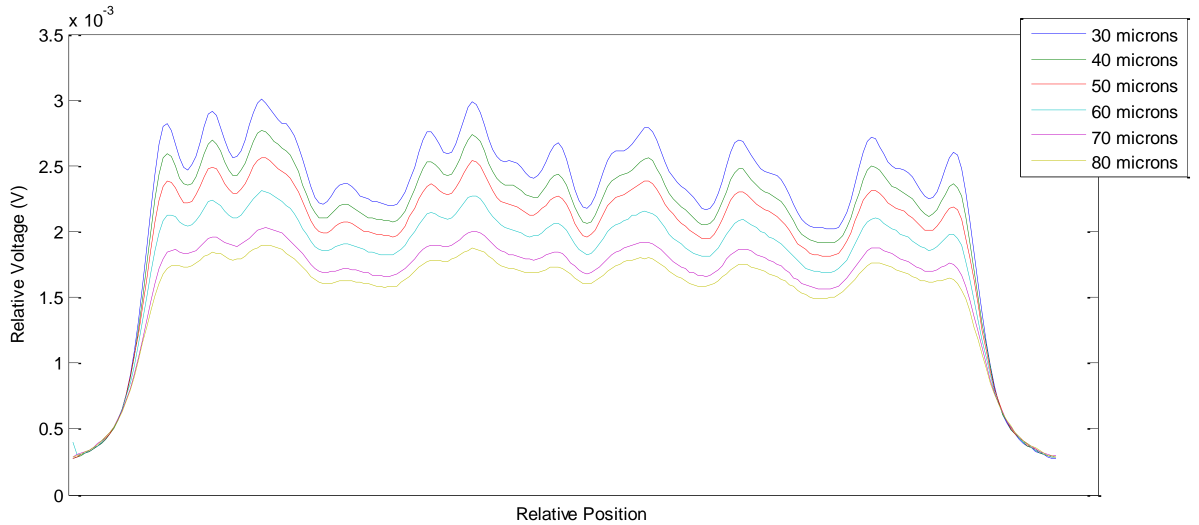

(a)

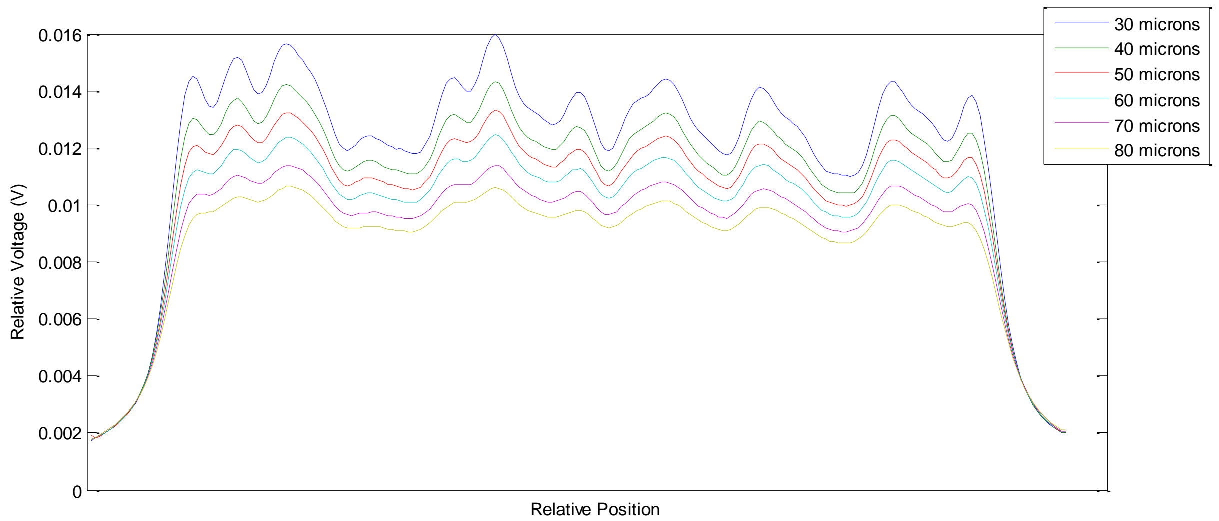

(b)

Figure 3.20: Resultant spatial resolution scans, with the transverse movement across the device with increased increments in the measurement plane using (a) EFP2 and (b) REFP; where the key indicates the separation of the measurement plane.

From figure 3.20 it is evident that, regardless of the initial signal strength, an increase in measurement separation produces a reduction of 40-50% of the probe output. The increase in separation also compromises the achievable resolution. The probes under scrutiny are unable to fully resolve individual fingers at the

separation of 30μm, increasing the measurement plane diminishes any initial resolution made.

3.2.4. The effect of the probe and the resulting measured field

Analysis of a foreign metal object placed within an electric field would result in alteration and distortion of the field distribution. Therefore it can be said that the distribution measured by the probe is not the actual distribution, but in fact the modulated version of the initial field. Considering this perturbed analysis, the distortion of electric field caused by the presence of the probe would be a relative and continuous distortion. Thus resulting in a relative measurement at the probe output.

Where in fact, it is the extent of this distortion that will dictate the validity of the results. As previously mentioned, by reducing the dimensions of the EFP, the disturbance caused to the resultant electric field is also reduced [23]. Therefore the measurements conducted, with the EFP dimensions discussed, should cause little disturbance on the measured field.

Measurement analysis of S_{11} will show the extent of any disturbance caused to the DUT. By increasing the measurement plane, any resulting disturbance will be evident in the S_{11} measurement.

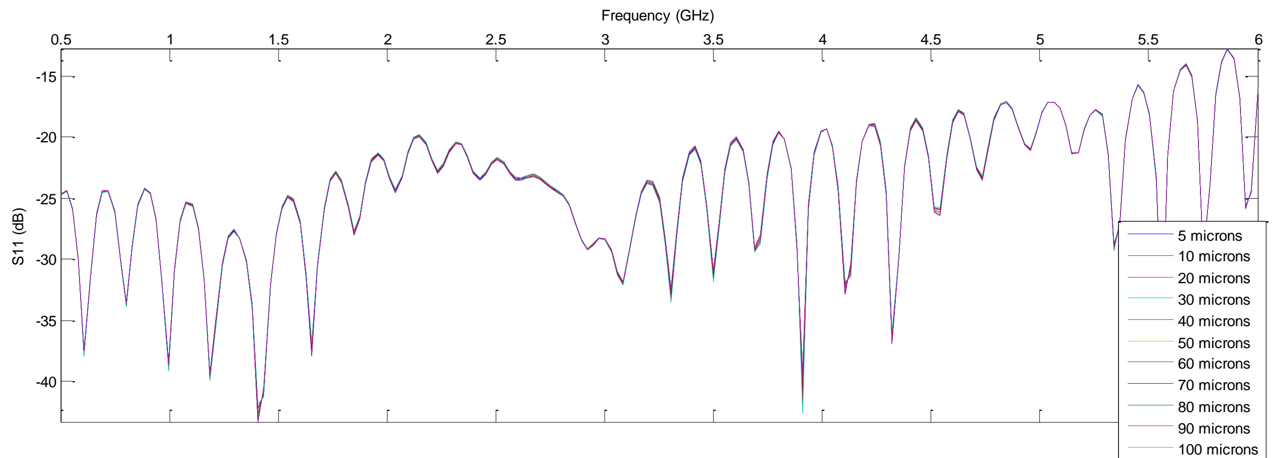

Figure 3.21: Resultant S_{11} measurement conducted on a terminated 50Ω transmission line with increased separation of the measurement plane using EFP2.

Figure 3.21 above, shows the resultant measurement made on a terminated 50Ω transmission line, with the initial probe tip separation of around 5μm then increased to 100μm. No variation of the measured input reflection coefficient is found as a result of an increased measurement plane. Thus concluding the interaction between the presence of the probe and the field generated by the DUT negligible.

3.3. Conclusion

Preliminary design methods of the EFP probe has demonstrated a spatial resolution of better than 100μm. Comparison of the results obtained within sections 3.1.4 and 3.1.5 concludes a reduction of both the diameter of the inner conductor and outer conductor of the probe, substantial spatial resolution improvements can be achieved.

The improvements in spatial resolution from EFP2 and EFP3, shows the overall achievable resolution is not only dependent on the reduction of the inner diameter, but also the outer diameter. By decreasing the outer diameter, substantial improvements can be achieved as shown with the evolution between EFP2 to EFP3.

Comparing all of the probes presented within this chapter, neither outperformed the resolution capability of EFP3, which showed the resulting improvements in resolution is attained at the expense of the output.

However, with the introduction of silver paint in the design of EFP3, many additional losses were introduced to the system. The application of silver paint may not be distributed evenly along the length of the protrusion, meaning the newly formed coaxial line cannot be considered as a homogeneous cylindrical conductor. Variation in the outer diameter, due to the change in silver paint thickness, will have a direct effect on the characteristic impedance of the probe. This change in the characteristic impedance can lead to attenuation and signal propagation, will ultimately in result transmission losses. The relatively low conductivity of silver paint (3 orders of magnitude lower than copper) also increases the skin depth (by $\sqrt{1000}$) thus possibly allowing the field to couple through the outer wall. An ideal design of the EFP, would need the requirement of silver paint to be eradicated, further design considerations must be made for an alternative reduction in the dimensions of the probe.

When comparing the functionality of EFP2 and the REFP, the signal gain of 15dB of the resonant probe would seem to be a much needed advantage. However, comparing the practicality of the two probes, the length of probe tip required for the resonant frequency at 2.1GHz is too extensive. Due to the long and thin shape of the probe tip, it is very susceptible to damage and bending and can easily cause anomaly in the measured field. An intentional design for 2.1GHz operation will inevitably result in a restricted application of the REFP, whereby DUT characterisation can only occur at the specified and harmonic frequencies. The REFP resulted in higher signal gain but an inconclusive analysis on subsequent spatial resolution capability, therefore further investigation will be provided within chapter 4.

The measured voltage has been found to be extremely sensitive to the measurement plane, an increase in separation has resulted in a proportional decrease is observed in the output. This reinforces the importance of a constant and small separation plane.

Seen from the measurements of S_{11}, the presence of the probe and the perturbation of the resultant field measurement can be regarded as insignificant. Therefore for maximum pick-up and spatial resolution, the probe can be situated as close as possible to the device it is measuring without causing additional disturbance to the measured field.

4. THE EDM ELECTRIC FIELD PROBE

From chapter 3, it was concluded that a spatial resolution of better than 100μm was achievable; however the procedure required the use of silver paint, which has numerous undesirable side-effects. The methodology behind the construction of EFP3 was rather novel, enabling a miniature equivalent coaxial cable to be achieved. It was found that substantial improvement can be achieved by the subsequent reduction of both the inner and outer conductor of the EFP. However, an alternative method for this reduction must be considered without the need for silver paint; for future developments and improvements to the spatial resolution and response of the probe.

Throughout this chapter, different designs of the EFP were fabricated and tested. Unfortunately some designs, while novel in theory, proved impractical in testing and would be disregarded as an alternative EFP design. The biggest disadvantage faced in this chapter and those to follow, is the fragile nature of the newly designed miniature EFP. It will be seen that a large reduction in probe size, although resulting in favourable advancement in the spatial resolution, will also increase the delicate nature of the EFP. Many probes were unfortunately destroyed without full measurement of their capabilities recorded, with each probe taking many hours for its construction and a few seconds for its destruction; unavoidable delay can be caused in the measurement stage.

4.1. Construction of the EDM EFP and EDM REFP

4.1.1. EDM electric field probe and resonant electric field probe

The sourcing of commercially available miniaturised coaxial cable proved to be difficult beyond the diameters of EFP2. To achieve an outer diameter of smaller dimensions, efforts were concentrated in obtaining small copper tubes with an OD less than that of the coaxial cables used in chapter 3. These copper tubes could act as the outer shield, while an alternative inner conductor could be threaded through for a customised coaxial cable.

Fine copper tubes, used in Electrical Discharge Machining (EDM), can be used for the fabrication of smaller EFPs. Through a supplier in the United States, Saturn EDM Industries, copper tubes with an OD of 0.0098” (≈0.25mm) and an ID of 0.064” (0.1mm) were obtained. To accommodate the reduced diameter of the outer conductor, slight modifications was required to the existing brass ferrule. The drilled hole was reduced to 250μm to allow a tight fit for the EDM copper tube. The figure 4.1 below highlights the physical differences between the EDM EFP and EFP2.

Figure 4.1: Pictorial representation of the reduction in dimensions of the EFP with the use of EDM copper tubes.

The inner conductor of the EFP was constructed using an enamelled copper wire with an OD of 0.071mm. A diameter larger or smaller than this would pose great difficulty in the fabrication stage of EFP, highlighted in figure 4.2. A diameter too large can result in damage to the enamel coating when threaded through the EDM tube, thus shorting the EFP if contact is made by inner and the outer tube. The resulting disadvantages from a wire too small can include; a high reduction in the resultant output of the EFP, kinking of the copper wire during the threading

process, or result in a non-concentric positioning of the inner conductor. With the latter, the coaxial's ability to support TEM mode would be compromised as the position of the inner conductor to a non-central point would cause a non-uniform distribution of EM waves and cause "glitches" in the frequency response.

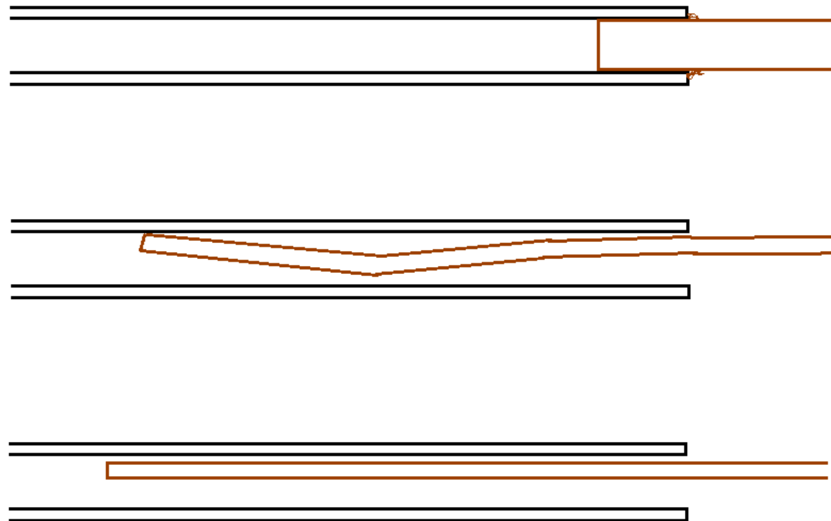

Figure 4.2: Potential unfavourable outcome if the diameter of the inner conductor is not fully considered (a) too large a diameter resulting in damage to the enamel of the copper wire (b) too small a diameter resulting in i) coiling or deformation or ii) non-concentric positioning of the copper wire.

The dimensions of the EDM EFP mentioned thus far requires fabrication underneath a microscope, as successful threading of copper wire through the EDM tube could not be achieved otherwise. For some perspective, the average human hair is of the same thickness as the copper wire, threading it through a copper tube just big enough to contain it, shows the level of difficulty, skill and the steady hand required for its fabrication.

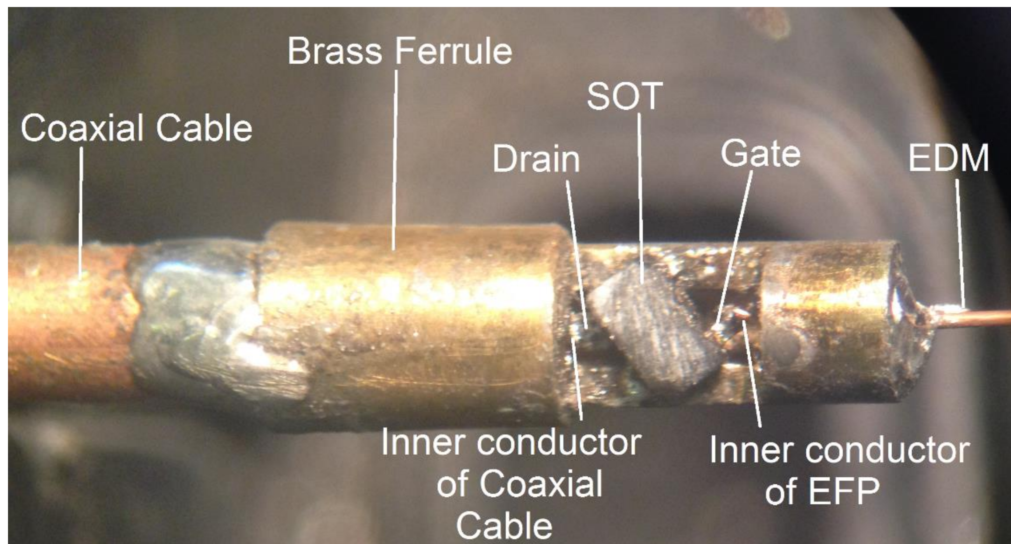

Figure 4.3: EDM EFP configuration, complete with brass ferrule, SOT package and EDM tube. Note: the ceramic casing of SOT has been filed to shape for the correct fit of the tight-fit brass case, not pictured above.

Fabrication of the EDM EFP and the EDM REFP, shown in figure 4.3, required a rather strict assembly procedure. A coaxial cable (RG405 U) is prepared with a SMA attachment at one end and with an open protruding inner conductor at the other. The open end of the cable is soldered to the brass ferrule. This protrusion is required for the attachment of the drain tab of the SOT package.

The EDM tube, of 9mm length, was then placed inside the 0.25mm drilled hole and soldered in place. The two final stages, proving to be the most difficult; required the soldering of the SOT package in the configuration shown above and threading of the central conductor through the EDM copper tube. Difficulty was presented in the attachment of the SOT package due to the material of the ferrule, which restricted the ease of solder flow. Precise positioning of the SOT package is vital for correct attachment of gate, drain and source connections, therefore the package required a steady positioning with simultaneous soldering.

The final stage involved the threading of the copper wire through the EDM tube and a final solder of the copper wire to the gate tab of the SOT. Once in place, the excess copper wire protruding from the EDM was cut flush.

Note: the frequency calibration of the constructed probe will be shown and discussed later in section 4.1.4.

As previously stated in chapter 3, it was concluded that the resonant EFP was deemed too fragile in comparison to a much shorter EFP tip. However, the

resulting increase in output of the probe did not provide conclusive evidence regarding its effect on the spatial resolution, and therefore further investigation was required. Its construction involved the same method as the non-resonant counterpart, and was designed to have a tip length i.e. EDM length of 34.9mm. Threading of the central copper wire through short sections of EDM tube posed great difficulty, which was only increased constructing the resonant probe.

The fabrication of the resonant EDM EFP was consistent to the same design specifications and procedures shown in section 3.2.1, where the fundamental resonance occurred at 2.15GHz. The frequency response of the REFP will be shown and discussed later in section 4.1.4.

4.1.2. Resolution of the EDM EFP and REFP

The newly constructed EDM EFP and REFP were used to scan the 19 bondwire structure shown in section 3.2.2. The measurement setup remains unchanged, with the probe stationary in height and position, while the DUT beneath is moved on an automated linear stage. From the results shown below, it can be seen that a reduction in the OD of EFP by the incorporation of the EDM copper tube, provides substantial improvement in the spatial resolution of both the non-resonant and resonant probe.

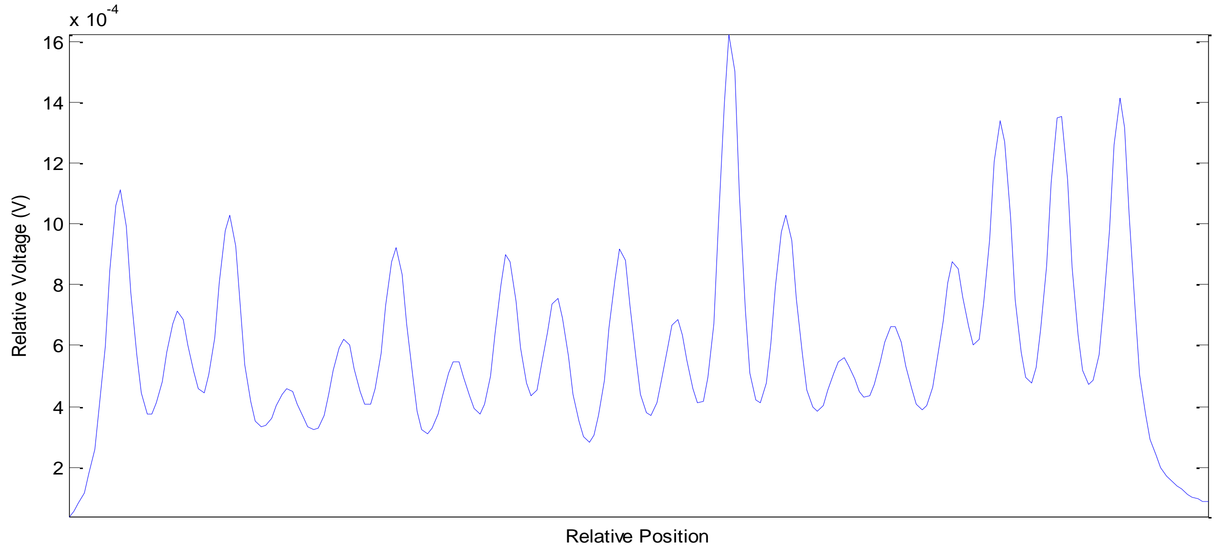

(a)

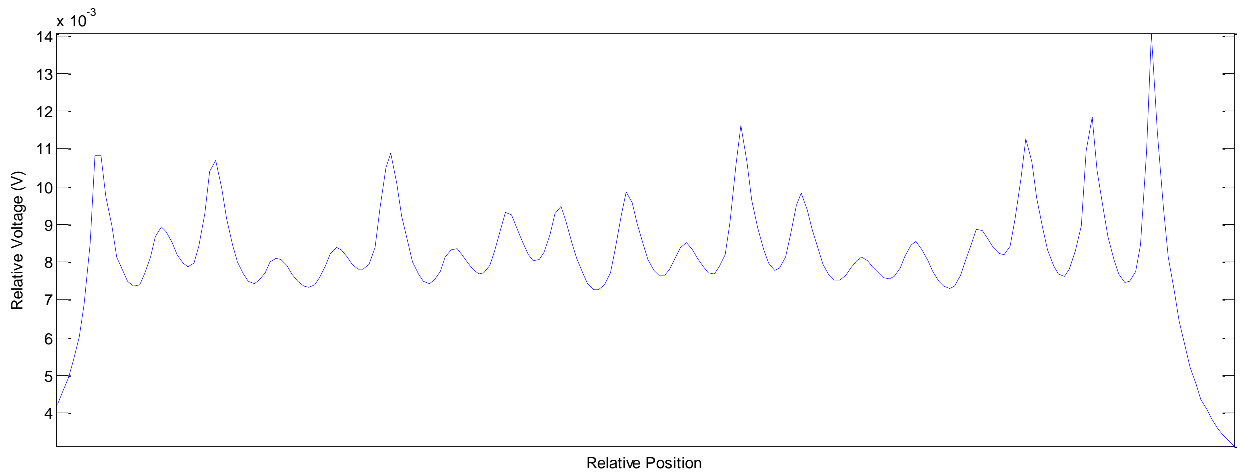

(b)

Figure 4.4: Resultant spatial resolution scans, with the transverse movement across the measurement plane using (a) EDM EFP and (b) EDM REFP of a 19 bondwire structure.

The sensitivity of the resonant probe is found to be much greater, of the order of times 10 the magnitude compared to the non-resonant probe. The subsequent scans conclude that both probes can clearly resolve the 19 individual bondwire fingers.

Application of equation 3.12 to figure 4.4 results in the following RFS:
$EDM\ EFP = 0.35$ and $EDM\ REFP = 0.32$.
Thus showing that the resolution capability of EDM EFP is slightly better than that of EDM REFP. Although lacking in magnitude, the non-resonant EDM probe has a clear advantage, with better defined maxima's and minima's.

In the previous chapter, it was highlighted experimentally how detrimental the separation between probe tip and DUT can be on the spatial resolution. Therefore the initial separation of both the EFP and REFP must be equal for a fair and comparative analysis. The results presented in section 4.1.5 will show experimentally, a quantitative analysis of the separation plane. It will be seen that a difference of 15dB in the probe output will require a change of greater than 20μm in the measurement plane. To achieve such a difference in the initial probe output, would therefore be observable through the microscopic system utilised for probe positioning. However, for reassurance and confirmation on the validity of the results, separation of the probe tip and DUT was again varied with both the resonant and non-resonant probes. These measurements shown in figure 4.5. The initial separation is 30μm with an increment of 10μm between each scan.

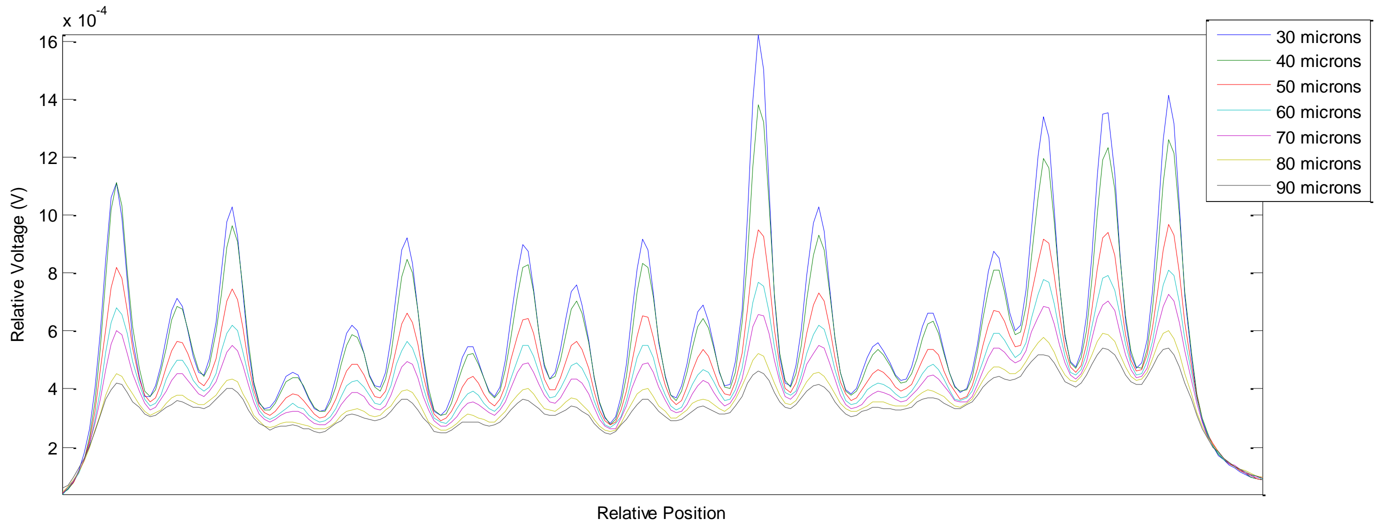

(a)

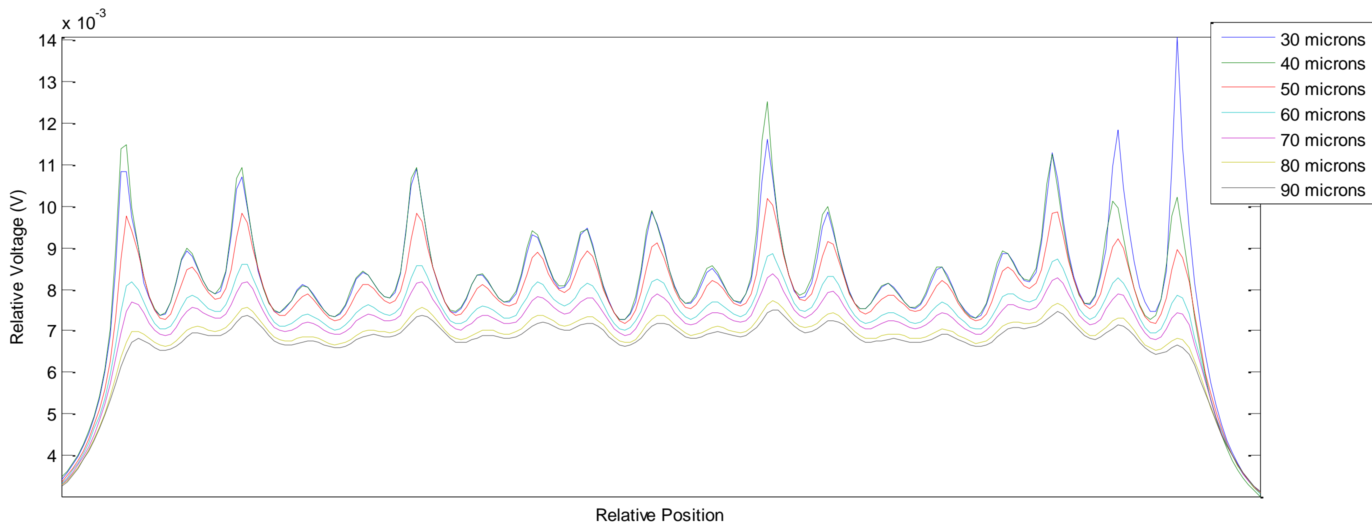

(b)

Figure 4.5: Resultant spatial resolution scans, with the transverse movement across the device with increased increments in the measurement plane using (a) EDM EFP and (b) EDM REFP.

From the data above it can be seen that the measurement plane must be increased beyond 80μm in order to achieve a noticeable degradation in the resultant resolution. A magnitude of such extent would be clearly visible and avoidable, therefore a difference in separation of the order of a few microns can be considered negligible.

4.1.3. The effect of inner conductor protrusion on the spatial resolution

One important factor which can dictate the resultant spatial resolution, is the protrusion of the inner copper conductor present at the end of EDM. Although contradicting numerous citations found in the literature on EFP, it had been noted that the presence of a protrusion can increase the sensitivity of the probe but at the cost of the spatial resolution [30].

It should be noted that the EDM EFP and REFP were constructed under a 0.7X-3X Bausch & Lômb microscope, this means that the highest available desktop magnification was used when cutting the excess copper wire once threaded through the EDM tube. Although this seemingly produced a flush cut of the inner conductor, limitations can be present in the fabrication; these can include the sharpness of the cutting blade and the maximum magnification provided by a desktop microscope.

Upon closer inspection of both the resonant and non-resonant probe, with a Nikon MM-800 Measuring microscope (with Quadra-chek 200) both probes appeared to have a slight protrusion. These protrusions measured to be 0.05mm for the REFP and 0.03mm for the EFP.

The measurements conducted within the previous section were re-taken with the removal of inner conductor protrusion, to investigate the full correlation and effect on the spatial resolution.

The first attempt for the eradication of protrusion resulted in a signal decrease of 3dB with no improvement made to the spatial resolution of the REFP. Second attempt caused the unfortunate destruction of the probe. By re-cutting and slightly retracting the inner, any and all resolution of the bondwires were indistinguishable. The SOT placed inside the brass ferrule for amplification was no longer drawing the correct current of 130mA but a reduced magnitude of 92mA, which led to the conclusion that the newly cut inner conductor was making contact with the EDM tube resulting in a short.

The resonant probe was remade with a shorted inner conductor using replacement copper wire.

Comparison scans were subsequently made before and after the removal of the protruding inner conductor for both the resonant and non-resonant EDM probes.

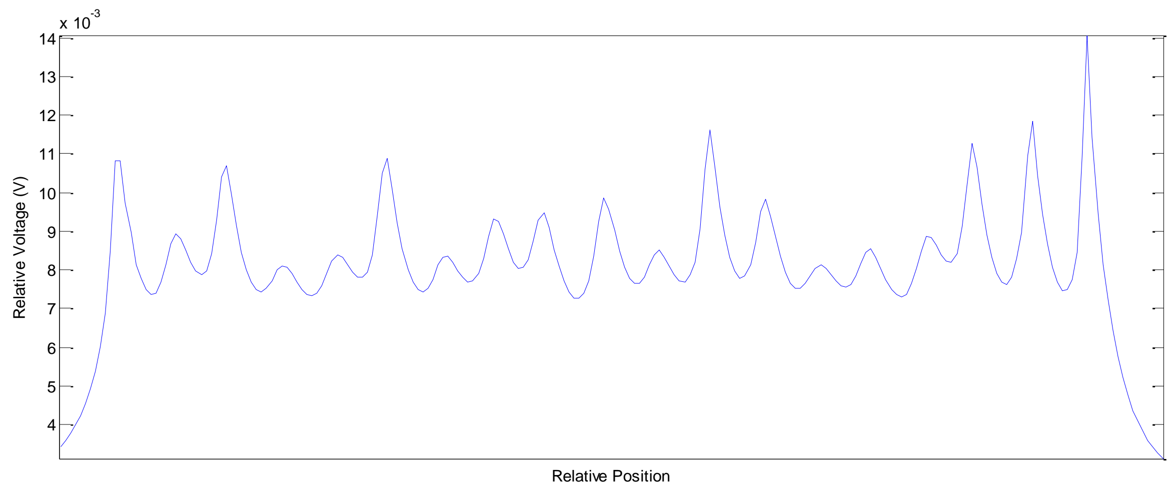

(a)

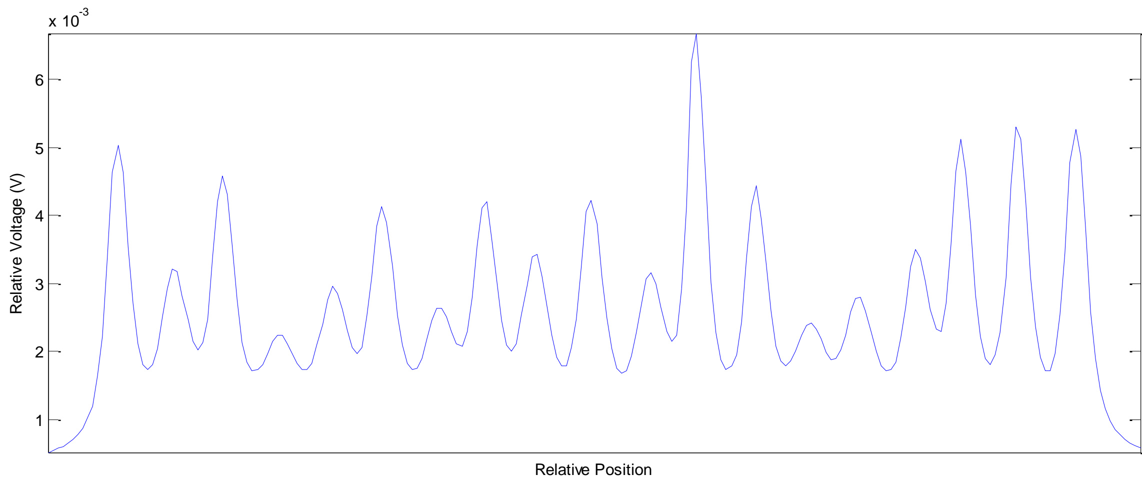

(b)

Figure 4.6: Resultant spatial resolution scans, with the transverse movement across the measurement plane using an EDM REFP with (a) an inner conductor protrusion of 0.05mm and (b) without an inner conductor protrusion, of the 19 bondwire structure.

The figure above shows the same scan of 19 bondwire structure with different inner conductor protrusions of the REFP. Figure 4.6(a) is the resultant scan of a present inner protrusion of 0.05mm; while the latter, figure 4.6(b), shows the result of no visible protrusion. The differences observed are substantial, the reduction of the central conductor protrusion diminishes the overall signal gain, by

almost four times. However, although considerable signal reduction can be seen, the improvement in spatial resolution is substantial.

Application of equation 3.12 to figure 4.6 results in the following RFS:

$REFP_{with\ protrusion} = 0.32$ and $REFP_{no\ protrusion} = 0.59$.

Showing such a reduction in the probe tip protrusion can yield a spatial resolution improvement of up to two times.

When the protrusion of the non-resonant probe is removed, the same observation is made, however to a lesser extent. The protrusion of the inner conductor present in the non-resonant probe was less than the original protrusion present in resonant probe, measuring at 0.03mm.

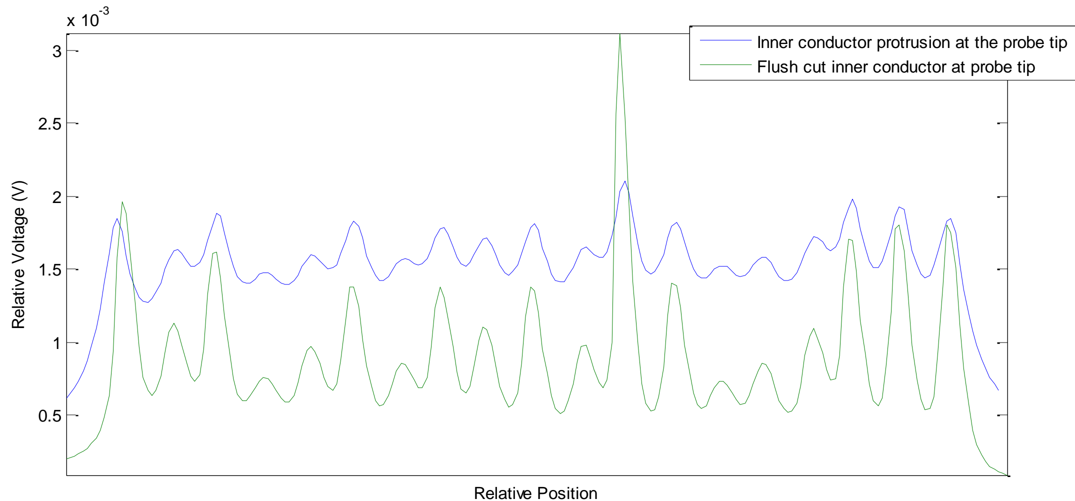

Figure 4.7: Resultant spatial resolution scans, with the transverse movement across the measurement plane using an EDM EFP with and without an inner conductor protrusion, of the 19 bondwire structure.

The eradication of the protruding inner resulted in a 50% reduction the overall measured voltage, without any compromise or degradation to the spatial resolution, but rather an increase in the spatial resolution.

Application of equation 3.12 to figure 4.7 results in the following RFS:

$EFP_{with\ protrusion} = 0.71$ and $EDM_{no\ protrusion} = 0.21$.

Clearly it can be concluded that the length of protrusion is proportional to the sensitivity which in turn is inversely proportional to the spatial resolution. Depending on the overall requirement of the probe, the protruding length must be carefully considered as this will severely compromise either its sensitivity or spatial resolution.

4.1.4. Frequency calibration

The ideal response of the EFP would be flat for frequency range that would extend to a minimum of the 3 harmonics for the intended measurements. For power amplifier systems with a fundamental at 2GHz, a flat response up to 6GHz will be the minimum requirement.

The initial construction of the EFP required probe line length of 9mm, however this length was chosen as a starting point. The full consequence of this length had not been investigated. To fully understand the consequence of the length of probe line, four subsequent EDM EFP were constructed with different conductor lengths and calibrated with regards to their frequency response.

In order to obtain the frequency response of a given probe, the probe is placed over a section of matched 50Ω microstrip line while the frequency is swept for the desired values, 500MHz to 13GHz, and the S_{21} was measured.

Due to the presence of the SOT package, the probe response will not remain perfectly flat at higher frequencies, as parasitic components will start to have a significant effect on the response.

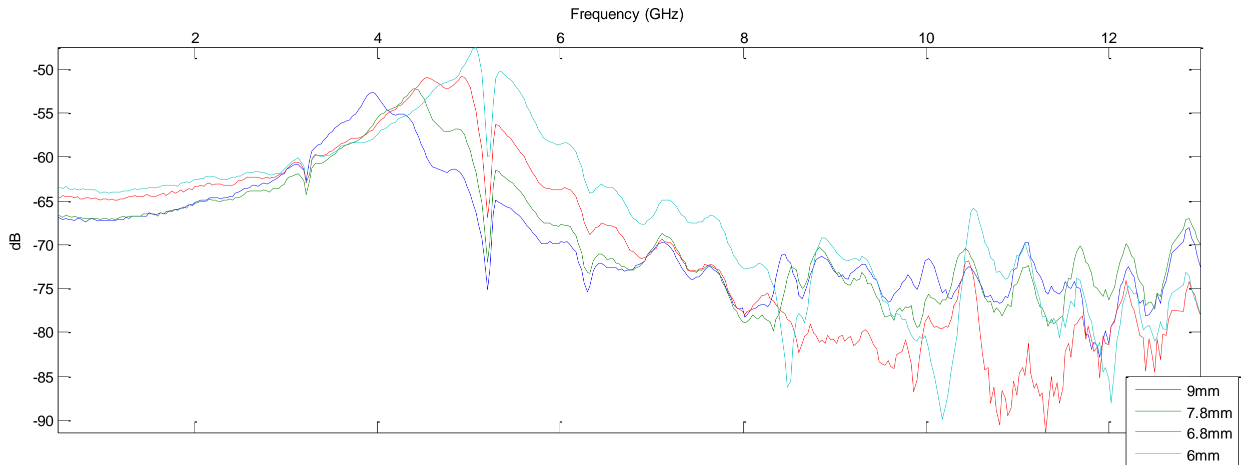

Figure 4.8: Resultant S_{21} measurement conducted on a terminated 50Ω transmission line for an EDM EFP with different line lengths.

The resonance present in the frequency response of the EFP is mainly a function of the probe line length, therefore altering the line length can subsequently shift the resonance for optimum results. Figure 4.8 shows four frequency responses for different lengths of probe line, showing the subsequent shifts in resonance. By reducing the length of the probe tip, the frequency resonance is shifted to a higher order, thus achieving a flatter response at the lower end. Although this reduction is beneficial, it has a direct impact on the separation between the brass ferrule and the DUT. Measurements conducted to determine the disturbance caused by the EFP regarded the effect of the miniaturised probe tip and the brass section, which in comparison is much larger in dimensions. It is known that the larger the foreign metal object, the greater the disturbance caused [23], therefore it would be unfeasible to reduce the probe line, such that the brass ferrule is too close in proximity to the DUT. Hence, a compromise between the optimum probe line length and therefore separation of brass ferrule to DUT must be chosen.

The design of the resonant EFP included a probe tip length of 139.55mm which yielded calculated fundamental resonance at $f_0 = 2.15$GHz, 1st harmonic of $f_1 = 4.31$GHz and a third harmonic of $f_2 = 6.45$GHz. The REFP was placed over the same section of matched 50Ω microstrip line and the S_{21} is measured for the frequency sweep of 500MHz to 8GHz, the response is shown in figure 4.9.

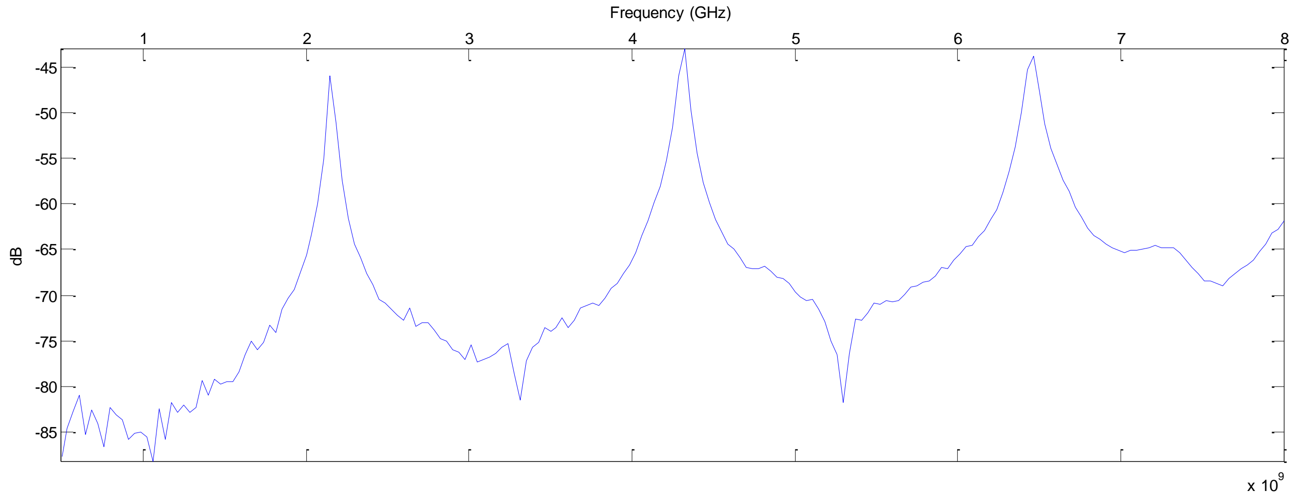

Figure 4.9: Resultant S_{21} measurement conducted on a terminated 50Ω transmission line for an EDM REFP with highlighted harmonic resonances.

The frequencies highlighted show the measured resonance and harmonic components, which is in accordance to that of the calculated values.

4.1.5. The effect of the separation between probe tip and DUT

In chapter 3 it was concluded that the effective voltage measured and the spatial resolution decreased as the separation between probe tip and DUT increased. Initial resolution scans showed a lack of complete resolution with regards to the 19 bondwire structure, therefore an increase in separation resulted in the loss of any valid data. However, with the construction of the EDM electric field probe, both the overall output and spatial resolution improved. The measurement plane under investigation within section 4.1.2 was conducted with the presence of a slight protrusion of the inner conductor. For a complete investigation of the EDM EFP with no protrusion, the measurement plane was again considered for full understanding of the resultant output and resolution.

Two experimental methods were used for this analysis, the effects of increasing the measurement plane on a terminated transmission line and transverse scans of a bondwire structure. Initial scans will show the effect as a function of measured output while the latter shows both the effect on the measured output and the resolution.

For initial experimentation two non-resonant EFP probes, with different initial outputs, were used. The first probe possessed the slight protrusion of 0.03mm therefore displayed a slightly higher initial output; while the second probe displayed a lower output as this was constructed to a flush cut. The same experimental procedure referenced in section 4.1.4 was repeated, whereby both probes were placed over a section of terminated transmission line at an initial measurement plane of 20μm. The frequency was swept between 1GHz and 3GHz, while measurements were taken at a marker frequency of 2GHz. At this marker value, the measurement plane was increased to 200μm and recorded for both probes, this is shown in figure 4.10.

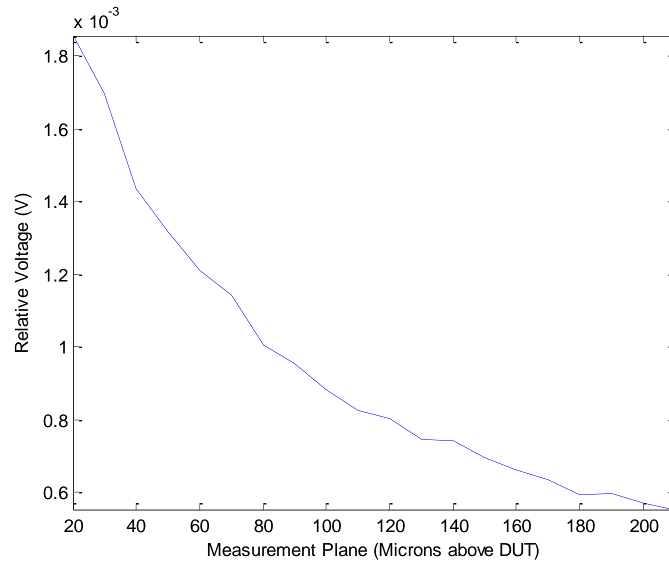

(a)

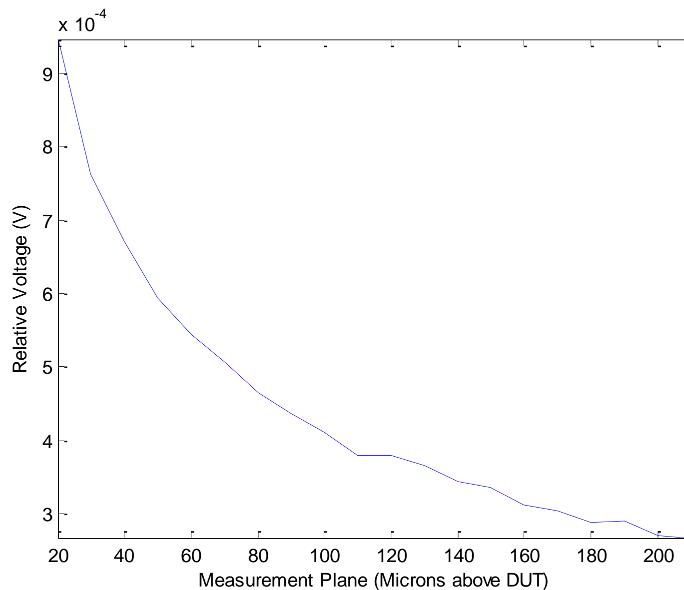

(b)

Figure 4.10: The effect of increasing the measurement plane as the probe is placed over a section of terminated transmission line for (a) a probe with higher initial output (0.03mm protrusion present at probe tip) and (b) a probe with lower initial output (flush cut at probe tip). Showing substantial degradation in the measured field as the plane is increased from 20μm to 200μm.

From figure 4.10 it can be seen, regardless of the initial output of the probe, as the measurement plane is increased, the resulting probe output is substantially reduced. Presenting a confirmation of the theory presented within previous

chapters, that the capacitive probe is heavily reliant on the air gap separation between its tip and the DUT.

Increasing the measurement plane of the EFP while conducting spatial resolution scans, the degradation seen in figure 4.11 can be quantified as a function of resolution. During this investigation both the 19 bondwire structures used for previous analysis of spatial resolution and the REFP were damaged beyond repair. At this point the REFP was deemed too fragile for consideration for future research. Although the design provided improvements in overall signal gain, its spatial resolution capability did not substantially outshine its smaller, less fragile counterpart. The difficulty presented for the construction of the 9mm EDM EFP was extremely high, the advantages of the REFP did not outweigh its disadvantages therefore could not justify the added level of difficulty required for its construction.

A new test structure was used for the effect of probe tip and DUT separation, due to the destruction of both the 7 bondwire and both of the 19 bondwire structures.

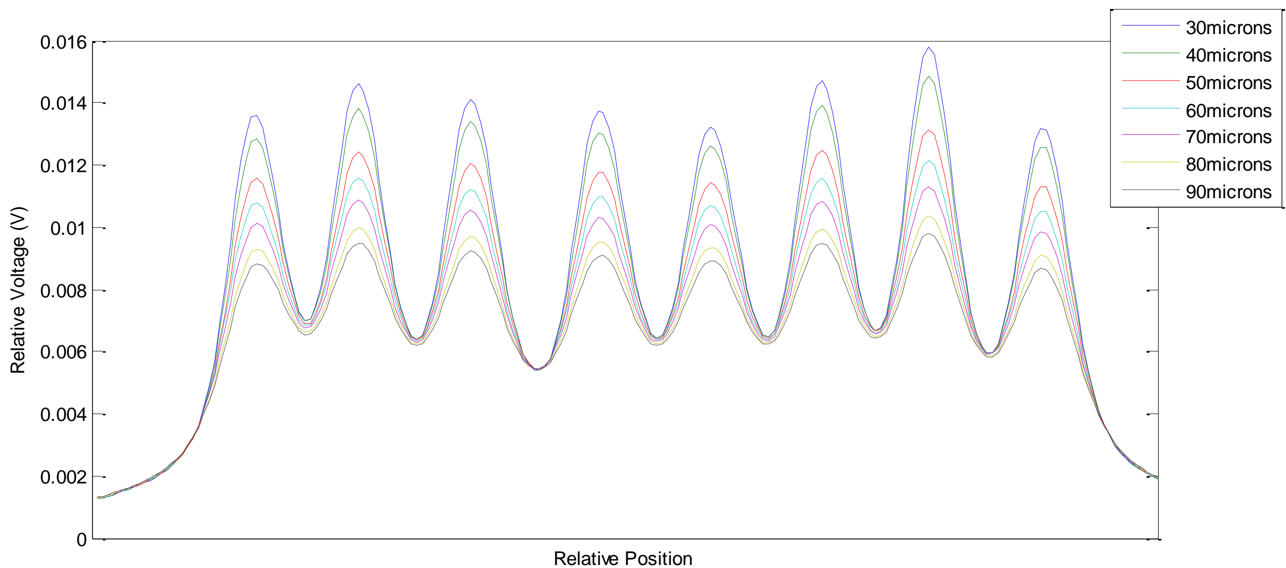

Figure 4.11: Resultant spatial resolution scans, with the transverse movement across the device with increased increments in the measurement plane using the EDM EFP for an 8 bondwire structure. Where the key represents the measurement plane, microns above DUT.

Figure 4.11 depicts the transverse scan along an 8 bondwire structure, which consists of two sections of separated transmission line joined by the bondwire array. The bondwire separation is 100μm with a bondwire diameter of 20μm. The initial scan is taken with a separation of 30μm, with subsequent scans increasing with 10μm increments.

The results seen above are in accordance to the measurement shown in figure 4.10, whereby the increase in measurement plane results in a proportional decrease in the measured voltage. Therefore it can be said that the field produced by the bondwires decays proportionally as distance is increased from the source.

One other important observation is the continued spatial resolution capability as the separation is increased, although the fingers are less defined, clear resolution can still be distinguished, unlike the results shown in figure 4.5.

The EDM EFP used for the measurement in figure 4.11 had no visible recordable inner conductor protrusion, therefore it can be seen that by minimising the protrusion present at the EFP tip, the spatial resolution can be maximised. With efforts concentrating on spatial resolution improvement, the resulting degradation of the probe output can be considered negligible.

4.2. The ultra-fine mini-coaxial EFP

With consideration of the research presented so far within this thesis, it can be concluded that the pursuit of spatial resolution can be attained by reducing the dimensions of the EFP, and minimising any inner conductor protrusion present at the probe tip. It has been previously mentioned the difficulty presented when sourcing materials which are considered 'specialist' entities or require a rather extensive budget. An ultra-fine coaxial cable was provided as a sample through private correspondence and was considered for investigation. The coaxial cable, which could be mistaken for a very thin silver wire, measured with an OD 0.096mm. Note: there was no measurement given for the ID for the conductor. With such small and rare coaxial cable, careful consideration was made for its incorporation in to the EFP design.

4.2.1. Construction of the ultra-fine coaxial EFP

Integration of the ultra-fine (UF) coaxial cable into a viable and working probe was devised and executed. The most convenient method of integration required the

insertion of the UF coax into the brass ferrule along with the extracting of the inner conductor for attachment to the gate of the SOT package. However, due to the thin and fragile nature of the UF coax, the lack of rigidity did not allow for the construction of a straight probe tip. Therefore the UF cable was inserted into a glass capillary, of diameter OD 0.097mm, to provide reinforcement and alleviate a bend in the EFP tip.

The extraction of the inner conductor was achieved by an undesirable method; whereby the outer conductor was scrapped away with a sharp blade. This method was initiated due to the nature of the application of the outer conductor, which was provided in a coil like method. The extraction of the inner conductor in such a manner will inevitably cause a certain degree of damage to the UF coax; however, this method was necessary for its extraction

Final construction of the EFP required a flush cut of the UF coax, for maximisation of spatial resolution. Cutting of the UF would prove unfeasible with laboratory cutting tools as an unavoidable pinching of the outer conductor over the inner conductor would occur. Therefore a Thales, 768nm femtosecond laser was used in order to achieve flush cut of the probe tip; resulting in a clean cut of the outer, dielectric and inner conductors. Figure 4.12, below, depicts the UF EFP with magnified pictures of the SOT package and probe tip.

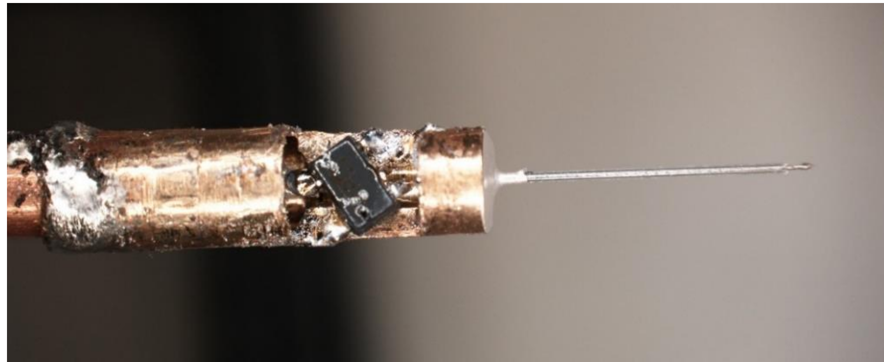

(a)

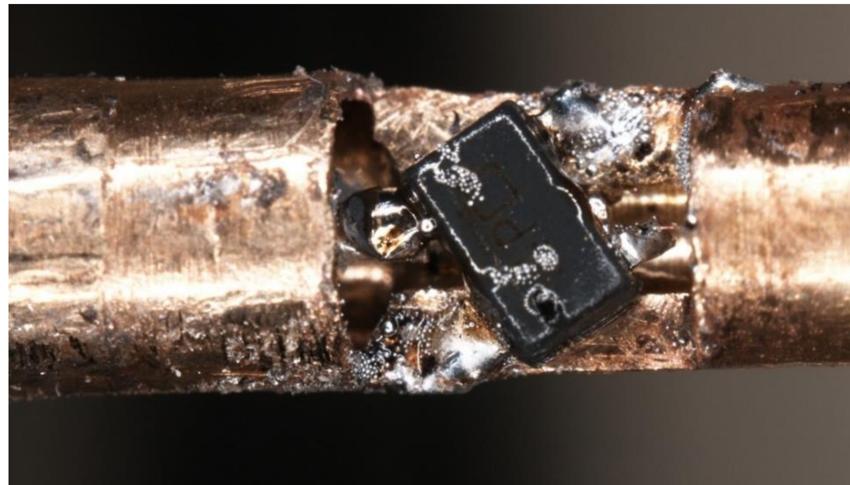

(b)

(c)

Figure 4.12: (a) Pictorial representation of the UF EFP, with magnified sections of (b) SOT package and (c) probe tip.

Note: that the construction of the UF EFP was prior to the destruction of the 19 bondwire structure, hence the spatial resolution scans include the 19 bondwire structure.

Initial spatial resolution scan provided an unexpectedly poor and inadequate resolution.

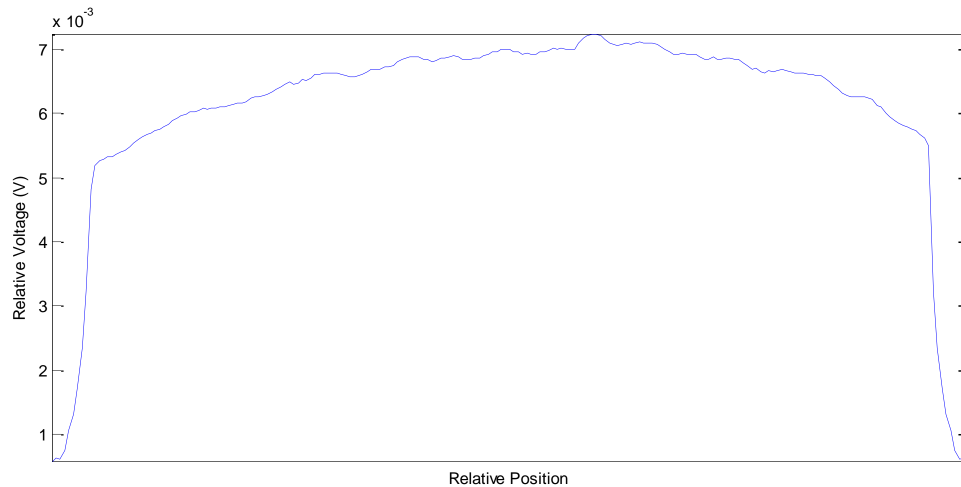

Figure 4.13: Resultant spatial resolution scans, with the transverse movement across the measurement plane using an UF glass capillary EFP of the 19 bondwire structure.

From the figure above, the results obtained from the UF EFP can be deemed unsatisfactory, despite the extreme reduction in dimensions of the coaxial cable. Although the measured voltage was distinguishable 'pre noise level' region, no resolution of the bondwires can be made.

From previous conclusions regarding the reduction of probe dimensions and the resulting improvement in spatial resolution, figure 4.13 did not correspond to such an improvement, therefore the UF EDM was assumed not to be functioning correctly.

The outer conductor of the UF coax was further investigated as the apparent coiling manner of its construction could have a direct effect on the functionality of the UF coaxial cable. Depending on an additional layer of metal beneath the outer conductor, the coiling outer layer observed will constitute in an inexorable gap in the metal sheath. Any gap, however small, will result in the coaxial cable not functioning in the correct manner. A coaxial cable, by definition, is a conductor which had been enclosed completely by another conductor, thus its ability to support TEM waves transversely along the length of the conductor. A gap would result in the radiation of electric field, as the field generated by the central conductor is not fully terminated by the outer conductor.

A closer inspection of the UF coax confirmed the method of fabrication, the cable under a high magnification is shown below in figure 4.14.

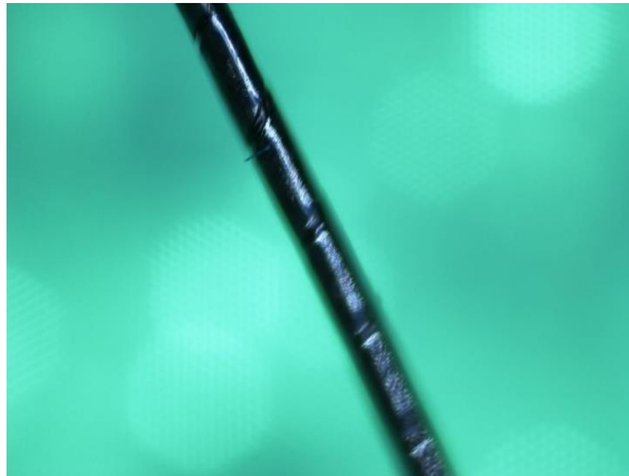

(a)

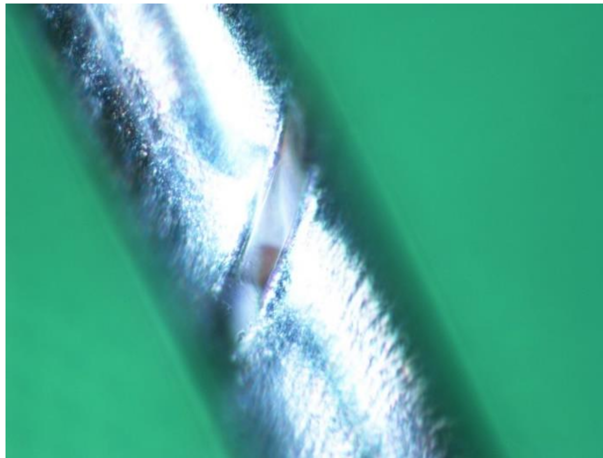

(b)

Figure 4.14(a) and (b): Magnified pictorial representation of the UF coaxial cable.

The application of the outer conductor in a coiling manor, with an increased magnification appeared to possess a gap in the metallisation.

For non-destructive analysis of the UF coax, a Wyko, NT3300, Veeco Interferometer was used for confirmation of the visual inspection. Utilising vertical-scanning interferometry (VSI), the instrument can make measurements with nanometer accuracy by the analysis of the displacement of incident waves. Accuracy of the reflected information is based on the subjects, in this case the UF coax, surface composition. Therefore resultant measurements can depict the reflectivity and continuity of a surface, this is shown in figure 4.15 below.

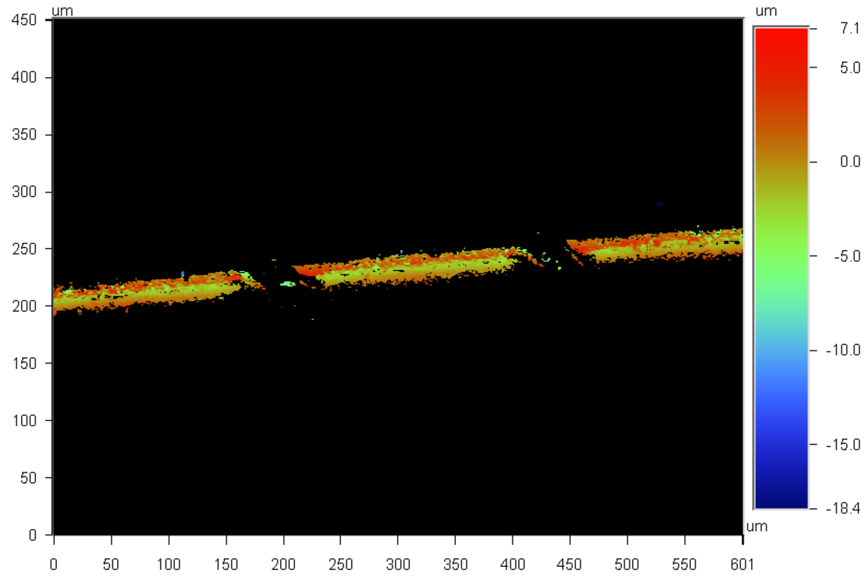

(a)

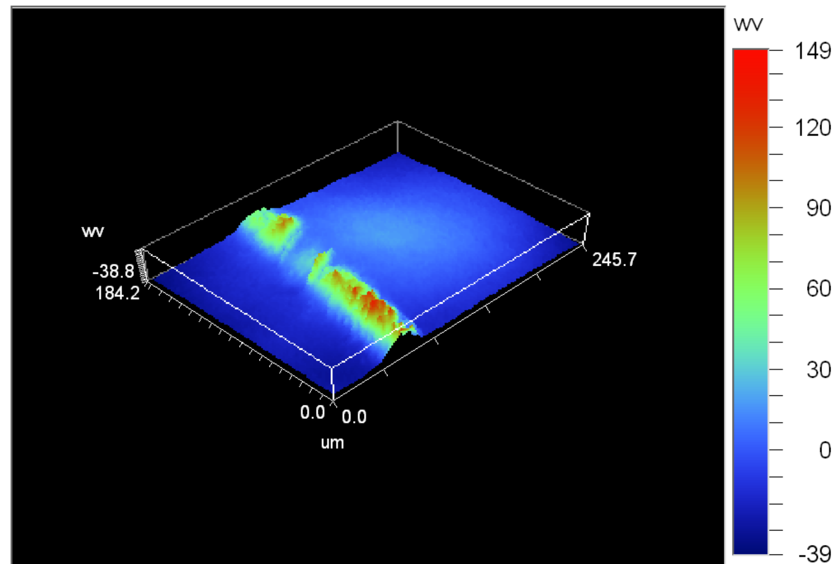

(b)

Figure 4.15: Confirmation of the air gap present within the outer diameter of the UF coaxial cable with (a) a VSI scan of 10.5X magnification and a (b) 3-dimensional reconstruction of the VSI scan with a magnification of 25.7X.

From the evidence provided, it can be concluded that there was in fact a gap present due to the coiling application of the outer conductor.

The eradication of the air gap was achieved through the application of a thin layer of silver paint to the outer of the UF coax. However, this resulted in an OD greater

than that of the glass capillary. From the materials available, the silver coated UF coax is inserted into the larger copper tube, from chapter 3, with the dimensions of: $OD = 0.58mm$ and $ID = 0.127mm$. Extraction of the inner conductor and cutting of the UF coax was achieved by the same process as previously mentioned. Subsequent repetition scan of the 19 bondwire structure would see much improvement in the spatial resolution, with no real effect on the magnitude of the measured voltage, which is shown below in figure 4.16.

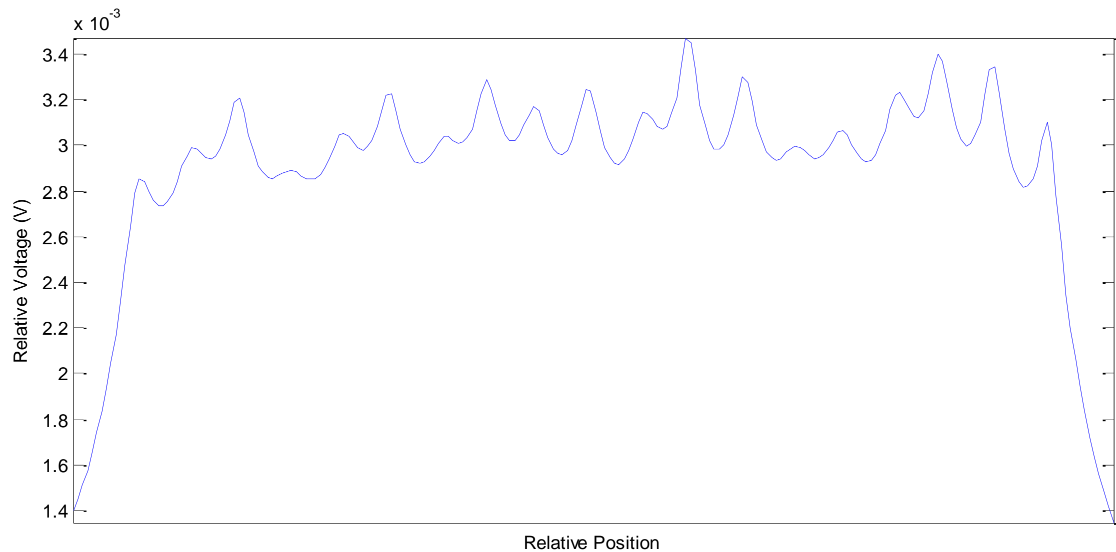

Figure 4.16: Resultant spatial resolution scans, with the transverse movement across the measurement plane using an UF silver coated, copper tube EFP of the 19 bondwire structure.

By adding the conductive paint to counteract the air gap present in the outer sheath of the UF coax, vast improvements to the spatial resolution were made. However, improvements made did not exceed the resolution capability of the EDM EFP. This is mainly due to the use of the larger copper tube which was required solely for rigidity of the flexible UF coax. Without a support frame, the silver coated UF coax was too fragile and susceptible to changes in its orientation i.e. the direction of the probe tip above the measurement phase. These changes would result in detection of orthogonal components, and without precise knowledge of detected fields, extraction of the normal electric field component would be unsuccessful. Although a promising direction for the EFP, the UF coaxial cable did not improve the spatial resolution therefore cannot be considered at this stage as a design alternative.

4.3. Conclusion

The design and construction of the EDM electric field probe has allowed for great improvements in the EFPs capabilities and characteristics. By systematically reducing both the inner and the outer diameter, the resolution capability far exceeded that of its predecessor in chapter 3. Improvements were seen in the both the spatial resolution and the sensitivity of the probes, despite its reduction in physical size. This increase in output by a factor of 10 is the result of fully understanding the effect of the probe tip protrusion and by eliminating the silver painted EFP, a concentric cylindrical miniature coaxial cable could be guaranteed. Experimental data has clearly shown that the resolution capability of the probe decreases as the protrusion present at the probe tip increased. With focus based on the importance of spatial resolution, the eradication of the inner protrusion is necessary, regardless if it is at the expense of the resultant output.

The frequency calibration of the constructed probes presented a resonance proportional to the length of the probe line. As the length of the probe line was decreased, the resonance was shifted to a higher and sought after frequency. The response shown beyond the resonance was greatly affected by the parasitic components of the buffer amplifier and unsuitable for measurement higher than 4GHz.

Unfortunately, both the resonant EFP and the UF EFP were deemed unsuitable for further consideration in this research. With the fragility of the REFP, even its storage overnight would result in an unintentional bend in the probe tip. The difficulty faced in construction of the REFP far exceeded that of the 9mm non-resonant equivalent, with its additional fragility, too much foreseeable time could be spent on making and re-making a probe which did not outperform the EDM EFP therefore could not be justified.

Although the sourcing of the UF coaxial cable seemed promising, the final construction of the UF EFP did not improve the spatial resolution, nor the sensitivity. This was primarily due to the final probe consisting of an effectively larger outer diameter than the EDM equivalent.

5. MMIC AMPLIFIED EDM ELECTRIC FIELD PROBE

This chapter will discuss the design, construction and implementation of an improved buffer amplifier which made use of a MMIC (Microwave Monolithic Integrated Circuit) technology. The MMIC amplifier will be described in detail and will show a major improvement in the frequency response of the EDM probe.

Discussion will be presented by the construction of four probes with different line and protrusion length, all integrated with a newly designed low-noise amplifier. For distinction between the probes constructed within this chapter and those in previous, the probes will be named probe A, probe B, probe C and probe D respectively.

The final section of this chapter will present an improved MMIC amplifier; designed and utilised for the improvement of the frequency response. The modification will show a flat frequency response to an improved 8GHz and result in the final EFP design used for the remaining work in the thesis.

5.1. Design and construction of the low-noise MMIC

The improvement of the resultant frequency response of the EFP required the redesign of the buffer amplifier. It has been shown that the resonance present in the frequency calibration is largely due to the length of the EFP line; however frequencies beyond this range are a result of the dominating parasitic components. The SOT, first introduced as a method of amplification of the small signal, its presence also resulted in the eradication the stray pickup from the feeder cable. Therefore measurements required beyond 4GHz need modification from the pre-existing method of amplification.

5.1.1. Design of the low-noise MMIC

The EDM EFP presented in chapter 4 provided excellent spatial resolution and adequate output for the measurement of passive devices. However, the frequency response of the EFP was not sufficient to satisfactorily measure high power devices due to the harmonic behaviour present at high frequencies. For minimisation of harmonic modulation, the frequency response of the probe must be improved beyond 4GHz. As previously mentioned, the resonance present in the frequency response can be shifted to higher frequency by reducing the line length. This reduction in line length will result in a closer positioning of the brass ferrule to the DUT, which will ultimately cause divergence and disturbance to the field produced by the DUT.

Re-design of the buffer amplifier is the only viable method for further improvement of the frequency response, reducing parasitic components and flattening of the resonance.

The pHEMT MMIC amplifier, for the replacement of the SOT package, is designed to operate over wideband frequency, from DC to 20GHz, and to facilitate an open circuit at the gate bias.

The layout of the new GaAs MMIC pHEMT is shown below in figure 5.1. The dimensions are in microns.

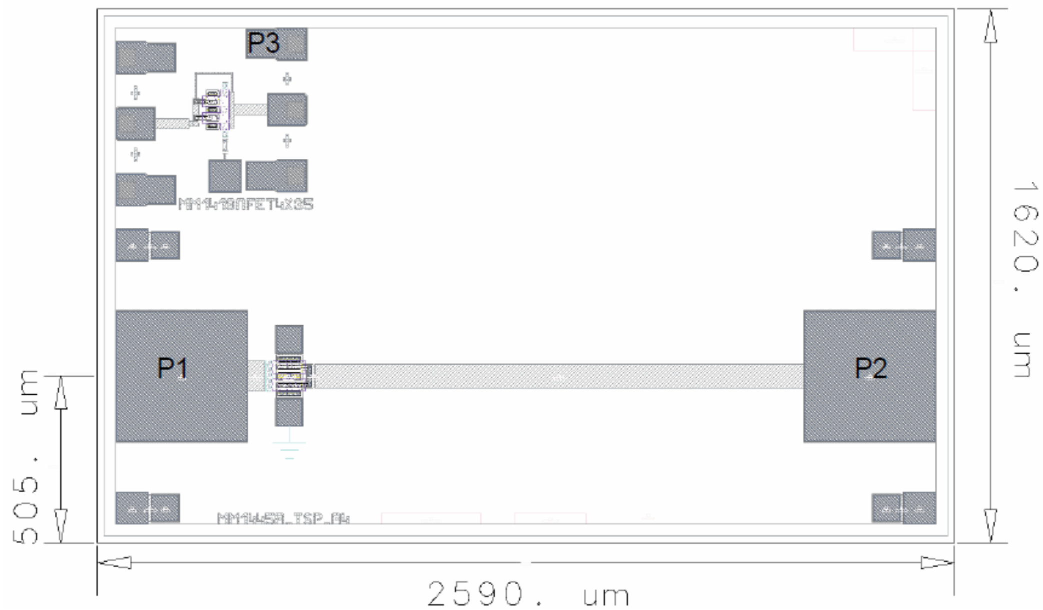

Figure 5.1: Layout of the pHEMT MMIC chip, with physical dimension highlighted.

The design of the MMIC was implemented using National Instruments, AWR Design Environment. Component parameters were chosen through optimal output requirements. By utilising the tuning tool, the required frequency response could be obtained. The circuit diagram is shown below in figure 5.2, where the following abbreviations have been made:

C1 represents the capacitance present between the probe tip and DUT, which has been estimated using the dimensions of the inner EFP conductor.

TL1 represents the length of the probe line, which can be altered in accordance to the optimal resonance required.

L1 is a small inductance required for a shift of resonance to a higher value.

L3 and C3 are shunt inductance and capacitance, respectively. Increasing their value sharpens the resonance peak as well as effecting the low-frequency roll-off.

Figure 5.3 indicates the simulated frequency response of the MMIC EDM EFP, predicting a flat response to 7GHz.

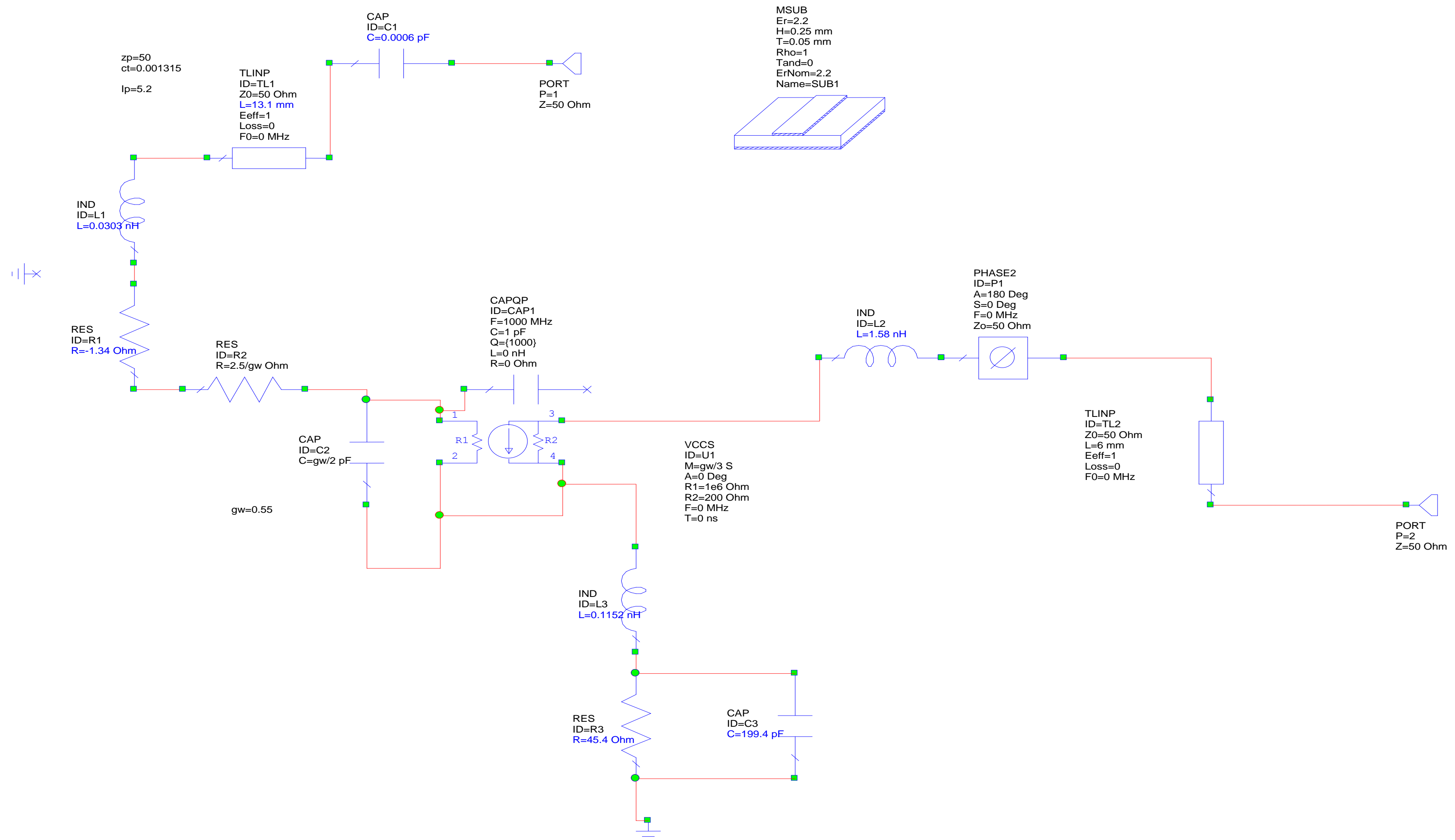

Figure 5.2: Circuit diagram of the simulation conducted for the design of the MMIC die. Tuned for an optimal flat frequency response beyond 7GHz.

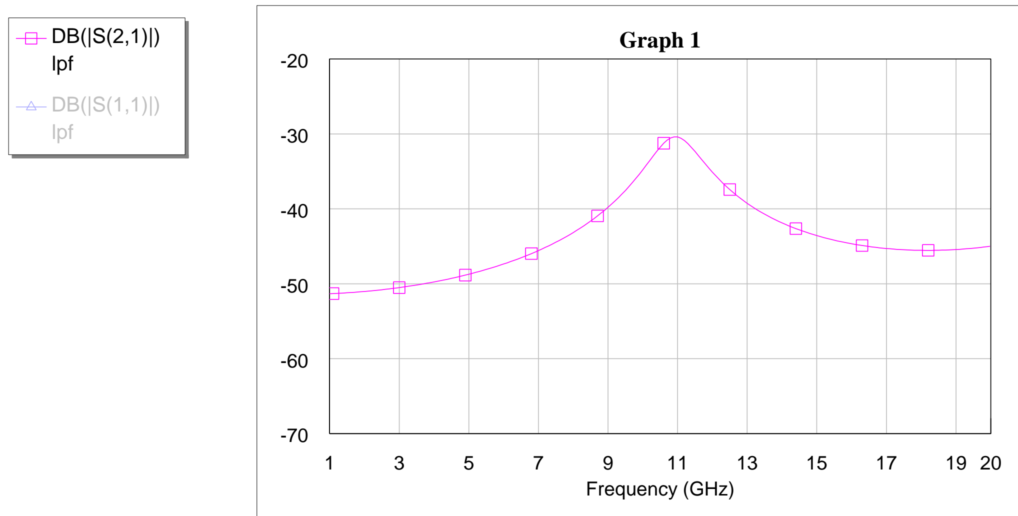

Figure 5.3: Simulation of the predicted frequency response for the MMIC amplified EDM EFP, with expectations of a flat frequency response to 7GHz. Note: the length of probe line used for the simulation is 9mm.

The dimensions of the new buffer amplifier are such that the existing brass ferrule required minimal modification for its housing. The previously hollow section beneath the SOT package was left flat, this resulted in a correct ground termination and attachment of the MMIC die was by epoxy. From the diagram seen in figure 5.1, the indicated labelling for the bonding pads are such; P1 is the gate, which is the open circuit at the probe tip, while P2 is the drain pad, to which bias is externally applied by an external biasing network. P1 and P2 both measure 400μm in length and width.

The MMIC chip, part number MM1445A_TSP_A4, was fabricated at RFMD (Newton Aycliffe) GaAs foundry.

5.1.2. Construction of the MMIC EDM EDF

Previous incorporation of the SOT package required the use of solder for correct connection of the SOT tabs. Unfortunately, this would not be suitable method of construction for the MMIC EDM EPF. Direct attachment of the drain pad cannot be made to the inner of the RG405U coaxial cable; an additional bondwire attachment was required for this connection.

A strategic and stringent method of construction was required for the successful construction of the probe. All the steps to be described are utilised underneath a high magnification microscope, with fabrication difficulties evident by the dimensions mentioned.

Initial steps for the construction of the MMIC EFP are similar to the SOT predecessor. A RG-4505 U coaxial cable is prepared with one end attached correctly to a SMA connection while the other end is left open, with a protruding inner conductor. The end with the protruding inner is slotted into and soldered to the brass section. To the protruding inner conductor of the coaxial cable, a small length of enamelled copper wire, with OD of 71μm, is soldered. The last section of solder required for this construction attachment of the copper EDM tube correctly within the 250μm drilled hole.

Subsequent attachment of circuitry requires the use of two-part silver epoxy; therefore between all uses of the epoxy, the probe is placed in a 100°C oven to speed up the epoxy curing process.

Firstly, the MMIC is attached and grounded to the flat section on the brass ferrule with epoxy and set aside to cure. Once secure and correctly in position, the small length of enamelled copper wire (attached to the inner of the protruding coaxial cable) is cut to length and placed on drain pad of the MMIC. Due to the size of the bonding pad (400μm) the copper wire is then secured in place with an extremely small amount of epoxy. The probe is placed to cure inside an oven to ensure no movement of the copper wire before it is securely in place.

Lastly, the inner conductor of the EDM tube is threaded, using a section of enamelled wire, 71μm in outer diameter, twice the length required. The copper wire is placed on the gate bonding pad and secured with a small amount of epoxy. This epoxy is placed within an oven to cure. Once secure, the surplus length of copper wire can be cut accordingly to the desired dimension.

Once completed the brass ferrule is encapsulated with the tight fit brass sleeve, in order to see the internal structure of the probe, figure 5.4 shows a picture of the probe without this sleeve.

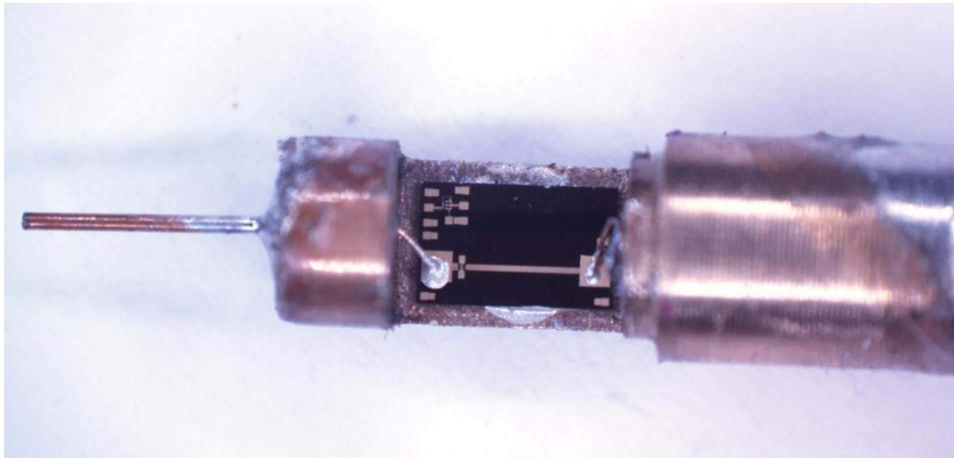

Figure 5.4: Pictorial representation of the MMIC EDM EFP, without tight fit case, highlighting the method of construction.

As previously mentioned in the introduction to this chapter, four different probes were constructed for the investigation of the frequency response, spatial resolution and the probe output. For clarity, probes were named; probe A, probe B, probe C and probe D. Although the design of the MMIC amplifier has been specifically tailored to dampen the resonance present in the frequency response, the length of the probe line will ultimately have an effect on this factor. For this reason two different lengths of probe tip were investigated, 9mm and 5mm. Thus probes A and B consist of line length of 9mm while probes C and D consist of a 5mm length.

In previous chapters, it was established that a protrusion of inner conductor can have a detrimental and proportional effect on the degradation of spatial resolution. Therefore the probes constructed have been intentionally fabricated with different and specific protrusion lengths. These are summarised below in table 5.1. Note: due to the hand-made construction of the probe, the protrusion length could not be fabricated in such a way that they are equal. The protrusion lengths were measured with a Nikon MM-800 Measuring Microscope with Qudra-chek 200.

Table 5.1: table highlighting the different dimensions and inner conductor protrusions present for constructed probes.

PROBE	*Line length (mm)*	*Protrusion length (mm)*
A	9	0.024
B	9	0.088
C	5	0.073
D	5	0.131

5.2. MMIC EDM EFP characteristics and resolution capability

The characteristics of the constructed probes were analysed for full determination of the impact of line length and inner conductor protrusion. The resulting analysis will conclude the corresponding frequency response and resolution capability.

5.2.1. Design of the flat inter-digital test fixture

The spatial resolution of each probe, tested within this chapter, has been performed on a different test fixture to that shown in the previous chapters. Section 3.1.4 showed the achievable resolution as the EFP was laterally scanned over a structure with bondwire arrays. However, due to imperfections in the fabrication stage of these fixtures, anomalies in the bondwire curvature and height existed and were subsequently present in the spatial resolution scans.

Due to the unintentional destruction of all the bondwire structures and for the eradication planarity related anomalies, a newly designed flat test fixture is described. The interdigital test fixture with gold film deposited on a 254μm alumina substrate, is aimed to emulate the previous bondwire array used in a 2-dimensional manner, thus eliminating the planarity issues. Three different test fixtures were constructed for full investigations of EFP resolution capability, which consist set of parallel 25μm thick fingers, with a separation of 25μm, 50μm and 100μm respectively, shown in figure 5.5.

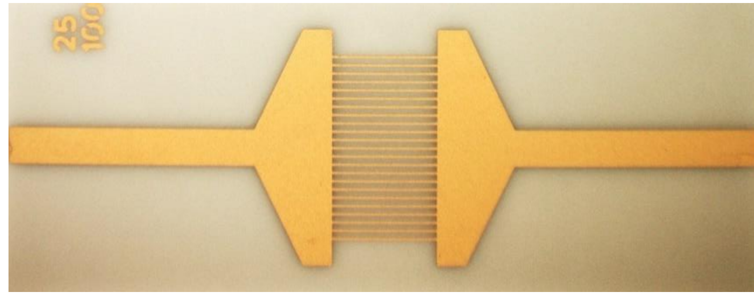

(a)

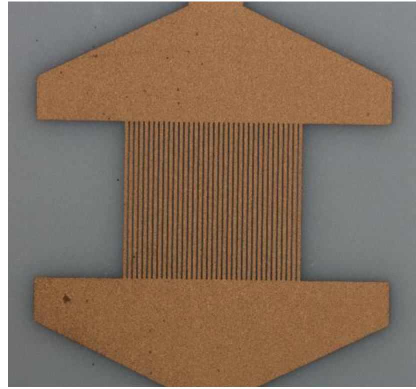

(b)

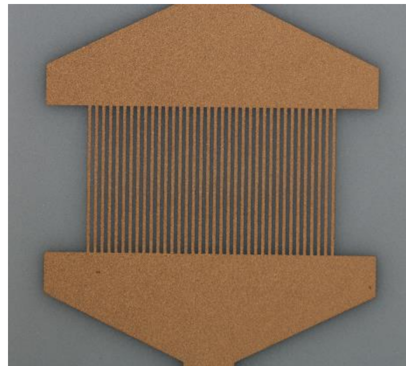

(c)

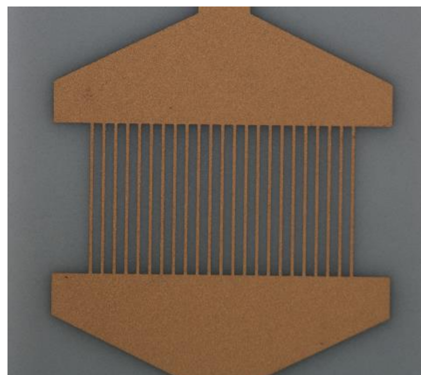

(d)

Figure 5.5: (a) Pictorial representation the interdigital test fixture designed to alleviate planarity issues, with magnification on different finger separation (b) 25μm (36 fingers), (c) 50μm (36 fingers) and (d) 100μm (23 fingers).

The test fixture shown above was designed to fit the H-block previously used for frequency calibration and resolution experimentation, with the same excitation through the input and the output connected to matched 50Ω termination.

Previous spatial resolution scans consisted of the movement of the DUT, while the probe remained in a stationary vertical position. For small test fixtures this method is satisfactory however, as the test fixture increases in dimensions and physical weight, this procedure becomes more impractical. At this point, the mechanism that allowed for the manual movement of the probe was altered and redesigned to incorporate a linear motorised stage. This resulted in the automatic movement of one axis, by moving the probe while keeping the DUT beneath stationary.

5.2.2. Frequency calibration of the MMIC EDM EFP

The frequency response, as previously established, is quite sensitive to the local geometry of the probe target area. As such, frequency calibrations are performed using the probes, mentioned in section 5.1.2. The experimental procedure described within section 4.1.4 was utilised for the calibration of probes A-D. Theoretical simulation of the probe predicts a flat response to 6.5GHz, with a resonance whose frequency is mainly a function of the length of the probe line. Figure 5.6(a) highlights the degree of protrusion required for, alteration of the frequency response and discussed later, the effect on the spatial resolution of the EFP. Figure 5.6(b) displays the four frequency scans for different lengths of probe line and inner conductor protrusions.

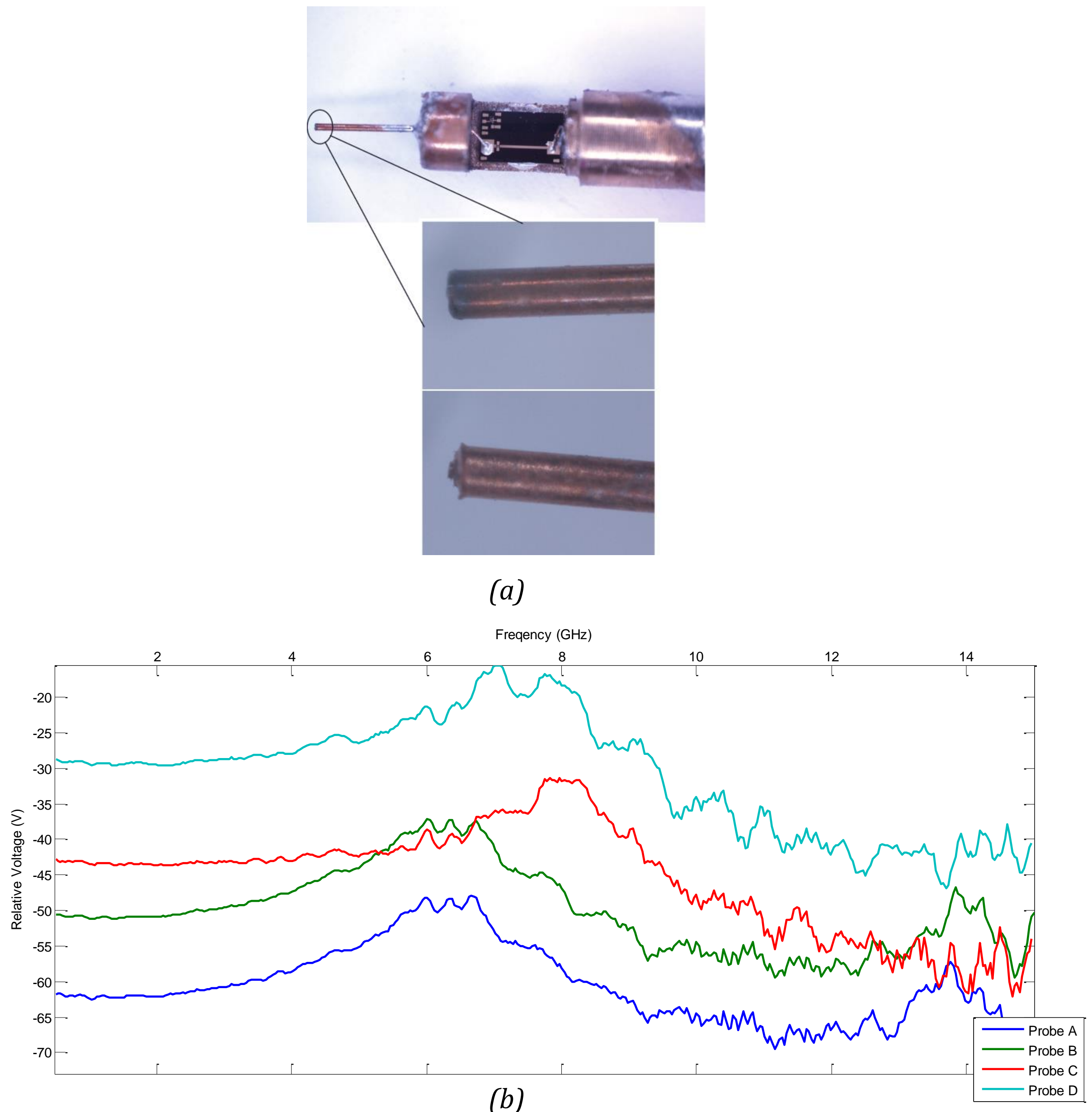

Figure 5.6: (a) A pictorial representation of the small protrusions present at the probe tip and (b) the resulting frequency response of four MMIC probes. Probe A and B have a probe line of 9mm and a monopole protrusion of 0.025mm and 0.10mm; Probe C and D have a probe line of 5mm and a monopole protrusion of 0.07mm and 0.13mm, respectively.

It can be clearly seen that an increase in probe line will result in a subsequent shift of the resonance to a lower frequency. A decrease of 4mm constituted in a resonance shift in the order of 2GHz. It has been previously discussed that a decrease in the probe line will ultimately result in the brass ferrule of the probe being situated much closer to the DUT. However, it will be shown that a probe line

of 5mm is sufficiently long enough for high power transistor measurements, required for both metallisation and bondwire measurements.

From figure 5.6, the response of the EFP is clearly a factor of both the protruding inner conductor and the length of the probe line. Consideration of the same probe line length, consistent in the 9mm and 5mm design; as the length of the protruding inner increases, so too does the probe output.

Consideration of only probes B and C, a contradiction is shown. Although the length of protrusion for probe B is greater than probe C, the output of probe C is greater than that of probe B (in the order of 8dB). Therefore the corresponding frequency response of the probe is dependent on both the length of inner conductor protrusion and the length of the probe line.

Figure 5.7 below highlights the resultant improvement in the frequency response between the SOT (taken from figure 4.8) and the MMIC amplified EDM EFP.

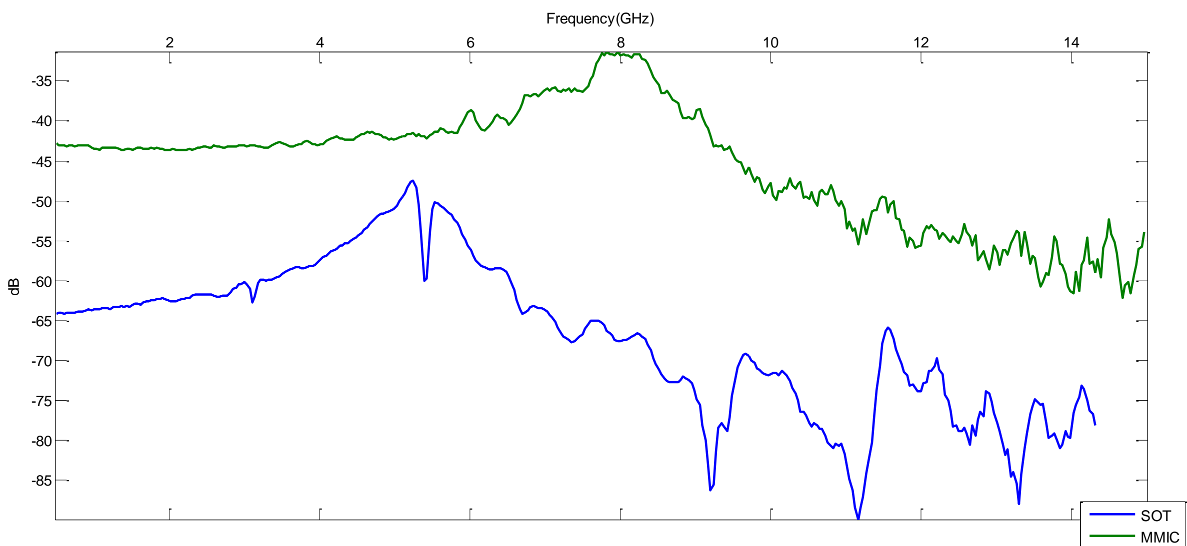

Figure 5.7: Comparison of the frequency response of the SOT and MMIC amplified EDM EFP. Showing a resultant improvement in the bandwidth and shift of resonance to higher frequencies.

The figure above clearly indicates the improvements in bandwidth of up to 2GHz with a subsequent shift of resonance. Beyond the resonant frequency both responses show a dominance of parasitic components.

5.2.3. Spatial resolution of the MMIC EDM EFP

Spatial resolution scans are conducted due to the successful completion of the frequency calibration of all probes within the previous section. From work citied in

previous chapters, there is an expectation for a degradation of spatial resolution with an increasing protruding inner. The subsequent spatial resolution scans of the flat interdigital test structure, with a finger spacing of 100μm, using probes A and B, are shown below in figure 5.8.

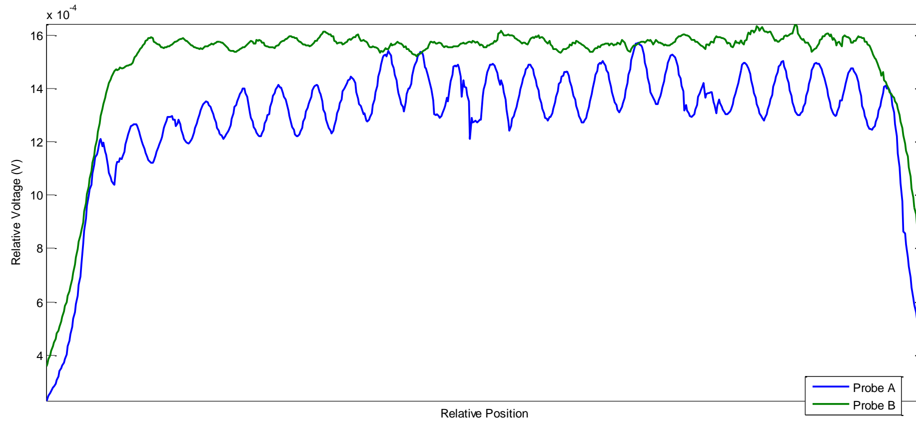

Figure 5.8: Resultant spatial resolution scans, with the transverse movement across the measurement plane using probe A and B of the 100μm *test structure.*

The figure shown above clearly indicates a substantial improvement in the spatial resolution as the length of the protruding inner conductor is decreased, as previously concluded, this is at the expense of lower output.

The same scan was repeated in order to test the spatial resolution of probes C and D, shown in figure 5.9.

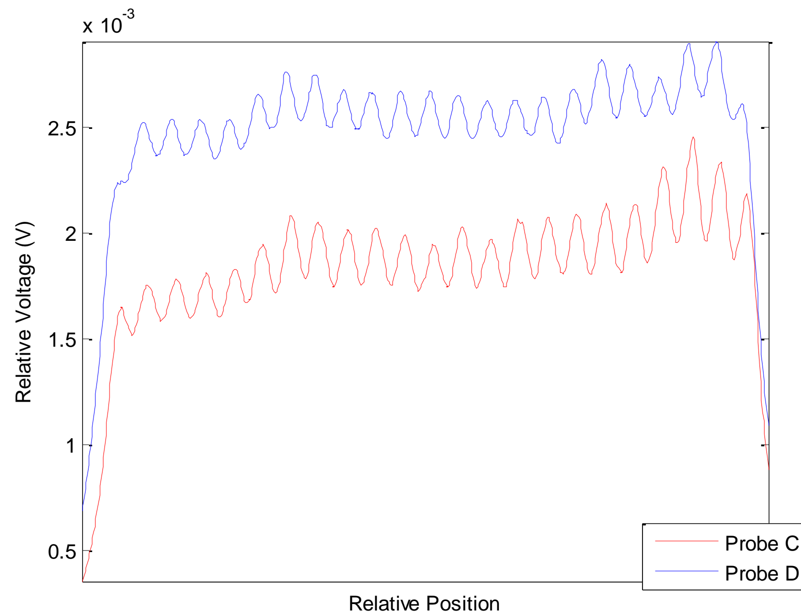

Figure 5.9: Resultant spatial resolution scans, with the transverse movement across the measurement plane using probe C and D of the 100μm *test structure.*

The transverse scans along the 100μm test fixture shows a less extreme variation in spatial resolution when comparing probes C and D. Disregarding the extremity, there is still a visible improvement in resolution by reducing the inner conductor protrusion. This is coherent to previous conclusions and measurements regarding probes A and B.

Comparing the two figures containing the spatial resolution scans, it can be seen that the relative voltage measured is in accordance to the frequency response, where by the output measured by probe D is the greatest, followed by C, B, and lastly A.

With further evidence verifying the effect probe tip protrusion and the resulting consequence on the achievable spatial resolution, probe construction must adhere to the most minimal protrusion possible. However, due to the impracticalities arising from hand-made construction, at no single time can two probes be made exactly the same. Though great efforts are made for uniformity, human error will inevitably have an effect, regardless if the materials used are consistent.

5.2.4. Spatial resolution capability beyond 100µm

The design and construction of the EFP's mentioned thus far within this chapter have all successfully resolved the finger separation of 100µm test fixture, however no scans have been conducted to further test the resolution capability. By replacing the 100µm test fixture with that of a 50µm fixture, further investigation can deduce the full extent of the EFPs resolution. Figure 5.10 below shows the transverse scans along the test fixture with finger separation of 50µm.

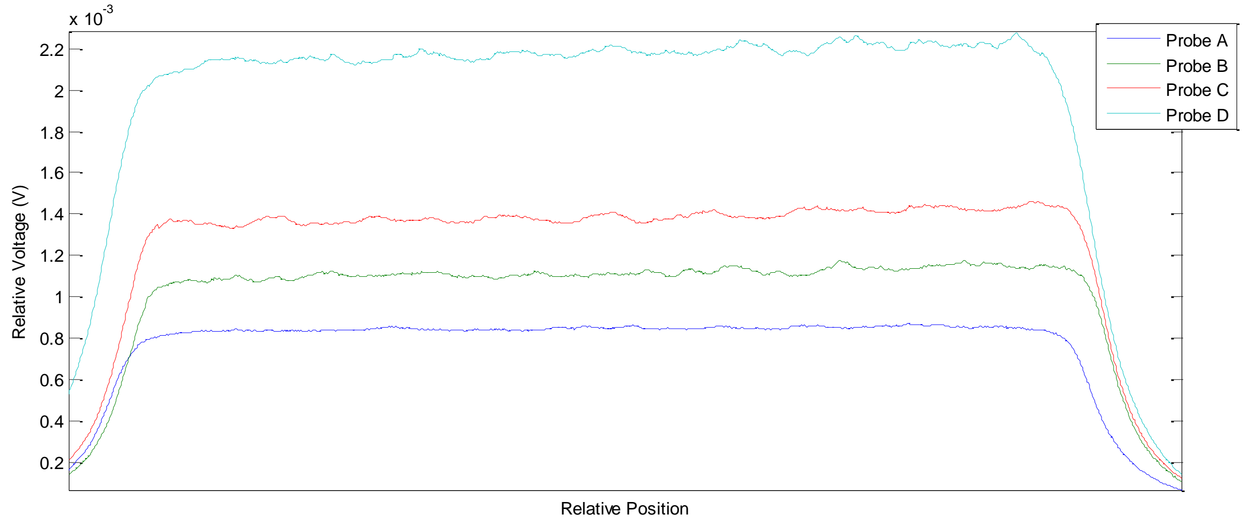

Figure 5.10: Resultant spatial resolution scans, with the transverse movement across the measurement plane using probes A, B, C and D of the 50µm test structure.

The corresponding scans along the 50µm test fixture clearly indicate the lack of detail with regards to the fingers resolution. The irregularity in the distribution, i.e. not completely flat, would suggest that each probe can slightly resolve the test fixture. If the dimensions of the test fixture are smaller than the resolution capability of the probe, the probe will not 'see' the fingers but rather depict a section of continuous microstrip line.

It should be noted that many versions of the EFP were constructed during the course of this research, due to their unintentional destruction. One such probe made, with the same EDM dimensions as in probe C, had the ability to resolve the 50µm structure, and the resultant scan is shown in figure 5.11.

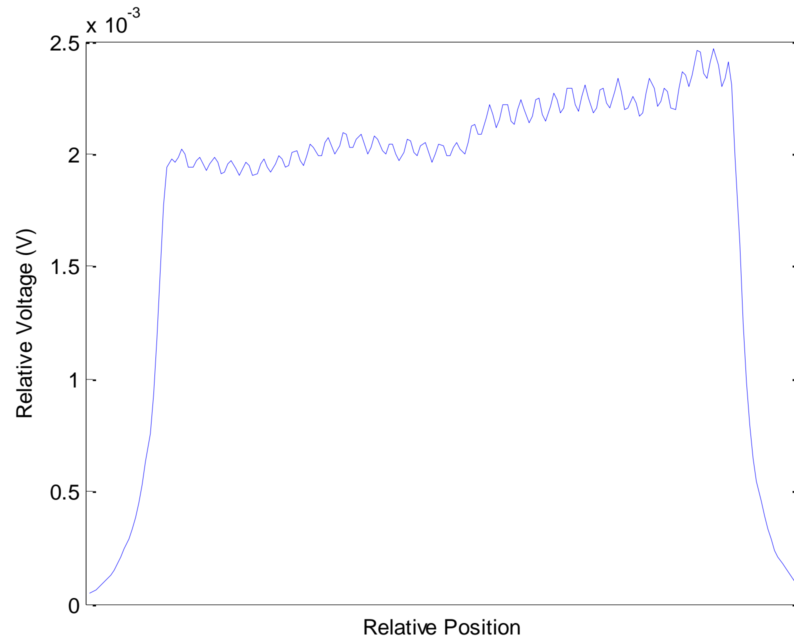

Figure 5.11: Resultant spatial resolution scans, with the transverse movement across the measurement plane using an EFP of the 50μm *test structure.*

From the figure above, clear resolution of the individual fingers are successfully made. However, no other probe constructed with the same dimensions and materials had the capability of this resolution. Resolution beyond the 100μm test fixture contradicts the theory presented in section 2.5.1; whereby the inner conductor of the electric probe would be expected to simultaneously couple with adjacent fingers due to their close proximity. Nevertheless, results presented in figure 5.10 clearly state otherwise. Possible explanation can arise from the method of construction. The threaded inner conductor was twice the required length, only when the opposing end is securely attached to the gate bonding pad of the MMIC, is the excess cut away. During the cutting stage, the copper wire can be potentially deformed, i.e. the introduction to a slightly sharpened tip. This would effectively reduce the coupling and plate area, which would result no further simultaneous coupling of adjacent fingers and therefore achieving 50μm resolution. This unintentional introduction of a sharpened tip can also explain the lack of repeatability with regards to the construction of further EFP's with increased resolution.

Further investigation of the probe tip and repeat scans of the 50μm structure resulted in the discovery of another unintentional fabrication by-product. The scan

produced above was repeated on different occasions, i.e. the probe was attached and re-attached between successive scans. Each scan conducted yielded different results, as some scans resulted in the resolution of the 50µm structure while others did not. Anomalous behaviour regarding the same probe questioned the validity of the results.

The probe tip therefore required further investigation. By placing the probe underneath a microscope, such that a top view of the probe tip was visible, positioning of the inner conductor revealed the cause of the anomalous behaviour. During the cutting of the inner conductor, not only was there a slight sharpening of the copper wire, but cutting resulted in the non-concentric positioning. At the probe tip, the copper wire was situated slightly closer to one side of the EDM tube. A marker placed on this side concluded that the orientation of the probes position coincided with the increased spatial resolution. If the probe was rotated 90°, 180° of 270° from the marker, resolution of the 50µm structure was not successful, however, complete 360° rotation to original marker position resulted in the 50µm resolution. With the central conductor positioned slightly closer to the EDM tube at the probe tip, a unidirectional increase in spatial resolution was achieved.

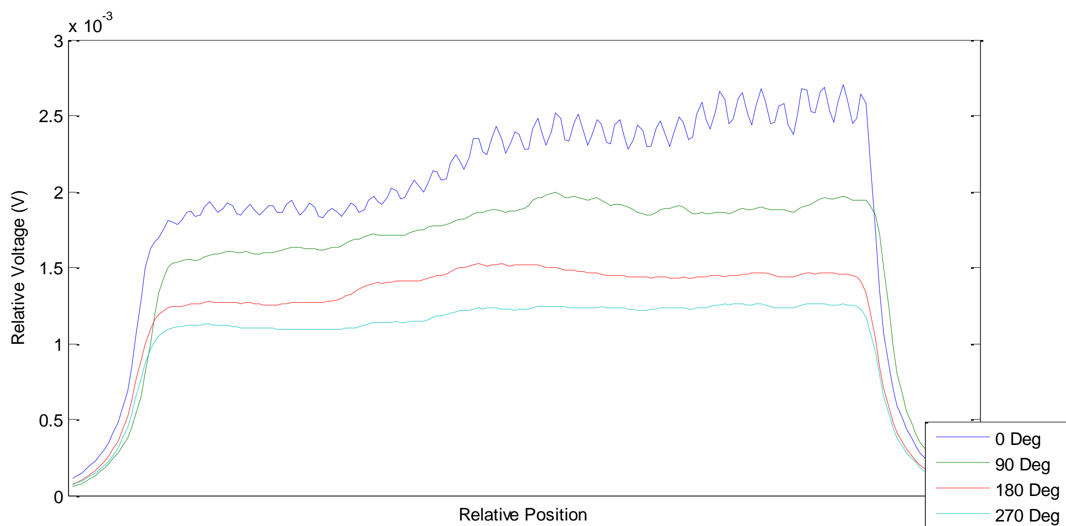

Figure 5.12: Resultant spatial resolution scans, with the transverse movement across the measurement plane of the 50µm test structure using an EFP at different orientation to the 'working' marker. Where the key represents: '0 Deg' is defined as the 'working' orientation with further rotations from origin '90 Deg', '180 Deg' and '270 Deg'.

From the results shown above, the orientation of the probe tip dictates the resolution achieved due to the non-central positioning of the inner conductor at the probe tip. The 'working' orientation was achieved due to the concentration of electric field distribution at the tip resulting from the reduced air gap between the two conductors. Therefore at this given orientation, the potential coupling between probe tip and DUT was increased further, resulting in a unidirectional behaviour.

The simulation shown below, shows an increase in the resulting field produced by the probe tip as then inner conductor is misplaced closer to the inner walls of the EDM tube.

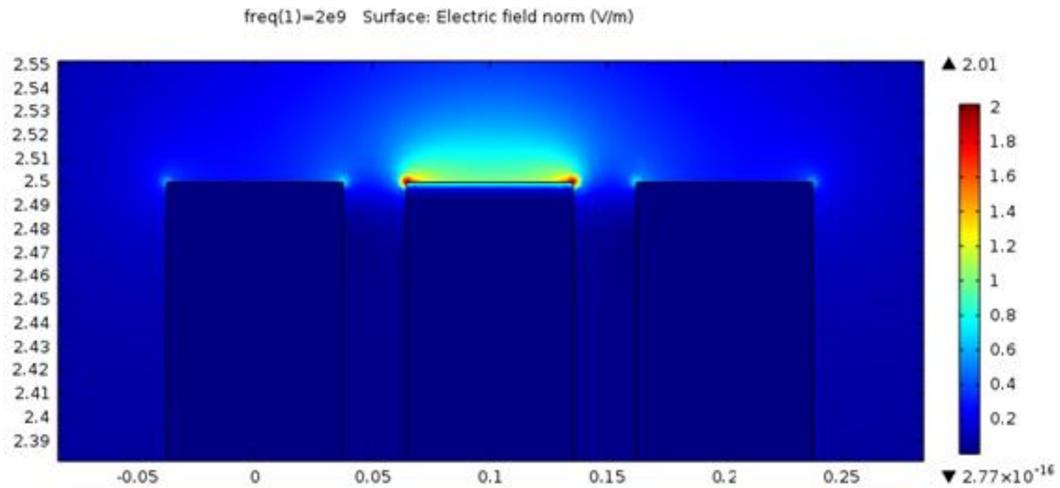

(a)

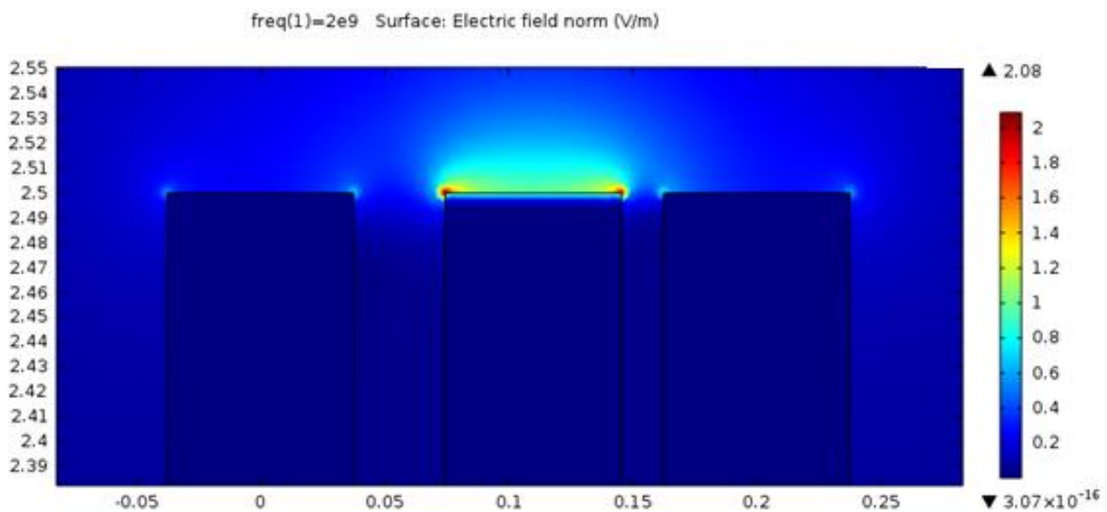

(b)

Figure 5.13: EM simulation supporting the 'unidirectional' behaviour of the probe; where (a) displays a central inner conductor placement and (b) displays a central inner conductor misplaced by 0.01mm. Showing a higher resultant field magnitude with a displaced inner.

It should be noted that closer inspection of previous probe tips, with regards to the EFP's used for the resultant scans, shown in figure 5.8; proved to have no axial displacement of the inner conductors, nor was there evidence of a sharpened tip. For this reason, no resolution can be made of the 50μm structure, regardless of the orientation of the probe tip.

5.3. Design and characteristics of alternative MMIC EDM EFP

From the previous section, the design standard for the MMIC incorporated EDM EFP has been successfully constructed and verified through frequency calibrations and spatial resolution investigations. During the design and construction stage, alternative variations of the MMIC EDM EFP were tried and tested in hope for greater improvement. Although a useful tool, the design of alternative EFPs not initialised using three dimensional software packages. For achievable expectations of the fabrication stage, alterative designs have been executed directly without prior simulation. As previously mentioned, a trial and error method of fabrication is more practical process of fully testing the abilities of the hand-made construction.

5.3.1. Glass dielectric EDM EFP

Improvements to all designs of the MMIC EDM EFP requires the development from the brass ferrule onwards, with either improvements to the buffer amplifier or reduction to the probe tip. This section describes the construction of two subsequent probes, which from theory, a lower performance would have been expected. By fabricating a design with an expectantly lower performance, confirmation is given to the theory used for previous design methods.

From the same supplier of EDM tubes, alternative diameter dimensions of tube were sourced. The EDM tube consisted of a smaller outer diameter and a larger inner diameter, measuring at an OD 0.23mm and ID 0.013mm.

From work cited in previous chapters, it has been shown a reduction in both the inner and outer diameter of the probe tip will constitute in an improvement in spatial resolution. However, the newly sourced EDM tube, although having a smaller outer diameter, has a larger inner diameter. Meaning any benefits arising from the smaller OD will be counter acted by the disadvantages of the larger ID.

A method that can be utilised for further improvements is a change in the dielectric medium present in the probe tip. The EFP described within the previous section required an enamelled copper wire to be threaded through the EDM tube. The enamel coating acted as an insulating barrier between the inner and outer conductors. The surplus of space surrounding the inner conductor is in the region

of 0.019mm, this separation is considered as the dielectric medium of the EFP i.e. air. The alteration of the dielectric medium will effect the resultant spatial resolution and output of the EFP and therefore was investigated.

Alteration of the dielectric medium will have a direct effect on the attenuation, α, of the wave propagation of the measured electric field, as seen in equation 5.1.

$$\alpha \approx \frac{R}{2Z_0} \approx \frac{R_s\sqrt{\varepsilon_r}}{2Z_{fs}\ln(D/d)}\left(\frac{1}{d}+\frac{1}{D}\right) \qquad 5.1$$

where:

R_s is the surface resistance.

D and *d* are the radius of the outer and inner conductors, respectively.

Therefore, integration of a glass capillary, with $\varepsilon_r = 4.7$, would achieve the change in the dielectric medium. The resulting probe will be expected to achieve a poorer outcome in signal strength and resolution, due to the increase in wave amplitude attenuation. By threading the inner conductor through a glass capillary, then threading both through an EDM tube, the dielectric medium can be successfully changed.

With two alternative probe constructions, spatial resolution scans were carried out in order to quantifiably test degradation of the probes characteristics; where probe E is constructed with the alternative EDM tube and probe F is constructed with both the alternative EDM and a glass capillary as the dielectric.

Figure 5.14below shows the resulting resolution as both the alternative EDM tube probe and glass capillary probe are moved transversely across the flat alumina structure, with 100μm finger separation.

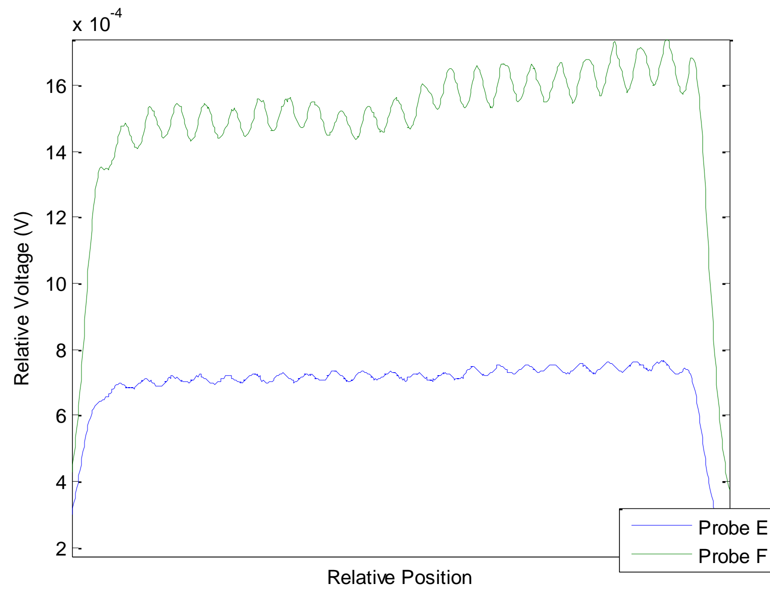

Figure 5.14: Resultant spatial resolution scans, with the transverse movement across the measurement plane using probe E and F of the 100μm *test structure.*

Although both probes are able to resolve the finger separation, they can be considered providing less signal than that of probe C, shown in figure 5.9. Probe E and probe C both yield similar resolution; however, the output of probe E is almost half than that of probe F.

With consideration of probe F, both the output and spatial resolution has degraded when compared to that of probe E. Both probes have been constructed to be identical, with only the addition of a different dielectric medium. With respect to equation 5.1, it is clear that the loss in output is consistent to the increase of attenuation by a factor of $\sqrt{\varepsilon_r} = 2.16$.

5.3.2. Construction of the 'control' EDM EFP

Previous work conducted on the EFP has found that the introduction of the buffer amplifier, close to the probe tip, can improve low pick-up while amplifying the desired signal and alleviating the problem of stray pick-up [35]. The investigation of this buffer amplifier is tested with the construction of an alternative EDM EFP. A probe without the inclusion of an amplifier is fabricated by means of the same method and materials as the MMIC EDM EFP. The inner conductor of the probe tip is extended and directly attached to the inner conductor of the standard RG 405 U coaxial cable, shown in figure 5.15.

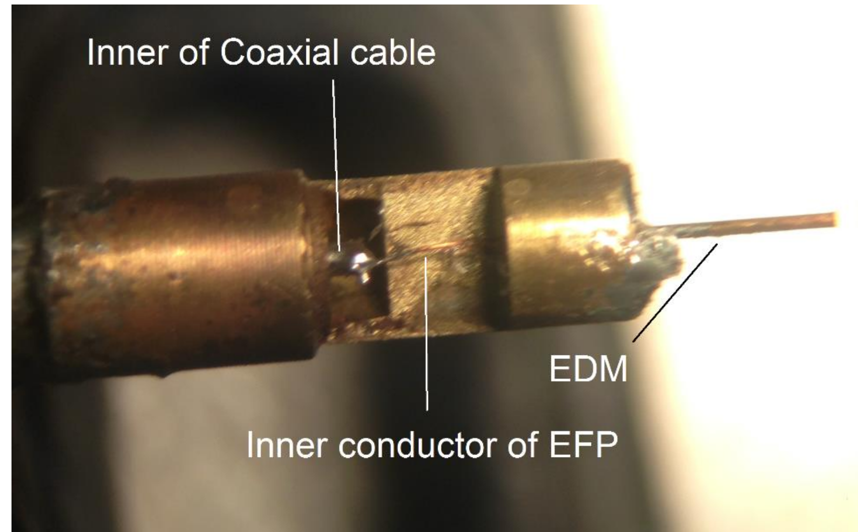

Figure 5.15: Pictorial representation of the EDM EFP constructed without MMIC amplifier for control experimentation. Picture above is shown without tight fit case.

The new orientation of the EDM EFP is still considered as a capacitive probe, where the output of the probe is still dependent on the proximity and local geometry of the DUT. However, the removal of the MMIC amplifier eliminates the gate to source capacitance, therefore the new orientation can no longer be considered as a capacitive divider.

Frequency calibration of this probe consisted of the same experimental setup and procedure referenced in sections 4.1.4 and 5.2.2. The resulting sweep is shown in figure 5.16.

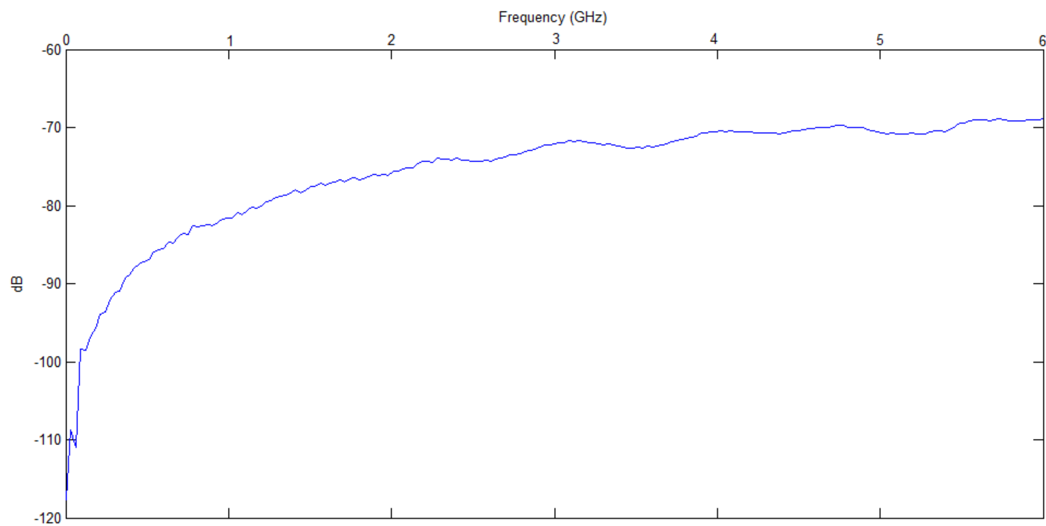

Figure 5.16: Frequency response of the EDM EFP without buffer amplifier close to the probe tip. Showing a flat frequency response free from parasitic components with a reduced output when compared to the MMIC EDM EFP.

The EFP was constructed with no visible probe tip protrusion therefore comparisons made to the frequency response of the MMIC amplified probe, shown in figure 5.6, yields a degradation of up to 40dB in the probe output. This degradation will have an effect on the performance of the probe.

Spatial resolution analysis of the non-amplified probe was performed on the 100µm interdigital test fixture and compared to the resultant scans of a MMIC amplified EFP.

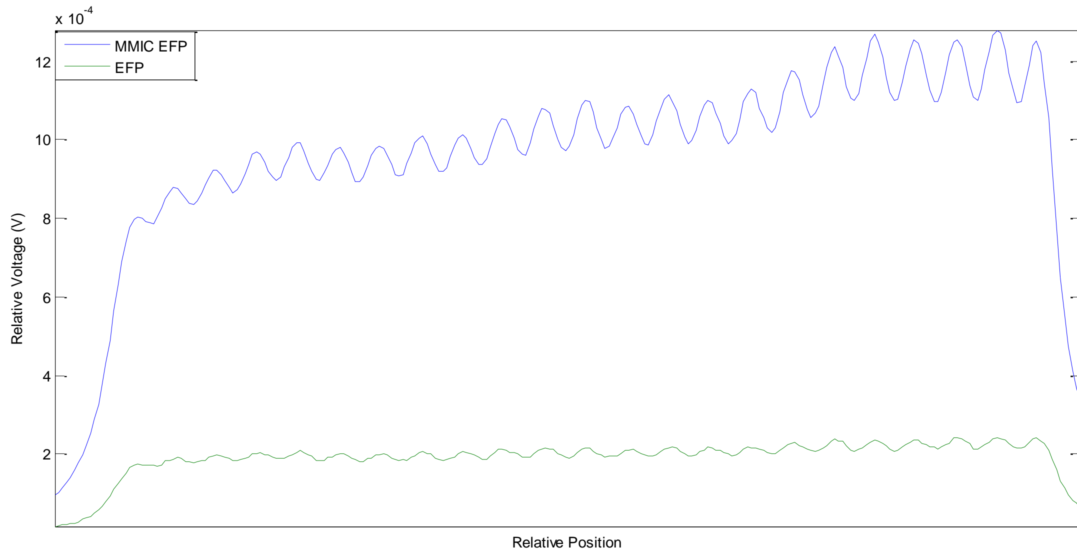

Figure 5.17: Resultant spatial resolution scans, with the transverse movement across the measurement plane using a MMIC amplified EFP and the 'control' EFP, for the 100μm *test structure.*

The importance of the buffer amplifier can be concluded from the results presented in figure 5.17. The incorporation of the MMIC amplifier improves the over performance of the probe in both output and resolution capability. The uneven nature of the 'control' EFP scan, not present in the MMIC EFP, indicates its susceptibility to stray pick-up.

It can also be stated that the response of the 'control' EFP has no dominating parasitic components, highlighting two important facts. Firstly the parasitic components present in the frequency response of the MMIC EFP are a result of the amplifier and not the construction or design of the probe; secondly, these parasitic components can be further improved with additional design enhancements of the MMIC amplifier.

Experimental data so far has shown an EFP probe capable of in-situ measurements on passive devices. Within chapter 5 the MMIC amplifier designed and incorporated for the alleviation of small signal pick-up, due to the miniaturised dimensions, had vastly improved the probes response. A flat frequency response of up to 6.5GHz has been presented, with the measurements conducted in this range have proven to be successful and accurate. However, for measurements requiring

higher frequency, due to the harmonic behaviour of the DUT the response of the probe should be further improved. By altering the existing MMIC design a theoretical frequency response beyond 10GHz can be achieved, extending the range of devices that can be potentially characterised.

5.4. MMIC design improvements

5.4.1. Extending the frequency response of the MMIC amplifier

The construction of the control EFP shown in section 5.3.2 provides conclusive evidence that the dominant parasitic components present in the high frequency response of the EFP, was a result of the MMIC design and not the construction of the EFP. Therefore, further improvements to the MMIC amplifier design can systematically improve the response of the EFP.

Theoretical improvement of the MMIC circuit response was achieved with minor design alterations of the existing layout within AWR. The addition of circuit componentry, tuned to optimal operation, theoretically improved the response of the EFP. The resulting design layout is shown below in figure 5.18

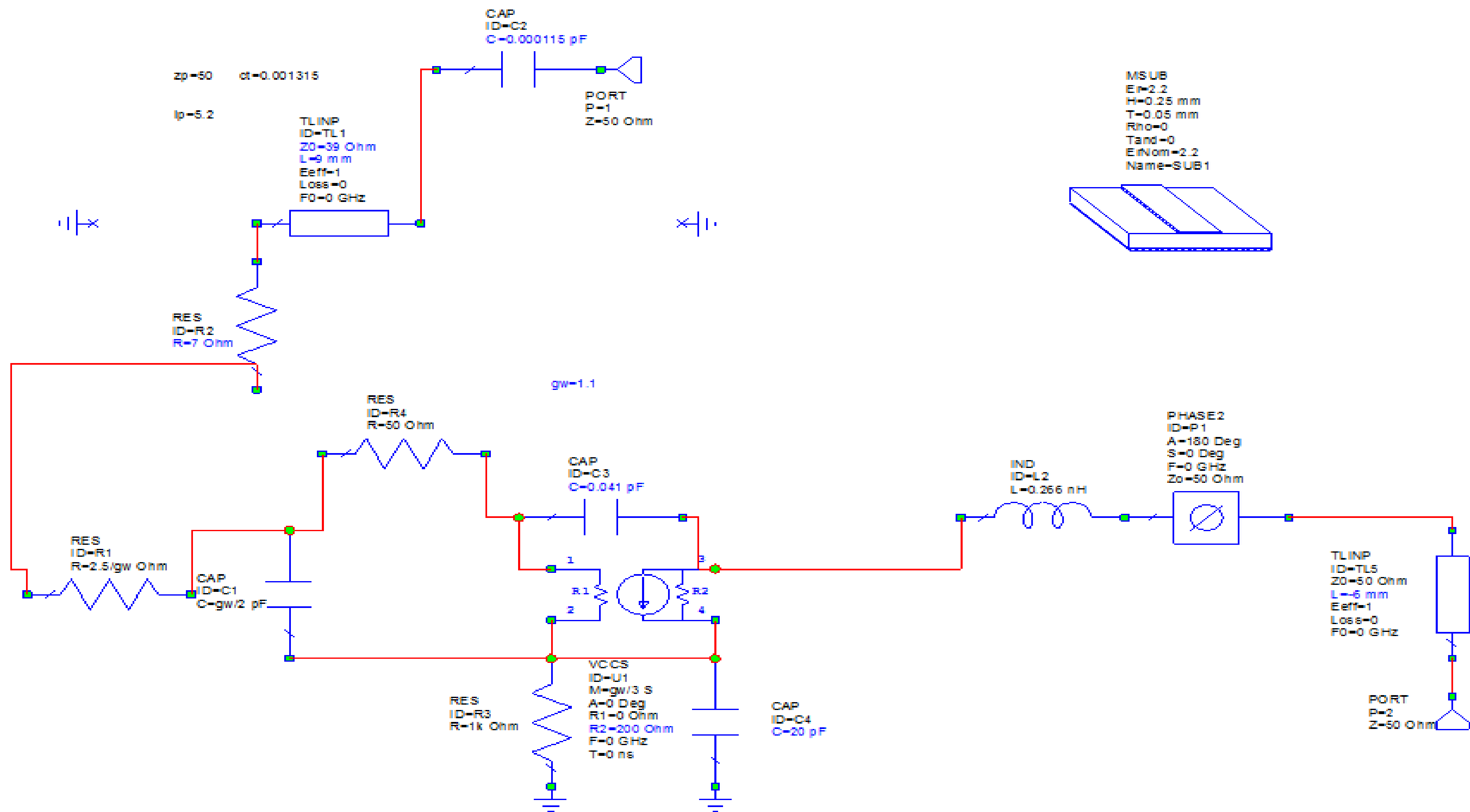

Figure 5.18: Circuit diagram of the simulation conducted for the revised design of the MMIC die. Tuned for an optimally flat frequency response beyond 10GHz.

Simulation of the circuit diagram, shown in figure 5.18, yields a theoretical expectation of a flat frequency response to 10GHz, shown in figure 5.19. Note: the shift in resonate is a result of reducing the simulated probe line to 5mm (from figure 5.3 the probe line was 9mm) and the addition and alteration of circuit componentry.

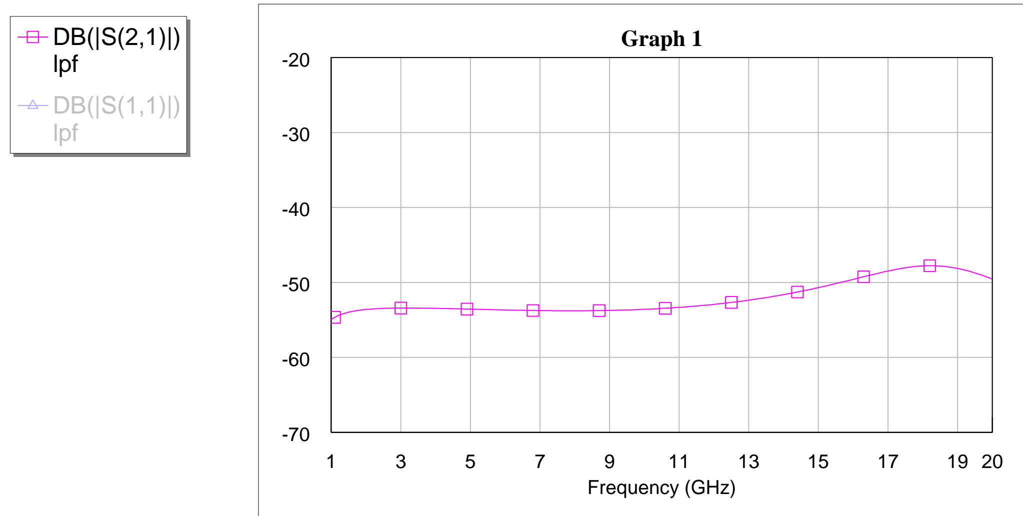

Figure 5.19: Experimental simulation of the predicted frequency response for the MMIC amplified EDM EFP, with expectations of a flat frequency response to 10GHz. Note: the length of probe line used for the simulation is 5mm.

5.4.2. Frequency calibration of improved MMIC EFP

The fabrication of the improved MMIC EFP was consistent to the method mentioned earlier within this chapter. Figure 5.20 is presented for the visualisation of the dimensions of the MMIC and probe tip.

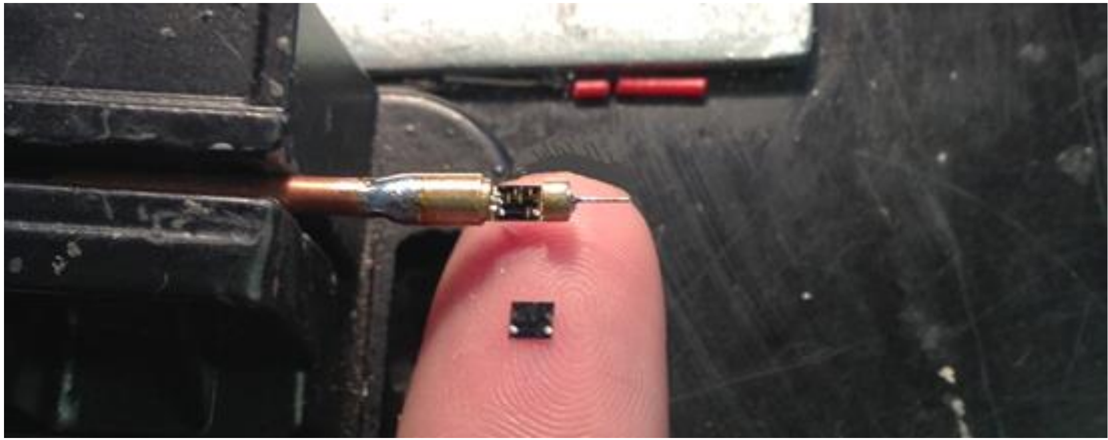

Figure 5.20: A picture of the improved MMIC amplifier in comparison to a human finger shown for visualisation of the dimensions presented for EFP construction.

Frequency calibration of the MMIC, consisted to the method utilised in section 5.2.2, yielded the result shown in figure 5.21.

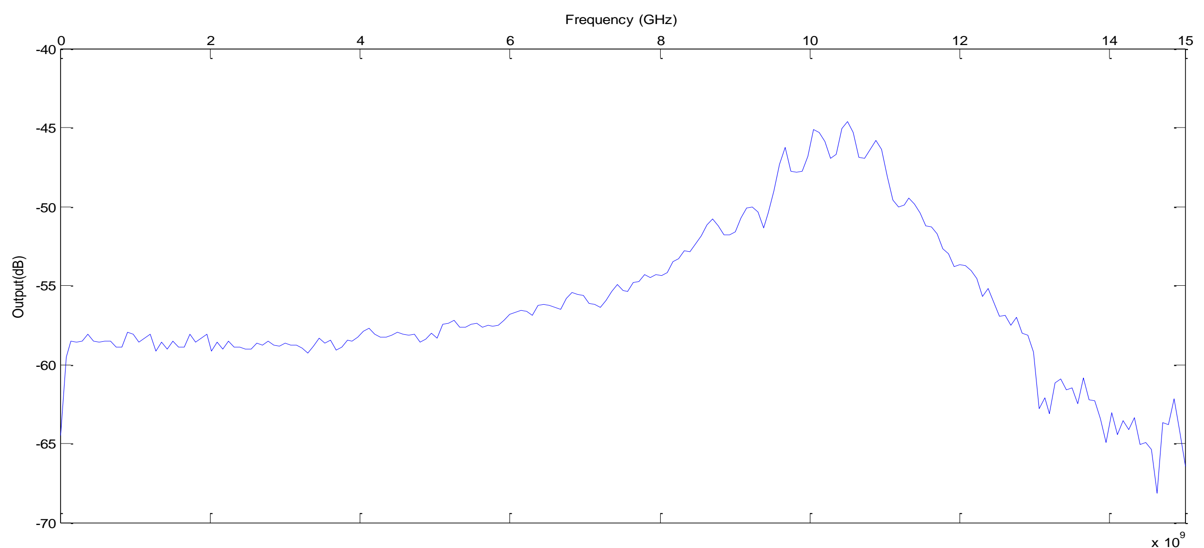

Figure 5.21: Frequency response of the improved EDM EFP. Showing an extended flat frequency response to 9GHz.

The frequency calibration of the improved MMIC EDM EFP shows enhancement in the frequency response, which has been extended beyond 8GHz, along with a dampening of the probe line dependant resonance.

Due to the improvements in the EFP response, results presented within chapters 6-8 will utilise the improved MMIC EDM EFP. However, it will be shown that this

MMIC design will not be practical for application within chapter 9 due to its low frequency response.

5.5. Conclusion

The introduction of the custom designed MMIC amplifier as a replacement of the previous SOT package has shown substantial improvement in the frequency response of the probe. The frequency response has been flattened and extended to greater than 8GHz, which is a 4GHz improvement to its SOT predecessor. The re-design of the buffer amplifier does not however improve the spatial resolution capability of the probe, as this is a function of the local geometry and dimensions of the probe.

The full effect of spatial resolution dependence by the presence of inner conductor protrusion has been shown. Further evidence has been provided by the detrimental effect that inner conductor protrusion has on the spatial resolution of the probe. The presence of the protrusion increases the effective area of coupling, therefore resulting in a higher output however, this increase systematically degrades the resolution as there is an increase in the effective inner diameter. This therefore reinforces the need for minimal inner conductor protrusion for spatial resolution maximisation.

Advantages have been shown by purposeful construction of an EFP with inferior characteristics. Although reductions made in the outer diameter of the EFP will constitute in a higher spatial resolution, this will only occur if there is a reduction in the inner diameter of the outer conductor, as shown with the construction of probe E.

The introduction of a dielectric with a higher constant has shown a proportional decrease in output and resolution, due to the attenuation of the measured signal, regardless if initial coupling of probe tip to DUT is kept constant. There is also confirmation that an air spaced EFP will have less loss associated with signal propagation.

The lack of resolution beyond the 100μm test fixture is to be expected from previous theory; as resolution of the probe is related to the dimensions of the inner conductor. Therefore, a decrease in the DUT dimensions and no corresponding reduction of the ID of the probe would indicate the reasoning behind the lack of

resolution. As the probe is moved transversely across the 50μm structure, simultaneous coupling may occur as a result of a summation in measured electric field, therefore clear distinction and resolution of the fingers cannot be made.
Unintentional resolution of the 50μm structure, although promising was deemed a result of accidental practice, and very difficult to repeat. Unintentional sharpening of the inner conductor resulted in a slight displacement in its positioning. The close proximity to one edge of the EDM tube resulted in an increased unidirectional spatial resolution. However, due to the unrepeatability of this unintentional result, the EFP cannot be considered as a probe with a resolution capability greater than 50μm.

6. HIGH POWER AMPLIFIER DIAGNOSTIC

With the successful design and construction of an EFP, with the spatial resolution capability of greater than 100μm, the transition between passive characterisation testing and in-situ active measurements can be made. The EFP can be potentially used as a diagnostic tool, with the ability to measure the electric field or waveform distribution along a given device. The first transistor under investigation is a 2000 to 2170 MHz, Freescale field effect transistor, N--Channel Enhancement--Mode Lateral MOSFET (see Appendix 4). This transistor was mounted to a test circuit also designed by Freescale. This chapter will discuss the measurement techniques required for the acquisition of the relevant data, and how these results can be used as an alternative method of device characterisation. This will be achieved by in-situ drain voltages measurements and its corresponding waveform information, which until now, have not been extracted at the device plane.

6.1. The high power amplifier, the transistor and its test circuit

As previously mentioned, the device under test was a 150W Freescale MRF8S21100H enhancement mode MOSFET, with an operational frequency of 2110 to 2170MHz. The transistor itself was packaged with a ceramic lid, which for purposes of in-situ on-chip measurements will be removed. Before the de-lidding process, each device was tested, and retested after de-lidding; by comparing the input and output characteristics of the device. The resulting variation can be compared. The removal of the ceramic lid required the use of a hot plate, in the

region of 200°C; by placing the transistor, ceramic side down, for a short period of time, the adhesive joining the lid to the metal contact below melts. With a well-practiced movement, the ceramic can be clicked off cleanly. However it should be noted that numerous transistors were in fact damaged during this process, but never used in the characterisation testing. Once the ceramic lid has been successfully removed, the transistor is placed within the test circuit for re-testing the initial power sweeps and in-situ measurements with the EFP. All measurements were taken at the device plane, therefore there were no EFP measurements before the de-lidding process.

The figure below shows the test circuit and the de-lidded transistor presented to the measurement system.

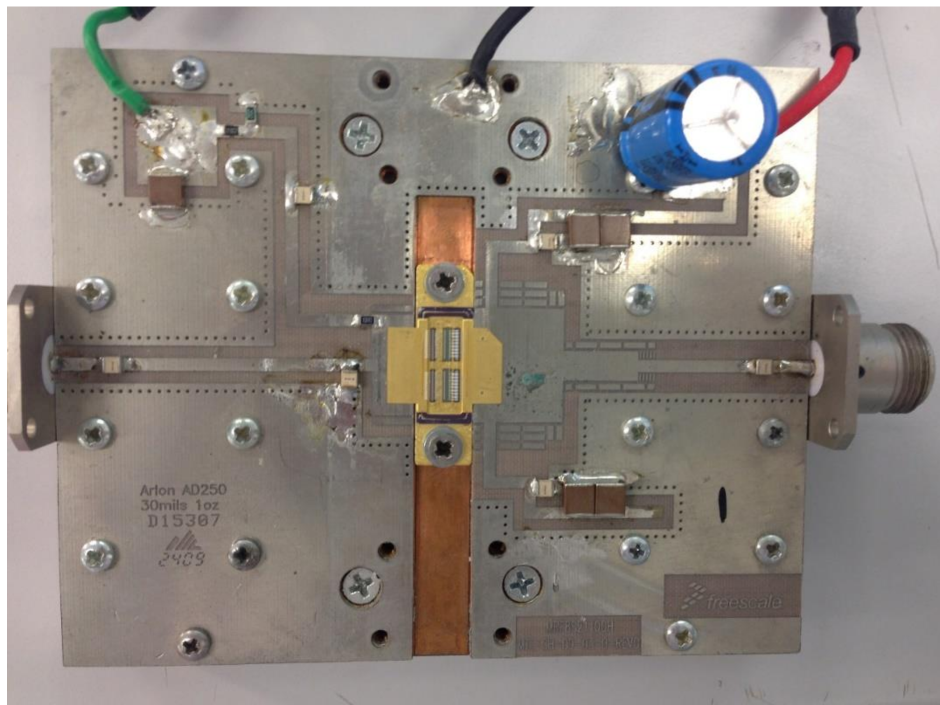

Figure 6.1: Pictorial representation of the 150W MOSFET, with ceramic lid removed, within the test circuit for its characterisation. All components provided by Freescale.

Continuous wave (CW) measurements were made on the test fixture shown above, at two frequencies 2.05GHz and 2.15GHz; for the comparison of the performance at mid-band and at the band-edge frequencies, respectively.

Using the VNA as a signal source, the input RF power to the test circuit was swept with an applied DC drain bias of 28V. For measurements requiring the electric field distribution of the device, the VNA was used as a detector and an external signal generator was used to supply the input signal.

A clearer picture of the de-lidded transistor is shown below in figure 6.2.

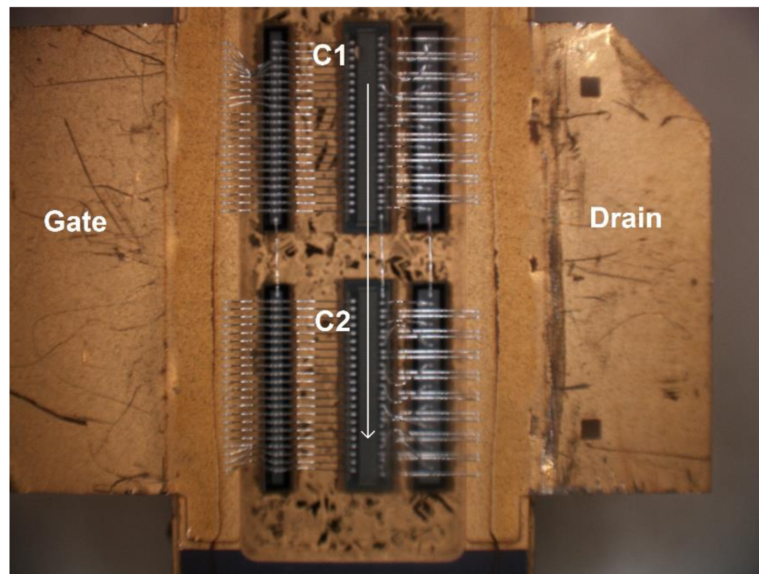

Figure 6.2: A magnified image of the 150W MOSFET, with ceramic lid removed, before its connection to the test circuit for its characterisation, with highlighted abbreviations.

The transistor shown in figure 6.2 is an example, this particular device has not been used for characterisation measurements as there was evident damage to the bondwire array. The damage shown is an example of incorrect removal of the ceramic lid, if removed before the adhesive has un-bonded, more force is required for correct removal and therefore can cause destruction of the delicate bondwire array beneath. Dis-regarding the broken bondwires, it can be seen that the device consists of two main sections of circuitry, for clear indication of the results obtained later in this chapter, these will be referred to as sections C1 and C2, respectively. Lateral scans described in the upcoming chapter will require the movement of the probe in the direction indicated above while the DUT beneath is kept in a stationary position.

6.1.1. Device characterisation before and after de-lidding process

As previously mentioned, the direct impact of the de-lidding process must be considered and measured before in-situ probing can be carried out. The gain and efficiency of the amplifier is tested and shown below in figure 6.3.

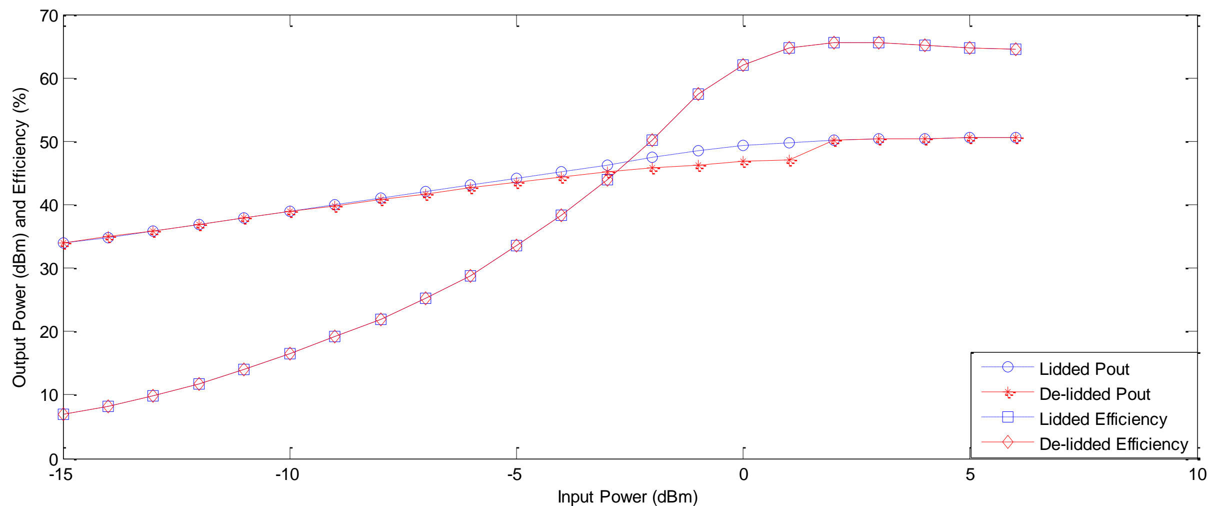

Figure 6.3: RF input and output characteristic of the HPA with increased input power and an operational frequency of 2.05GHz; before and after the removal of the ceramic casing.

The figure above indicates the removal of the ceramic casing can be considered negligible with regards to little performance degradation of the amplifier.

6.1.2. *Automated spatial resolution and the electric field distribution*

The successful removal of the ceramic casing, along with the confirmation of no performance degradation, subsequent testing can be initialised.

It should be noted: with limited supply of transistors, and destruction of 3 devices through the de-lidding process, the resultant investigations in this section are not extensive.

For the successful extrapolation of waveform information, automated scans for spatial resolution were conducted with limited attempts. As previously mentioned, the EFP is extremely sensitive to its local geometry, therefore for the maximisation of coupling and reduction of unwanted orthogonal field components, the EFP and DUT separation was kept to a minimum.

For spatial resolution scans of the active device, the probe is placed over central curvature point of the drain-side bondwire array. At a constant separation of 30μm above the bondwire height, the EFP was then moved along the direction indicated in figure 6.2, from section C1 to C2.

Unfortunately, fabrication of mass produced devices results in variation of the product. The quality of the device should not vary due to the sophistication of the

bonding machines utilised for their construction, however, in reality variances will occur from device to device. This is evident in the subsequent lateral scan acquired as the probe is automatically moved down the device, shown in figure 6.4.

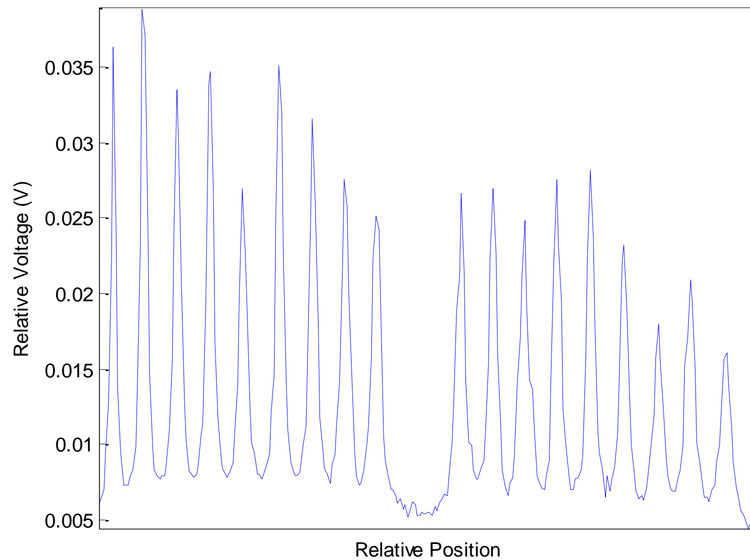

Figure 6.4: Resultant spatial resolution scan of the voltage distribution along the drain-side of the MOSFET from section C1 through to C2.

From the figure above, clear depiction of the two sections of 9 bondwires can be seen, however variation across the device is the most notable observation. Variation in the peak values indicate one of two fabrication anomalies; variation in the height of the bondwires and variation in the curvature of the bondwires. However, the distinct roll-off would indicate a variation in the distribution of current through the bondwires. This observation indicates an undesirable outcome, as matching networks are designed for the even distribution of current throughout the device.

If the roll-off present in the distribution is a result of a gradient in the automation of the EFP, as the probe is measuring section C2, the separation required for a degradation of half the peak value, would be evident by visual inspection. For this reason it is believed that the roll-off present in the voltage distribution is in fact a true representation of an in-situ measurement for the active device.

6.1.3. Calibration and Data processing of waveform information

In order to obtain waveform information in the time-domain, measurements are obtained by a digital signal oscilloscope. The probe is placed above the required position, and the relative waveform information can be extracted. The waveform information presented in this and upcoming chapters have undergone data processing for two purposes. The first, as a method for the extraction of the fundamental component for later analysis and second, a method to smooth the raw data obtained from the oscilloscope. For the extraction of fundamental components the waveform is over sampled and as a result an effective method for smoothing raw data is established.

Before waveform measurements can undergo Fourier analysis, a form of experimental calibration must be performed. By constructing a waveform with a distinct polarity, the subsequent waveform can be measured directly from the source (i.e. from the signal generator) and compared with the output of the probe. The distinct waveform is constructed by two phase locked signal generators, with the combination of the fundamental and 2nd harmonic, a class J waveform is produced. The combination is measured directly by a digital sampling oscilloscope and recorded. The same waveform is then injected through a section of matched 50Ω microstrip line while the EFP is placed over this section, at a separation of 30μm. The subsequent output of the probe is recorded and displayed in figure 6.5.

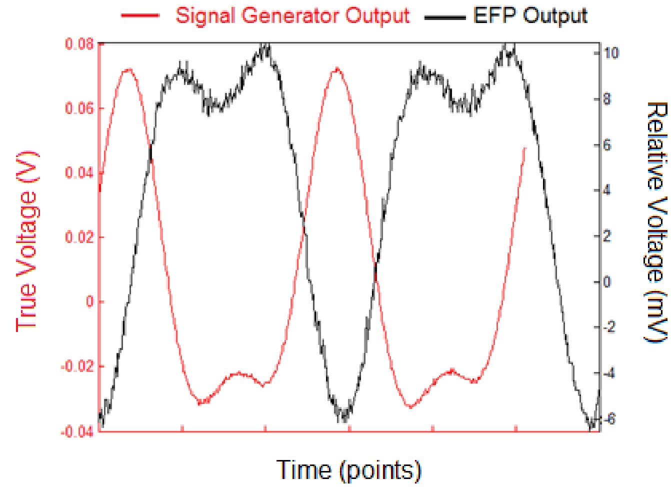

Figure 6.5: Comparison of a class J waveform measured directly from the signal generator to output of the probe. The probe output results in an inverted and scaled down measurement of the original waveform showing a true scaled voltage at the DUT target.

The resulting measurement can conclude that the EFP has the ability to successfully measure a true scaled representation of the voltage present at the DUT, as mentioned in section 2.3.1. The field generated at the probe tip and its effective coupling to the field generated by the DUT results in the change of waveform polarity, hence the inversion present in figure 6.5. Therefore, resulting waveforms will undergo inversion before further analysis can be performed.

Due to the positioning of the EFP over the drain manifold, device plane voltages can be measured. The time-domain waveform obtained, is the AC output voltage swing around the DC operating conditions. For this reason, Fourier analysis can extract the fundamental component, and therefore the DC characteristics can be constructed as a function of input drive.

By identifying one full cycle of the waveform, Fourier analysis can be performed on the raw data, for the given position relevant to the waveform.

$$f(x) = \frac{1}{2}a_0 + \sum_{n=0}^{\infty}(a_n \cos nx + b_n \sin nx) \tag{6.1}$$

where

$$a_0 = \frac{1}{\pi}\int f(x)dx \tag{6.2}$$

$$a_n = \frac{1}{\pi}\int f(x)\cos(nx)\,dx \tag{6.3}$$

$$b_n = \frac{1}{\pi}\int f(x)\sin(nx)\,dx \tag{6.4}$$

a_n *and* b_n are Fourier coefficients and relevant to each data point within the raw data obtained from the waveform.

For two cycles, extraction of the fundamental, where *n=1* and the conduction angle, α, is based on the radian angle for each data point, v_t, the root mean square voltage value can be calculated:

$$v_{fundemental} = \sqrt{\left(\sum v_t \cos\alpha\right)^2 + \left(\sum v_t \sin\alpha\right)^2} \tag{6.5}$$

The smoothed waveform data can be obtained from the summation of all harmonic component voltage values, not just the fundamental.

$$v_{smoothed} \sum_{n=1}^{\infty}\left(\left(\cos n\alpha \sum_{n=1}^{\infty} v_t \cos n\alpha\right) + \left(\sin n\alpha \sum_{n=1}^{\infty} v_t \sin n\alpha\right)\right) \tag{6.6}$$

By calculation, the raw waveform information obtained from the output of the EFP, can be smoothed and the fundamental voltage component can be extrapolated. This method will be imposed on all raw waveform data and fundamental plots.

6.1.4. Waveform distribution with varying input power

For a given measurement, the position of the EFP can be lowered such that the probe tip is 30µm above the metallisation of the transistor die. Measurements requiring the drain-side waveform information were obtained by positioning the EFP directly over the drain manifold, due to its miniaturised size and flexibility in the positioning was achieved.

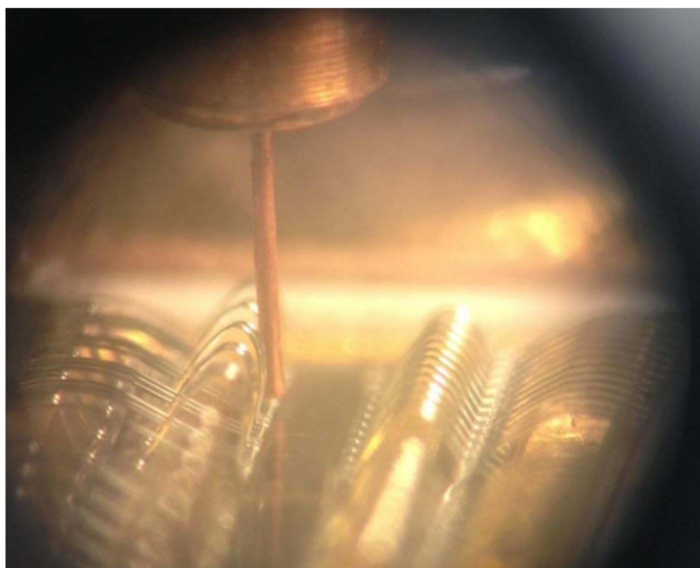

Figure 6.6: Example of the EFP positioning above the DUT i.e. above the drain manifold.

With the EFP in its fixed position, the RF input was increased, to take the device into compression. As the drive power levels are increased, the probe can make relevant measurements of the waveform information at each given level.

For the given position, measurements were taken at two frequencies, one at mid-band frequency, 2.05GHz, and the other slightly past the upper band edge, at 2.15GHz as the input RF power is increased from -5dBm to +7dBm.

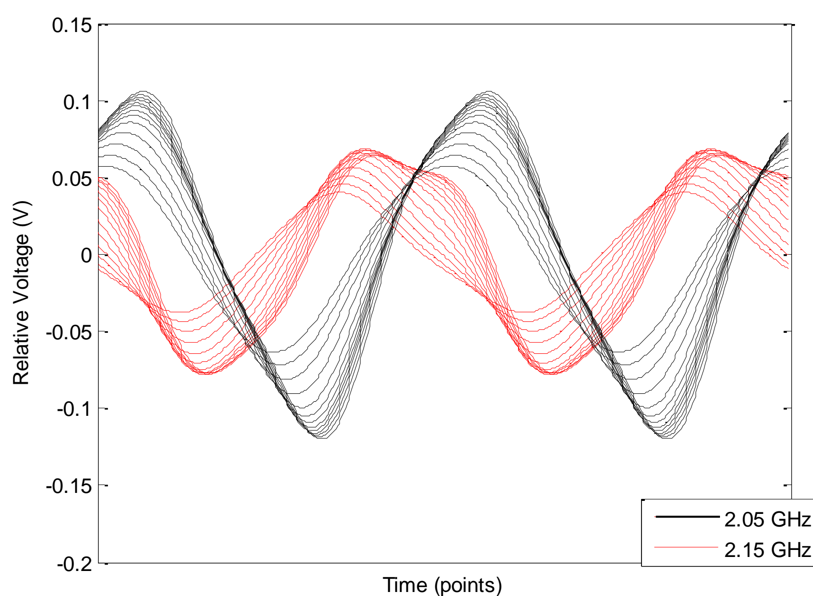

Figure 6.7: Drain-side voltage waveforms, for the device as the power level is increased to saturation, at the two different frequencies. 2.05GHz and 2.15GHz.

From figure 6.7, it can be seen that the impedance match at the band edge has dropped to a low value, so that the voltage never reaches the clipping level. With the capability of in-situ measurements in working amplifier, such information is of great value to the circuit designer.

6.1.5. Waveform distribution before and after broken bondwire

The results shown in the previous section required measurements of stationary EFP position. However, the measurement system has capability of lateral and transverse scan. For the analysis of the waveform information along the length of the device, the probe is no longer kept in a stationary position and moved laterally down the device; at constant measurement plane. Two alternative measurements can be performed during this automation; the input power can remain constant or be increased, dependent on the measurement required.

During in-situ measurements, a build-up of static charge caused destruction to the measuring probe and resulted in a broken bondwire of the transistor; the damage was specific and confined to the point of discharge. The resulting accident caused no visual damage to the metallisation of the die. The damage caused to the bondwire was not extensive, a small section of the metal had melted away. This unfortunate occurrence did however have its advantages. Re-measuring the output power and efficiency of the broken device resulted in no indication of such occurrence, there was no degradation in the output characteristics. Using a new EFP, whose performance was equal to the damaged probe, the waveform distribution down the device was repeated.

Figure 6.8 below shows two different lateral scans of the device at a constant input power of +7dbm; where figure 6.8(a) was conducted pre-accident and (b) was conducted after the knowledge of the broken bondwire.

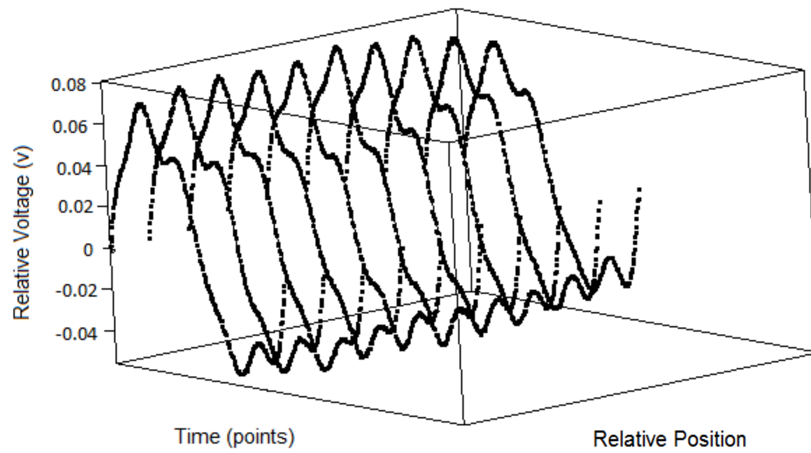

(a)

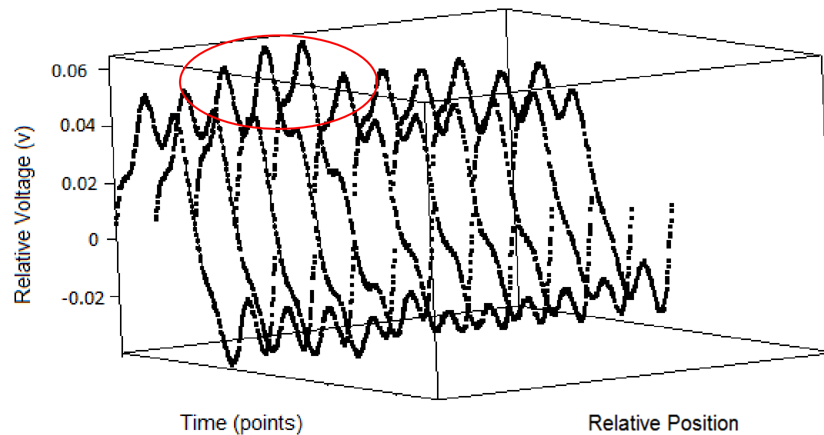

(b)

Figure 6.8: Lateral scans down the metallisation of the die driven close to saturation from section C1 to C2 (a) for a device with no imperfections (b) the device after a broken bondwire. Where the highlighted section indicates the difference in peak magnitude caused by the broken bondwire.

Two highly significant observations can be made from the waveform distribution presented in figure 6.8. The initial scan, shown in figure 6.8 (a), clear differential behaviour between the two separate die is evident as the probe is moved from die C1 to C2; and in figure 6.8 (b) there are well-defined discontinuity in the measured voltage at one specific point on one die. Close inspection of the device at this point revealed the position damaged bondwire. Note: both measurements have been conducted at a constant separation plane.

The EFP shows the ability to characterise a given device by analysis of the waveform behaviour; such anomalies as those shown in figure 6.8 (b), can be of great importance. In this particular scenario, no indication of potential damage to the device could be detected if measurements were only conducted at the input and output of the device. The EFP has therefore been successfully utilised as a diagnostic tool, with the ability of conducting in-situ internal measurement capable of detecting physical anomalies.

6.1.6. Amplitude calibration

Measurements made in previous sections have been conducted with the philosophy of relative voltage measurements, without absolute calibration. Within the literature review of this thesis, it has been noted that probe calibration can be difficult, with very little mention made to absolute calibration. Any citations found required the calibration of the EFP to a non-relevant method, e.g. using an axially suspended conducting wire for calibration when the intended function of the probe was to measure MMIC test structures [24]. Effective information regarding the characteristics of the probe can be extracted by comparing theoretical to experimental results of a 'known' structure. However, it has been repeatedly mentioned that the probe itself is extremely sensitive to its local geometry. Therefore, calibration attempts made in a non-relevant manner, to that if the intended measurements, cannot be systematically translated and cannot be accepted as an absolute calibration method. For an accurate method of absolute calibration, the probe must calibrated in-situ to the particular DUT under investigation.

The method presented follows the philosophy whereby either "known" voltage, and/or known features of the waveform such as mean, peak and minimum levels, can be used to give direct in-situ calibration with a particular probe position.

Figure 6.9 shows a set of probed waveforms taken on the high power device at the drain manifold; with a constant RF drive level, whilst decreasing the DC supply voltage.

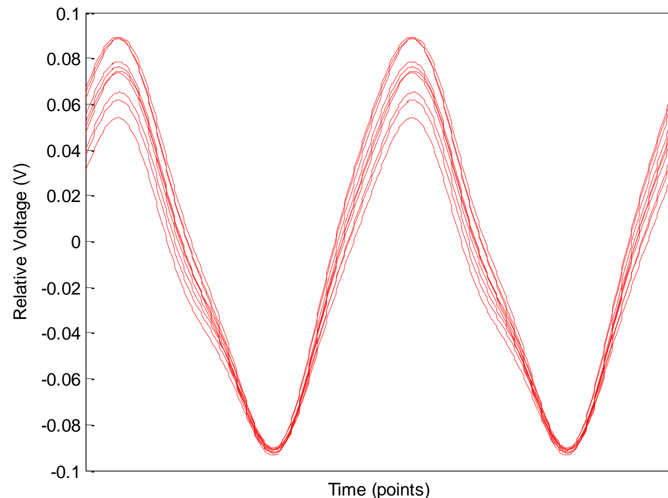

Figure 6.9: Probe voltage waveforms, at constant RF, with uniform decrease of supply voltage over a 1ns sweep; traces have been lined up at the device knee point.

Given that these traces all represent the device in hard compression, it is a reasonable assumption that the successive minima represent conditions where the device voltages are close to the knee, or turn-on value, which is a known and measureable characteristic of the device, 3.5v (±0.5v) in this case. Along with the mean level, which can be set to the DC supply value, a workable in-situ voltage calibration can be obtained [37].

6.2. Conclusion

This chapter has successfully shown the full extent of the EFP's capability, the ability to conduct in-situ measurements within a working amplifier, direct and valuable information can be achieved. Due to the miniaturised size and flexibly within the measurement system, the EFP can be used to directly measure over the drain side manifold. Therefore the resulting positioning yields the most accurate and relevant method of measurement and characterisation. The EFP has been successfully utilised as a diagnostic tool, with the ability to detect anomalies and unexpected behaviour, such as uneven distribution along a device. The drain voltage has a direct effect on the depletion region of the device, and therefore channel width; an uneven distribution can have a detrimental effect on the functionality of its performance.

Transverse scans conducted at constant drive, of two nominally identical devices successfully resulted in the EFP ability to expose the deformity present within a topology. This particular measurement displayed the presence of a broken bondwire. Without the aid of the EFP, measurements conducted at input and output terminals would not detect the deformity; as output power and efficiency of the device remained constant.

All the information presented within this chapter would greatly aid the work of a designer, giving vital information which could not be obtained through other measurement techniques.

7. DOHERTY POWER AMPLIFIER DIAGNOSTIC

The successful measurement of a high-power amplifier was presented in the previous chapter. The EFP was shown to be effectively utilised as a diagnostic tool, therefore this chapter will show the resulting measurement of a more complicated system. As discussed in section 2.1.2 Doherty power amplifier, consists of two active transistors. Employed as a method of efficiency enhancement, potential complications in the resultant characteristics have been observed. The anomalies present in the Doherty configuration have perplexed designers, with no diagnostic tool available for in-situ measurement. Undiagnosed and unpredicted errors in the design stage have resulted in the necessity for further understanding in the testing stage. With direct access to the device, on-chip measurements can be utilised to detect such anomalies and conclude if each device is working correctly or coherently to design specifications.

7.1. Symmetrical Doherty power amplifier

7.1.1. Theoretical DPA behaviour

The Doherty power amplifier tested in this chapter is symmetrical, i.e. with two identical LDMOS devices BLF7G21LS-160P, consisting of a main and peaking device. The circuitry of the 50W 2GHz DPA and transistors are all supplied by NXP, Netherlands, shown below in figure 7.1.

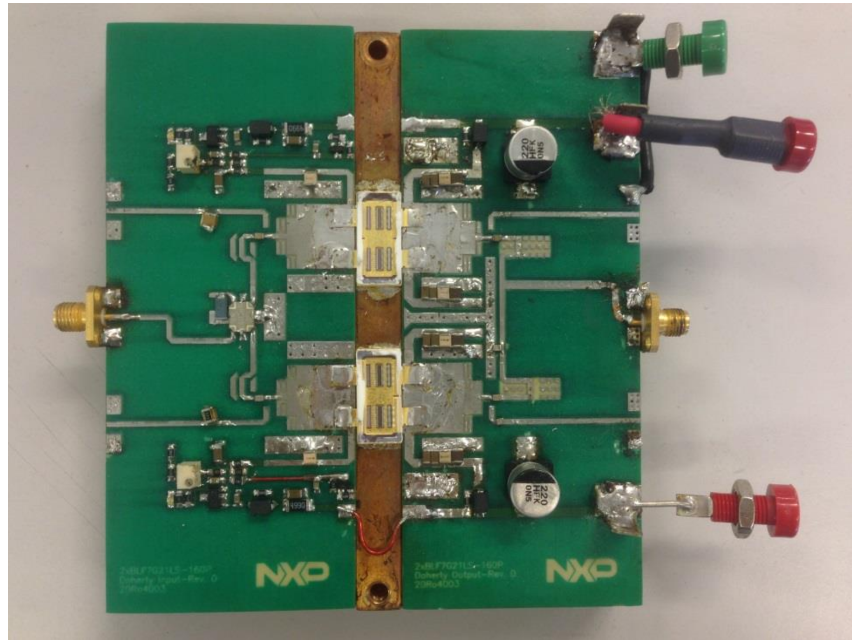

Figure 7.1: Pictorial representation of the symmetrical 50W Doherty PA, showing LDMOS devices with ceramic lid removed. All components provided by NXP.

Theory would dictate that at low input power levels, the peaking device is off, so the main device receives the entire input signal. As the power level is increased, the main device reaches a level of voltage saturation; at this point, due to its biasing arrangement the peaking device switches on. This switch-on results in a current contribution from the peaking device. Therefore, resulting in the main device to behave like a controlled voltage source; while the peaking behaves as a controlled current source. As the input power is increased further, the impedance seen by both devices are now equal to that of the characteristic impedance of the quarter-wave transformer.

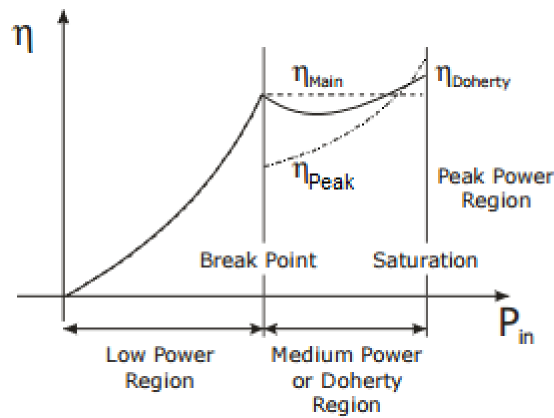

Figure 7.2: Generic efficiency plot for a Doherty power amplifier with increased input power, defining the low power and high power region behaviour [1].

In theory, the classical Doherty behaviour is shown to be rather abrupt. Literature on the topic will illustrate the efficiency to be similar to that shown above, in figure 7.2. Displaying a linear efficiency at low input power and a peak efficiency at the 6dB back-off point.

In practise, this idealised behaviour is not always evident. Actual measurements of the efficiency and device voltages show a much tamer representation.

For accurate representation of the device plane voltages, in-situ drain-side measurements must be conducted, along with the data analysis shown in section 6.1.3. This will allow for the extraction of the fundamental voltage components, therefore allowing potential anomalies to be identified.

7.1.2. RF input output characteristics before and after transistor de-lidding

As with measurements conducted on the HPA within chapter 6, the output characteristics of the DPA should be measured before and after the de-lidding process. However, this was not possible as the amplifier was provided with de-lidded transistors, therefore no direct comparison could be made. The figure 7.3 displays the RF input and output characteristics for the de-lidded DPA.

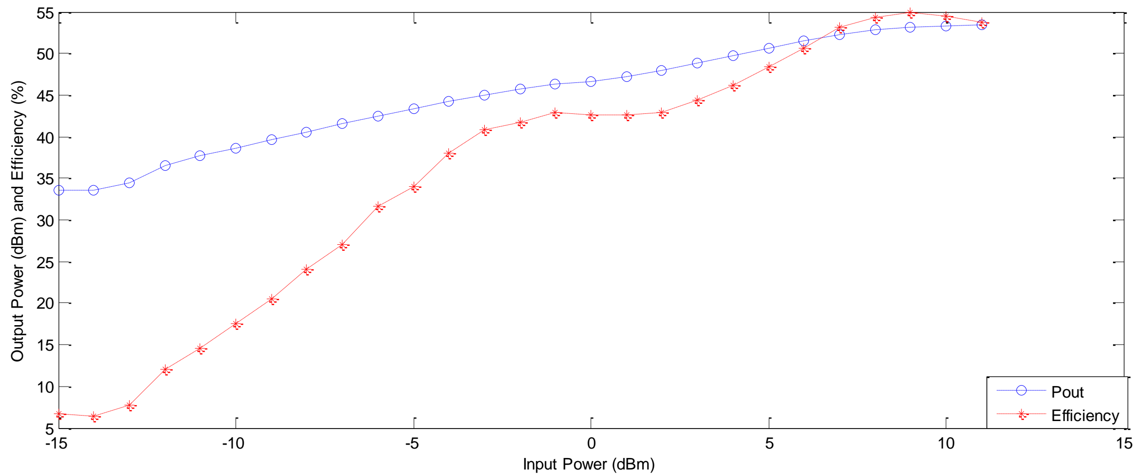

Figure 7.3: RF input and output characteristic of the DPA with increased input power and an operational frequency of 2GHz

7.1.3. Spatial resolution scans along the bondwire of the transistors

The figure below shows a magnified picture of the LDMOS device to be tested; both devices within the DPA are identical.

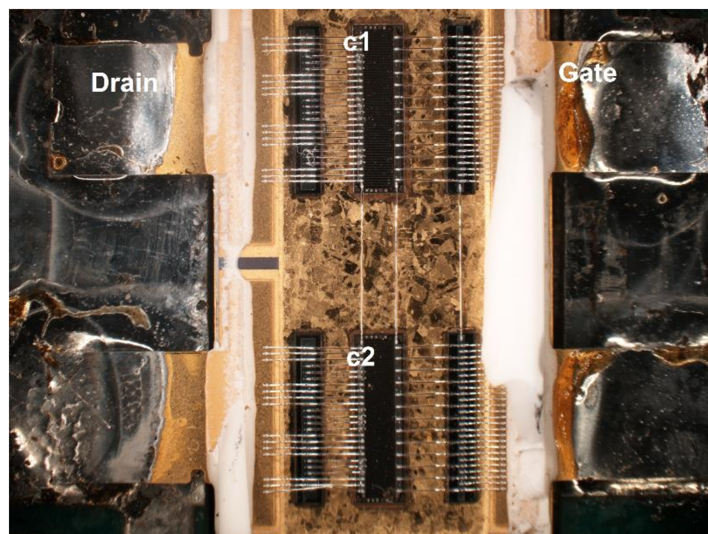

Figure 7.4: A magnified image of the LDMOS device, with ceramic lid removed, where the main and peaking devices consist of identical transistors; with highlighted abbreviations "c1" and "c2".

The transistor circuitry consists of two sections of separated die metallisation, connected through a bondwire array. For clear understanding of the proposed measurements, the labelling indicated above ("c1" and "c2") will be adopted.

Both the bondwire arrays on the drain and gate side of the LDMOS were separately scanned for the relative voltage distribution, note: the bondwire separation of the

array differed with each side. The bondwire separation on the drain side measured to be 30μm, while the spacing of the gate side bondwires measured to be 100μm. Initial resolution scans were conducted on the drain side, resulted in a lack of spatial resolution, due to the close proximity of the bondwires, i.e. the resolution required exceeded that of the probes capability.

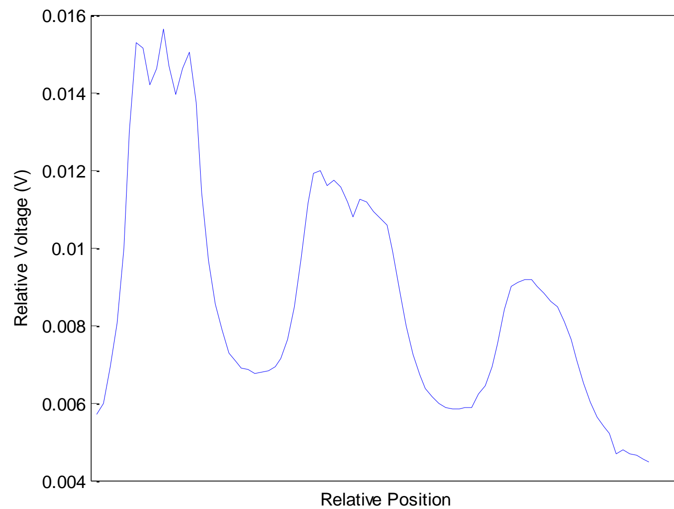

Figure 7.5: Automated spatial resolution scan along the bondwire array situated on the drain side of the peaking LDMOS device within the DPA, showing a lack of definite resolution due to the close proximity of bondwire (bondwire separation measured to be 30μm).

The DPA was measured at a constant RF input, close to compression, to ensure both devices were in the 'on' state. The scan shown above, in figure 7.5, is the result of a transverse movement of the EFP over the section c1 on the peaking device; measured at a constant separation plane. The drain side array consisted of 3 separated sections of bondwires; where section 1 and 3 contained 3 wires, while section 2 contained 4 wires. As the EFP is moved down the device, a degradation of magnitude and resolution is observed. The lack of resolution is mainly due to the close proximity of the bondwires (30μm separation). Repetition of drain side bondwires produced the same outcome for each section of each transistor, c1 and c2; with slight resolution of initial bondwires leading to a complete decay of resolution and measured magnitude along the device.

For confirmation of the spatial resolution capability of the EFP, transverse scans are conducted along the gate side bondwire array; where the separation between each wire is greater and more suited to the resolution capability of the probe. The initial separation of the probe tip and DUT is set to the same level as the previous scans, 30μm above the highest visible bondwire. This procedure is essential due to the natural anomalies in fabrication; this precaution avoids destruction of the probe and the DUT.

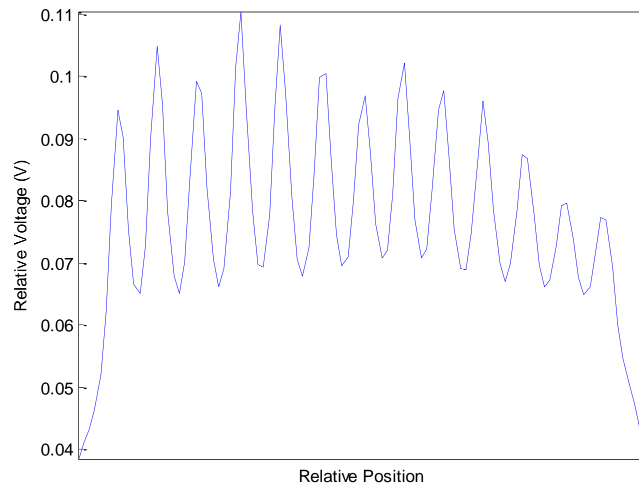

7.6 (a)

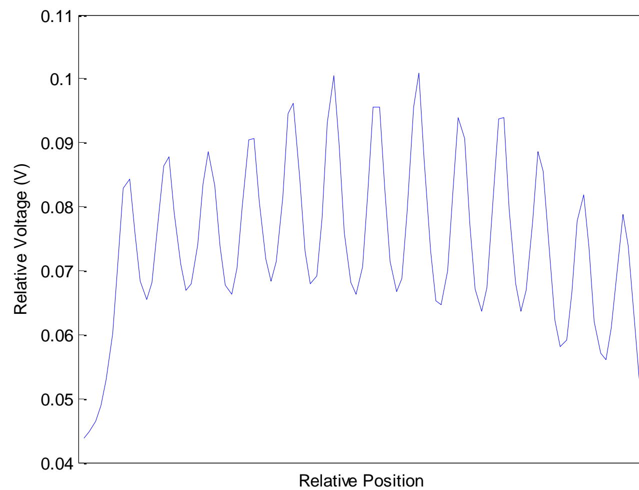

7.6 (b)

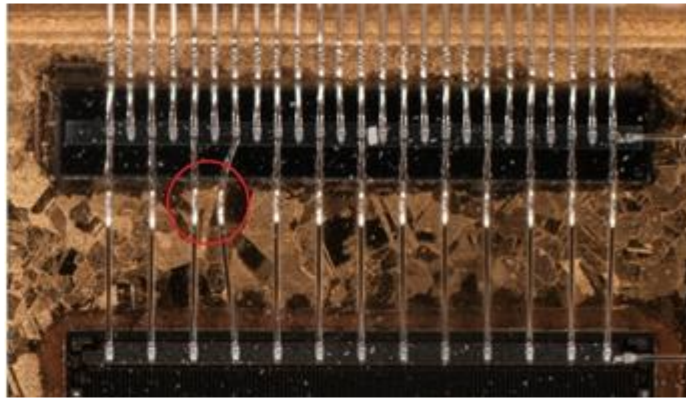

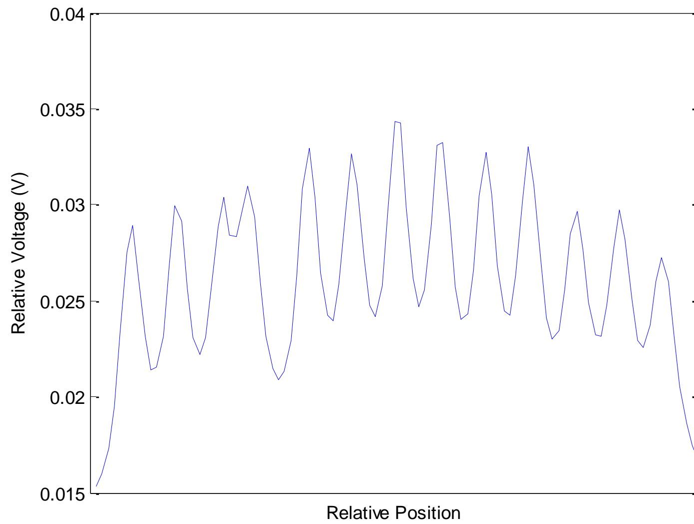

7.6 (c)

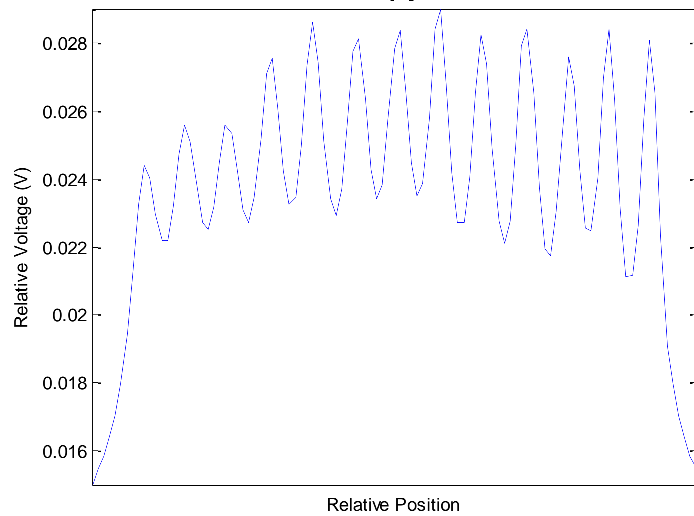

7.6 (d)

Figure 7.6: Automated spatial resolution scan along the bondwire array situated on the gate side of the LDMOS device within the DPA, of the main device (a) section c1 (b) section c2, and of the peaking device (c) section c1 (d) section c2.

Note: the picture shown along with plot (c) is to highlight the anomaly present within the bondwire array.

From the scans shown above, two important observations can be made; firstly that the distribution of voltage along the device varies as the probe is moved from section c1 to c2 and secondly, the considerable variation present between the peak magnitude of the main and peaking devices.

As the probe is transitioned between sections c1 and c2 of the same device, the decay in amplitude and resolution is presented not as extreme when compared to the drain side scans. The differences observed in peak values of the voltage distribution between the main and peaking devices are rather unexpected behaviour.

Again, the probe separation is kept constant throughout all measurements; any unintentional variance caused to the measurement plane would be noticeable by the microscopic positioning system used for initial positioning.

The degradation of the voltage distribution is evident in both the bondwire scans and scans conducted on the metallisation of the die. The EFP is placed at a constant measurement separation of 30μm above the central point of the die, i.e. midway between the drain and gate bondwire arrays, and moved transversely down one section of the device. Note: the results displayed below are obtained from a scan of c1 on the main device and c2 of the peaking device; this is due to the degree of variance present in their corresponding bondwire investigations.

The section of metallisation should be nominally flat, with no issues of apparent variation in the planarity. However, the scan shown below in figure 7.7 is consistent with the decay visible in the bondwire scans.

Figure 7.7: Automated spatial resolution scan along the metallisation within section c1 of the main and c2 of the peaking device, showing substantial and coherent variation in the resulting distribution.

The results shown above displays a coherent degradation in the measured magnitude across the device; such substantial variation across the device periphery is unexpected and not desired for the correct functionality of the transistor.

7.1.4. Experimental waveform measurements and fundamental voltage component

The measurements described within this section are intended as a relative measurement, the vertical scaling of the voltage is a representation of the true output of the EFP. The measurements below are taken at the device plane over the drain manifold, for a stationary EFP position as the input power is increased.

The EFP is lowered 30μm above the drain manifold, where the position chosen on the main and peaking devices are comparably the same. The input drive is increased in 1dBm increments beyond the saturation of the DPA and shown in figure 7.8 and figure 7.9 for the main and peaking devices, respectfully.

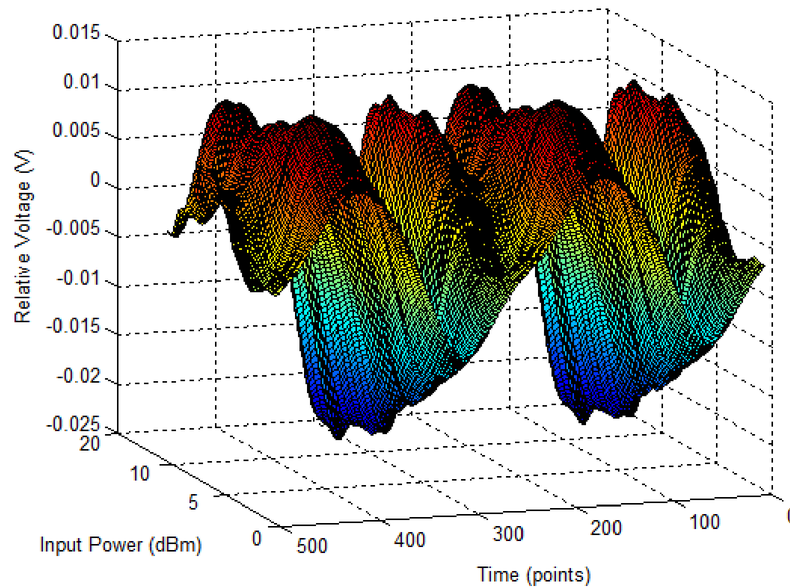

Figure 7.8: Voltage waveforms from the main device as the input power is stepped in 1dBm increments for a stationary position of the EFP, comparable to the position chosen on the peaking device.

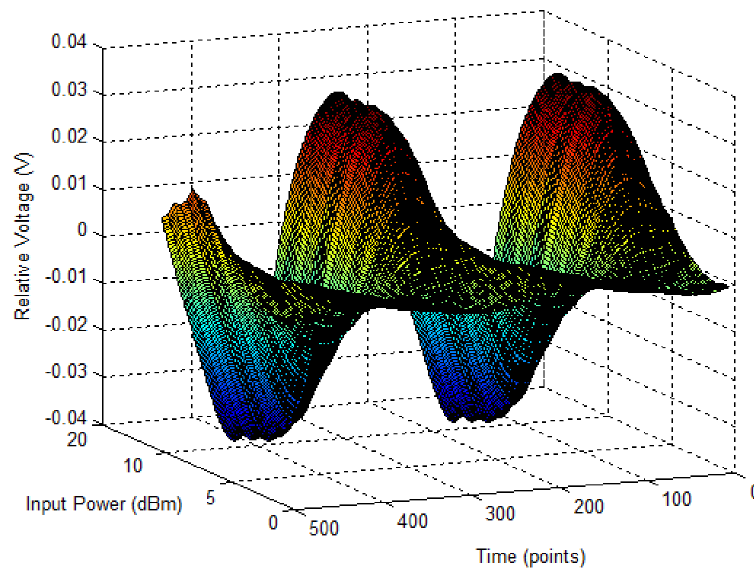

Figure 7.9: Voltage waveforms from the peaking device as the input power is stepped in 1dBm increments for a stationary position of the EFP, comparable to the position chosen on the main device.

From the waveforms plots shown above; a visible difference of almost a factor of two is present in the peak to peak voltage values, between the main and the

peaking devices. The separation plane of the EFP was kept constant for both devices, however, differences in magnitude were still observed.

Extracting the fundamental voltage component from the waveform information displays a coherent difference in the peak values. Despite this difference, clear Doherty behaviour is observed.

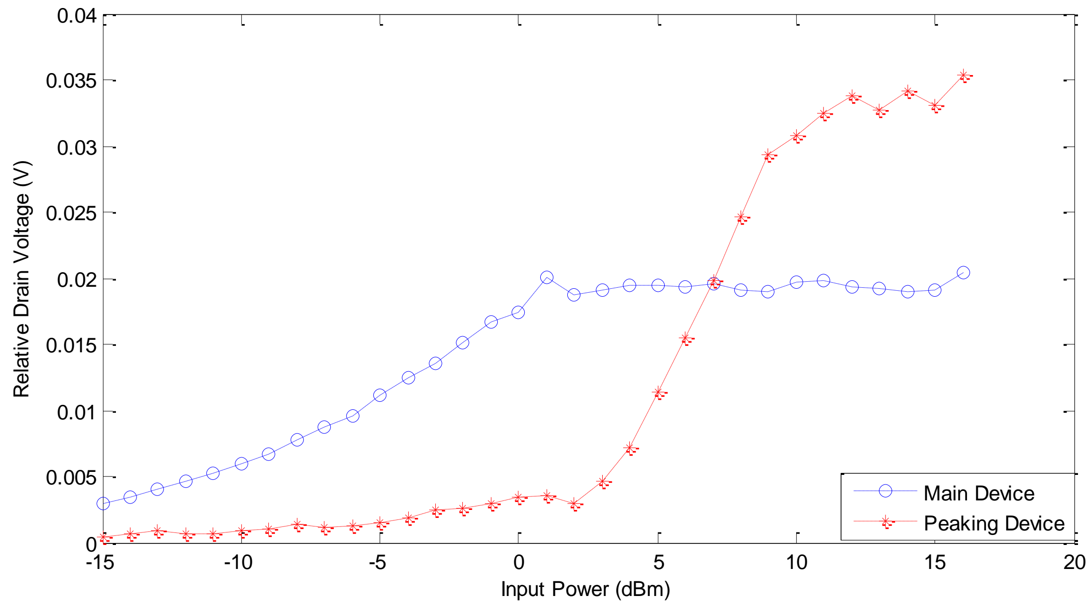

Figure 7.10: Fundamental voltage component extracted from the waveforms shown in figure 7.8 and 7.9; showing clear Doherty behaviour as the input drive is increased, with visible difference in the peak voltage values.

From the figure above, it can be seen that the main device is taken to saturation as the peaking device turns on. However, the peak value of the peaking device quickly exceeds that of the main, before saturating at a higher than expected magnitude.

Further analysis of both the main and peaking devices concluded that differences exhibited in the peak values, were due to the substantial variation in the voltages along the device periphery. Waveform analysis conducted at a constant input drive, as the EFP was moved along the device plane, showed the full extent of this variation. Figures 7.11 and 7.12 show the degree of variation along the main and peaking devices respectively; note that the vertical position of the probe does not

change. For clarity of the device periphery variation, the measured waveform has been reduced to one cycle.

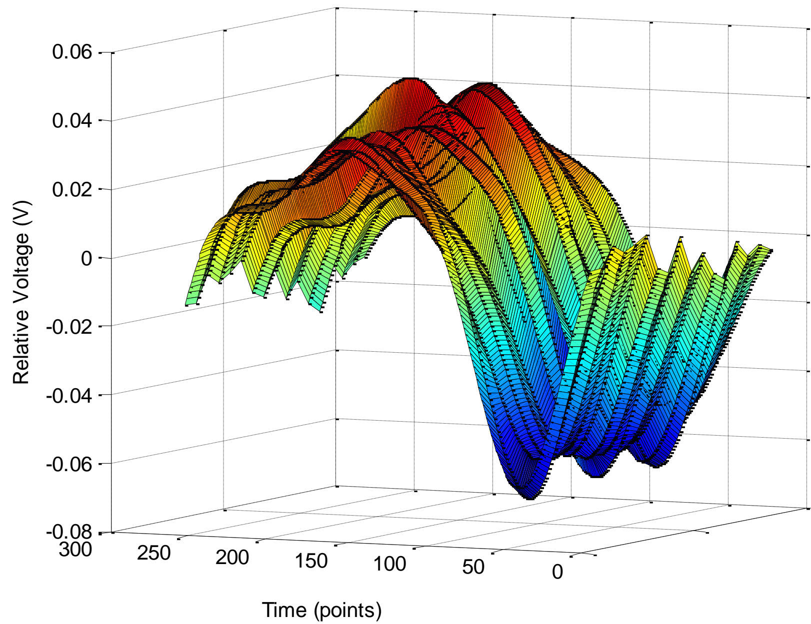

Figure 7.11: The extent of the voltage waveform variation, at a constant input drive of +7dBm, as the EFP is moved transversely down the main device. For improved visual inspection, the waveform has been reduced to one cycle.

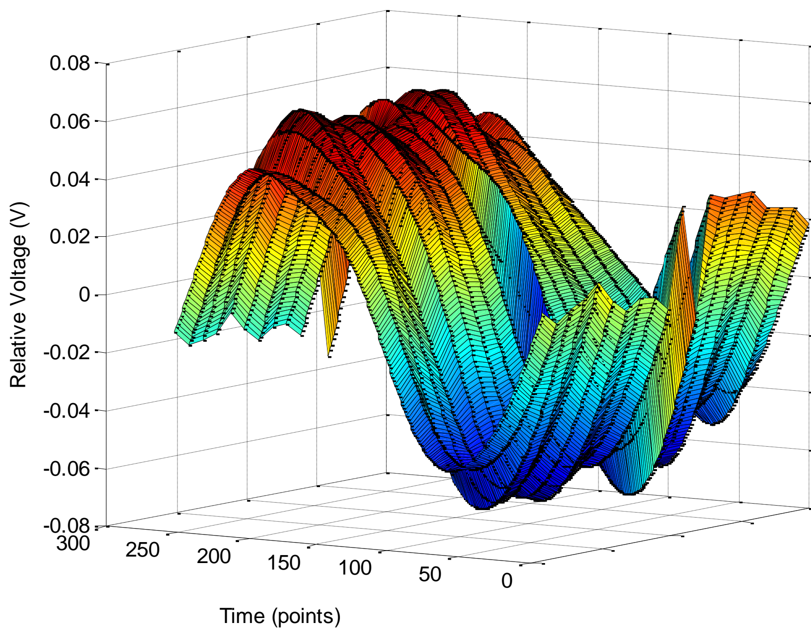

Figure 7.12: The extent of the voltage waveform variation, at a constant input drive of +7dBm, as the EFP is moved transversely down the peaking device. For improved visual inspection, the waveform has been reduced to one cycle.

From both figures 7.11 and 7.12, a clear observation can be made in the significant variation of peak voltage values along the devices. The devices used in the DPA are nominally the same, only under different biasing conditions. For this reason, similar points along the devices were used as a comparative point for the measurements displayed within figures 7.10, 7.11 and 7.12. However, the variation along each device was specific with no coherent deviation, showing a more extreme variation along the main device. With the variation specific to each device, the point of comparison chosen dictated the differences observed in the peak voltage value.

7.2. Conclusion

The initial spatial resolution scans conducted within this chapter have shown two major significances; the actual resolution capability of the MMIC EFP exceeded the original expectation of 100μm and the extent of the amplitude variation along the device periphery was highlighted. With partial resolution of the drain side bondwires, loss of resolution could be a result of the extreme roll off present in the voltage distribution. Thus, extending the expectant resolution of the EFP close to the region of 30μm.

The variation of the measured voltage extended to the time-domain measurements, where waveform distribution along the metallisation of the die also showed signs of anomaly. The deviation present along the device periphery showed an inconsistent variation in the distribution. The variation in the waveform distribution along the individual devices and the discrepancy present in the comparison of devices, are ultimately a result of an unintentional design flaw. Such anomies can theoretically affect the performance of the DPA.

The final comparison of fundamental components obtained from main and peaking devices depend specifically on the point of comparison. Due to the discontinuous variation along the device periphery, the extent of the discrepancy between the peak voltage values are dependent on point of comparison.

8. ASYMMETRICAL DOHERTY POWER AMPLIFIER DIAGNOSTICS

The measurements conducted within chapters 6 and 7 have shown successful application of the EFP as diagnostic tool, for the characterisation of high power amplifier systems. This chapter will describe the analysis of a 200W, asymmetrical, Doherty power amplifier, A-DPA.

The work presented within Chapter 7 investigated the operation of a symmetrical DPA, where the active devices within the system were identical devices. The A-DPA however, consists of two different LDMOS devices, a 130W transistor for the main and a 200W transistor for the peaking (designed and manufactured by NXP, Netherlands).

The classical DPA design displays a peak efficiency at 6dB back-off, which makes it most applicable to a signal with 6dB PAPR. A modern day system demands a higher peak to average ratio, PAPR, with a peak efficiency in the region of 8dB back-off. The A-DPA can be utilised for this reason, by altering the devices within the DPA, the peak efficiency can be shifted to the desired back-off point. By specifically increasing the size of the peaking amplifier, typically in the region of 1.5-2 times larger, the peak efficiency can be shifted to a higher back-off levels.

However, the implementation of an A-DPA increases the challenges faced by the designer. The two different sub-amplifiers within the system will alter the design consideration, as variances can occur independently due to the asymmetric nature of the devices. Variations as a result of the fabrication process can also occur, as components are not made on the same production run.

These uncertainties have overshadowed the potential efficiency improvements of the A-DPA design, and caused designers to favour the symmetrical orientation.
For this reason, diagnostic characterisation of the A-DPA with the EFP system, can give valuable information regarding the functionality of the design. Direct access to each device will allow for on-chip measurements which result in the most accurate characterisation of the A-DPA.

8.1. EFP diagnostic evolution of the A-DPA

8.1.1. Theoretical behaviour of the A-DPA

Theoretical behaviour of the 200W asymmetrical Doherty, has similarity to that of the symmetrical system described within chapter 7. At low input power levels, the device plane impedance is transformed from the 50Ω termination by the quarter-wave transformer. The impedance seen by the main device is a higher magnitude than in the symmetrical case, therefore the saturated voltage value at the main device is reached at a much lower drive level.
As the input power is increased, the peaking device starts to conduct, and modulates the main device impedance downwards, thus maintaining the saturated voltage value of the main device. The figure below summarises the generic theoretical characteristics of the main and peaking devices.

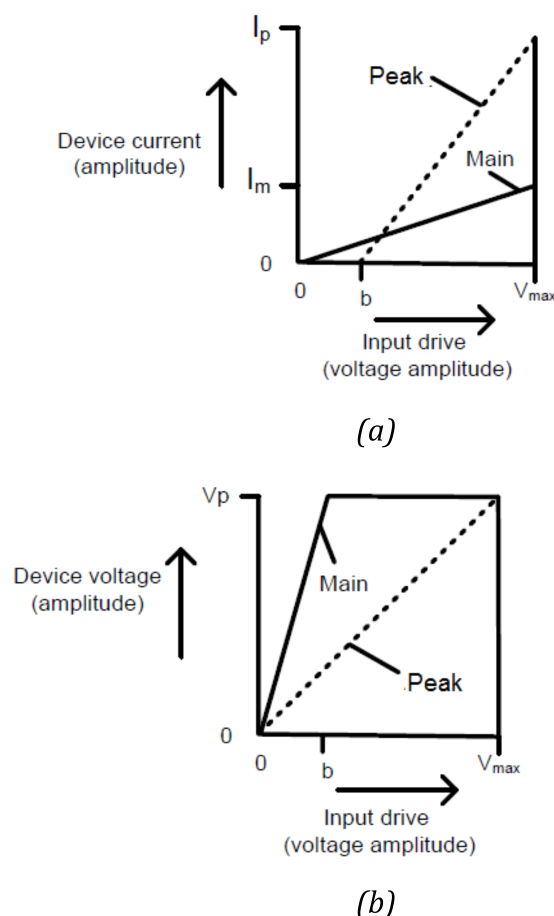

Figure 8.1: Generic characteristic behaviour of an A-DPA with increased input power, for (a) current and (b) voltage. Highlighting earlier current switch on, of the peaking device and voltage saturation of the main device [1].

From figure 8.1 it can be seen that the peaking device is designed to contribute at lower input power, therefore resulting in an earlier voltage saturation of the main. For this reason, the peak efficiency occurs at a lower back-off level. Depending on the ratio difference between the main and peaking transistors, the individual maximum current values, seen in figure 8.1 (a), will differ accordingly. It should be noted that the expected peak voltage values for the main and peaking devices are equal.

8.1.2. RF Pin-Pout characteristics before and after the de-lidding process

The RF input and output characteristics of the A-DPA are conducted before and after the removal of the transistors ceramic casing. For ideal back-off within a

lower region, the peaking amplifier has been chosen to be larger than the main device. Note the devices used within the A-DPA are BLF7G22LS-130 and BLF7G22LS-200, where the latter is the peaking device and is 1.5 times greater than the main device. Schematic diagram of the transistors and test circuit are shown below in figure 8.2.

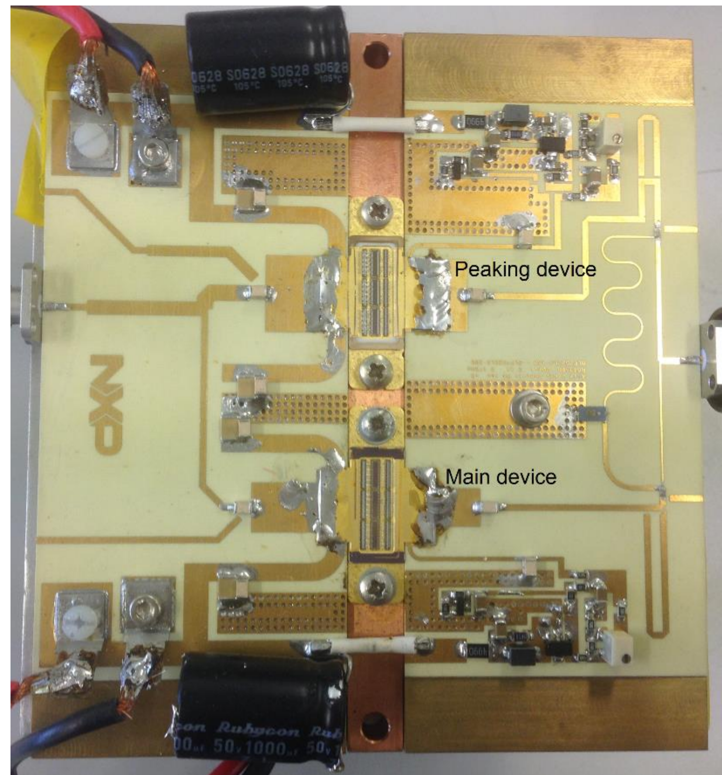

Figure 8.2: Picture of the symmetrical 200W Doherty PA, showing LDMOS devices with ceramic lid removed. All components provided by NXP.

In order to calculate the expected efficiency of the system, output data is analysed as the input excitation is increased. The A-DPA is excited by a CW of 2.14GHz provided by a VNA. This excitation is fed using an external driver amplifier, Mini-Circuits ZHL-30W-252+, UK, for addition gain. The output of the A-DPA is terminated via sufficient attenuation and measured by a power meter via a directional coupler.

Figure 8.3 below shows the efficiency and output power of the A-DPA, before and after the removal of the ceramic casing. The efficiency is calculated as the percentage ratio of output power as a function of the input power.

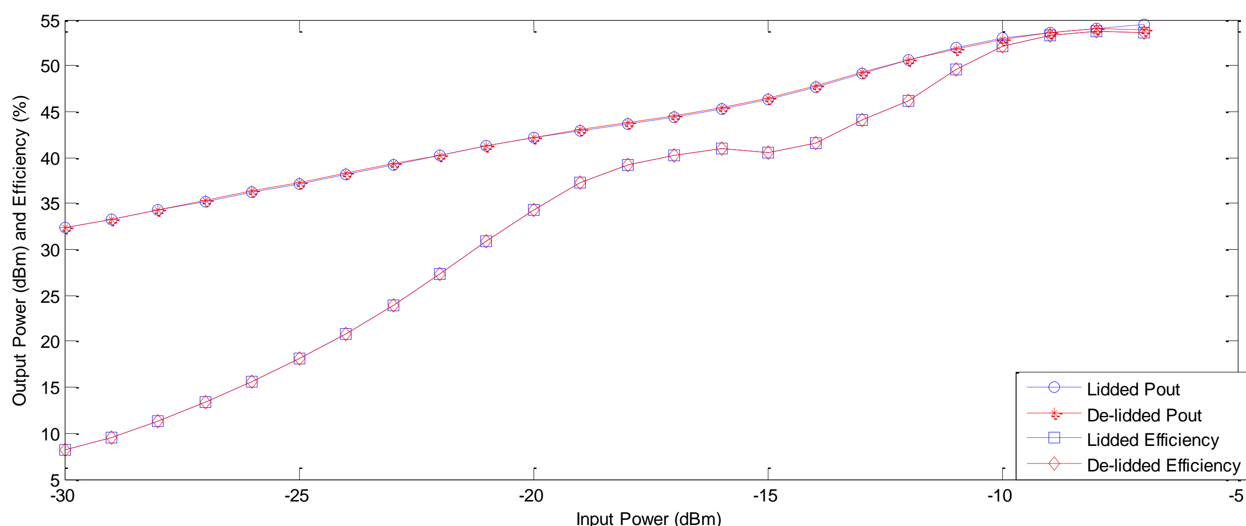

Figure 8.3: RF input and output characteristic of the A-DPA with increased input power and an operational frequency of 2.14GHz, for intact ceramic casing and removed ceramic casing.

From the figure above, the classical twin peak characteristic of the amplifier efficiency can be observed in the expected region of 10dB back-off. However, the backed-off efficiency peak is significantly lower than the maximum drive peak, as compared experimental to theoretical expectations.

Comparisons made between the plots displayed within figure 8.3 can conclude the de-lidding process can be regarded as having negligible effect on the performance of the A-DPA.

8.1.3. Spatial resolution analysis of the A-DPA

Spatial resolution scans were conducted on the main and peaking devices while the A-DPA was in full operational mode; for analysis of the voltage distribution along the device periphery. Figure 8.4 below shows a magnified image of the main and peaking devices, respectively; highlighting the direction of measurement, "*a*" to "*b*".

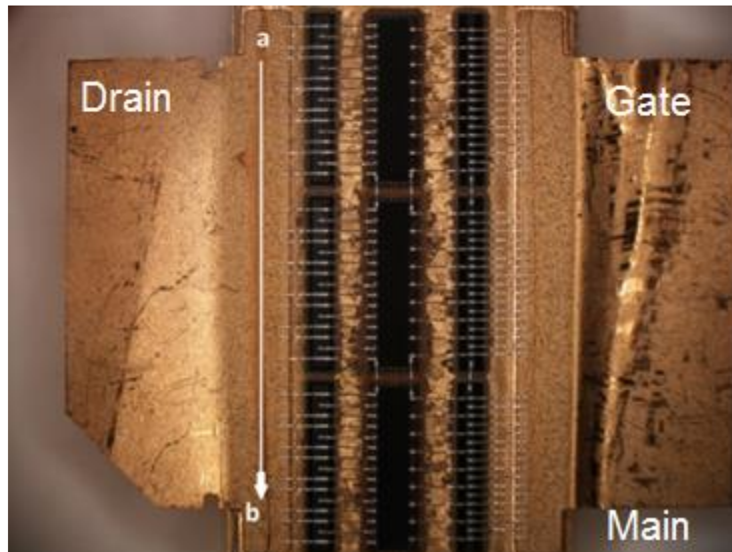

(a)

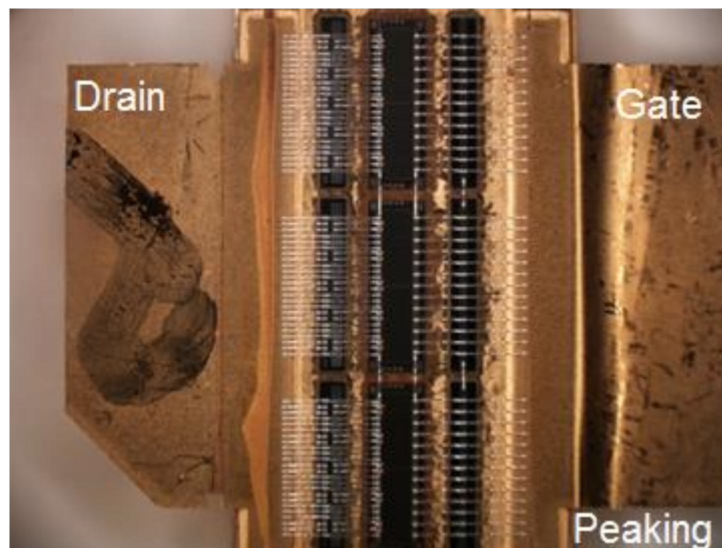

(b)

Figure 8.4: A magnified image of the LDMOS device, with ceramic lid removed, before its connection to the test circuit, for (a) the 130W main and (b) 200W peaking device. Highlighting the direction of the transverse spatial resolution scan.

From the figure above, it can be seen that the bondwire array differs between devices, which is to be expected given that the DPA is asymmetric. The spatial resolution scans conducted on the drain side bondwires, between the main and peaking devices, are expected to have a difference in distribution. This is due to the difference in bondwire proximity. The bondwire separation of the main device measures at 100µm, while the peaking device measures at 50µm. The spatial resolution scans, within this section, were conducted at two power levels on each

device. One at mid-level input and one deep within saturation level of the device. Note: the difference in RF input between figure 8.5 (a) and (b) and between figure 8.6 (a) and (b) is +7dBm. The resulting scans shown below were conducted with no alteration in the vertical measurement plane.

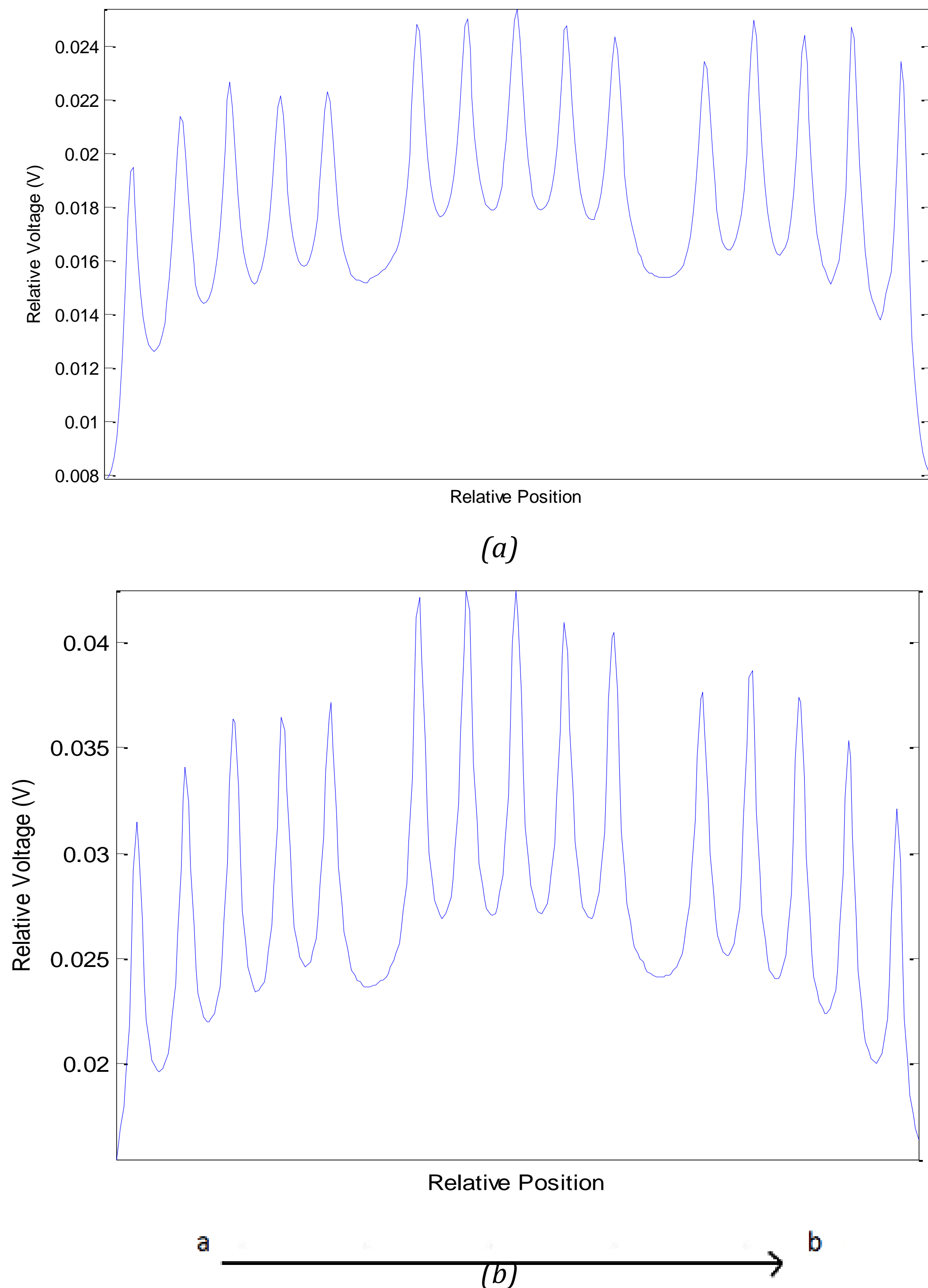

Figure 8.5: Automated spatial resolution scans along the drain side bondwire array, of the main LDMOS device within the A-DPA, as the probe is transversely moved in the direction of "a" to "b" for a (a) lower RF input and a (b) RF input deep within saturation.

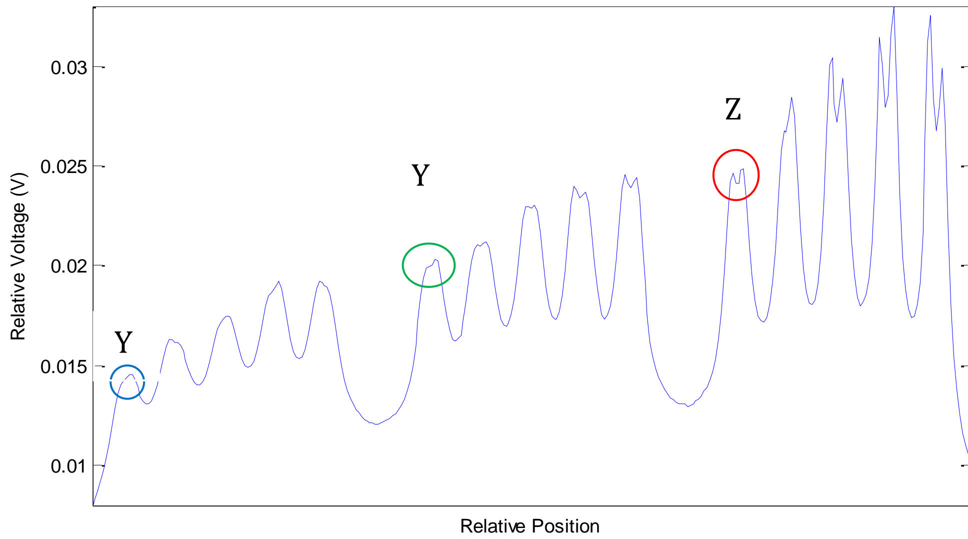

(a)

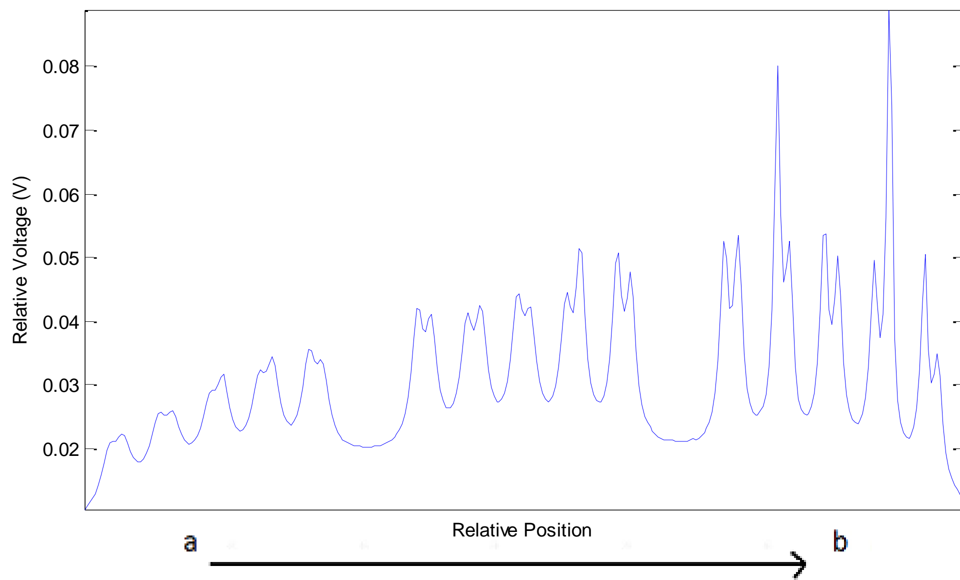

(b)

Figure 8.6: Automated spatial resolution scans along the drain side bondwire array, of the peaking LDMOS device within the A-DPA, as the probe is transversely moved in the direction of 'a' to 'b' for a (a) lower RF input and a (b) RF input deep within saturation.

Comparing the automated scans within 8.5 (a) and (b), the increased RF input is observable in the resultant measurement of the probe output. The significant observation from the figures above is the clear and visible trend is present in the

voltage distribution of the main device. Both the peaks and the troughs exhibit an umbrella shaped distribution, showing maximum voltage in the central position of the device. This trend is more substantial at higher input power levels.

The variation in the voltage distribution of the peaking device yields an interesting analysis. Considering figures 8.5 (a) and (b), the output measured by the probe is consistent to the increase in the input power, however this observed increase is to a much higher magnitude. The resulting increase in the input power has a direct effect on the spatial resolution of the probe, the subsequent scan shown in figure 8.6 (b) shows a more distinguished bondwire resolution. The visible trend in both scans display a dominant linear increase in the resulting magnitude, this trend has a direct effect on the spatial resolution recorded. As the measurement plane is moved from 'a' to 'b', a noticeable improvement is present in the spatial resolution of the EFP, which suggests that the EFP has capability of resolution within the 50μm range.

The variation observed in the peak voltage values, of both the main and peaking device, are clearly due to non-planarity of the bondwires. It has been well documented that the EFP is sensitive to both planarity and the local geometry, therefore any variation present as a result of fabrication error will be translated to variation in the distribution.

The increments chosen between each movement of the EFP was a critical decision, where the resulting step-size must be comparable to the desired resolution. If the increment was too large, maximum resolution cannot be achieved; while an increment too small will result in over sampling and increase the scanning time beyond a necessary rate. Although the optimum increment has been chosen for both transverse scans shown in figure 8.5 and 8.6, an increase in the step-size can fully investigate the differences in the resolution achieved within figure 8.5. The highlighted sections of the peaking device annotated in figure 8.6 (a) is repeated with a decreased step-size of two times the standard rate.

The probe is then chosen to re-scan the first two bondwires within each section of the peaking device's bondwire array, which have been annotated as 'X', 'Y' and 'Z'.

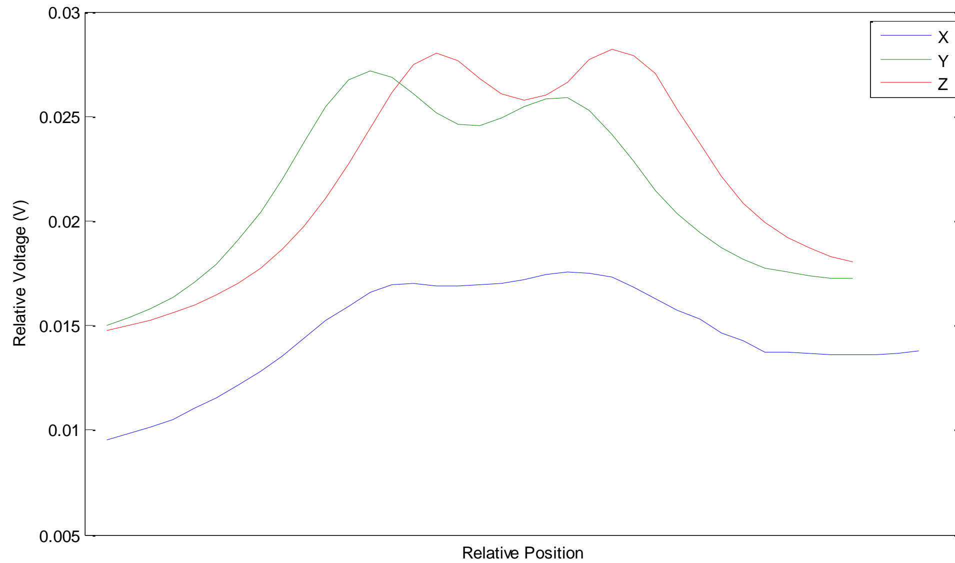

Figure 8.7: Spatial resolution scans, with and increased data point along of the twin bondwires within the peaking device shown in figure 8.5 (a). Any differences observed in the horizontal scale are due to the variance in the initial scanning point of the EFP.

From the scans shown above, it can be seen that the resolution of the EFP is not improved as the increments between the automated movements are increased. The resulting scan shown in figure 8.7 is in accordance, and provides confirmation, of the resolution achieved within figure 8.6 (a). Showing a measured magnitude where, $Z > Y > X$ and the measured resolution where, $(Z \approx Y) > X$.

Additional spatial resolution analysis was conducted on the metallisation of the die for both devices within the A-DPA. Distributions measured were expected to exhibit a proportional variance present in the bondwire measurements. However, due to the nominally planer surface of the die, the planarity issues present in the bondwire measurements can be reduced.

The spatial resolution scans resulting from the metallisation of the die are conducted mid-way between the drain and gate bondwire arrays. The probe was lowered to this position, at a measurement plane of 30μm and transversely scanned from position "*a*" to "*b*". The resulting transverse scans for the main and peaking devices are shown in figure 8.8 and 8.9, respectively.

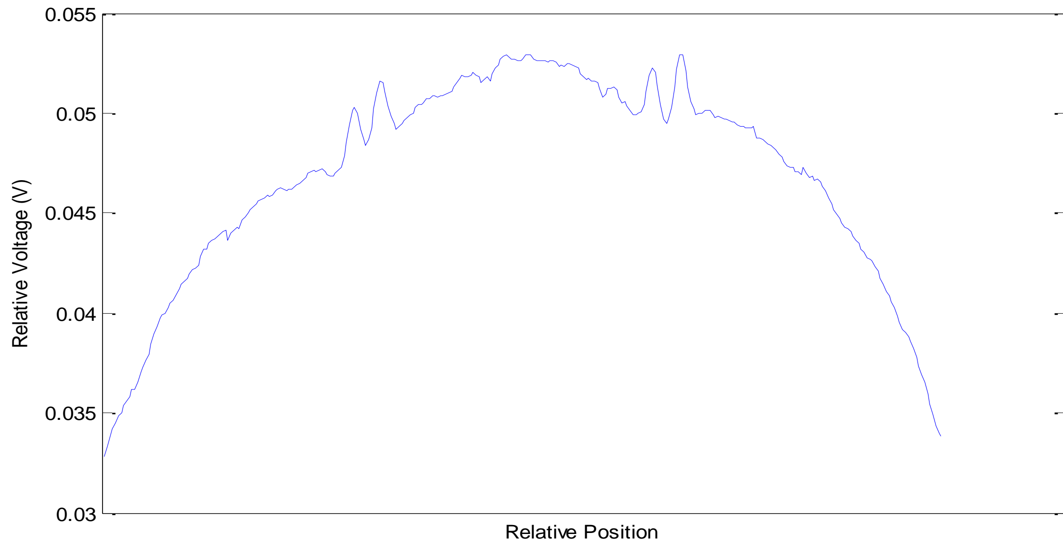

Figure 8.8: Automated spatial resolution scan along the metallisation of the die, within the main LDMOS device, as the probe is positioned in a central location, with a separation of 30μm as it is transversely moved down the device in the direction of a to b. The resulting distribution presents a dominant "umbrella" shaped trend with a "mysterious" double peaks.

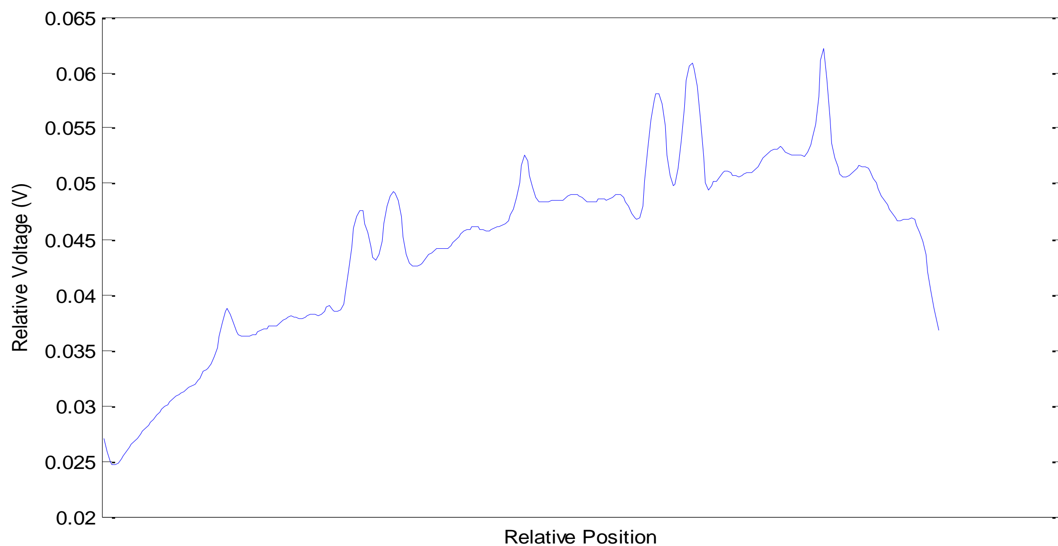

Figure 8.9: Automated spatial resolution scan along the metallisation of the die, within the peaking LDMOS device, as the probe is positioned in a central location, with a separation of 30μm as it is transversely moved down the device in the direction of a to b. The resulting distribution presents a dominant trend with a "mysterious" double and mid-die peaks.

From both scans presented within figures 8.8 and 8.9, confirmation is given to the coherent distribution presented in figures 8.5 and 8.6. The distribution of the main device exhibits a clear and more predominant "umbrella" trend, displaying a maximum magnitude in the central section of the transistor with substantial roll off at the end sections of die.

The distribution present in figure 8.9, shows a clear increase in the measured magnitude as the probe transitions between the scanning range of "*a*" to "*b*".

It must be noted that both measurements conducted above exhibited an unexpected twin peak and mid-die peak. Both exhibit a twin-peak as the EFP is moved over adjacent sections of die; with an addition mid-die peak present in the peaking device.

Further visual inspection of both the main and peaking device revealed the cause of the mid-die and twin-peaks.

Figure 8.9 below shows a magnified image of the square pads present between two adjacent sections of metallisation die.

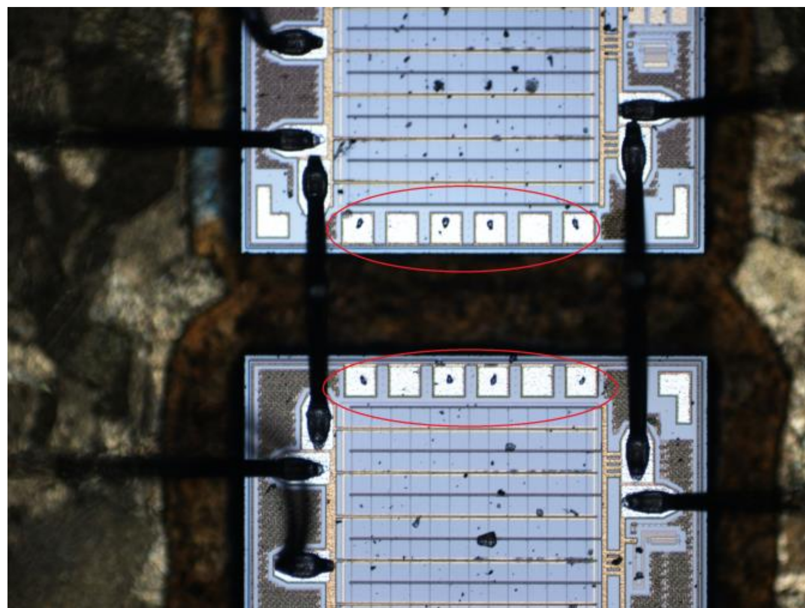

Figure 8.10: A highly magnified image of the LDMOS device, showing the pads present between adjacent sections of die metallisation. Highlighting the cause of the observed twin-peak measured in spatial resolution scans.

Both the main and peaking device contained the pads, shown above, and ultimately resulted in the measurement of the twin-peaks.

Additional mid-die peaks, within the peaking device, were understood with visual inspection. The mid-point within each section of die contained a cluster of 3 closely positioned interdigital fingers, shown in different magnifications within figure 8.11.

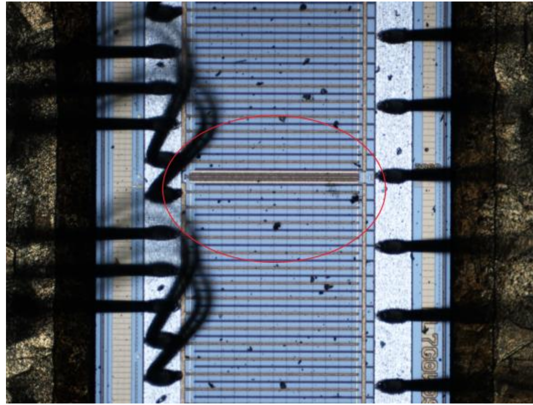

(a)

(b)

(c)

Figure 8.11 (a) (b) (c): A highly magnified image of the peaking LDMOS device, showing an unexpected finger orientation in the interdigital array of the die metallisation. Highlighting the cause of the observed mid-die peak measured in spatial resolution scans.

From figure 8.11 (c), it can be seen that this cluster of interdigital fingers is of a comparable size to that of a bondwire, therefore the resultant distribution of electric field can be accordingly measured by the EFP. It will be shown, within section 8.1.4, that waveform distribution along the metallisation will too vary as a result of this intentional design orientation.

8.1.4. Waveform analysis of the A-DPA

The work conducted within the previous section has shown conclusive evidence to the extent of variation present along the device periphery. Such measurements can provide vital information with regards to the amplifiers functionality; as it is generally assumed that the device behaves in a much simpler manner, therefore characterisation has not been as accurate. In reality the high power transistor is a complex and distributed device, with the ability to display substantial variation along the device periphery. Waveform analysis performed on the A-DPA can provide further information to aid the understanding of such a complex device.
This section will show two forms of data measurement, one required a stationary position of the EFP, while the other required an automated movement. For the extraction of the fundamental component and observation of classical Doherty behaviour; measurements will be conducted as a function of increased RF input, for a stationary position of the EFP. To display the full extent of variation along a device periphery, the EFP is transitioned between different positions at a constant RF input.

Initial waveform analysis was performed for the verification of the mid-die peaks present in the spatial resolution scans, conducted within section 8.1.3. Preliminary measurements required the same plane of movement across the metallisation of the peaking device. The probe was placed in the same position, between the drain and gate side bondwire arrays, at a separation plane of 30µm. As shown in figure 8.4 (b), the peaking device consisted of three sections of die metallisation. The scan shown in figure 8.11 was a result of intensive measurements of one section of die, at a constant RF input close to saturation.

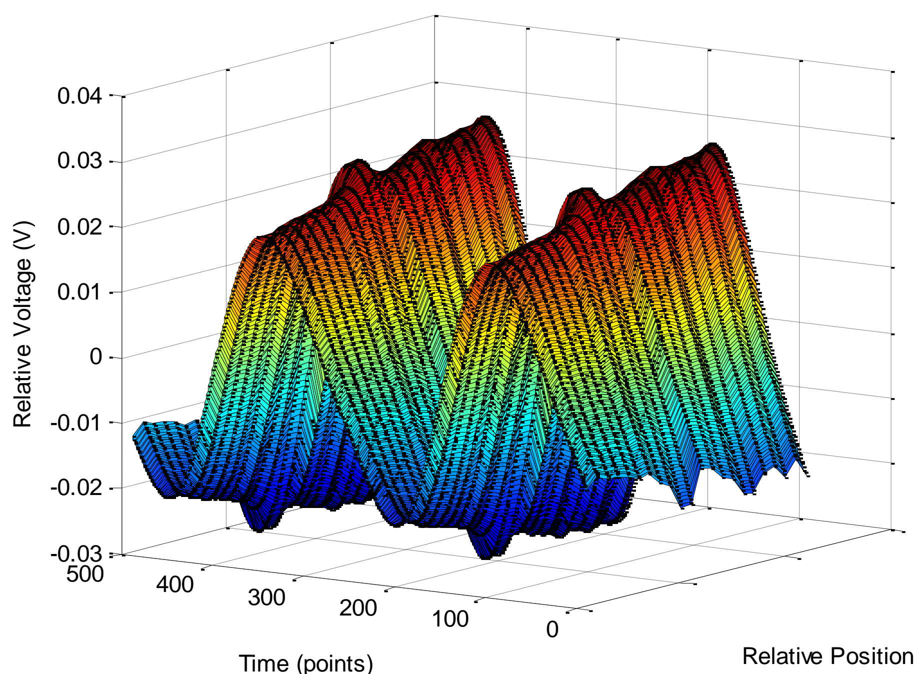

Figure 8.12: Scan depicting the waveform distribution of the middle die of the peaking device, at a constant RF input close to saturation, with waveform evidence of the mid-die peak.

The figure above displays consistent mid-die peak behaviour within the waveform distribution. Therefore showing the design of the interdigital cluster directly effecting the resulting waveform distribution of the device. This intentional design will therefore have a repercussive effect on the distribution fed to the drain bondwire array.

For the extraction of the fundamental drain voltage component, equivalent positions along the main and peaking device were chosen for comparison.
Due to the high degree of variation along the devices, the results displayed solely depend on the two points of comparison. For example, the plots shown below, in figure 8.13 (a) and (b), are an examples the differences present in the fundamental values. Figure 8.13 (a) displays the results of two comparative positions a central point on the central die, while 8.13 (b) displays comparative position at the die edge on the central die.

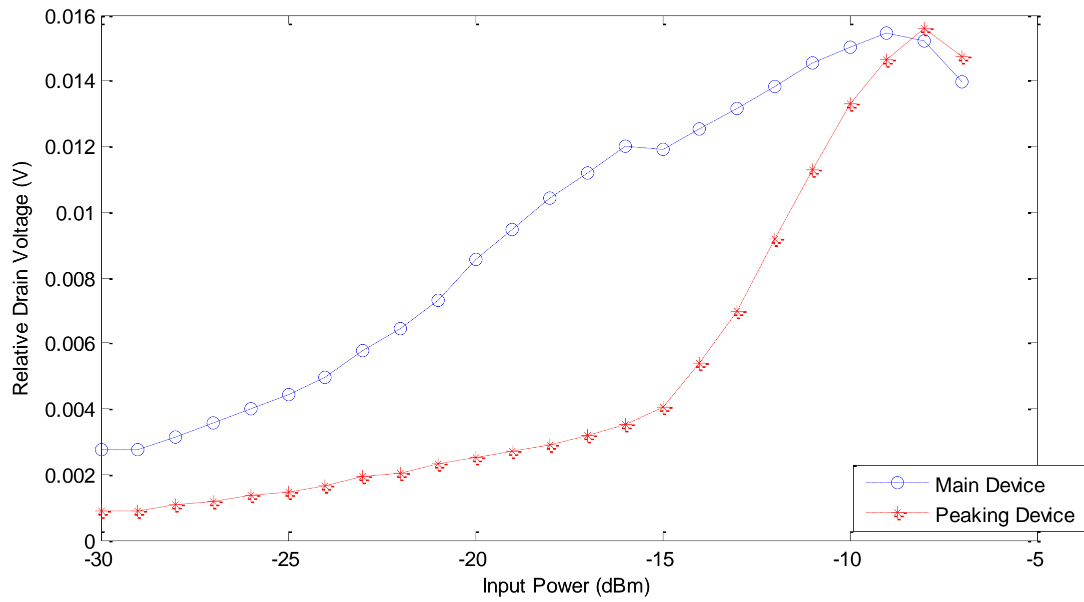

(a)

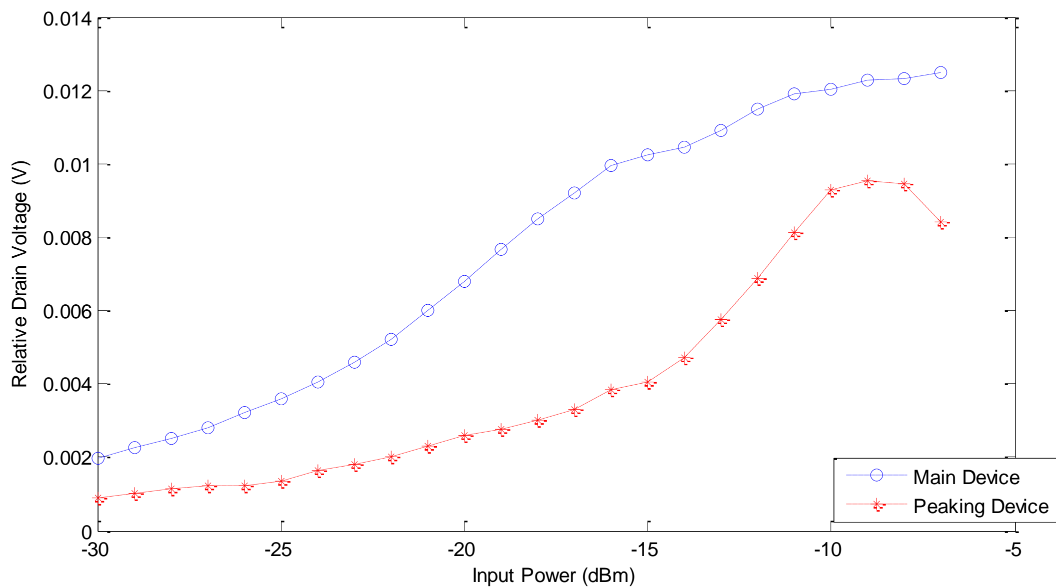

(b)

Figure 8.13: Fundamental drain voltage component of the main and peaking device as a function of increased RF input, where (a) is a central position down the device and (b) is at the device edge.

Due to the substantial variation along the device, the point of comparison chosen greatly effects the fundamental plot. Discrepancies are presented in the saturated values of the main and peaking voltages. It can be seen that in specific sections of the die, that although the "on" state of the peaking device results in the main device

to be taken into saturation, the peaking voltage does not reach the maximum main voltage. This variation is not a favourable outcome as the device is not performing to the expected characteristic behaviour.

To show the full extent of the variation present along the main and peaking device, different positions along each periphery were chosen and plotted. Figure 8.14 shows the positions of measurement, while figure 8.15 displays their result and the extent of variation present within each subsection.

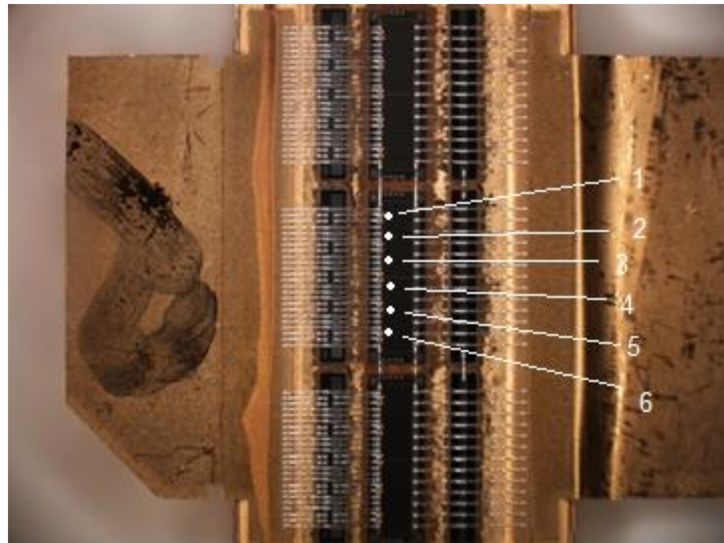

Figure 8.14: A magnified image of the LDMOS device, with ceramic lid removed, displaying the positions for further measurement.

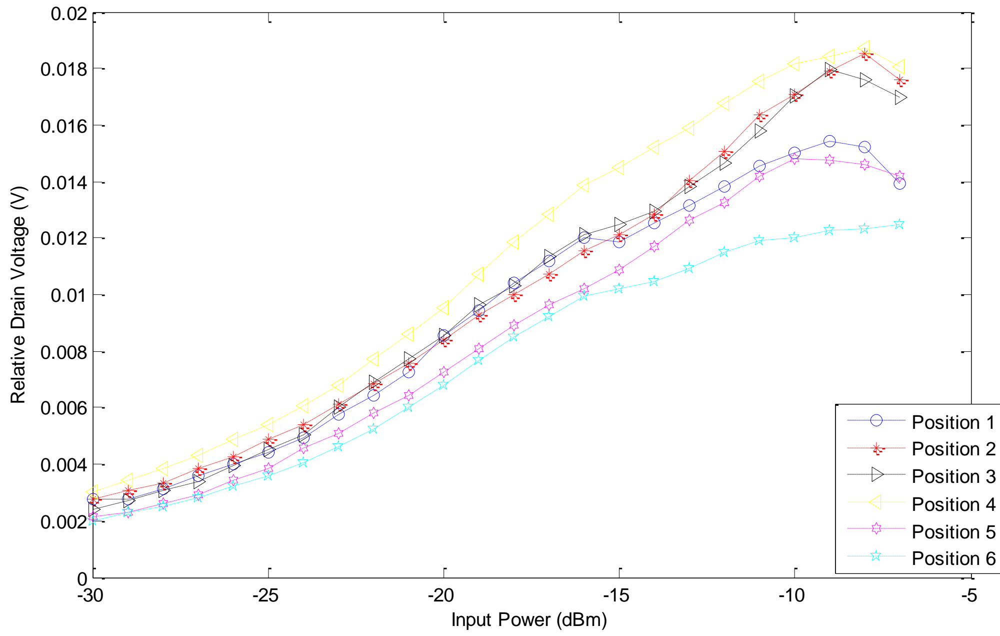

(a)

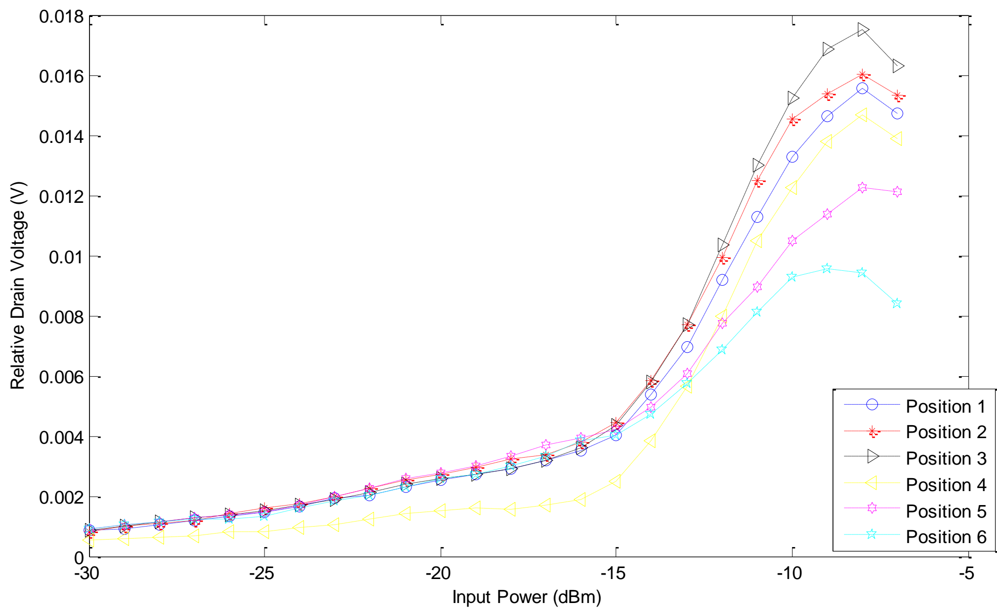

(b)

Figure 8.15: Fundamental drain voltage component of the main and peaking device as a function of increased RF input; where (a) shows the variation along the main device and (b) shows the variation along the peaking device.

From figure 8.15 (a) and (b), the extent of the variation along both devices can be clearly seen. Variation in the peak and saturated values of this kind are a result of

an unintentional design flaw. Discontinuity in the power distribution can potentially have detrimental effects; most notably linearity and reliability. With the aid of the EFP as a diagnostic tool, the designer can pre-empt potential errors within the matching network, which is clearly the cause of this variation. It must be stipulated that the measurement plane was not altered, and that the variation in the amplitude is a true representation of the variation measured at the output of the EFP.

The deviation of magnitude, measured across the device periphery, will result in the proportional variance exhibited in the waveform distribution. Specific comparison of two separate positions, shown below in figure 8.16 (a) and (b), shows the extent of the potential variation present within the main device.

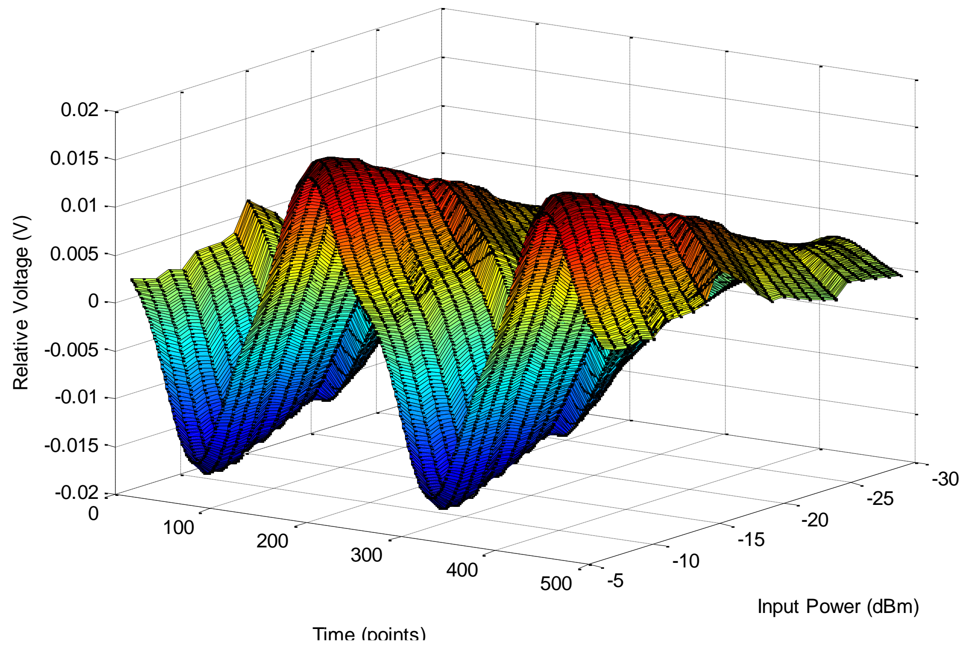

(a)

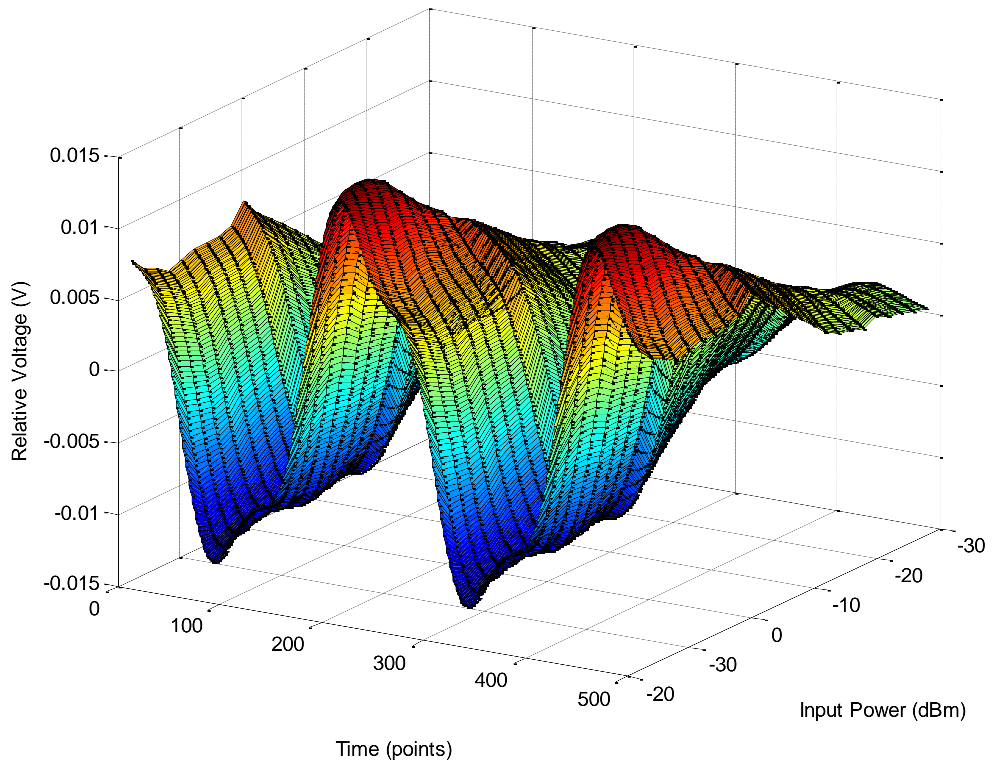

(b)

Figure 8.16: Voltage waveforms from the main device as the input power is stepped in 1dBm increments for (a) midway down the device and (b) the beginning of the

device; where substantial differences in the shape and magnitude of the distribution can be observed.

The figure shown above depicts the waveform distribution of two specific points along the main device of the A-DPA, as the RF input is increased in 1dBm increments. A clear difference in the measured peak to peak voltage values are observed between the two points. The waveform measurements shown in figure 8.16 (b), show a visible growth of a second harmonic component within the main device, a characteristic not predicted by classical Doherty analysis, and possibly beyond the range of conventional CAD simulators.

8.1.5. Waveform analysis of the A-DPA at band-edge frequencies

The 2.14GHz A-DPA can be measured at the band-edge for further characterisation and the understanding of anomalous behaviour. An amplifier designed at a particular frequency will exhibit ideal and optimum performance within this bandwidth. However, frequencies beyond the specified bandwidth will result in a degradation in performance. Measurements within this section will highlight potential disadvantages arising from the out of band excitation.

Further measurements are therefore taken at the upper and lower band edges, of 2.12GHz and 2.16GHz, respectively. RF input and output measurements at these frequencies show an improved peak efficiency at 2.16GHz, while the lower band edge exhibits similar efficiency to the recommended frequency of 2.14GHz.

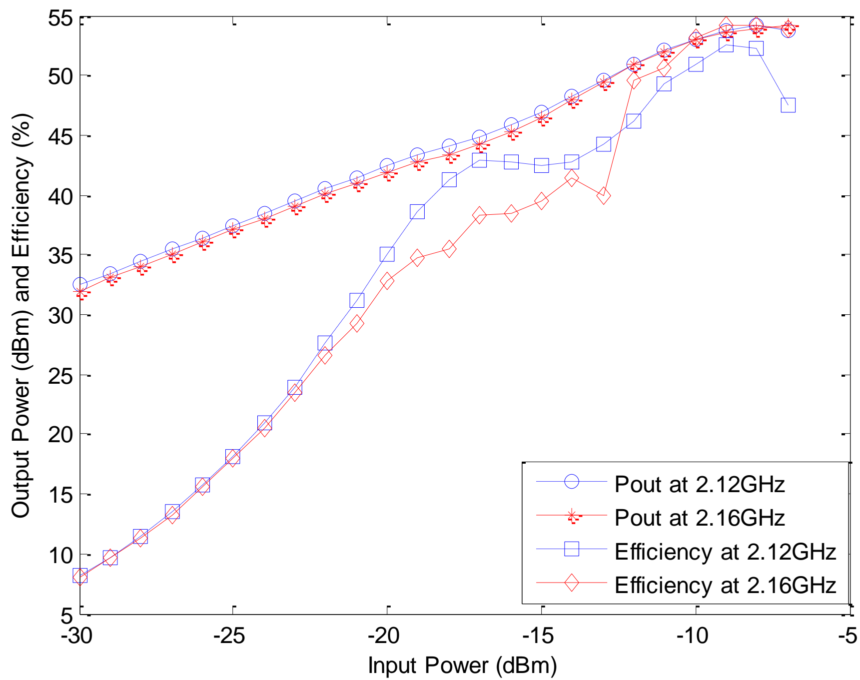

Figure 8.17: RF input and output characteristic of the A-DPA with increased input power, for band-edge frequencies 2.12GHz and 2.16GHz.

The measurements shown below display the variation in the fundamental voltage component, with respect to increasing input drive, along the device periphery; at both band-edge frequencies. For direct comparison of the two frequencies, while in one position, the EFP was used to measure at both band-edge frequencies i.e. the EFP position was not altered as the excitation frequency was interchanged.

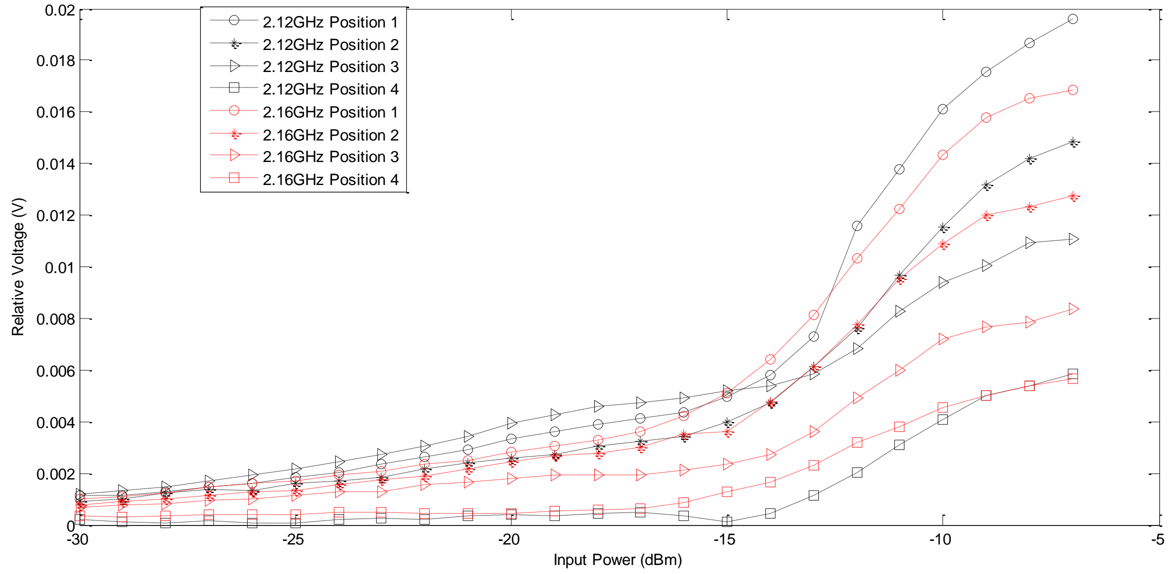

(a)

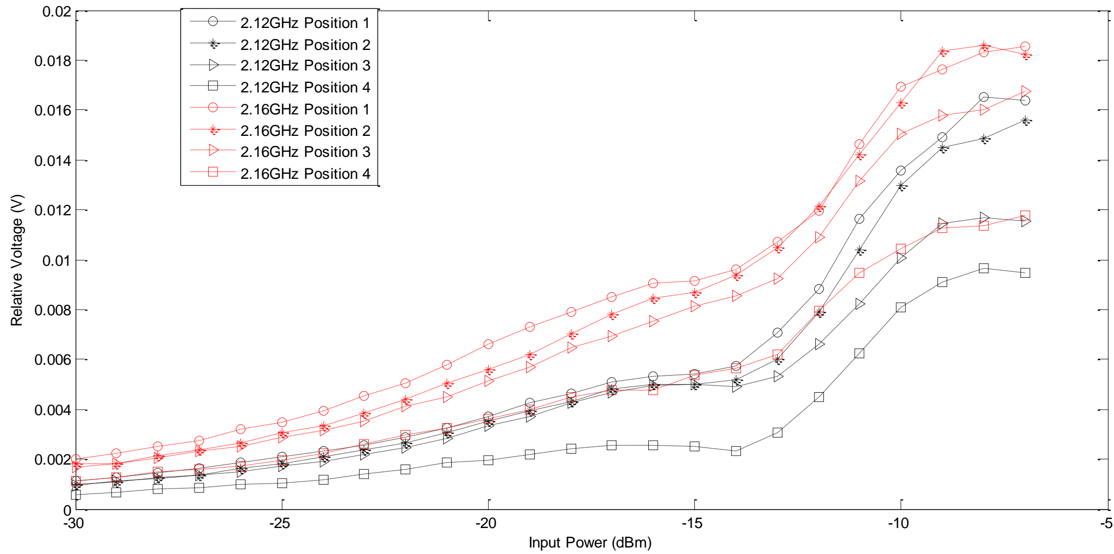

(b)

Figure 8.18: Fundamental drain voltage component for four different positions along the device, as a function increased RF input, at both 2.12GHz (shown in black) and 2.16GHz (shown in red); where (a) shows the variation along the main device and (b) shows the variation along the peaking device.

Although the position of the probe was not changed between different frequency measurements, the resulting variation in the fundamental component is evident. With a greater variation in the main device, the operational frequency has dictated the saturated drain voltage and as well as the functionality of the device.

From the evidence presented in the fundamental components, it would suggest that the matching network on the main device presents a low impedance at low input power; therefore the voltage rises at a much lower rate in the pre-peaking regime. As the RF input is increased, the contribution of the peaking device to the system, the voltage moves to a higher and saturated level, as a result of correct load modulation.

8.2. Conclusion

Within this chapter, further application of the EFP has successfully shown extended analysis of Doherty systems. The ability to obtain real-time waveform measurements can give valuable information about internal characteristics of an active device within the amplifier, which has been previously un-reported.

The extent of variation along the periphery of the device has been demonstrated, in both spatial resolution and waveform distribution analysis. This variation is specific to the individual device, which is to be expected of an asymmetrical configuration. The central point of the main device has been shown to have the maximum measured voltage value, with substantial and unexpected roll-off at both edges. Whereas the peaking device has shown a gradual increase in its amplitude distribution, as the measurements were conducted down the device.

Theoretical and ideal expectations of the A-DPA require an equal and constant voltage distribution, both anomalies mentioned above can result in great disadvantages to the overall intended design. This can result in a deviation of internal behaviour from the idealised characteristics between the input and output of the device. Without the EFP technique, these highly significant deviations could not be observed and measured. Other methods of device characterisation assume a single node device, though it has been clearly shown that the transistor behaves inconsistently throughout the device periphery.

Further measurements at the band-edge has resulted in the knowledge of characteristic behaviour at the out of band frequencies; fundamental measurements have shown the true impact on the matching network as a result.

At low input power levels, the peaking device is considered off, with no contribution to the net current. Although there is no expected current contribution, it is evident from the resulting voltage analysis, that there is some form of

contribution present. At the bandedge, this voltage contribution at low levels of input power is much higher than at the mid-band frequency, thus the deviation from the expected Doherty behaviour.

9. "IN-SITU" CALIBRATION METHOD FOR EFP

This thesis has successfully described the design, fabrication and implementation of an EFP. The measurements thus far have been made relatively, with no absolute calibration performed in-situ during the measurement process. Various references have been made to the lack of calibration techniques conducted in previous documented electric field probe research, while any mentions made have not utilised in-situ measurements, but rather a measurement and comparison of a 'known' DUT.

The work conducted within this thesis has described a novel method for the internal measurements of device plane voltages within the packaged high power transistor devices. Absolute calibration of this unique measurement technique has posed somewhat difficult. This chapter will go on to describe a novel in-situ calibration technique for the electric field probe, which has the capability to be utilised before every probe measurement. Unfortunately, due to time constraints this method of in-situ calibration was not performed on the measurements presented within previous chapters. This technique was developed at the late stage of this research, therefore it has been included to show the possibility for absolute calibration of the EFP system.

9.1. Basic concepts of proposed technique

The miniaturised size and the flexibility in its positioning has allowed the EFP to perform measurements in various positions along a packaged transistor device. The coupling factor has been shown to be an extremely sensitive function of the

spacing of the probe to the circuit element. The probe output is therefore a very complex function of the spacing and the local geometry of the probing target.

A successful method of absolute calibration requires the development of a 'known' voltage, which would subsequently result in the comparison of measured EFP output. Due to the sensitivity of the probe to the local geometry, in-situ calibration should be conducted with every probe movement, i.e. as the probe target is altered between the planar surface and the bondwire array of the semiconductor device.
However, at microwave frequencies, development of a 'known' voltage poses some difficulty as the measurement point is deeply embedded in a distributed microwave circuit.
A possible solution is to recognise that the coupling of the probe to the circuit is essentially capacitive and "quasi-static". As such, the critical coupling factor can be measured at any convenient frequency, which can for example be much lower than the operational frequency of the circuit under test. In particular, a sufficiently low calibration frequency can be chosen such that the spatial variation of the voltage in the region of the probe target, is massively reduced and can be measured conveniently.
The intended low frequency measurements for the in-situ calibration of the EFP will require the use of the initial MMIC amplified probe, as seen in the beginning of Chapter 5. The improved MMIC amplifier designed later in that chapter provided much improvement in the frequency response, extending the flat response to a higher frequency. However, the addition of the input shunt resistor resulted in a sharp roll-off at extremely low frequencies <10MHz. For the measurement of the high frequency devices, this trade-off was considered negligible. However, for low frequency calibration, this probe was not practical and therefore the probe designed initially in Chapter 5 will be utilised.

The broadband frequency response of the MMIC EFP is shown below in figure 9.1.

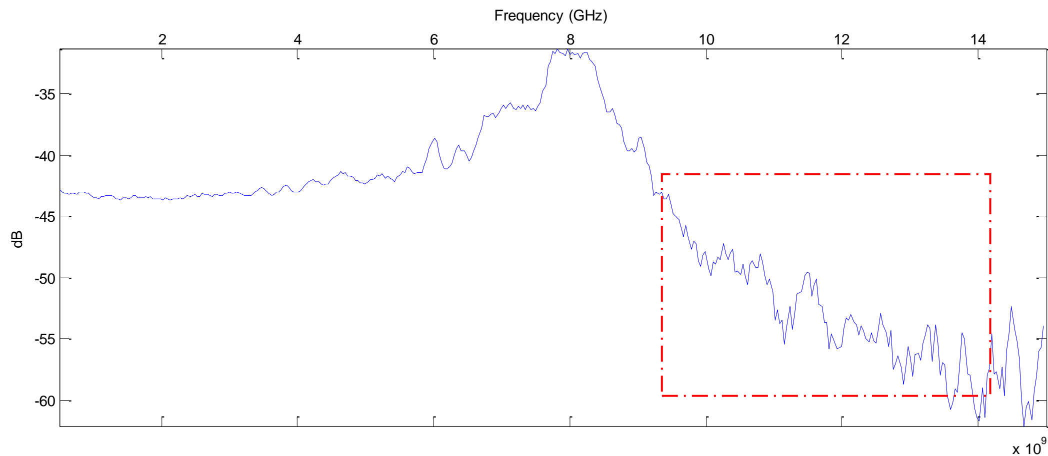

Figure 9.1: Frequency response of MMIC probe to be utilised for the 1MHz calibration. Showing a flat response at very low frequencies to 8GHz, where the response indicated within the dotted box is a result of parasitic components of the amplifier and not the design of the probe.

The frequency calibration of the EFP shows the nominally flat response extends to low frequencies <1MHz, thus reiterating the suitability for low-frequency calibration. At higher frequencies the response of the EFP is no longer flat beyond the resonance as parasitic components begin to dominate; this is indicated by the dotted box. These parasitic components have been shown, in section 5.3.2, to be a function of the MMIC amplifier and not a result of the EDM EFP design, and in particular the spacing from the DUT.

9.1.1. Low frequency analysis

The frequency calibration of the EFP has shown its suitability to be utilised at very low frequencies. The necessity of this result will be shown in this section for the novel 1MHz in-situ calibration. The calibration method will require the measurement and comparison of a DUT at two alternative frequencies, 2.1GHz and 1MHz. A microwave circuit excited at very low frequencies will exhibit an even distribution of voltage across the whole device. Therefore a voltage measured on the feed lines of a transistor will be similar to the voltage measured at the device bonding pads. Using a high impedance oscilloscope probe, direct measurement of the voltage at a given point can be compared to the output of the EFP. The scope used for direct measurement of the DUT was a 350MHz-5GS/s Tektronix, TDS5032B Digital Phosphor Oscilloscope (DPO).

Thus a 2-step calibration procedure can be described: (1) the frequency response can be measured as a relative function using any convenient structure, such as a microstrip line. (2) With the probe in position to make a measurement in the target structure under test, the target is "illuminated" by a known low frequency signal (e.g. 1MHz). This allows absolute calibration of the actual microwave frequency measurement, along with a suitable frequency correction obtained in the first step (1).

Initial analysis of the EFP considered a simple capacitive coupling model. In order to investigate the validity of this model, the spatial resolution of the EFP must be evaluated at low frequencies. The spatial resolution of the EFP can potentially be compromised due to the change in the penetration of electric field through the wall of the thin co-axial line; the skin depth for copper at 1MHz is approximately 30 microns which is not much lower than the wall thickness of the EDM tube. Experimental analysis can however eliminate this concern, as shown in figure 9.2, where the bondwire array of the drain side of the DUT has been scanned at 2.1GHz, 10MHz, and 1MHz. The DUT used for the 1MHz calibration is a 10W 3.5GHz GaAs pHEMT FET, mounted on a simple test fixture with a pre-designed matching network (part number: MRFG35010). Biased at $V_{ds} = 12V$ and $V_{gs} = -0.9V$.

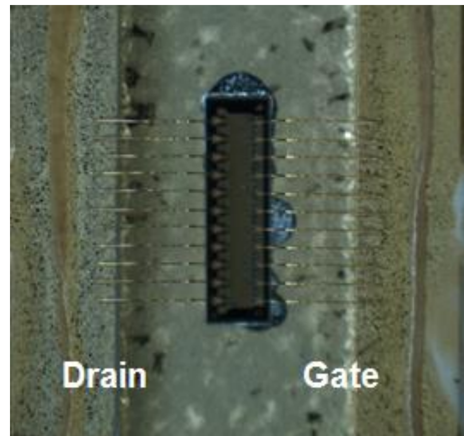

(a)

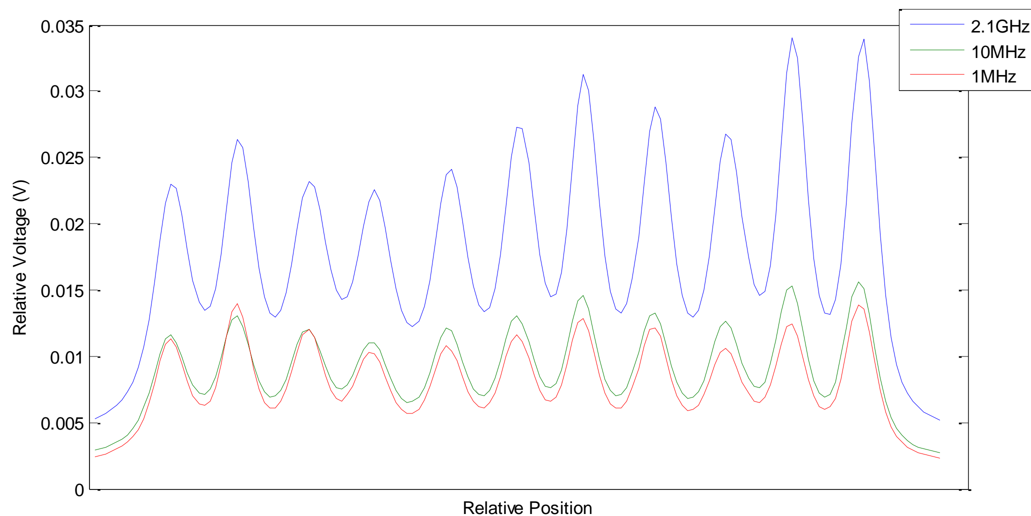

(b)

Figure 9.2 (a) Shows the structure of the 10W GaAs transistor under investigation, de-lidded for device plane analysis. (b) Shows the resultant spatial resolution scans of the drain side bondwire array, conducted at different frequencies 2.1GHz, 10MHz and 1MHz, respectively; where the decrease in frequency has no effect on the spatial resolution of the EFP.

From the figure above it can be concluded that no degradation of resolution occurs with the decrease of excitation frequency. Anomalous differences present in measured peak values of the relative voltage, are solely due to the planarity issues existing in the bondwires of the GaAs device. As mentioned previously, the probe output is a function of its local geometry, thus the highly sensitive EFP subjected to

changes in the curvature and bondwire height, will exhibit a proportional variance in its output.

9.1.2. RF input and output characteristics of the 10W GaAs device

The device shown in figure 9.2(a) depicts the GaAs transistor once the ceramic casing had been removed. Prior to the removal, the RF Pin/Pout sweeps were conducted and compared to the de-lidded sweeps. The resulting comparison is found to be negligible and shown in figure 9.3.

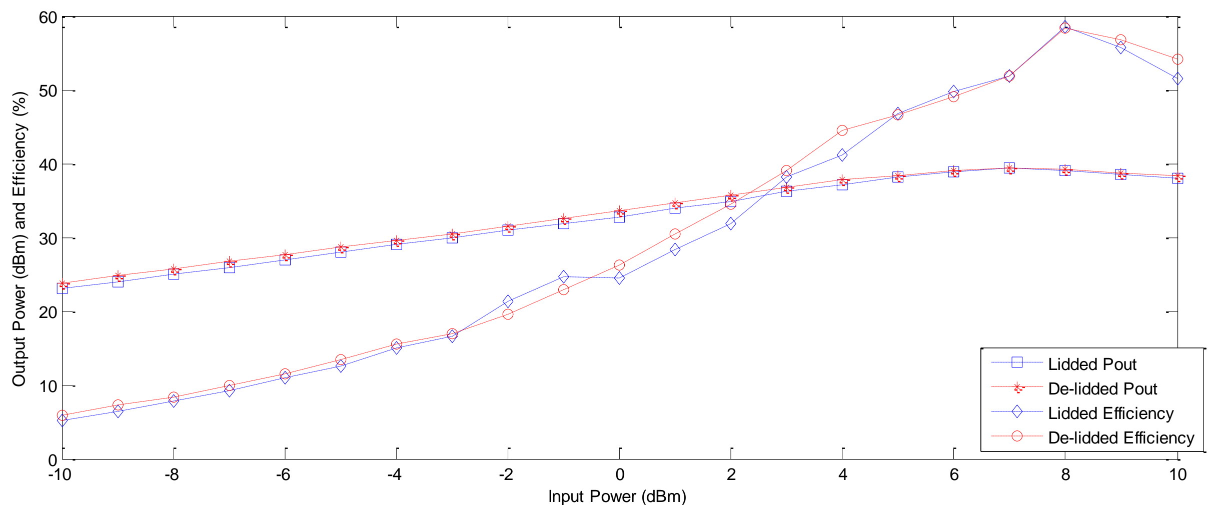

Figure 9.3: RF input and output characteristic at 2.1GHz of the 10W GaAs device with increased input power before and after the removal of the ceramic casing, showing negligible impact on the device performance.

9.1.3. Measurement setup

In order to meet the objective, stated in section 9.1.1 of a two-step in-situ calibration technique, the resultant measurement must be conducted with a constant measurement plane as the injected excitation is interchanged between 2.1GHz and 1MHz. During this time, waveform information from the output of the EFP, at a constant position, is captured by a DSO at both frequencies. Direct measurement of the voltage at 1MHz can be obtained with a high impedance

oscilloscope probe, resulting in a calculated scaling factor for the 1MHz waveform. This scaling factor can then be applied to successive EFP measurements at 2.1GHz.

For a successful interchange of excitation, two separate sources are used for the supply of 2.1GHz and 1MHz, this procedure insures the equivalent positioning of the EFP. Figure 9.4 shows a block diagram for the measurement setup, 2.1GHz and 1MHz. The measurements obtained at 1MHz required the increase of the gate voltage to the pinch-off level, thus insuring no current to be drawn (V_{gs} is increased from -0.9V to -1.5V).

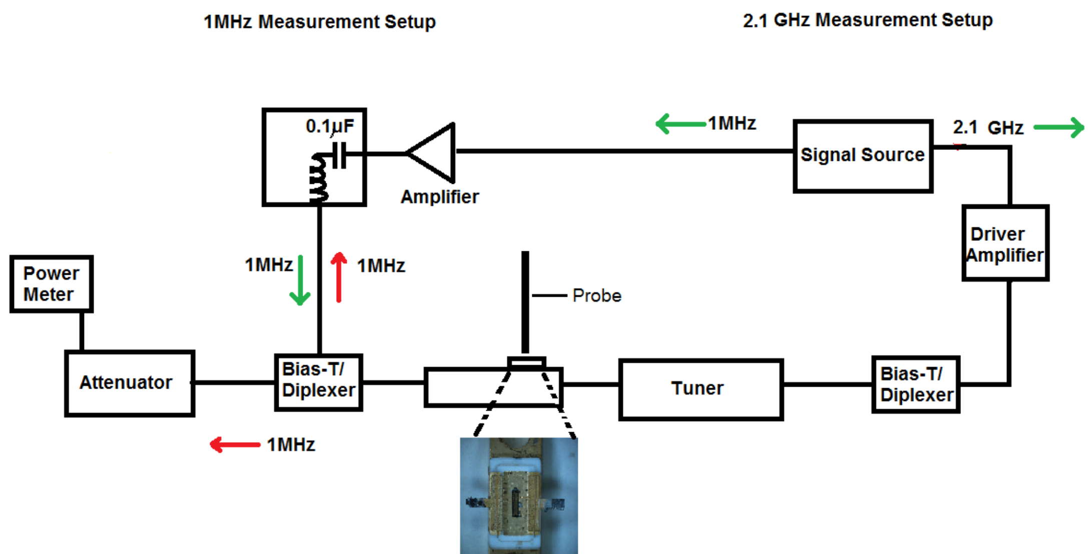

Figure 9.5: Block diagram of the measurement setup required for the 1MHz and 2.1GHz measurement; where green arrow indicates the direction of flow, while red arrows represents the blocking of flow.

9.1.4. Experimental results

Utilising the experimental setup shown in the previous section, the waveform information is captured by the EFP at 2.1GHz and 1MHz. Using a DPO with a probe attachment, the direct contact is made on the microstrip line leading to the GaAs device at 1MHz. From this captured waveform, a suitable scaling factor can be achieved for the EFP measurement at 1MHz. This scaling factor is found to be 615. Figure 9.5 shows the resultant waveform measurements obtained from the DPO and the scaled up waveform measured from the EFP, both at 1MHz.

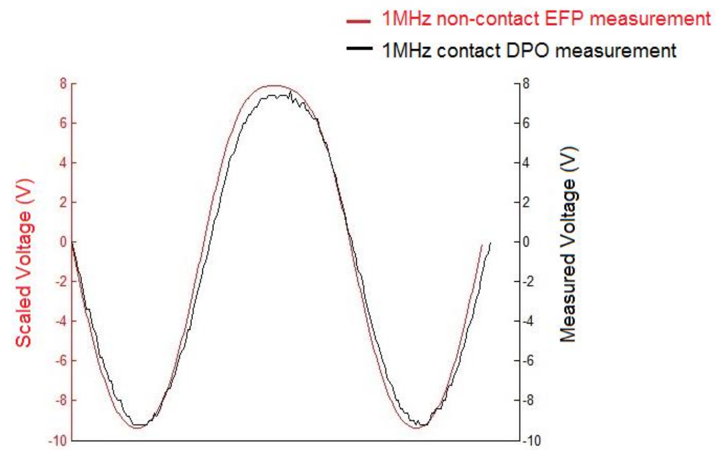

Figure 9.5: Superimposed waveforms measured at 1MHz from contact measurement of DPO and the scaled EFP measurement.

The calculated scaling factor is applied to the waveform measurements obtained by the EFP for a power sweep of 0-9dBm at 2.1GHz, the results are shown in figure 9.6.

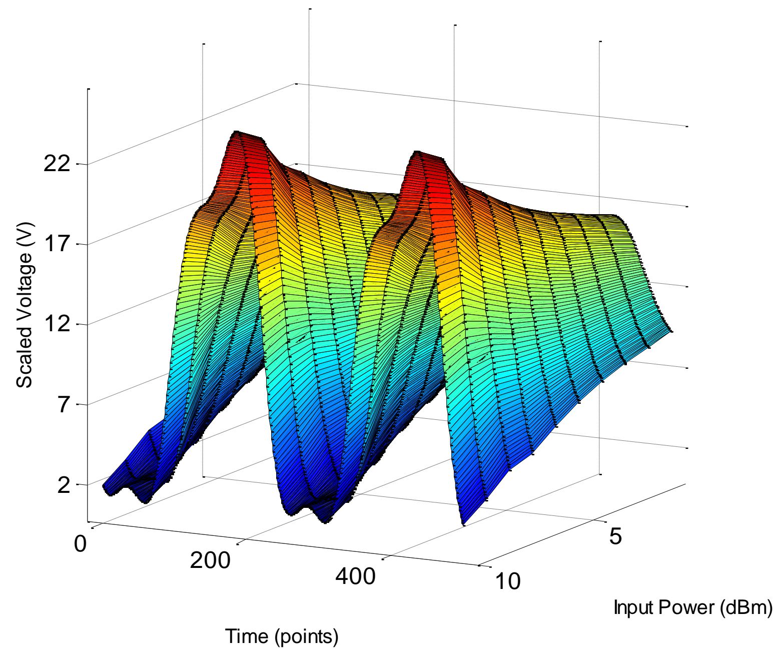

(a)

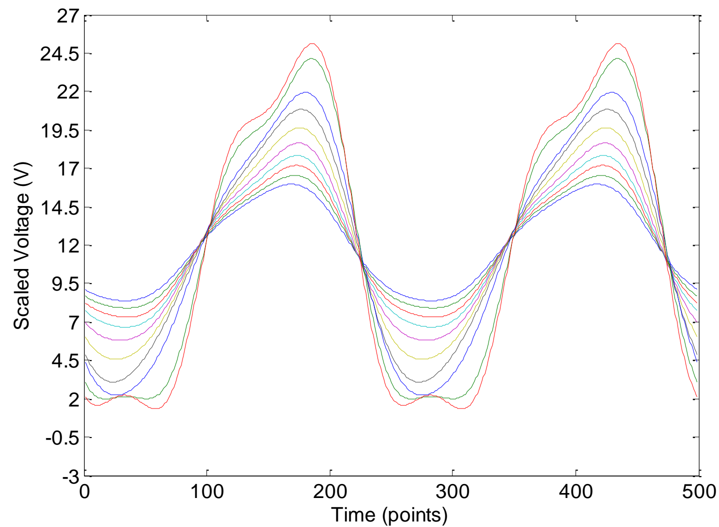

(b)

Figure 9.6: Power sweep of 0-9dBm conducted at the frequency 2.1GHz, where the EFP output has been accordingly scaled by the calculated factor of 615; represented in (a) 3D and (b) 2D format. Note probe is AC coupled, the actual Vdc value of 12V.

9.2. Conclusion

This chapter has successfully introduced and employed a novel in-situ calibration technique for a high resolution EFP. By exploiting the low frequency response of a system, whereby at such frequencies, even the most complicated structures behave in a much simpler manner. This resulted in an equal voltage distribution across all parts of the device. Due to the resolution capability and flat low frequency response of the EFP, it has been demonstrated that its spatial resolution is independent of the measuring frequency. With a suitable scaling factor obtained from the 'known' voltage measurement, absolute calibration can be determined and applied.

It should be noted that this novel method of in-situ calibration was designed and implemented at the latest stage of the research presented within this thesis. Unfortunately due to time constraints, this calibration method was not applied to measurements shown in previous chapters. However, this method can be executed as an initial procedure in all future works of the EFP.

10. DISCUSSION

10.1. Design methodology of the EFP

Initial work presented required the construction and evolution of the EFP. Although a method utilised for decades for the measurement of electric field [13, 14, 16, 17, 18] referenced work can be regarded as incomplete. Spatial resolution of the EFP is a common goal throughout the literature, with many understanding that miniaturisation of the probe can achieve this result. However, the disadvantage of this miniaturisation is the loss in the measured output voltage of the probe. Commonly it has been seen that this particular disadvantage is resolved by the addition of a monopole protrusion of the inner conductor [14, 16, 19, 24]. Full consideration of this design methodology has not been thoroughly investigated and the detrimental effect the protrusion has on the spatial resolution is not understood. This thesis has intensely examined the effects of a protruding inner conductor, showing that an increase has a positive effect on the output voltage while providing an extremely negative effect on the spatial resolution. A protruding inner conductor greater than 0.05mm, has been shown to significantly reduce the spatial resolution when compared to a flush cut EFP. Literature has commonly presented inner conductor protrusions varying from 0.3mm [19], 1mm [24] to 5mm [16].

Increasing the inner conductor protrusion proportionally increases the output voltage of the probe, this is due to the increase in coupling between the EFP tip and the DUT. This increase in coupling is a result of an overall increase in effective probe tip surface area i.e. hypothetically larger probe; which ultimately results in

an increase of non-parallel e-field coupling and simultaneous coupling. Hence, the increase in probe output and a decrease in the spatial resolution.

For this reason the novel design of a buffer amplifier, placed close to the probe tip, is a more favourable method for signal amplification than probe tip protrusion.

10.2. Continuity of the measurement plane and the resulting output

Throughout this thesis, comprehensive investigation with regards to the EFP and the resulting measurement plane have been conducted. It has been well documented that the output of the probe is extremely sensitive to the local geometry of the DUT and the separation between probe tip and DUT. Questions concerning alteration in the measurement plane may exist with results presented within chapters 7 and 8, where in certain scenarios the device plane voltages differed by up to twice the minimum measurement. Differences in the peak values existed along the device periphery and between the adjacent main and peaking devices. However, the results shown in section 4.1.5 clearly indicate an increase of up to 100μm is required to achieve a difference of measured V_{pp} to decay by half. Such a substantial difference would be notable by the microscopic system used for precise positioning of the EFP. A simple experiment to disregard questions concerning the measurement plane requires an in-situ movement of the EFP. In the region where the measured peak voltage is at its maximum, the EFP can be backed-off gradually in order to achieve the half-point decay, the final change in the measurement plane is noticeably obvious through the microscopic equipment. Therefore it is believed that the results presented within chapters 7 and 8 are true representations of the device plane variation and not a result of measurement plane variation.

10.3. Response of true voltage

Waveform measurements presented in this thesis have undergone an intentional inversion before the process of Fourier analysis. The necessity of the inversion was discovered through a form of waveform calibration. By constructing a waveform with a distinct polarity, comparisons could be made with the EFP output and direct measurement of the signal generator (required for the excitation). This excitation, with a distinct waveform, was injected through a terminated section of

transmission line and subsequently measured. Results presented in section 6.1.3 showed the EFP has the capability of measuring a true representation of the DUT voltage. Further confirmation was presented within chapters 7 and 8 by the measurement of Doherty drain voltage characteristic. Placing the EFP directly over the drain manifold, the resulting response is a true representation of the drain voltages. During these measurements, the input drive is increased in single increments, where if the EFP was purely responding to this increase, the output would yield a linear proportional increase. However, with consideration of the main device, clear and evident saturation is recorded with the activation of the peaking device, therefore reinforcing that the EFP has the capability of directly measuring the DUT voltage.

10.4. Calibration

Chapter 2 discussed previous literature available regarding the EFP, where it has been commonly seen that absolute calibration poses great difficulty. Absolute calibration of the EFP within this work was presented in the final chapters, however due to time constraints the technique was never fully employed before the measurements shown in previous chapters. The data presented within chapter 9 provided the technique and theory behind the process, and successfully showed that a suitable scaling factor can be determined and applied to the output of the EFP, for actual representation of device plane voltage.

Without the employment of the calibration technique on passive and active measurements, the validity of the EFP output can be questioned. Before the design of the 1MHz technique, all prior measurements were performed on the 'relative' assumption. With this basis, the information presented can provide valuable insight to the functionality of the devices measured.

The calibration technique presented is an extremely novel method, it has been well documented that the EFP is very sensitive to the local geometry of the DUT, therefore requires a form of calibration applicable for all intended measurements. Thus the calibration technique can be applied as and when the probing target is altered. Previous methods of published calibration, although valid in its own right, can be questioned by the relevance of the intended measurement. Methods have included the measurement and comparison of a known entity such as a microstrip

line [23, 24] and shielded current carrying conductor [13]. However if the intended purpose of the probe is to characterise complex high power structures, then questions can arise to the applicability of these techniques. The response of the probe changes significantly depending on the DUT target, therefore calibrated measurements over a microstrip line cannot be compared to measurements of an active bondwire array.

Supplementary forms of calibration have been provided throughout this thesis, mainly as form of EFP characterisation and verification of the measured results. Measurements shown in section 6.1.3 can be regarded as a form of absolute calibration, as the EFP output is suitably compared to a 'known' target. Although the results presented show that the EFP has the ability to measure an inverted and scaled output, this technique is regarded as a verification method confirming the capability of the probe. Measurements conducted for this verification are required over a section of microstrip line, therefore the suitable scaling factor calculated, would only be applicable for similar circumstances and cannot be considered as a form of absolute calibration.

11. Conclusions and Future Works

11.1. Conclusions

Internal waveform information of high power transistors, within an operating amplifier system, has been a somewhat mysterious entity. EM simulation up to now has provided the most accurate interpretation of expected behaviour, but with no experimental verification, the simulators have only provided a guideline for these expectations [38]. Alternative methods including such as load-pull systems have successfully measured device plane waveforms, but usually at low power levels and not in actual working amplifiers [2, 3, 5]. However, the work presented in this thesis has successfully shown the design and implementation of a high-resolution EFP highlighting the true operating complexities of a high power transistor.

This thesis has been primarily split into two main sections; the evolution of the high-resolution EFP and its implementation as a diagnostic tool capable of characterising simple passive structures and highly complex active devices.

Chapter 2 discussed the theoretical expectation and functionality of the EFP, where it was first introduced that the resulting probe will essentially be capacitive. The EFP can 'connect' to the DUT due to the capacitive coupling between the inner conductor of the probe and the surface of the DUT. Due to the miniaturised size of the probe tip, the effective coupling that occurs is very low, thus requiring amplification. The small capacitance therefore represents a very high impedance, allowing the outer conductor of the probe to be considered as a virtual ground.

The introduction of buffer amplifier (required to combat low output voltages) close to the probe tip provides a series gate to source capacitance to the effective coupling present in the air gap between the probe tip and DUT, thus the system can be considered as a capacitive divider. This results in a frequency independent measure of the voltage across the gate to source of the buffer amplifier, a highly desirable feature of the novel EFP design.

Chapter 3 presented initial EFP analysis, highlighting the key factors effecting the resultant resolution and output of the measurement system. The construction of EFP3 showed the resulting resolution was a function of both the inner and outer diameters of the EFP. A reduction in both these dimensions will ultimately improve the resolution presented, however at the expense of the probe output. The loss in this output can be compensated for with the introduction of an intentional resonance. Signal improvement of up to 15dB have been shown, however this increase in the response had no positive implication on the resultant resolution. The REFP proved an extremely fragile design, very susceptible to damage due to its long and thin nature.

It has been well documented that increasing the level of miniaturisation of the EFP will cause less of a disturbance to the measuring field [23]. The probes presented within chapter 2 contained the largest EFP design within this thesis, subsequent analysis of the S_{11} parameter showed no negative effect by the probes presence. Therefore, systematic reduction in the dimensions of the probe shown in chapters 3 and 4 will ultimately reduce further potential disturbances.

Significant advancement in the EFP design was presented within chapter 4 by the incorporation of thin copper tubes for construction of custom made miniature coaxial cables. Drastic reduction in the outer diameter of the EFP by a uniform and rigid entity, allowed for improvements in spatial resolution and the resultant output of the probe, which vastly improved the results obtained by EFP3. Clear resolution of passive bondwire array structures were presented of the order of 100μm. Construction of the REFP was again investigated, with identical materials used for the fabrication of the EDM EFP, providing a much needed amplification in the output of the probe. Intentional design of a dominating resonance in the response of the probe, signal pick-up increased in the order of 15dB. Although the amplification of the output signal is highly desirable feature, two major disadvantages would compromise this result. The increase in the probe line length

further underlined the fragility and difficulty for construction, while the intentional resonance limited the EFP to a specific measuring frequency range. Results present within chapter 4 of the REFP showed no significant improvement in the resolution with the improved output, therefore the non-resonating EFP was considered a more favourable design.

Initial alleviation of low output required the incorporation of a low-noise SOT transistor package at the probe tip, however frequency calibration concluded only a flat response up to 4GHz. For the measurement of high power transistors within a PA system, the flat response must be extended to a much higher frequency. This led to the design and construction of an alternative amplifier in the form of a low-noise MMIC pHEMT transistor. Frequency calibration of the newly constructed MMIC EDM EFP showed substantial improvement in the resulting response, where the frequency response remained nominally flat up to 8GHz. However, with no additional reduction in the EFP dimensions, no further improvements were made with regards to the spatial resolution. Resolution of the 50μm structure presented within chapter 5, with many attempts made, could unfortunately not be recreated, therefore must be disregarded.

Chapters 3-5 show the design, construction and evolution of the EFP system successfully displaying a resolution of better than 100μm. The remaining sections of the work presented within this thesis implemented the EFP for the diagnostics of high power transistors within an operational PA system.

Initial work presented, within chapter 6, were conducted on a more simple system, containing one high power transistor. The removal of the device's protective ceramic casing allowed for internal in-situ measurements to be conducted. Transverse movement of the EFP, for a constant measurement plane, displayed anomalous distribution of the measured voltage. Theoretical behaviour would expect an even distribution in both waveform and relative voltage distribution, therefore the measured result is an unexpected characteristic of the high power device. Alternative methods of device characterisation relies on the simplification of the high power device; assumption that the complex and distributed device is merely a three terminal device. Such over simplification can blind designers to the extent of complexity present and result in reliability problems in the finalised system.

Measurements conducted on two nominally identical devices, placed independently within the HPA, contained differential waveform behaviour occurring in a specific region along the device. Further inspection of this region concluded a damaged and broken bondwire, where the differential behaviour was not evident in the output characteristics, therefore its consequence cannot be fully known if alternative methods of device diagnostics were used.

Chapter 7 and 8 presented the analysis of much more complicated structures containing two sub-amplifiers within their system. Due to the size, resolution and flexibility in positioning, the EFP was capable of measurements directly above the drain manifold within the active bondwire array. Such measurements allowed for direct, highly accurate and informative representation of the drain voltages within the DPA. Extraction of the fundamental component showed clear Doherty behaviour, whereby the sudden activation of the peaking device provided the sufficient contribution to maintain and saturate the main device's voltage. However, this clear depiction presented differences in the peak voltages, consistent in both the DPA and A-DPA measurements. Measurements conducted along the main and peaking devices showed that this difference was due to the substantial variation along the device periphery. The point of comparison chosen would therefore dictate the extent of the difference measured.

The variation measured at the device plane by the EFP was not visible in the output characteristics of the DPA or the A-DPA, if these variations led to potential reliability problems they would go undetected.

Measurements conducted within this thesis have consistently shown the application of the EFP as a diagnostic tool for the characterisation of complex devices. The ability to conduct in-situ on-chip measurements for time-domain analysis has given a valuable and alternative insight to the functionality of the device. Anomalous behaviour measured within the device package was not present in the output characteristics of the amplifier systems, thus highlighting the importance of a diagnostic tool capable of making such measurements.

The final chapter displayed a novel in-situ calibration method for the EFP, capable of being utilised before diagnostic measurements. By exploiting the low frequency response of a system, a 1MHz excitation can be used for the comparison of the EFP output to that of a contacted high impedance oscilloscope probe. A low frequency

excitation results in an even voltage distribution across all entities of the device, therefore a suitable scaling factor can be calculated and applied to further EFP measurements. This calibration method can be applied to every measurement as the DUT changes, thus making the calibration relevant and unique to each measurement. However, due to time constraints, this calibration method was not employed before the RFPA measurements. The delayed method for absolute calibration does not however disprove the results presented thus far, as they have been conducted on a relative manner. A relative measurement of such sorts provides valuable information not capable by other field methods.

11.2. Future works

The work presented within this thesis can be continued in various directions. Firstly, all further measurements would be conducted using the 1MHz calibration method, thus ensuring a fully calibrated measurement.

Improvements to the system can include:

- Calibration of the measurement plane. For situations where the low frequency in-situ calibration (mentioned in chapter 9) cannot be applied, an alternative technique for the determination of the measurement plane separation must be considered. This can be achieved simply through visual verification by improving the optical microscope system utilised. Improvements can include: higher magnification and the use of an optical microscope capable of measuring specific positioning.
- The measurements within this thesis have been conducted with only one automated axis. The incorporation of an additional automated stage can allow for full 3-dimensional scans of the DUT.
- Initial work has shown substantial improvement in the spatial resolution of the EFP can be made with systematic reduction in the probe dimensions. Further miniaturisation of the probe, with alternative materials, will improve beyond the current range and enable the system to probe interstage behaviour in multifunction RFICs.
- Further miniaturisation will ultimately lead to a loss in the output of the probe, therefore further improvements must be considered in the MMIC amplifier used. Incorporation of a two-stage amplifier can increase the

output and frequency response to a theoretical 19GHz. Such a design was in consideration for this thesis but due to time constraints it was never implemented. Primary design of the 2-stage MMIC amplifier is shown in figure 11.1, where the bias to the 2nd stage is provided through the addition of a feedback resistance.

- For the measurements of the amplifier system with two active devices to be investigated, for example a DPA, a system with two EFPs can be developed for simultaneous measurements of the main and peaking device.
- With all improvements thus far considered a permanent test bench can be developed for the measurement of hardware provided by external customers.
- Incorporation of EFP system and load-pull systems. A collaboration of the two methods can display any errors within the respective measurement technique and provide an absolute method of characterisation and diagnostic. [20]
- Final consideration includes the development of a current probe with similar dimensions, resolution and technologies. The measurement of device plane voltages, although a valuable measurement, only provides limited information about the system. Specifically for the measurement of high power amplifiers, the construction of a current probe will allow for the device plane drain current to be fully investigated.

.

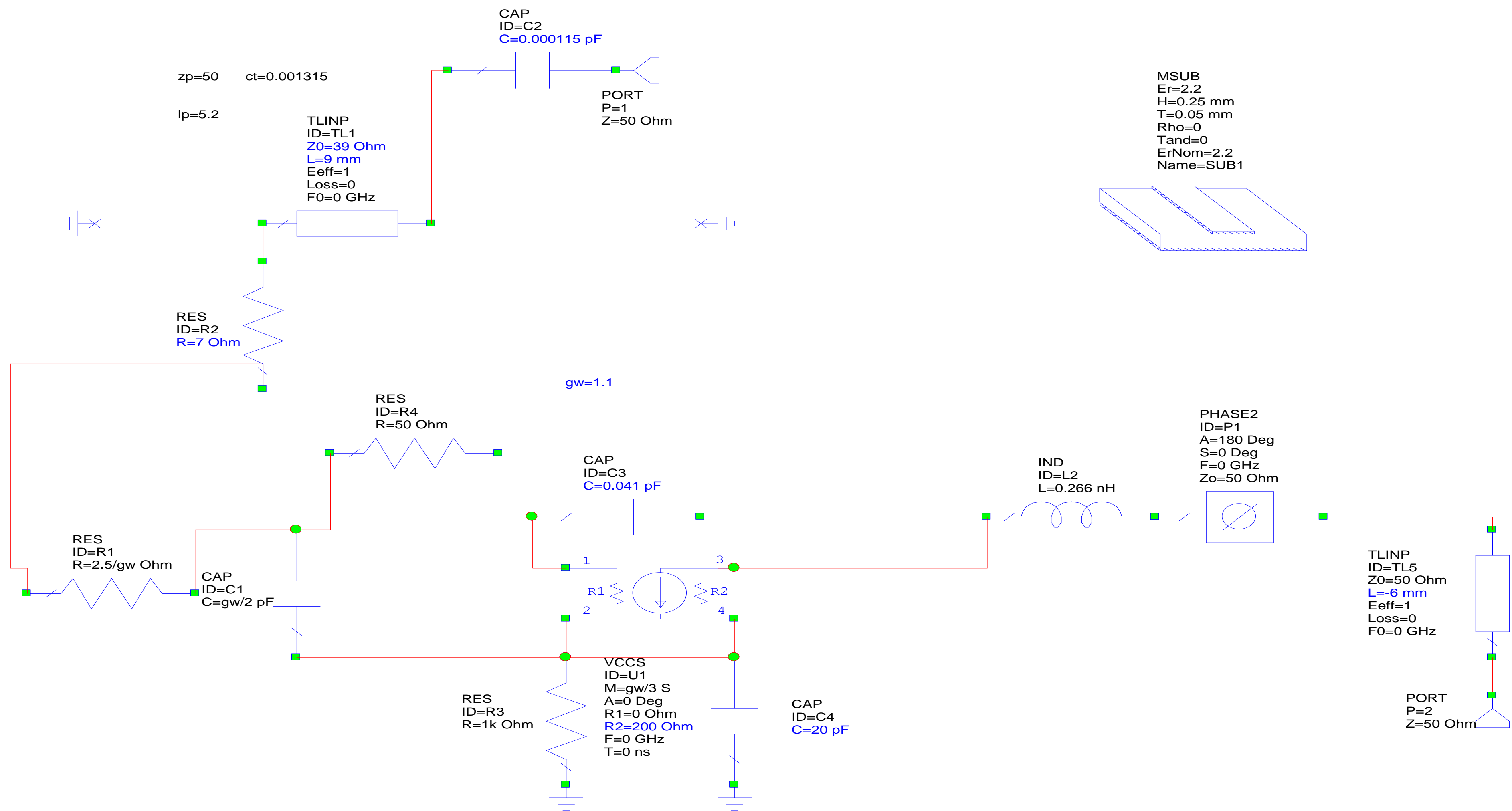

Figure 11.1: Circuit diagram of the simulation conducted for the design of the 2-stage MMIC die. Tuned for an optimal flat frequency response beyond 19GHz.

12. BIBLIOGRAPHY

[1] S. C. Cripps, RF Power Amplifiers for Wireless Communication 2nd ed., Artech House, 2006.

[2] M. A. Casbon, P. J. Tasker, W.-C. Wang, C.-K. Lin, W.-K. Wang and W. Wohlmuth, "Advanced RF IV Waveform Engineering Tool for use in device technology optimization: RF Pulsed Fully Active Harmonic Load Pull with Synchronized 3eV Laser," in *IEEE 978-1-4799-0583-6/13*, 2013.

[3] D. Barataud, F. Blache, A. Mallet, P. Philippe Bouysse, J.-M. Nebus, J. P. Villotte, J. Obregon, J. Verspecht and P. Auxemery, "Measurement and Control of Current/Voltage Waveforms of Microwave Transistors Using a Harmonic Load–Pull System for the Optimum Design of High Efficiency Power Amplifiers," *IEEE TRANSACTIONS ON INSTRUMENTATION AND MEASUREMENT,* vol. 48, no. 4, pp. 835-842, 1999.

[4] V. Carrubba, A. Clarke, S. P. Woodington, W. McGenn, M. Akmal, A. AlMuhaisen, J. Lees, S. C. Cripps, P. J. Tasker and J. Benedikt, "High-Speed Device Characterization Using an Active Load-Pull System and Waveform Engineering Postulator," in *IEEE 978-1-61284-961-4/11*, 2011.

[5] R. Ishikawa, Y. Takayama and K. Honjo, "Experimental Design Method for GHz-Band High-Efficiency Power Amplifiers Based on MHz-Band Active Harmonics Load-Pull Technique," in *Proceedings of APMC*, Kaohsiung, 2012.

[6] B. V. Rao, K. B. R. Muryy, K. R. Rajeswari and P. C. R. Pantulu, Electronic

Devices and Circuits, India: Chennai Micro Pront, 2007.

[7] J. Pritskutch and B. Hanson, “Understandinf LDMOS Device Fundamentals,” ST Microelectronics, Italy, July 2000.

[8] R. L. Boylestad and L. Nashelky, Electronic Devices and Circuit Theory, New Jersey: Pearson Education Ltd., 2006.

[9] F. Raab, P. Asbeck, S. Cripps, P. B. Kenington, Z. B. Popovic, N. Pothecary, J. Sevic and N. O. Sokal, “RF and Microwave Power Amplifiers and Transmitter Technologies- Part 1,” *High Frequency Electronics,* vol. 2, no. 3, May 2003.

[10] W. H. Doherty, “A new high efficiency power amplifier for modulated waves,” *Institute of Radio Engineers,* vol. 24, pp. 1163-1182, 1936.

[11] E. d. Silva, High Frequency and Microwave Engineering, Butterworth Heinmann, 2001.

[12] D. M. Pozar, Microwave Engineering, John Wiley & Sons INC, 1997.

[13] J. S. Dahale and A. L. Cullen, “Electric Probe Measurements on Microstrip,” *Microwave Theory and Techniques,* Vols. MTT-28, no. 7, 1980.

[14] Y. Gao and I. Wolff, “A simple electric near-field probe for microwave circuit diagnostics,” *MTT-S Digest,* Vols. TH3C-4, pp. 1537-1540, 1996.

[15] Z. Riah, D. Baudry, M. Kadi, A. Louis and B. Mazari, “Post-processing of electric field measurements to calibrate a near field dipole probe,” *IET Science, Measurement & Technology,* vol. 5, no. 2, pp. 29-36, 2009.

[16] T. Hiraoka, C. P. Chen, T. Anada, J. P. Hsu, Z. W. Ma and C. Christopoulos, “Electric Field Distribution in Microwave Planar Circuits by Small Coaxial Probe with comparison with FDTD Method,” in *European Microwave Conbference*, 2-9600551-2-8, 2005.

[17] R. Hou, M. Dprinto, B.-J. Kooij, F. van Rijs and L. C. de Vreede, “Contactless Measurement of In-circuit Reflection Coefficients,” in *978-1-4673-1088-8/12*, 2012.

[18] D. Uchinda, T. Nagai, Y. Oshima and S. Wakana, “Novel high-spatial Resolution Probe for Electric Near-Field Measurement,” in *RWS 978-1-4244-7685-5/11*, 2011.

[19] R. Hou, M. Spirito, J. Gajadharsing and L. C. de Vreede, “Non-intrusive

Characterization of Active Device Interation in High-Efficiency Amplifiers," in *978-1-4673-2141-9/13*, 2013.

[20] D. Baudry, A. Louis and B. Mazari, "Characterization of the open-ended coaxial probe used for near-field measurements in EMC applications," *Progress in Electromagnetics Research,* vol. Pier 60, pp. 311-333, 2006.

[21] C. j. Wei, Y. A. Tkachenko and J. C. Hwang, "Non-Invasive Waveform Probing for Nonlinear Netwrok Analysis," *IEEE MTT-s Digest,* Vols. CH3277-1/93/0000-1347, pp. 1347-1350, 1993.

[22] C. J. Wei, Y. A. Tkachenko, J. C. Hwang, K. R. Smith and A. H. Peake, "Internal-Node Waveform Analysis of MMIC Power Amplifiers," *IEEE Tansactions on Microwave Theory and Techniques,* vol. 43, no. 12, pp. 3037-3042, 1995.

[23] L. Navitel, M. Marchetti, P. Falgayrettes, M. Castagne, D. Gasquet, P. Gallborrut and M. Castel, "MMIC's Characterization by Very Near-Field Techniques," *Microwave and Optical Technology Letters,* vol. 41, no. 3, pp. 209-213, 2004.

[24] R. Kantor and I. V. Shvets, "Method of increasing spatial resolution of the scanning near-field microwave microscopy," *American Institute of Physics,* vol. 93, no. 9, pp. 4979-4985, 2003.

[25] R. Kantor and I. V. Shvets, "High Resolution Near-Field Measurements of Microwave Curcuits," *Microwave and Optical Technology,* vol. 5445, pp. 318-323, 2003.

[26] J. Chisum, M. Ramirez-Velez and Z. Popovic, "Planar Circuits for Non-contact Near-Field Microwave Probing," in *39th European Microwave Conference*, Rome, 2009.

[27] K. Yang, L. P. Katehi and J. F. Whitaker, "Electric Field Mapping System Using an Optical-Fiber-Based Electrooptic Probe," *IEEE MICROWAVE AND WIRELESS COMPONENTS LETTERS,* vol. 11, no. 4, pp. 164-166, 201.

[28] Y. Gao and I. Wolff, "Electric field investigations on active microwave circuits," in *26th EuMC*, Prague, 1996.

[29] Y. Gao, A. Lauer, Q. Ren and I. Wolff, "Calibration of Electric Coaxial Near-Field Probes and Applications," *IEEE TRANSACTIONS ON MICROWAVE THEORY AND TECHNIQUES,* vol. 46, no. 11, pp. 1694-1703, 1998.

[30] H. H. Barjawi, "Electromagnetic field mapping of microwave circuits using

transmission line probes," Cardiff University, UK, Cardiff, 2009.

[31] B. H. Kolner and D. M. Bloom, "Electrooptic Sampling in GaAs Integrated Circuits," *IEEE JOURNAL OF QUANTUM ELECTRONICS,* vol. 22, no. 1, pp. 79-93, 1986.

[32] M. Fukunda, Optical Semiconductor Devices, Canada: John Wiley & Sons Inc., 1999.

[33] K. Yang, T. Marshall, M. Forman, J. Hubert, L. Mirth, Z. Popovic, L. P. Katehi and J. F. Whitaker, "Active-Amplifier-Array Diagnostics Using High-Resolution Electrooptic Field Mapping," *IEEE TRANSACTIONS ON MICROWAVE THEORY AND TECHNIQUES,* vol. 49, no. 5, pp. 849-857, 2001.

[34] G. David, W. Schroeder, D. Jager and I. Wolff, "2D Electro-optic probing combined with field theory based multimode wave amplitude extraction: a new approach to on-wafer measurement," *IEEE MTT-S Digest,* Vols. CH:3577-4/95/0000-1049$01. OO, pp. 1049-1052, 1995.

[35] S. C. Cripps and A. Porch, "An Active, Non-intrusive, High Resolution Microwave Field Probe with Applications in High Power RF Device and Circuit Design.," in *978-1-4244-6689-0/10*, Crown, 2010.

[36] P. Aaen, "Private correspondence," 2011.

[37] N. Dehghan, S. Cripps, A. Porch and J. Lees, "An improved electric field probe with applications in high efficiency PA design and diagnostics," in *81st ARFTG*, Seattle, 2013.

[38] P. Aaen, J. Wood, D. Bridges, L. Zhang, E. Johnson, J. A. Pla, T. Barieri, C. M. Snowden, J. P. Everett and M. J. Kearney, "Multiphysics Modeling of RF and Microwave High-Power Transistors," *IEEE TRANSACTIONS ON MICROWAVE THEORY AND TECHNIQUES,* vol. 60, no. 12, pp. 4013-4023, 2012.

[39] N. Dehghan, A. Porch, S. C. Cripps and P. H. Aaen, "A Novel High Resolution E-Field Microscope System with Applications in HPA Diagnostics," in *ARFTG-978-1-4673-0282-1/11*, Tempe, 2011.

13. Appendix 1

A Novel High Resolution E-Field Microscope System with Applications in HPA Diagnostics

N. Dehghan, A. Porch, S.C. Cripps, School of Engineering, Cardiff University, UK

***Abstract*—A new type of high resolution E-field microscope system is described. The system is based on a novel design of an active E-field probe (EFP) probe, which is both non-intrusive and displays high spatial resolution. This paper focuses on the construction and spatial resolution of the probe, which shows significant evolution from that previously reported [1], and some measurements on passive structures which indicate that features smaller than 100 microns can be individually resolved. The probe construction lends itself to further improvements in spatial resolution. Measurement results are presented which demonstrate the high resolution of the probe, and its potential utility in measuring waveforms with high spatial resolution at individual points on microwave circuits, discrete devices, and integrated circuits.**

INTRODUCTION

WITH the development of ever increasingly sophisticated high frequency systems, it vital to have an understanding of each component and their interactions. With the aid of electromagnetic simulation software, designers have been able to reduce the number of prototype systems produced, as errors and design flaws can usually be flagged before fabrication. However this does method does not pinpoint all potential errors. The development of a non-intrusive E-field microscope system has proved to be vital as a method of evaluating the field distribution at a device plane, as each component may not perform in the expected manner in real life application.

This paper describes the design and fabrication of an E-field probe (EFP), and its in-situ applications. The design

of the EFP, is a development of a probe described in [1], and is constructed using an open-ended co-axial transmission line which can respond to local normal electric fields with a spatial resolution of about 100 microns.

From previous papers [1], knowing that the probed signal is small and the unwanted presence of stray signal pick-up problematic, the design of the EFP includes an amplifier close to the probe tip. This feature evidently amplifies the small signal but also eliminate the stray pickup from the feeder cable.

PROBE CONSTRUCTION

The basis of the EFP is an open-ended co-axial transmission line, which can be shown to have an increasingly sharp radiation pattern as the inner conductor is retracted inside the outer sleeve [2]. The use of such a retracted configuration is an important novel feature of the probe design, and differentiates it from previously published work in this area [2].

Conventional EM thinking, backed up by simulations [3], suggests that the spatial resolution of such a probe will be limited to the diameter of the inner conductor. On this basis, the spatial resolution can be improved indefinitely by using thinner co-ax. But a practical limitation becomes evident; as the capture area of the probe is reduced, the amount of coupling also reduces, and the desired signal soon becomes indistinguishable from the stray pickup on the co-axial leads. In previous literature [4], the EFP is coupled to a resonant transmission line in order to counteract this problem and to achieve a high spatial resolution with thinner inner conductor.

This problem is exacerbated by the high reflection presented by the probe to the 50 Ohm co-axial measurement system. Both of these problems can be greatly alleviated by the use of a buffer amplifier located close to the probe tip, and this is the second novel feature we describe in this paper.

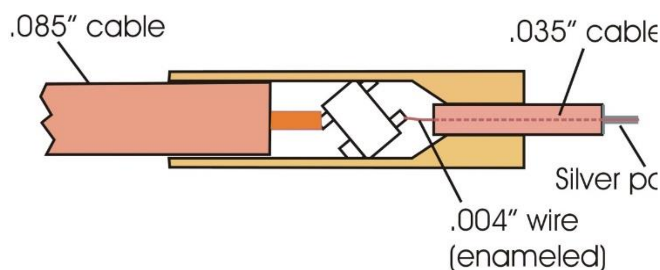

Fig. 1. Schematic diagram of E-field probe.

Such a configuration requires some innovative construction techniques, which have been substantially improved since the basic design was initially reported [1]. The construction of the present probe is shown in Figure 1. A small brass ferrule is machined to take a small diameter semi-rigid cable (1mm dia. approx.) at one end, and a conventional .085 semi-rigid feed cable at the other. Inside the ferrule there is just sufficient space to emplace an SOT packaged, small signal PHEMT transistor (Avago ATF34143). The ferrule has a tight fitting cover (shown removed in Figure 2). Although useful results can be obtained by simply flush-cutting the end of the protruding 1mm cable, much higher resolution can be obtained by removing the original inner conductor and replacing it with a much thinner piece of enameled copper wire. The actual probe then comprises the short protrusion of the wire beyond the semi-rigid cable, and this is transformed into a very thin co-axial line by coating it with conductive silver paint. The wire diameter for the present set of reported measurements was 100 microns (.004 inch).

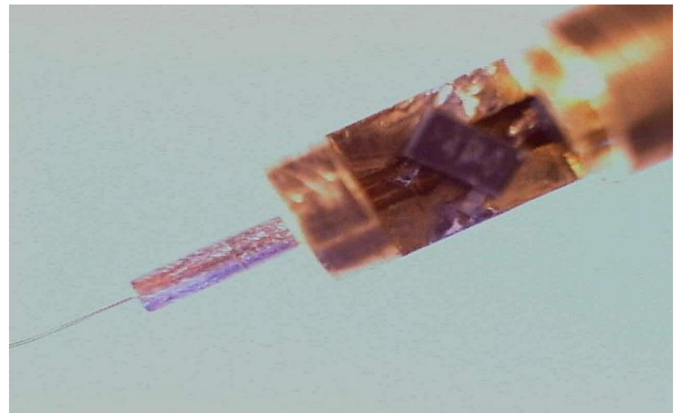

Fig. 2. Picture of the ferrule with the cover removed.

MEASUREMENTS.

Figure 3 shows a 3-D view of a typical test structure that is being used to demonstrate the probe’s spatial resolution. It consists of a microstrip line which has an end termination consisting of a fan of multiple 20 micron ground bonds. Various structures were measured, having different bondwire counts and different spacings. Figure 4 shows the measured spatial response as the probe is moved transversely along the bond wires shown in Figure 3. We measure a dc voltage proportional to the power picked up by the probe, which is itself proportional to the square of the local electric field generated at the probe’s tip

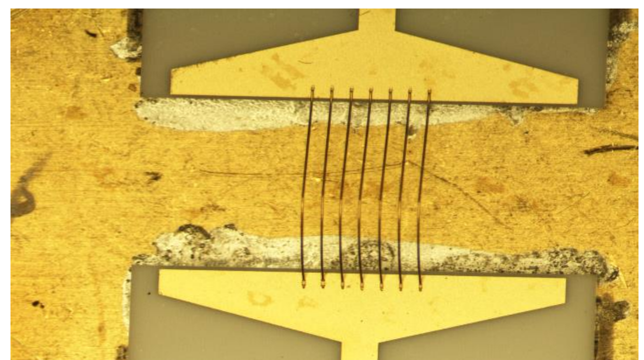

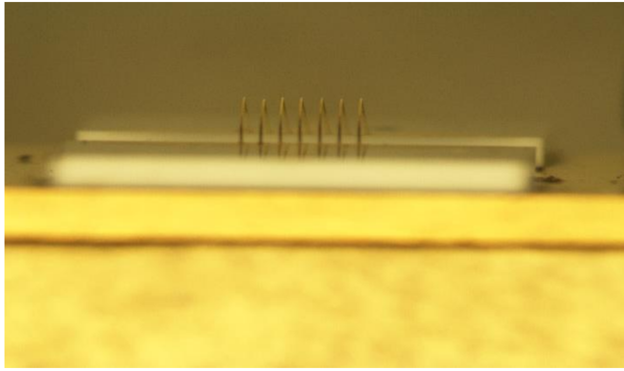

Fig.3. Plan and side view of a 7 bond test structure.

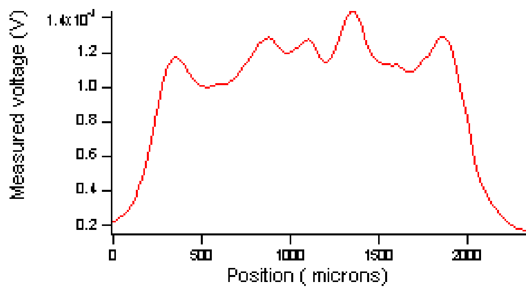

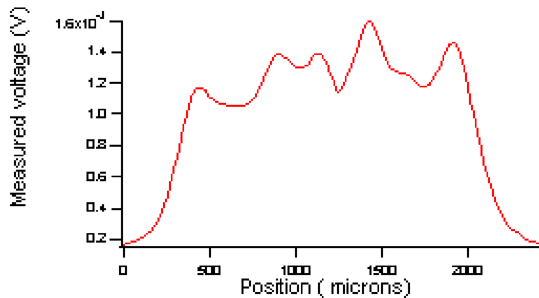

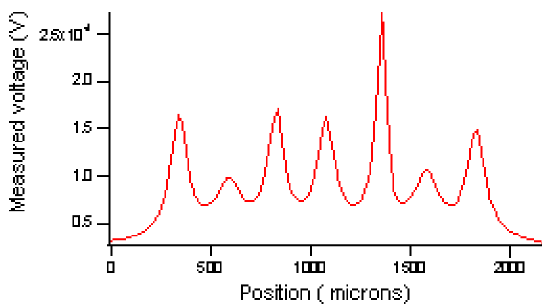

Fig. 4. Voltage distribution transversely along the 7 bond structure shown in Fig 3 Shown in the order, Probe 1, Probe 2 and Probe 3. Probe inner conductor diameters: Probe 1 : 0.007 inch. Probe 2: 0.005 inch. Probe 3:0.004 inch (wire probe)

In previous work [1] we have presented evidence that this probe geometry responds only to the electric field, and almost entirely to the vertical component of the local electric field at the measurement tip; this in turn bears a close physical relationship with the voltage on the wires. Figure 4 shows the same measurement using three different probe inner diameters. It is interesting to note that the thinnest available semi-rigid cable has an inner conductor diameter of .005", which is only slightly larger than the wire probe, yet the wire probe clearly has substantially higher spatial resolution.

Figure 5 shows a measurement taken along a more extensive bondwire structure, having 19 bondwires and closer spacing. Figure 6 shows the 3-D view of the 19 bondwire structure. It is clear that the magnitude of the field peaks are very sensitive to the planarity of the bondwires, but there is a clear overall trend visible, whereby the field has a smooth maximum at the center of the structure and a substantial roll off towards the edges. This is in apparent disagreement with a 3-D EM simulation shown in Figure 7, although the full consequences of this comparison are still under evaluation.

The magnitude of the field peaks is not just dependent on the planarity but to the curvature of each individual bondwire. Imperfections in the fabrication stage leaves slight variations in the curvature and may ultimately contribute in the overall trend which has been observed.

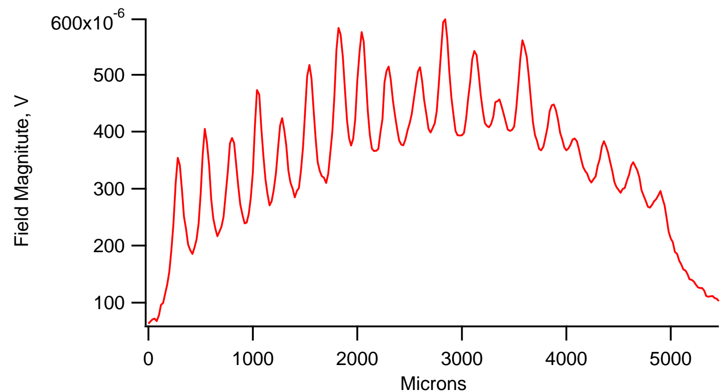

Fig. 5. Voltage distribution transversely along a 19 bond structure.

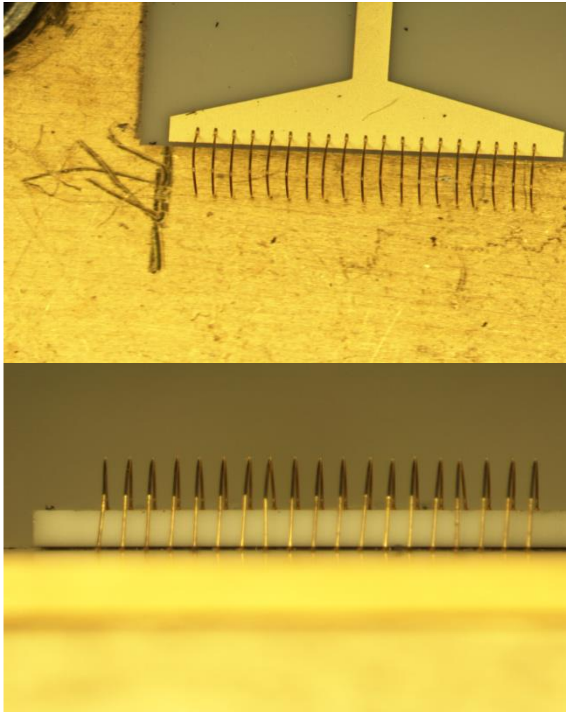

Fig. 6. Plan and side view of a 19 bond test structure.

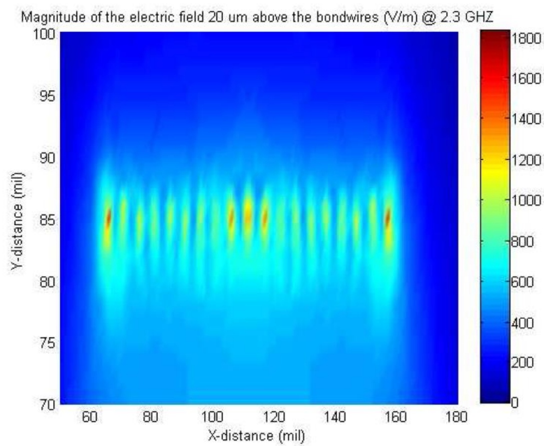

Fig. 7. EM simulation of 19 bond structure.

CONCLUSION

In conclusion, we have built and demonstrated a novel E-Field microscope system which has a spatial resolution of better than 100 microns. We believe substantial further improvements can be made to the resolution, for example enabling voltages within RFICs to be probed directly. We are also pursuing applications where the device plane voltages and currents in working PAs (as opposed to devices in load pull systems) can be measured directly. One specific goal in this area is an investigation of device voltages, and potential reliability issues resulting therefore, in high power Doherty PAs.

REFERENCES

[1] Cripps S.C, Porch, A., "A High Resolution, Non-Intrusive Field Probe", Wamicon 2000

[2] Kantor, R., Shvets, I.V., "Measurement of electric field intensities using scanning near-field microwave microscopy", Trans. Microwave Theory Tech., MTT-51, no. 11, Nov 2003, pp2228-2234.

[3] H. Barjawi, MSc thesis,2009, Cardiff University, UK.

[4] C. P. Vlahacos, R. C. Black, S. M. Anlage, A. Amar, and F. C. Wellstood, Appl. Phys. Lett., Vol. 69, No. 21, Nov. 1996, pp3271-3274

14. APPENDIX 2

An Improved Electric Field Probe with Applications in High Efficiency PA Design and Diagnostics.

Abstract — An Electric Field Probe is described, which has substantially improved bandwidth and spatial resolution compared to previously reported work [1]. Calibration tests on the reported probe shows a flat amplitude and phase response up to 6GHz. A novel calibration technique is described, which has enabled direct observation of device plane voltages in high power RFPAs. Results show evidence of various anomalous effects, including variation of voltage across the periphery of high power RF devices.

Index Terms — High power amplifiers, microwave measurements, microwave imaging, microwave transistors.

INTRODUCTION

This paper describes a non-intrusive, non-contacting high electric field ("E-field") probing system which has much improved frequency and resolution performance over that described in previously published literature [1-4]. The current design evolution is shown to display better than 100 micron spatial resolution, with a clear path to further improvement through dimensional reduction. Flat frequency performance, in both amplitude and phase, are demonstrated up to 6GHz, with potential for extension well beyond 19GHz. These improvements have been obtained through the novel use of fine geometry components and a customized RFIC probe head amplifier. The probe has been used to make both spatial and power-swept scans on high power LDMOS transistors operating in high efficiency amplifiers.

PROBE DESIGN AND CONSTRUCTION

Fig.1 shows a schematic diagram of the probe. It consists of a short length of co-axial line, constructed using a short length of fine diameter copper tube, threaded internally by an enameled copper wire. The actual pickup structure is a very short monopole and it will be shown in this paper that the length of the monopole protrusion has to be carefully controlled in order to obtain optimum spatial resolution. It is observed that the monopole "protrusion" needs to be very short, or even slightly retracted into the outer sleeve, but this greatly reduces the magnitude of the pickup. There comes a point where the probe pickup signal becomes comparable to the "stray" pickup that will inevitably occur on the outer conductor.

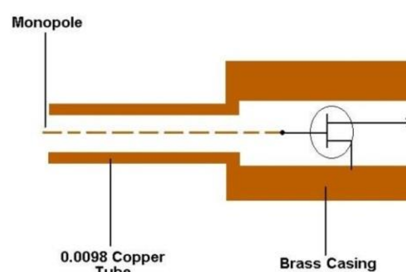

Fig. 1. Schematic diagram of e-field probe.

It is therefore essential that an amplifier is placed as close as possible to the probe pickup point in order to amplify the desired signal; the construction in effect places the amplifying device in a Faraday cage which greatly improves the dynamic range for this reason. In this reported work, the probe head amplifier was a common source PHEMT. This was originally implemented using an SOT-packaged device but this gave a poor frequency and phase response above 3GHz. The present RFIC implementation has greatly improved the frequency

performance. The RFIC design provides a low parasitic interface with the probing structure, allows for optimum biasing of the active device, and enables an optimum device periphery to be selected. Fig.2 shows a photograph of the probe head amplifier casing, with the probe structure itself emerging on the left hand side, and the 50 Ohm cable output on the right. This casing would have a close-fitting cover in normal use.

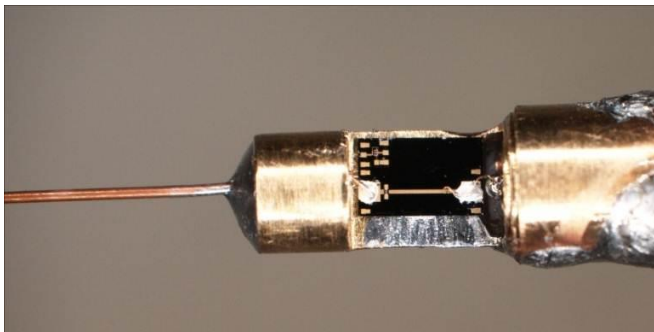

Fig. 2. Picture of the probe casing with cover removed.

PROBE CALIBRATION

A. Frequency Calibration

It has been established that the relative frequency response of this probe is quite insensitive to the local geometry of the probe target area, or to the precise spacing between the probe and the target. As such, frequency sweeps are measured using the probe placed above a section of matched 50 Ohm microstrip line. Theoretical simulation of the probe predicts a flat response, but with a resonance whose frequency is mainly a function of the length of the probe line. Fig. 3 shows four frequency scans for different lengths of probe line, showing the shift in resonance, and different monopole protrusion lengths, showing different coupling factors. Several previous workers [1, 3] have shown that such a probe will respond almost entirely to the E-field parallel to the monopole.

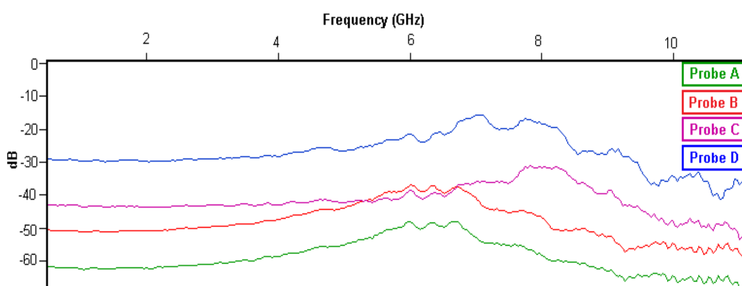

Fig. 3. Frequency Response of four MMIC probes. Probe A and B have a probe line of 9mm and a monopole protrusion of 0.025mm and 0.10mm; Probe C and D have a probe line of 5mm and a monopole protrusion of 0.07mm and 0.13mm, respectively.

B. Spatial Resolution

Fig. 4 shows a test pattern that has been used to measure the spatial resolution of the probes. It is a set of parallel 25 micron fingers, deposited on a 10mil alumina substrate. For the present generation of probe dimensions, a finger spacing of 100 microns (4 mil) was used.

Fig. 4. Resolution test substrate with 25 micron fingers, 100 micron spacing.

Fig. 5 shows the result of scanning this structure with two probes, each having a different length of monopole protrusion; clearly the probe with the shorter (almost flush) protrusion shows substantially better resolution, but at the expense of lower output.

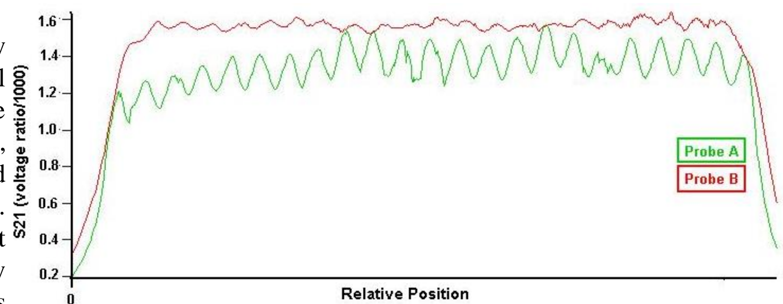

Fig. 5. Automated scan along the test substrate using Probe A and Probe B.

The probe was then used to scan a 50W 2GHz Doherty power amplifier. The scan was taken over the gate region of an LDMOS device, where the enclosing lid has been removed, exposing the bondwires. Fig. 6 shows this region and the resulting measured voltage. The probe is able to depict the position and placing of the bondwires, showing the deformity of two that are closer together, highlighted in red.

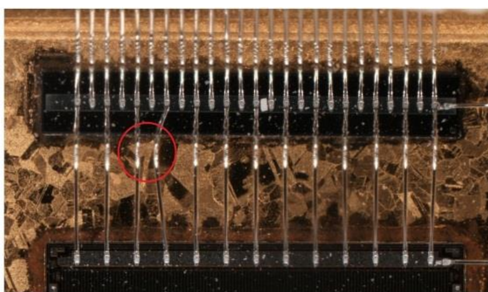

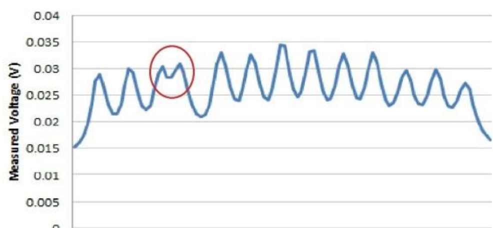

Fig. 6. Automated scan along the gate-side bondwires of an operating 50W 2GHz Doherty power amplifier.

C. *Amplitude Calibration*

It should be noted that useful and informative observations on high power active devices can be taken using relative readings from a fixed probe position (e.g. as shown in Figs. 7 and 9). Absolute calibration of this kind of E-field probe poses some difficulties. The pickup signal is highly sensitive to the spacing and local geometry of the probing target and the pickup itself is proportional to the vertical electric field component, rather than the voltage to ground. In this work we have followed a calibration philosophy whereby either "known" voltage, and/or known features of the waveform such as mean, peak and minimum levels, are used to give direct *in situ* calibrations with a particular probe position setting.

For example, Fig.7 shows a set of probed waveforms taken on a high power LDMOS drain at a constant RF drive level but with decreasing supply voltage. Given that these traces all represent the device in hard compression, it is a reasonable assumption that the successive minima represent conditions where the device voltages are close to the knee, or turn-on value, which is a known and measureable characteristic of the device (3.5v $\pm$0.5v) volts in this case. Hence, along with the mean level which can be set to the DC supply value, a workable *in situ* voltage calibration can be obtained. This is the calibration technique used to define the voltage scale in the HPA waveform measurements presented in section IV (Fig.8).

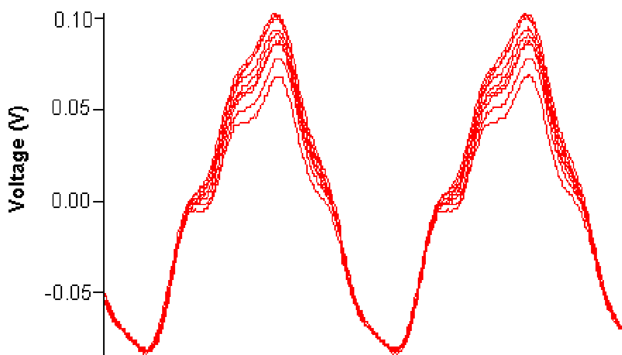

Fig. 7. Probe voltage waveforms, at constant RF, with uniform decrease of supply voltage over a 1ns sweep; traces have been lined up at the device knee point.

HIGH POWER PA (HPA) MEASUREMENTS

This section presents some results obtained using the described E-field probe to display the device plane voltages of a twin-die high power (200W) LDMOS device in a fully operational high efficiency PA module. For these measurements, the active device was de-lidded, and the probe was place very close to the on-chip drain metal manifold. Fig.8 shows a series of voltage waveforms in the center of one of the die, for drive power levels that took the device into compression.

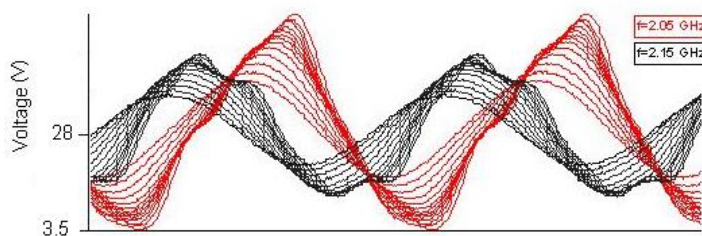

Fig. 8. Voltage waveforms for the LDMOS device as the power level is increased, for two different frequencies (individual waveforms have been displaced horizontally for clarity).

The two sets of waveforms in Fig.8 represent the same test taken at two different frequencies: the larger amplitude set (in red) was taken at the designed mid-band frequency, 2.05GHz, the lower amplitude set (the black) was taken at a frequency slightly past the upper band edge, 2.15GHz. Clearly, it can be seen that the impedance match at the band edge has dropped to a low value, so that the voltage never reaches the clipping level. Such information is of great value to the circuit designer. Fig. 9 shows a spatial scan taken across the two die that comprise the complete packaged device; this scan was performed at a drive level close to the saturation level and shows one cycle of the waveform. Fig. 10 shows the same scan for a nominally identical but different device. Two highly significant observations can be made from these plots: in Fig. 9 there is clearly some differential behavior between the two separate die, and in Fig. 10 there is a well-defined discontinuity in the voltage at one point on

one die. Close inspection of the device at this point revealed a damaged bondwire.

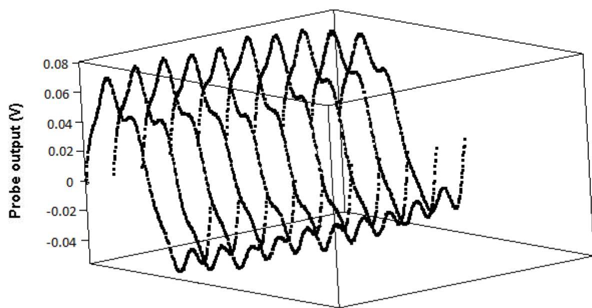

Fig. 9. Lateral scan across LDMOS device close to saturation, (1ns sweep).

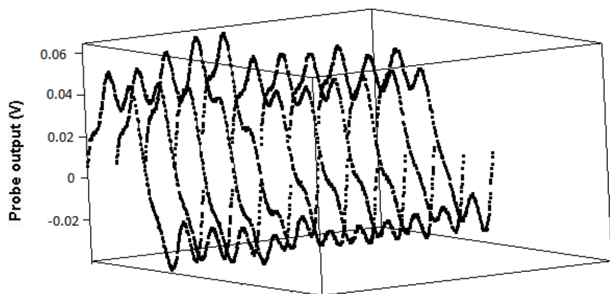

Fig. 10. Lateral LDMOS device scan, damaged bondwire.

DOHERTY POWER AMPLIFIER (DPA) MEASUREMENTS

The same probe was then used to measure the voltage waveforms of a 50W 2GHz Doherty power amplifier, with equal transistor size. Both devices were de-lidded, and the probe was placed over, very close to, the drain manifold. Fig.11 shows the voltages waveforms of the main device as the input drive is increased in 1dBm steps, where Fig.12 shows the waveforms from the peaking device.

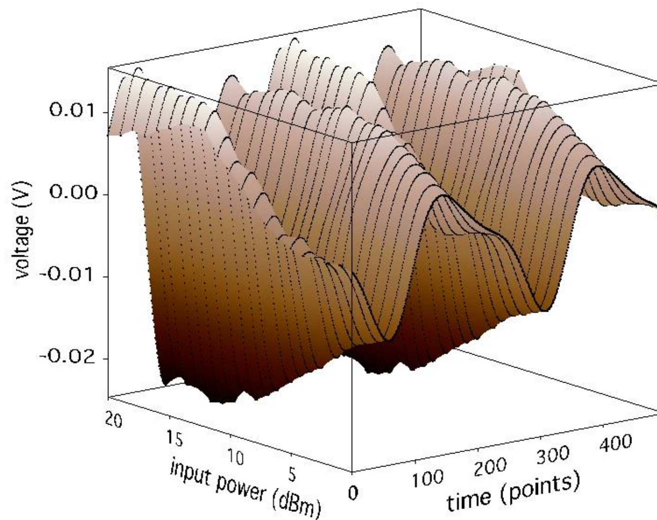

Fig. 11. Voltage waveforms from the main device, for 1dBm stepped input power, attained from one position of the probe.

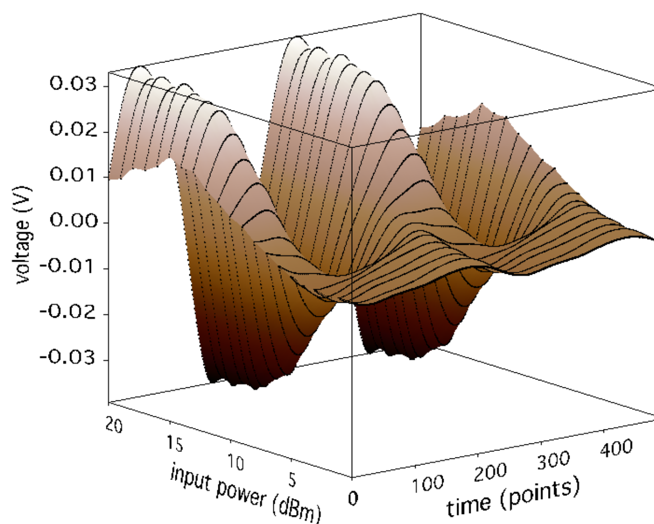

Fig. 12. Voltage waveforms from the peaking device, for 1dBm stepped of input power, attained from one position of the probe.

It can be seen that there is almost a factor of two in the difference in the peak to peak values of the voltages in the main and the peaking device. The position of the probe over both devices were in the same positions of the die manifold, but showed such differences in the magnitude. Further investigation of the main device concluded that this difference was due in part to variations in the voltages along the device periphery. Fig.13 shows the extent of this variation as the probe is moved along the main device; note that the vertical position of the probe does not change.

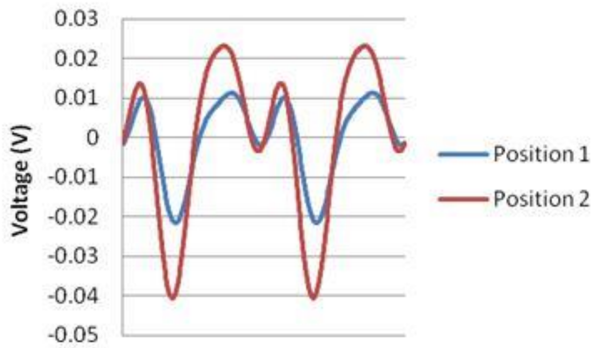

Fig. 13. Voltage waveforms from the main device, at a drive level close to the saturation, in two different lateral positions.

These plots have been included in order to demonstrate the enormous potential of the described probing technique, in obtaining more detailed insight into the behavior of complex high power microwave amplifiers. The full implications of these plots, in terms of DPA design methodology, are still under intensive study at the time of submission. The growth and phase shift of a strong second harmonic component in the main device voltage waveform is, for example, a significant feature that is not predicted by classical DPA analyses.

CONCLUSIONS

A high resolution, broad band E-field probing system has been described. The construction techniques used will allow for substantial further reductions in probe dimensions, resulting in finer resolution, for example enabling an ability to resolve individual finger voltages in high power RF transistors, and inter-stage voltages in RFICs. Improvements in the probe head amplifier will also enable higher sensitivity and dynamic range. This technique will provide a unique insight into the operation of microwave active devices in actual operating circuits.

REFERENCES

[1] N. Dehghan, S.C.Cripps, "A Novel High Resolution E-Field Microscope System with Applications in HPA Diagnostics" (ARFTG, Tempe AZ, 2011)

[2] R. Kantor, and I.V.Shvets. "Measurement of electric field intensities using scanning near-field microscopy," *IEEE Trans. Microwave Theory & Tech.,* vol. 51, no. 11, pp. 2228-2234, November 2003.

[3] J.S. Dahele, A.L.Cullen, "Electric probe measurements on microstrip," *IEEE Trans. Microwave Theory & Tech.,* vol. 28, no. 7, pp. 752-755, July 1985

[4] Y.Gao, A.Lauer, Q.Ren, I.Wolff,, "Electric probe measurements on microstrip ," *IEEE Trans. Microwave Theory & Tech* 1985 vol. 48, no. 11, Pt. II, pp. 1694-1703, Nov. 1998.

15. APPENDIX 3

A Novel In-Situ Calibration Technique for a High Resolution E-Field Probe

N. Dehghan, S.C. Cripps, A. Porch, School of Engineering, Cardiff University, UK

Abstract— **The potential of E-Field probes as diagnostic tools in operational microwave circuits and devices has been widely recognised but little used. Progress in this area has always been hampered by the lack of an absolute calibration technique. As such, these measurements are usually only useful for relative measurements over a range of electrical conditions where the probe remains stationary. This paper describes a probe design which can be calibrated in-situ each time the probe is moved. The calibration technique is demonstrated by measurements of RF waveforms at the device plane of a medium power (10W) GaAs FeT power amplifier.**

INTRODUCTION

With the recent growth in multifunction microwave integrated circuits (MMICs), the availability of a probe with suitably high spatial resolution would be a very useful diagnostic tool for the MMIC designer. For example, the ability to measure internal voltages within a MMIC would be most valuable in diagnostic activities. The use of E-Field Probes (EFP) in other applications, such as antenna measurements, has been widely reported for many years [1-3]. Such probes usually comprise a dipole or monopole sensing element connected to a 50 Ohm feeder cable. The spatial resolution of such a probe is of great importance in the measurement of tiny microwave devices. In principle this requirement predicates a suitable scaling down in the physical size of the probing element, although this will proportionately reduce the sensing aperture. This can be partially resolved by the use of an amplifier at the probe tip [4-5] but the fundamental problem of calibration remains.

Figure 1 highlights the main aspect of calibrating an EFP. The probing structure "hovers" above the target measurement point. The coupling factor is clearly a very sensitive function of the spacing of the probe to the circuit element, which itself may not be planar and can have a wide range of geometry. The probe output is therefore a very complex function of the spacing and the local geometry of the probing target. So in Figure 1, for example, a different response can be expected in the two cases of an extensive planar surface (such as a microstrip line) and a more local structure such as a bondwire or a pad on a semiconductor device.

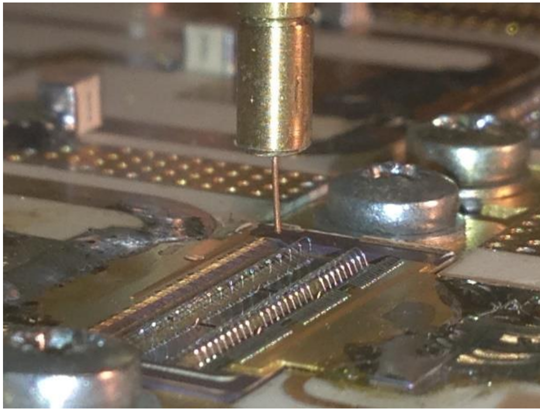

Fig. 1. Depicts an example of the EFP and how it can be positioned for an in-situ measurement of a de-lidded power transistor.

Nevertheless, if it were possible to develop a “known” voltage in the target area, calibration would be straightforward, so long as a new calibration is performed every time the local geometry changes, usually due to movement of the probe. Difficulties can arise at microwave frequencies as the measurement point is deeply embedded in a distributed microwave circuit.

LOW FREQUENCY RESPONSE

A possible way around this problem is to recognise that the coupling of the probe to the circuit is essentially capacitive and “quasi-static”. As such, the critical coupling factor can be measured at any convenient frequency, which can for example be much lower than the operational frequency of the circuit under test. In particular, a sufficiently low calibration frequency can be chosen such that the spatial variation of the voltage in the region of the probe target is massively reduced and can be measured conveniently. For example, if a microwave circuit is excited at 1MHz, the same voltage will be measured on the feed lines to a transistor as will appear at the device bonding pads. The voltage can thus be conveniently measured using a high impedance oscilloscope probe at a point some distance from the device itself.

This approach assumes however that the probe itself has a suitable low frequency response. Conventional EFPs, where typically the probing element is connected to a 50 Ohm system, will display an R-C roll-off characteristic, so that at very low frequencies the probe output will be too low to be useable. The probe used in the present work has been described previously [5] and consists of a short length of miniature co-axial line, fabricated using a 0.25mm diameter EDM tube, which is connected to the input of a high frequency GaAsFET transistor. The gate input of the GaAsFET is essentially capacitive, so this probe construction gives a flat response down to very low frequencies, limited in practice only by the drain biasing arrangements, as shown in the measured response (Fig.3).

THEORY

Fig. 2 shows the frequency response of the probe as it measures a section of matched 50 Ohm microstrip line. The probe response will not remain perfectly flat at higher frequencies, where the parasitic components beyond 9GHz will start to have a significant effect on the response. *But these parasitic are not affected by the position of the probe, or the local geometry of the probe target*.

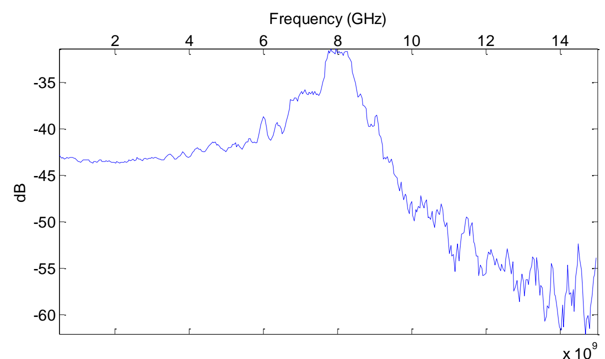

Fig. 2. Frequency calibration of the EFP resulting in a flat response from 1MHz to 7.5GHz before the resonance due to the length of probe line and parasitic components dominate.

The only component that is sensitive to the probe position is the coupling capacitor. Thus a 2-step calibration procedure is possible: (1) the frequency response can be measured as a relative function using any convenient structure, such as a microstrip line, (2) with the probe in position to make a measurement in the target structure under test, the target is “illuminated” by a known low frequency signal (e.g. 1MHz), which allows absolute calibration of the actual microwave frequency measurement, along with a suitable frequency correction obtained in the first step (1).

It may still be questioned as to whether the simple capacitive coupling model will remain valid at the low calibration frequency. In particular, the spatial resolution of the probe will ultimately change due to the penetration of electric field through the wall of the thin co-axial line; the skin depth for copper at 1MHz is approximately 30 microns which is not much lower than the wall thickness of the EDM tube.

Transverse scans across the 11 bondwire array on the drain side, shown in Figure 3, at frequencies 2.1GHz, 10MHz, and 1MHz, as in Figure 4, can however eliminate this concern.

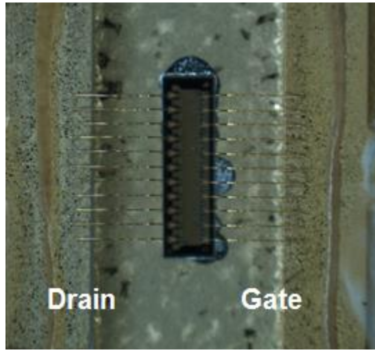

Fig. 3. 10W medium power GaAs transistor, de-lidded for in-situ calibration and spatial resolution measurements; highlighting the drain and gate.

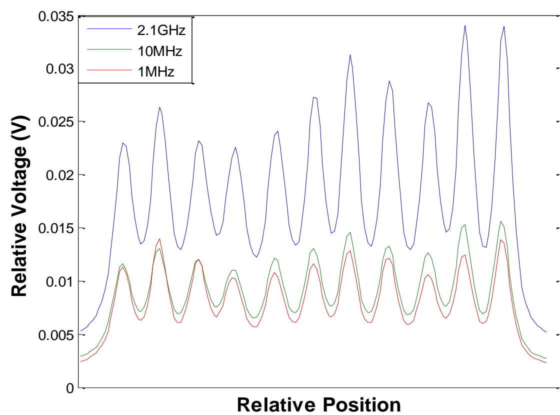

Fig. 4. Transverse scans along the 11 drainside bondwire array resulting in no degradation of spatial resolution as the excitation frequency of the GaAs device is lowered.

Anomalous differences present in measured peak values of the relative voltage magnitude are solely due to the planarity issues existing in the bondwires of the GaAs device. As previously mentioned the probe output is a function of its local geometry, thus the highly sensitive probe, when subject to changes in the curvature and bondwire height, will measure a proportional change in the field produced by the bondwires and hence the variance in the voltage.

Measurement Setup

In order to meet the objective of an in-situ calibration technique, the resultant procedure must be such that the probes position above the DUT remains constant while the injected excitation is interchanged between 2.1GHz and 1MHz. During this time, waveform information is captured by a DSO at both frequencies in the same exact position. With direct measurement on the a section of metallisation a high impedance oscilloscope probe, the suitable scaling factor for the 1MHz waveform can be calculated. The measurement setup is such that 2.1GHz and 1MHz excitation does not occur simultaneously, but can be interchanged with ease. This ultimately results in a constant separation and positioning of the EFP at both frequencies they are utilised independently.

For measurements taken at 1MHz, the gate voltage is increased to the pinch-off level in order draw no current.

Experimental Results

Following the experimental setup shown in the previous section, the waveform information is captured by the EFP at 2.1GHz and 1MHz. Using a DPO with a probe attachment, the direct contact is made on the microstrip line leading to the GaAs device at 1MHz. from this captured waveform, a suitable scaling factor can be achieved for the EFP measurement at 1MHz. This scaling factor is found to be 615. Figure 5 shows the waveform measurements obtained from the DPO and the scaled up waveform measured from the EFP both at 1MHz.

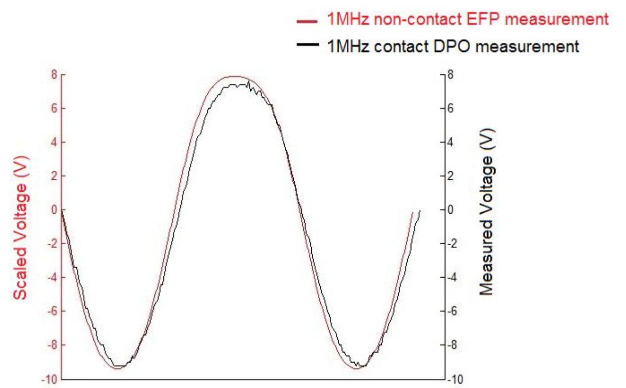

Fig. 5. . Superimposed waveforms measured at 1MHz from contact measurement of DPO and the scaled EFP measurement.

The same scaling factor is applied to the waveform measurements obtained from a power sweep, from 0-9dBm at 2.1GHz, the results are shown in Figure 6.

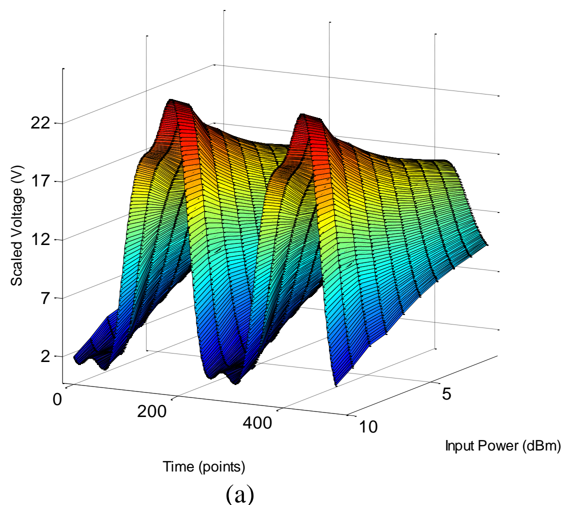

(a)

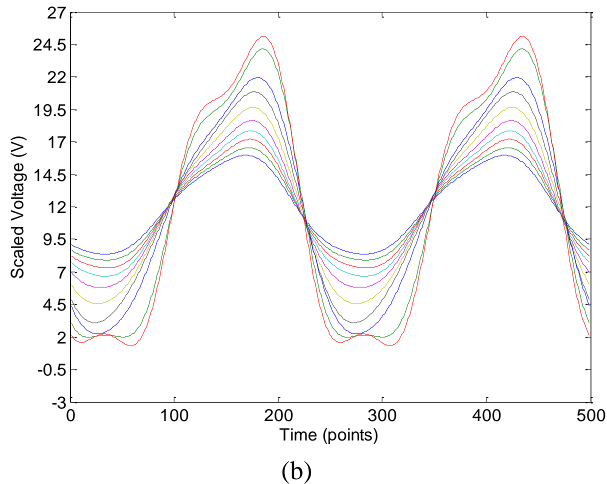

(b)

Fig. 6. Power sweep of 0-9dBm conducted at the frequency 2.1GHz, where the EFP output has been accordingly scaled by the calculated factor of 615 scaled using the scaling factor; represented in (a) 3D and (b) 2D format. Note probe is AC coupled, the actual Vdc value of 12V.

CONCLUSION

A novel in-situ calibration technique for a high resolution e-field probe [5] has been suitably demonstrated. By exploiting the low frequency response of a system, where by at such frequencies, even the most complicating structures behave much simpler, resulting in an equal voltage distribution across all entities of the device. Due to the resolution capability of the e-field probe, it has been demonstrated that its spatial resolution is independent of the measuring frequency. With suitable scaling factor obtained from the 'known' voltage measurement, absolute frequency calibration can be applied and determined.

REFERENCES

R. Kantor and I.V. Shvets, "Measurement of electric-field intensities using scanning near-field microwave microscopy" *IEEE Transactions on Microwave theory and Techniques,* vol. 51, no. 11, November 2003.

J.S. Dahele and A.L. Cullen "Electric probe measurements on microstrip" *IEEE Transactions on Microwave theory and Techniques,* vol. MTT-28, no. 7, July 1980.

D. Uchida, T. Nagai, Y. Oshima and S. Wakana "Novel high-spatial resolution probe for electric near-field measurement" *IEEE,* 2011, pp. 978-1-7685-5/11.

N. Dehghan, S.C.Cripps, "A novel high resolution E-Field microscope system with applications in HPA diagnostics" *IEEE,* 2011, pp. 978-1-4673-0282-1/11.

N. Dehghan, S.C.Cripps, "An improved electric field probe with applications in high efficiency PA design and diagnostics." *IEEE,* 2013, pp. 978-1-4673-4983-3/

16. APPENDIX 4

Zaber automated stage.

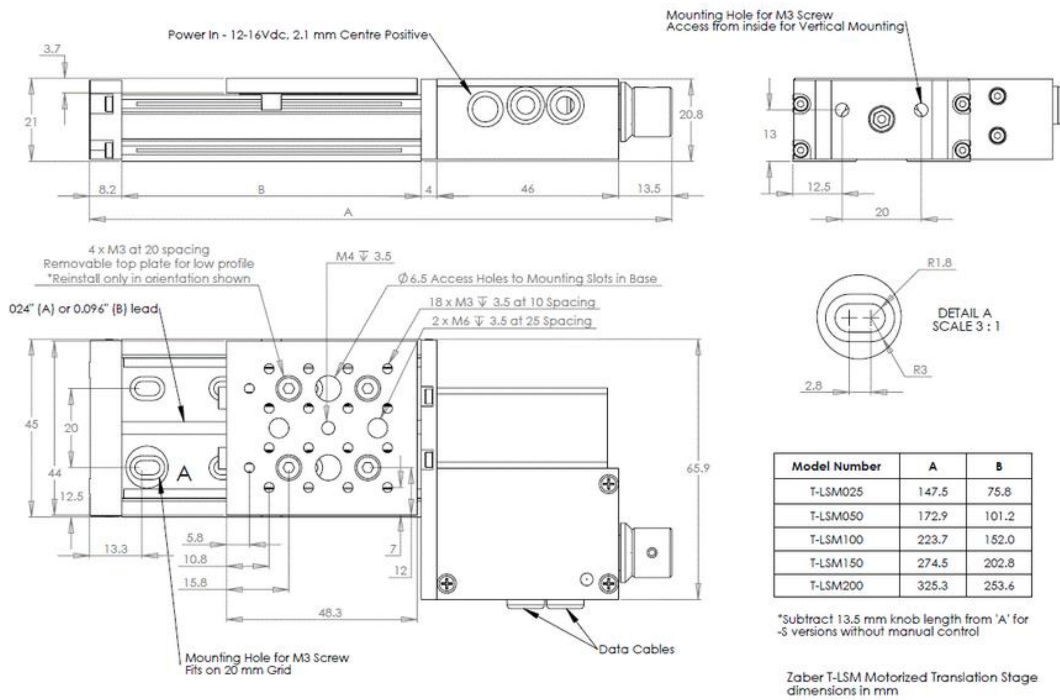

Model Number	A	B
T-LSM025	147.5	75.8
T-LSM050	172.9	101.2
T-LSM100	223.7	152.0
T-LSM150	274.5	202.8
T-LSM200	325.3	253.6

Figure A: Schematic of the Zaber automated stage.

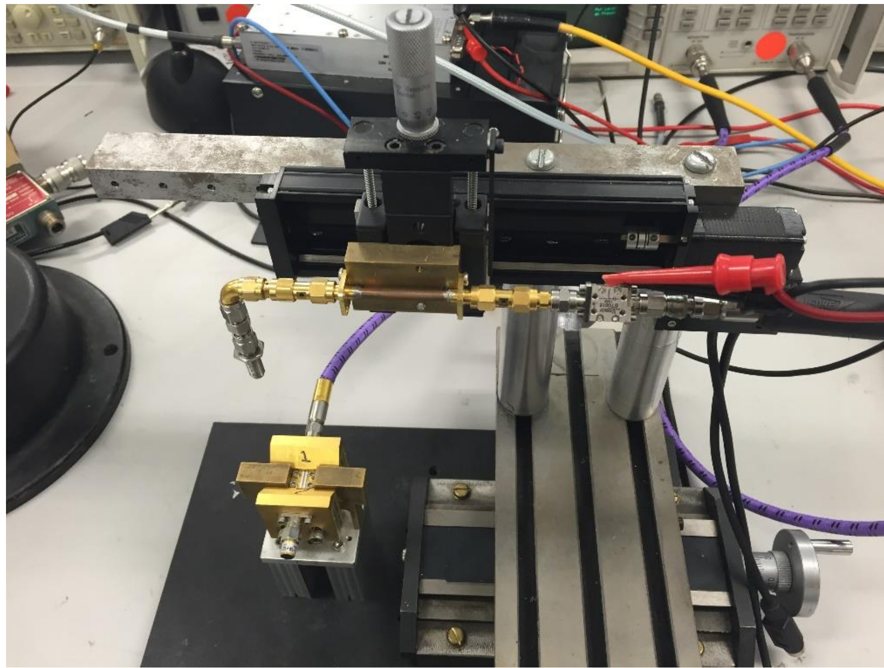

Figure B: Schematic of the incorporated Zaber automated stage and x-y-z positioner used for measurements throughout the work presented.

17. APPENDIX 5

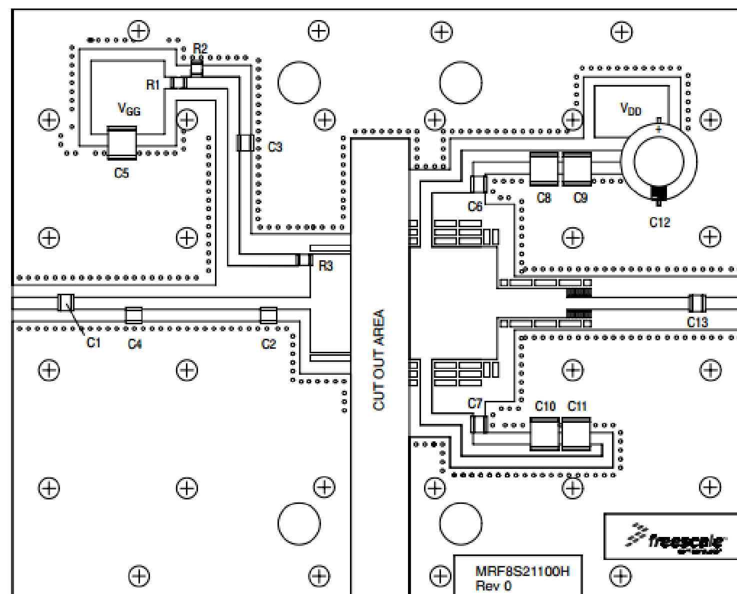

Figure 1. MRF8S21100HR3(HSR3) Test Circuit Component Layout

Table 5. MRF8S21100HR3(HSR3) Test Circuit Component Designations and Values

Part	Description	Part Number	Manufacturer
C1, C3, C6, C7	6.8 pF Chip Capacitors	ATC100B6R8CT500XT	ATC
C2	1.6 pF Chip Capacitor	ATC100B1R6BT500XT	ATC
C4	0.2 pF Chip Capacitor	ATC100B0R2BT500XT	ATC
C5, C8, C9, C10, C11	10 μF, 50 V Tantalum Capacitors	293D106X9050E2TE3	Vishay
C12	220 μF, 50 V Electrolytic Capacitor, Radial	227CKS050M	Illinois Capacitor
C13	5.6 pF Chip Capacitor	ATC100B5R6CT500XT	ATC
R1, R2	2 KΩ, 1/4 W Chip Resistors	CRCW12062K00FKEA	Vishay
R3	10 Ω, 1/4 W Chip Resistor	CRCW120610R0JNEA	Vishay
PCB	0.030″, ε_r = 2.55	AD255A	Arlon

Figure C: Schematic of the HPA test fixture used within chapter 6.